Titanium Milling Strategies

The University Of Sheffield.

Thesis submitted to
The University of Sheffield
for the degree of
Doctor of Philosophy

Sam Turner

Advanced Manufacturing Research Centre
University of Sheffield

November 2008

ACKNOWLEDGMENTS

I would like to thank Professor Keith Ridgway for the opportunity to undertake this piece of work and his support throughout the last few years and without whom none of this would have been possible.
I would like to thank the many people at the AMRC who have supported me in numerous ways.
I would like to thank the Phantom Works team at The Boeing Company, St Louis for the opportunity to work with them and the focus on titanium machining. I would like to thank Dr Scott Smith and Dr Yusuf Altintas for their support and guidance and the opportunity to spend some time with their respective research groups.
I would also like to thank my family for their support and particularly Grace for her faith and patience and for keeping me sane throughout.

ABSTRACT

This thesis explores the subject of titanium milling and identifies the need for development of titanium milling strategies to address the key process limitations of chatter and tool wear. These subjects are typically studied in isolation and little work has previously been undertaken on titanium milling dynamics. Titanium is often perceived as difficult to machine as the very properties such as high strength at high temperature and low thermal conductivity that make it an attractive engineering material can cause rapid tool wear and limit process parameters. Titanium alloys are increasingly popular within the aerospace industry due to the high strength to weight ratios and titanium and carbon fibre composites have replaced many steel and aluminium components within aerostructures. Titanium is still seen by many as expensive to process and there is not the same degree of understanding and process optimisation within the machining industry as there is for aluminium and steel alloys.

The literature review considers both advances in titanium tool wear mechanisms and research into machining dynamics. From the literature review three research hypotheses are developed around the knowledge gaps pertaining to titanium milling stability and process optimisation. The limitations on milling performance and productivity are considered and three areas are identified where the research could be advanced to improve titanium milling productivity through manipulation of parameters and tool geometry, these areas are pocketing strategies, special tooling geometries and process damping.

A method for controlling radial immersion for pocketing strategies is developed and it is proven that through control of parameters and toolpaths that tool life and productivity can be optimised and controlled. A study is then undertaken into the performance and modelling of variable helix end mills to explore the hypothesis that the tools will outperform standard and variable pitch cutters and that the performance can be modelled. As part of the validation process an analysis of the linearity of machine tool dynamics is undertaken and it is demonstrated that under speed and load, spindle and machine tool frequency responses can differ from those measured in the static condition. The final part of the research investigates process damping performance and sensitivity to cutting tool geometry and feed rates. A method for evaluating process damping performance is developed and through optimisation of tool geometry and feed per tooth increases in productivity up to 17 fold are demonstrated. A method is then presented for tuning machine tool dynamics to optimise process damping performance and stabilise sub optimum tooling and machine tools.

The three core strands of the thesis are brought together and demonstrated in an aerospace case study. Through application of the techniques developed in the thesis a titanium aerostructural component is machined at the same rates as an equivalent steel component and at less than 50% of the planned titanium milling process time.

TABLE OF CONTENTS

FIGURES

TABLES

NOMENCLATURE

a_e – *Radial depth of cut (mm)*
a_{emax} – *Maximum radial depth of cut in trochoidal toolpath*
aT – Time delay for first pitch angle
a_{xx} *-Directional dynamic coefficient (x) direction*
a_{xy} – *Directional dynamic cross coefficient (xy) direction*
a_{yx} – *Directional dynamic cross coefficient (yx) direction*
a_{yy} – *Directional dynamic coefficient (y) direction*
b – Length of chip (axial depth of cut) (mm)
b_{lim} *- limiting depth of cut for stability (mm)*
$b_{limcrit}$ *-critical limit of stability (mm)*
b_m = *Average pitch for engaged flute length*
bT – Time delay for second pitch angle
f_c – *Chatter frequency (Hz)*
f_n – *Natural frequency (Hz)*
fr – Table feed rate (mm/min)
f_t – *Feed rate per tooth (mm)*
j – tooth number
k – Constant relating to Taylor's tool life equation
k_c – *static stiffness*
k_w – *thermal conductivity*
k_{wc}– *thermal conductivity of tungsten carbide*
k_{wt} – *thermal conductivity of titanium*
$g(\phi j)$ *- Step function to determine whether tooth is in cut*
h – Chip thickness (mm)
l – tooth pitch
l_a – *First pitch angle*
l_b – *Second pitch angle*
m – Number of teeth
m_{avg} – *average number of teeth engaged in cut n – Spindle speed (rpm)*
q_c*- Average heat flux entering the tool from tool chip interface*
q_{cLy}*- Average heat flux calculated for full flute engagement(Ly)*
q_{cLyt}*- Average heat flux for instantaneous engagement considering helix (Lyt)*
r – ratio of ω/ω_n
r_1 – *constant relating force to variation in chip thickness*
r_c – *Coupling coefficient*
s – Constant
t – Time (s)
tpf – Tooth passing frequency (Hz)
vj - Dynamic displacement of present tooth
vj_{-1} *- Dynamic displacement of previous tooth*
ω – *excitation frequency (radians)*
w_c – *Chatter frequency (radians)*
ω_n*- natural frequency (radians)*
(x) – Feed direction
x_p – *surface position on heat source*
x_t *- Empirical constant for Palmai's tool life equation*

(y) – Normal direction
y_p- surface position on heat source
z – depth of thermal field normal to plane x,y
A – Tool position at peak of vibration wave
[A] - Matrix of time varying periodic directional coefficients
$[A_0]$ – Average matrix of time varying coefficients periodic directional
$[A_\rho]$ – Average matrix of time varying coefficients for harmonic ρ
$[A_{\rho j}]$ – Average matrix of time varying coefficients for harmonic ρ, tooth j
$A(\phi_t)$ - Average transfer function
Am – Start point of elliptical vibration path
B- Tool position at downwards mid-point of vibration wave
Bm- Mid point of elliptical vibration path
BUE- Built Up Edge
C – Tool position at trough of vibration wave
CMM – Coordinate measuring Machine
C_t – Empirical constant for Palmai's tool life equation
D – Cutter diameter (mm)
DCFC-Dynamic Cutting Force Coefficients
DD- Tool position at upward midpoint of vibration wave
Dt- Characteristic dimension for the penetration of the temperature field
E- Regenerative delay term
FEM – Finite Element Modelling
FFT – Fast Fourier Transform
F_n – Resultant cutting force (N)
F_v – variable component of cutting force (N)
F_r – Radial cutting force (N)
F_{rj} – Radial cutting force for tooth j (N)
FRF- Frequency Response Function
F_t – Tangential cutting force (N)
F_{tj} – Tangential cutting force for tooth j (N)
F_x – Force in feed direction (N)
$\overline{F_x}$ - Average x direction cutting force
$\overline{F_{xc}}$ - x direction component of shearing force
$\overline{F_{xe}}$ - x direction component of edge force
F_y – Force in normal direction (N)
$\overline{F_y}$ - Average y direction cutting force
$\overline{F_{yc}}$ - y direction component of shearing force
$\overline{F_{ye}}$ - x direction component of edge force
$\overline{F_z}$ - Average z direction cutting force
$\overline{F_{zc}}$ - y direction component of shearing force
$\overline{F_{ze}}$ - x direction component of edge force
G- Gradient of cutting force coefficient curve
$G_{ij}(w)$ – Calculated cross transfer function at i and j
$G_{(w)}$ Transfer function of system
$H_{ij}(w)$ – Measured transfer function at i and j

Hex – Maximum chip thickness
I- Radial immersion
ImK_{ij} - Imaginary part of cutting force coefficient
Im[G] – Imaginary part of transfer function
Im[G]min- minimum point of imaginary part of transfer function
K_{ac} – Axial cutting force coefficient for shearing force
K_{ae} – Axial cutting force coefficient for edge effect
K_{di} - Cutting force coefficient for inner modulation in normal direction
K_{do} - Cutting force coefficient for outer modulation in normal direction
K_{ci}- Cutting force coefficient for inner modulation in tangential direction
K_{co} - Cutting force coefficient for outer modulation in tangential direction
K_{ij} - Cutting force coefficient with real and imaginary parts
K_r – Radial cutting force coefficient
K_{rc} – Radial cutting force coefficient for shearing force
K_{re} – Radial cutting force coefficient for edge effect
K_R -the ratio between the radial and tangential coefficients
K_s – Cutting stiffness (average cutting force coefficient)
K_t – Tangential cutting force coefficient
K_{tc} – Tangential cutting force coefficient for shearing force
K_{te} – Tangential cutting force coefficient for edge effect
L- length of uniform line heat source
L_x - Dimension x of heat source (mm)
L_y - Dimension y of heat source (mm)
L_{yt} – Total length of flute engaged in cut
M – Modal mass (kg)
MRR – Metal removal rate (mm^3/min)
N – Integer (lobe number)
N_c- Number of cycles in temperature computation
OTF- Oriented Transfer Function
P – Power consumed in cut
Q – Source of heat flux
R1 – Directional factor for first pitch angle
R2 – Directional factor for second pitch angle
ReK_{ij} - Real part of cutting force coefficient
Re[G] – Real part of transfer function
Re[G]max- maximum point of real part of transfer function
Re[G]min - minimum point of real part of transfer function
S – Cycle period for one revolution of a trochoidal pass
T - Time delay between teeth due to spindle rotation
T_l – Tool life (mins)
T_{AVE}- Average temperature over the heat
T_{emp} – Temperature (°C)
T_j - Time delay between tooth j and previous tooth
T_M- Max temperature
Vs – Surface speed (m/min)
Y_0 – surface position from previous tooth pass
Y_1 – surface position generated by tooth pass

α_1 – *Rake angle of tool*
α_2 – *Effective rake angle of tool*
α_s – *specific heat*
α_{xx} – *Integrated directional coefficient (x) direction*
α_{xy} – *Integrated directional cross coefficient (xy) direction*
α_{yy} – *Integrated directional coefficient (y) direction*
α_{yx} – *Integrated directional cross coefficient (yx) direction*
β- *Chatter vibration wavelength*
β_0 _ *Wavelength for initial condition*
β_j _ *Wavelength for between tooth j and its predecessor*
χ - *Angle of engagement of cutter*
δ – shear angle
ε - *Phase (radians)*
ϕ - *Helix angle of tool*
ϕj – *angular position of tooth*
ϕ_{pj} _ *Pitch angle of tooth j*
ϕ_{st} - *Start immersion angle of cut*
ϕ_{ex} - *Exit immersion angle of cut* γ_n – *relief angle of tool*
γ_{min} – *Minimum effective relief angle of tool*
γ_{max}- *Maximum effective relief angle of tool*
η – *Relative vibration between tool and workpiece (x,y)*
η_0 –*Vibration between tool and workpiece from previous tooth(x,y)*
$\eta_{(t)}$ – *Relative vibration between tool and workpiece at time t (x,y)*
$\eta_{(t-T)}$ – *Relative vibration between tool and workpiece at time t-T(x,y)*
ι – *relative vibration between tooth j and previous tooth*
κ- *Ratio of* Λ_I/Λ_R
λ – *Vibration wavelength (mm)*
λc – *Critical process damping wavelength*
μ – *directional coefficient for transfer function*
ρ – *Harmonics of dominant vibration frequency*
τ - *point in time*
τ_1 – *Time period that tooth is in cut*
τ_2 – *Time period that tooth is in cut*
ψ- *Phase shift of eigenvalue*
ζ – *damping ratio*
Δ - *phase variation*
$\Delta(t)$ - Δx, Δy *as a function of time t*
Δx- *change in x position of tooth between current and previous pass*
Δy- *change in y position of tooth between current and previous pass*
$\Phi_{(w)}$- *Transfer function of system*
$\Phi_{xx(w)}$- *Transfer function of system in (x) direction*
$\Phi_{xy(w)}$- *Cross transfer function of system in (xy) direction*
$\Phi_{yx(w)}$- *Cross transfer function of system in (yx) direction*
$\Phi_{yy(w)}$- *Transfer function of systemin (y) direction*
$\Phi_{0(w)}$- *Oriented transfer function of system*
Λ- *Eigenvalue*
Λ_R – *Real part of eigenvalue*
Λ_I – *Imaginary part of eigenvalue*

1 INTRODUCTION

1.1 Background

1.1.1 Challenges of Titanium Milling

Within the last decade there has been a steady increase in the use of titanium components within the aerospace industry. The advent of composites on commercial aircraft has further increased titanium usage as its traditional alternative aluminium reacts with carbon based composites and has too high a differential in thermal properties. Titanium has often been termed a difficult to cut material [1], [2], [3] and with its continued increase in application, machining strategies are sought where titanium parts can be produced cost effectively. Much work has been carried out in defining high speed machining strategies for aluminium and steels which aid design engineers, programmers and machine operators in selecting an optimum process or troubleshooting existing problems [4] [5]. Guidelines have been well established and software is commercially available for this purpose. A greater understanding of the titanium milling process has been sought through industry and academia and has not yet been achieved to the levels of aluminium or steel milling. Within the first two chapters of this thesis it is suggested that to develop optimised strategies for titanium milling it is necessary to first understand the critical path limitations on any process. Titanium is perceived as difficult to machine due to excessive tool wear at high speeds. The very properties that make titanium alloys a popular engineering solution for high temperature high strength performance contribute to making it difficult to machine. Poor thermal conductivity, high strength at temperature and chemical reactivity with tool steels and coatings all mean that under typical milling conditions high localised temperatures occur which can lead to excessive wear of cutting tools or chemical dissolution. The mechanisms and causes of wear are studied in detail in the first part of chapter 2 and it is concluded that it is difficult to consider titanium milling without understanding the influence of cutting parameters on the wear mechanisms and understanding the limitations that this in turn puts on the machining process. A further critical path limitation on titanium milling is chatter. Chatter in titanium milling is a problem due to relatively high cutting force coefficients and limitations on surface speed that mean that traditional techniques for stabilising chatter cannot easily be applied. There has been extensive research on chatter and high speed machining

dynamics. Research was pioneered by Tlusty and Tobias in the 1960's and Tlusty went on to establish stability lobe theory where pockets of stable machining exist throughout the spindle speed range [6], [7]. The stable pockets are at their greatest at high speeds when the tooth passing frequency is equal to the dominant natural frequency of the system. A stable region exists for tooth passing frequencies at every harmonic of the dominant frequency although the pockets become smaller in depth and width as a small change in rpm results in a large change in chatter phase and they become more closely packed together (chapter 2). This results in stability lobes being of no practical use in the regions where titanium milling typically occurs. A milling strategy is therefore required that addresses the issues of tool life and chatter.

Many of the dominant factors restricting machining optimisation are interrelated and it is difficult to study one in detail without some knowledge of the others.

Great advancements have been made in machine tool technology with spindle speeds and feed rates increasing. This is a vast science in itself and will not be studied in detail here, although machine tool stability plays an important role in controlling chatter in the machining process. Some of the advancements in machine tool technology can either inhibit performance for titanium machining or complicate the process by which chatter is controlled.

Part integrity and tolerance can be a limitation on any machining process. Within the aerospace industry tight tolerances are often set that push the boundaries of machine tool and measurement control. Cutting parameters and strategies can influence part tolerance due to cutter push off and surface finish. Surface integrity can be influenced as a result of introduction of poor or aggressive parameters and this often leads to reluctance to accept new techniques or technologies. Specifically within the aerospace industry where parameters are often locked into long build programs, there is little opportunity to further optimise for fear of damaging the integrity of a component. Surface integrity will not be covered in detail but is always considered when proposing and validating new parameters and techniques as this is a fundamental requirement within the aerospace industry. Fig1.1 shows a mindmap of the research problem, considering the factors that limit titanium milling performance.

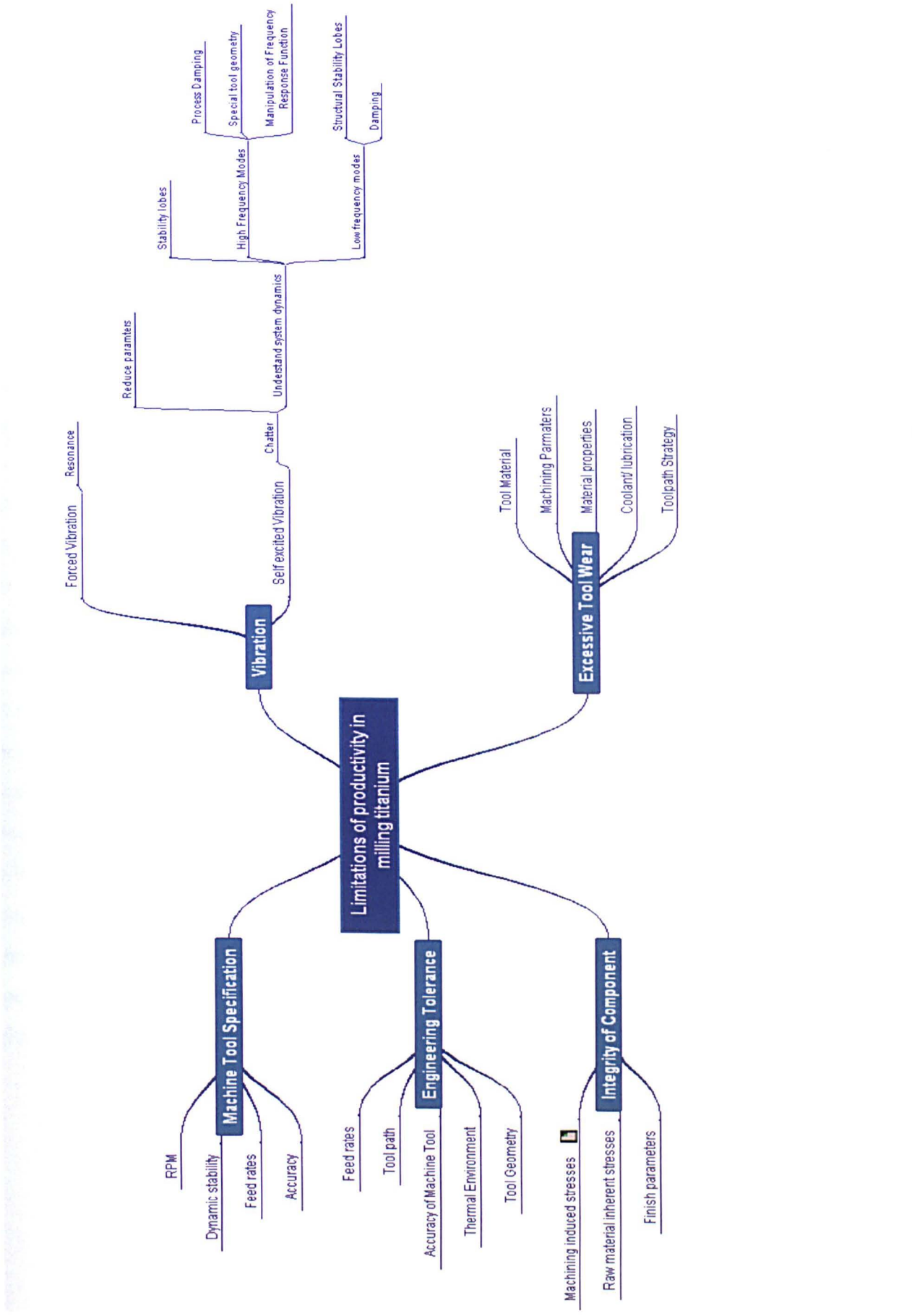

Fig1.1 Mindmap of Research Problem Scoping

In the specific case of titanium machining there has been a huge amount of work focussed on prolonging tool life. Titanium is perceived as 'difficult to cut' due to excessive tool wear and consequently high spindle speeds are typically unattainable. Advancements have been made in cutter material grades and coatings, coolant application, understanding of the chip formation process and tooling geometries. This is a vast topic and is fundamental to any understanding of the titanium milling process. A review of research will therefore be carried out in this thesis as tool life limitations have a major impact on the control of chatter within the machining process. Tool wear in titanium milling will most likely remain the principle challenge to overcome for the machining community, if all the other factors listed above are optimised, it is excessive tool wear as a result of the inherent material properties that will prevent titanium from being machined at the rates of lighter alloys such as aluminium.

A significant part of this work will focus on the development of machining strategies to limit tool wear and chatter. This work will be supported by research to further the understanding of the influence of cutting parameters and tooling geometry on tool wear in titanium machining.

It is the author's experience that the limitation of a titanium milling operation is often not the result of insufficient machine tool specification, excessive tool wear or an inability to produce components to specification. Although all of these issues have been discussed above it is common to find that chatter inhibits performance well within the boundaries of machine tool and cutting tool capability. Understanding and controlling chatter with regards to titanium machining will be the main focus of this thesis. The aim is to control chatter to the extent that cutting tool and machine tool technologies become the critical path limitation on titanium milling processes so that chatter does not limit performance.

1.2 Research Strategy

This thesis furthers the current field of research by seeking a comprehensive solution to the challenges presented by titanium machining. Through the course of this thesis a suite of solutions are developed, through experimental and theoretical techniques, to overcome the issues outlined in the previous section, these are then demonstrated on a typical aerospace component.

The research is unique in providing strategies that consider both the effects of tool wear and vibration. The two have been studied in isolation but as explained in the next chapter they strongly influence one another and should not be considered in isolation. The restrictions of tool wear have a major impact on the spindle speed range and the dynamics encountered during titanium milling and the introduction of chatter, particularly through tool path selection, have a significant impact on tool life.

Research in the field of machining dynamics has been largely focussed on high speed machining and there has been little research in the field of low speed machining dynamics applicable to titanium machining largely due to non-linearities in the process. Further understanding is required in this field and this thesis makes a contribution to the development of machining dynamics for low speed/titanium machining. Due to the restrictions on surface speed and the propensity to chatter, three key areas have been identified that can be combined to create a coherent strategy for titanium milling.

The thesis adds to the current state of knowledge by:

- Developing a toolpath strategy to minimise tool wear and chatter during titanium pocketing and optimise productivity.
- Evaluating and modelling the performance of variable helix end mills.
- Exploring the factors that influence the process damping phenomena and developing practical techniques to employ process damping and optimise cutting performance.

1.3 Research Methodology

The thesis begins in ***Chapter 2*** with a summary of the state of current research in the field of titanium machining and machining dynamics. A review is developed into three research hypotheses which are:

1 Tool life and chatter in titanium milling can be controlled through effective toolpath selection
2 Variable helix end mills can provide enhanced stability and productivity and can be modelled using a frequency domain solution
3 Process damping can be controlled and utilised to optimise milling stability through control of cutting parameters, tool geometry and tool set-up

These hypotheses are then explored in ***Chapters 3,4 &5***.
In ***Chapter 3*** a study is undertaken to examine the influence of toolpath on tool life when milling square pockets in titanium. The increased radial immersion when milling into a corner typically causes detrimental tool life and chatter. Tool path strategies are proposed to overcome this problem and each strategy is demonstrated and evaluated. The toolwear is measured after the completion of each pocket and charted against a benchmark 'standard' pocketing routine. The influence on stability of the toolpaths is also demonstrated. These toolpaths are then applied to a range of typical aerospace pocket geometries in a study sponsored by Sandvik Coromant. The results of this study were used to create the Sandvik Coromant Best Practice Guide for titanium milling [8].
In ***Chapter 4*** an analytical model is developed to predict the stability of variable helix end mills. This is compared against an established time domain model and experimental results. Research into tools with non-uniform pitch has been published in the past, demonstrating improved stability particularly in low speed regions where traditional stability lobes cannot be reached.
A detailed experimental procedure is outlined for the plotting of empirical stability lobes. The empirical study in Chapter 4 compares variable helix tools with equivalent

variable pitch tools with uniform helix, providing for the first time a clear comparison of the performance of the two types of tools.

In ***Chapter 5*** a technique is developed for characterising the process damping performance of an end mill. This technique is used to explore the influence of feed rate, rake angle and relief angle on process damping and performance. The study offers an insight into the mechanism of process damping and a theory is proposed as to the influence of process damping on the stability boundary, encouraging further work in this area. The results are then used to demonstrate how cutting parameters can be optimised through attenuation of dominant machine and toolholder parameters to eliminate chatter as a critical constraint during semi-finishing operations in titanium.

A case study is carried out in ***Chapter 6*** where the three hypotheses are brought together to demonstrate productivity savings on an aerospace component in a production environment.

The findings of the research are discussed and the conclusion to the thesis is presented in ***Chapter 7***. The flow of the thesis is outlined in Fig.1.1.

The following publications have emanated from the research described in this thesis:

1. 'Modelling of the stability of variable helix end mills' Turner, Merdol, Altintas, Ridgway, International Journal of Machine Tools and Manufacture 2007.
2. 'Modelling of the stability of variable helix end mills' Turner, Merdol, Altintas, Ridgway, Proceedings of CIRP 2nd International conference on High Performance Machining 2006.

The research has also contributed to the section on pocketing strategies in:

1 Application Guide, Titanium Machining, Sandvik Coromant 2004.12.

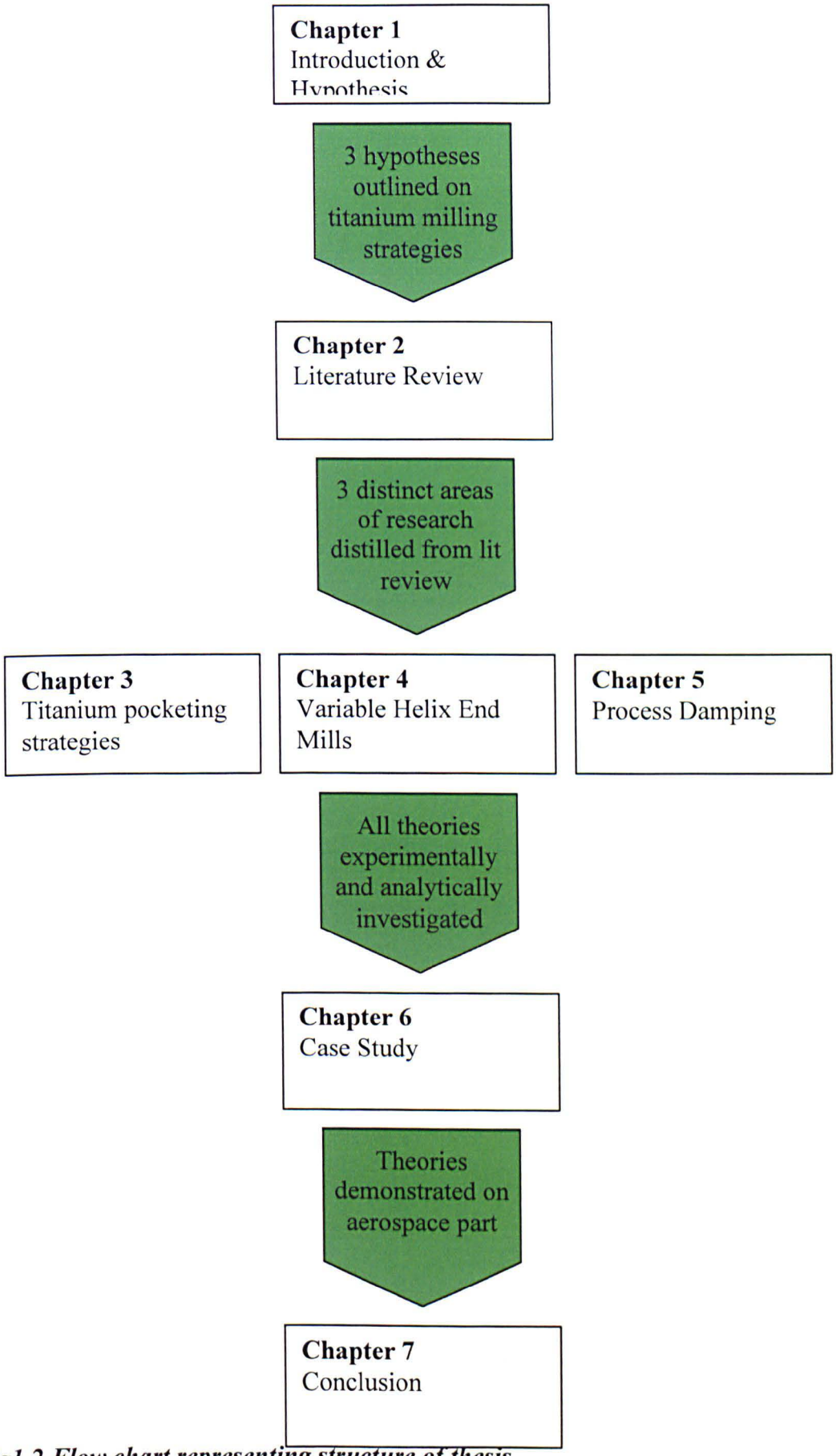

Fig1.2 Flow chart representing structure of thesis.

2 LITERATURE REVIEW

2.1 Introduction

This chapter summarises the state of current research in the fields of tool wear in titanium milling and dynamics of the milling process. Each of these subjects is explored in some detail and they are then brought together in a review, identifying gaps in the current research and combining the two fields. The review is developed into an argument that the two fields should not always be considered in isolation and that there is a need for a coherent strategy for approaching titanium milling applications. The strategy is defined as a critical constraint analysis and some of the most common critical path constraints on the titanium milling process are identified. These constraints are focussed on three problem areas from which the research hypotheses are developed.

2.2 Tool Wear in Milling

2.2.1 Wear Mechanisms

The dominant wear mechanisms in titanium machining are as follows; adhesive, attrition, abrasive, oxidation and adhesion, fracture and chipping, diffusion, super-plastic deformation, plastic deformation, fatigue cracking. At low speed the tool wear mechanisms are largely mechanical with little thermal effect.

Adhesive wear is when a bond occurs between the clean tool and clean cut workpiece surface due to micro-welding (Wright & Bagchi [9]), generating a Built Up Edge (BUE). If the bond is greater than the local tool strength particles are removed upon exit from the cut with the chip [10]. Venuvinod [11] noted that adhesive wear was influenced by hardness.

Abrasive wear is due to hard inclusions in the material which score the surface of the cutting tool, removing material through sliding wear [9]. Abrasive wear is greater with hard metals and at higher speeds the tool softens due to thermal effects and abrasive wear increases.

As speeds increase then thermo-mechanical wear mechanisms take hold; attrition, fracture & chipping, superficial plastic deformation, plastic deformation and fatigue cracking.

Attrition wear starts with particles being plucked away from the surface, often due to adhesion. The void left by the particles creates a stress differential and cracks initiate along grain boundaries resulting in lumps being plucked off as cracks propagate

(Bhattacharyya [12] and Shaw [10]). Dearnley & Grearson [13] noted that the rate of wear related to the grain size of the carbide with the wear rate increasing with the grain size.

Fracture and chipping occurs due to high stresses during cutting or sudden unloading. This is common for tool materials such as carbide that retain their hardness at elevated temperatures. When compressive stress becomes higher than hot compressive strength, cracks and edge rounding occur leading to fracture and breaking of particles. This is common for carbides as they begin to lose strength above 1100°C. High Speeds Steels have higher transverse rupture strength than carbides and are less prone to fracture, making them popular with many titanium machining houses. Hoshi & Okushima [14] noted that sudden unloading after cutting strong materials at high speeds and feeds led to fracture. Fracture is also common in carbides experiencing severe loads through chatter.

Superficial plastic deformation is when the tool surface sees high shear stresses and is dragged away with the chip. This is common with High Speed Steels (HSS) but not carbide [15].

Plastic deformation changes the form of the tool due to large normal stresses on the cutting edge at high temperature [12]. Zarev [16] noted that the stress is extremely high at the edge and decreases exponentially with distance along the rake face. When the normal stress on the edge becomes greater than the elevated compressive strength then the tool edge fails through plastic collapse or chipping.

Plastic collapse is common in HSS tools where the edge becomes rounded with a negative rake angle resulting in high temperature and force, higher deflection and failure.

Fatigue cracking is initiated by thermal stresses. Fatigue cracking is common at high speeds with intermittent cutting and high normal stresses. Chandrasekara [17] found that all cemented carbides crack due to ***thermal fatigue***.

The dominant thermal wear mechanism is ***diffusion*** through ***dissolution*** of tool particles into the chip. Wright & Trent [18] noted that atoms from the tool are taken away with the chip and this is due to the solubility of the tool material in the workpiece. This is particularly a problem with carbides and certain coatings. Kramer [19] noted that a layer of TiC forms on the tool and acts as a barrier to diffusion wear but the layer is then removed by the chip (diffusion limited wear). For very high speeds the layer remains in equilibrium and steady state diffusion exits. Kramer [20]

believed that diffusion and diffusion limited wear were related to continuous and segmented chips.

2.2.2 Tool Failure modes

Crater wear develops on the rake face and is dependent upon tool/workpiece combinations and cutting speeds. Wright and Bagchi [9] observed that crater wear was related to diffusion and plastic deformation and therefore the chemical stability of the tool is important to restrict crater wear. Abrasive wear can become dominant after diffusion has weakened the surface and Wright & Bagchi [15] showed score marks on the rake surface indicating abrasion. Rake wear occurs next to the tool tip and can accelerate flank and edge wear.

Notching can occur at both ends of the cut engagement and is believed to be caused by oxidation as the notch area is hot but not protected from the atmosphere [21]. Shaw [10] found that for nickel alloys the temperature at the edge of the chip was higher than in the middle as the material at the edge is sheared twice. Dearnley & Grearson [13] noted that the notch wear due to oxidation grows with feed and a low approach angle. Tonshoff & Bartsch [22] also showed that notch wear depended upon entry angle. Dearnley & Grearson [13] claimed that cracking and chipping occurred due to the stick/slip of the segmented chip fretting the edge of the tool.

Flank wear is the most common wear mechanism at low surface speeds with rake wear being prevalent at high speeds [23]. Flank wear is largely a mechanical process and not influenced by coatings, attrition wear being dominant for titanium [13]. The form of the wear relates to the hardness of the carbide with rough wear due to brittle fracture for hard carbides and smooth wear due to edge rounding for softer grades. Flank wear results in edge rounding which in turn creates rubbing of the flank face and accelerates the wear process. Flank wear is dominant in milling whilst crater wear on the rake face is thermally activated and more common in turning.

Merchant [24]observed ***edge chipping*** during rapid unloading and thermal cycling of the tool. Albati [25] claimed that edge chipping sometimes occurred due to defects in the tool. Trent and Wright [26] observed that edge chipping was caused by high temperatures and thermal / mechanical cyclic stresses and adhesion of the chip. Initial flank wear can weaken the edge and enhance chipping especially in the case of high hardness tools as mentioned above. Cobalt lends ductility to the cutting tool and low

cobalt content increases the risk of edge chipping. Attrition and fatigue resulting in edge chipping are the dominant wear mechanisms in low speed titanium milling.

Factors Influencing Tool Wear

Climb milling was found to reduce wear due to BUE in titanium milling [27], due to a reduction in the shock loading on exit that would break away the BUE and tool particles when conventional milling. Eckstein [28] also noted that conventional milling causes high tensile stress on exit. For these reasons climb milling is adopted where possible in titanium milling operations.

Dearnley & Grearson [13]found that coatings were quickly removed from carbides via attrition wear for high feeds and by smooth wear for lower speeds. 'Quick-stop' tests showed that the tools fractured such that the cutting edge remained bonded to the chip, showing that titanium will stick to the tool material. Small grain carbides are suggested as having superior attrition wear to other carbides. Smooth wear is dependant upon the solubility of the tool material in the work piece. The high temperature and intimate contact between tool and work piece provide an ideal environment for diffusion of tool material.

Elbestawi [29]carried out cutting tests with Through Spindle Coolant (TSC) on carbide tools and studied the effect on tool-life. It was noted that tool life for full and quarter immersion was double that of half and three quarter immersion. This was believed to be due to the mechanical shock experienced during entry to the cut. When a full slot is made the cutter will deflect away from the direction of feed and the balance of forces will maintain the cutter in its programmed location between the two walls. When the cutter is experiencing less than full immersion the cutter will deflect away from the cut for climb milling at an angle dependant upon the radial immersion, the impact experienced as the cutter first makes contact with the material causes mechanical shocking in the tool. For cuts less than half immersion the effect is reduced due to the decrease in force. This is an important factor when selecting roughing parameters for titanium.

2.2.3 Titanium and its alloys

Tool life is a critical factor in machining of titanium. Although in many cases the cost of the tools is not of major concern, in relation to the overall cost of the part, there comes a point where tool wear is prohibitive. Also tool changes mid-way through a

process can be problematic and time consuming. Pure titanium changes from Close Packed Hexagonal (CPH) alpha phase to Body Centred Cubic (BCC) Beta phase at 882°C and titanium alloys become increasingly difficult to machine with increase in Beta content. Trigger [30], Zlatin & Field [2] and Trent & Wright [26] have all observed higher temperatures with an increase in the higher strength Beta content. Alloy elements are used to stabilise the alpha or beta phase. The alloys focussed on within this thesis are Ti 6Al 4V and Ti 5Al 5V 5Mo 3Cr, both of which are now prevalent within the aerospace industry. Ti6Al4V is the most commonly used alloy within the aerospace industry and is an alpha-beta phase alloy. Ti5Al5V5Mo3Cr contains beta stabilising elements and is used in high strength applications such as landing gear.

2.2.4 Titanium Tool Wear

Tool wear in titanium machining has often been seen as a limitation on productivity and much research has focussed on this area. A number of factors result in titanium having poor tool life relative to steels and other aerospace alloys and the models used to predict the chip generation become more complex due to segmented chip formation. Many models such as Shaw's partition model [31] focus solely on continuous chip generation. Komanduri [32, 33] stated that the friction effect at the tool chip and tool flank were opposite to that of continuous chip formation. Titanium has high temperature strength, low thermal conductivity, low modulus of elasticity and high chemical reactivity, many of these properties make it attractive in its final application but make it difficult to machine. Due to the low thermal conductivity Konig [3] claimed that 80% of the shear deformation heat was transferred to the tool, compared to only 50% for most steels. As a result of these characteristics some believe that machining of Ti and its alloys would always be a problem no matter what techniques are employed [27].

Titanium is hard to machine because;

1 High strength at high temperature opposes plastic deformation required to form the chip.
2 Thin chip results in small contact area causing high stresses on the tool.

3 High coefficient of friction between chip and tool.

4 Strong chemical reactivity with tool steels, diffusion wear.

5 The low specific heat and small contact area lead to v. high temps up to 1100C. (Siekmann, [27], Ashiura et al. [34]).

6 Built Up Edge (BUE) at low cutting speeds gives poor surface finish Komanduri [32].

7 Low modulus of Elasticity can lead to deflection and rubbing; (Siekemann [27], Konig [3]).

8 Some work hardening occurs during machining. This can cause problems with subsequent cuts.

Tool wear in titanium milling can be broadly broken down into thermally activated, mechanical and thermo-mechanical causes. A large amount of work has focussed on understanding the thermal effects of titanium milling and this will now be explored in more detail after which chip generation in titanium milling is considered.

Temperature

Peak temperature in titanium machining is closely related to the time that the cutter is engaged in the cut. Milling is an interrupted process unlike turning, with the cutting tooth engaging and exiting the cut with each cycle such that the cutting edge experiences a heating then cooling process, creating stress conditions on the tool. Tlusty[35] in a study on thermal cycles in High Speed Machining (HSM) observed that the tool quickly cooled to ambient when out of contact and that the period of cooling had little impact on temperature or wear, however maximum stresses were observed when the tool was cooling and therefore the number of thermal cycles has a significant impact. Maekawa [36] and Palmai [37] all demonstrated that the heating cycle was more influential than the cooling cycle and that time engaged in the cut influences maximum temperature. Salomon [38]claimed that beyond a certain surface speed, named 'the valley of death', chip mechanics altered and tool wear improved as surface speed increased. No data was available to substantiate these claims but this formed a foundation for high speed machining development and has been further explored by Palmai. Harting & Kramer [39] and Zlatin & Field [2], found that the rate of temperature increase was high at low speeds and reduced towards the melting point. Smart & Trent [40], Trent [26] and Konig [3] found that the maximum temp

and the heat affected zone in the cutting tool , power and stresses were much greater than when machining steels, iron or copper and that the maximum temperature occurred close to the tool tip. Jensen [41] believed the higher temperatures to be due to increase in frictional heat, Chao and Trigger [42] suggested the higher temps were due to a decrease in chip contact area with the tool. At higher speeds there is an increase in thermal softening and localised shear which reduces the thickness of the flow zone and increases temperature. Zlatin & Field [2] found the cutting forces when milling titanium were equivalent to those of steel but the chip contact area was 3.5 times smaller, hence stresses are much higher and can cause cracking on the rake face. Stephenson [43] developed a model to predict cutting edge temperature for intermittent cutting which showed that a peak temperature was reached during each tooth engagement followed by a subsequent cooling cycle to a steady state temperature.

Surface speed and radial depth of cut appear to have the strongest influence on peak temperature. The influence of other parameters on peak temperature have also been investigated, Vaughn and Quakenbush [44] found that flank wear did not vary significantly with feed per tooth and Jensen [41] saw little change in peak temperature with increased chip thickness. Tyler [45] stated that by removing the surface layer of the work piece with slight depths of cut the heated zone is removed. The greater the proportional surface area, the lower the energy density and therefore heat generation is reduced.

Shorter contact time will lead to lower heat generation and reduce the level of thermal wear. By altering the helix angle to minimise the contact of the cutting edge, contact time is also reduced and tool life is again improved as demonstrated by Maekawa et al. [36]. As the heat cannot be dissipated through the tool due to the low contact time, the localised heat in the chip reaches high temperatures. There is then a danger of the chip welding to the tool. In this situation increasing the volume of the chip will decrease the average temperature. The contact time can be reduced through reducing the radial immersion and this requires a modification of milling strategy.

Chip Mechanics

Some of the difficulties that arise when machining titanium can be better understood through an exploration of the chip mechanics. The chip mechanics, particularly the formation of a segmented chip, of titanium machining can contribute to the high

temperatures discussed above. Understanding ductility in the chips is important for an understanding of the chip curl and evacuation and surface finish. The bend strength offers an important clue to the mechanism of the chip formation [33]. Cook [46]noted that titanium chips are brittle and discontinuous, a sign of poor ductility.
Titanium chips have low bend strength as the segments constituting the chip are held together by highly localised intense shear bands. When bent, the chips will break at these junctions.

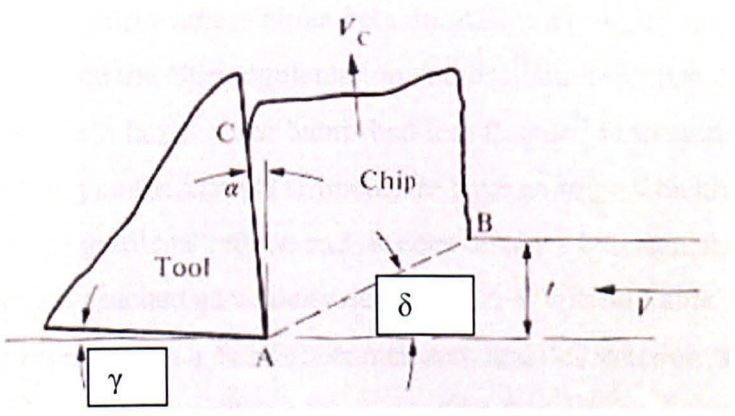

Fig 2.1 Orthogonal Plot of Chip Formation [10]
α_1 = rake angle, γ= relief angle, δ= shear angle

Titanium does not form a continuous chip and this is used as a defining factor for difficult to machine materials such as some nickel alloys. Periodic gross inhomogeneous deformation occurs in primary zone causing intense strain localisation.
Browne & Hinds [47] suggested that the oscillating force from chip segmentation may lead to fatigue type failure of the cutting edge. Loladze [48] found that shear stress decreased as rake angle increased. There are 4 recognised types of chip formation (Ernst [49], Merchant [50]) of which segmented chip is one. Segmented chip formation in titanium occurs as the shear to form the chip occurs on a particular shear plane. When the stress built up by relative tool motion exceeds the yield strength of the material the slip occurs. The energy associated with this deformation is converted immediately into thermal energy and because of titanium's poor thermal properties large temperature rises occur. This in turn causes temperature softening locally and thus the strain continues in the same plane instead of moving to a new plane in the colder material. As the deformation proceeds, the deforming shear plane rotates, thus

becoming larger until the increased force due to this rotation exceeds the force needed to plastically deform colder material on a more favourable plane. This process is referred to as 'adiabatic shear' Von Turkovitch [51]and results in cyclic process producing a saw tooth chip formation.

The initial contact on the chip face is very small and the contact length increases as the flattening of the wedge shaped work material ahead of the tool progresses.

The small contact area at the start of this process leads to the high pressures.

Chip formation varies with alloy content; alpha alloys do not form conspicuous serrated chip whereas alpha-beta do. Ashiura [34] found that alloying elements influenced the chip segmentation and oscillation frequencies. He found that alpha alloys with larger shear bands had less fluctuation in cutting force.

Cutting parameters and temperature have an impact on chip formation. At low speeds thermal gradients reduce and so does distance between shear bands. A critical cutting speed is reached as velocity decreases to a 'critical value' whereby the distance between the shear bands becomes zero and deformation becomes uniform. The critical cutting speed decreases with increasing feed rate as the temperature increases.

The thickness of segments decreases with a decrease in both depth of cut and rake angle [52].The critical cutting speed is based upon a purely thermally activated process and this may be unreliable.

The cyclic force is believed to enhance certain wear mechanisms. Some have claimed that the cyclic force can initiate chatter [34], the actual source of chatter will be covered in chapter 3.

2.2.5 Influence of parameters

Tool Material:

Tool materials for titanium milling require low chemical reactivity, high hot hardness for stresses, good thermal conductivity, toughness, fatigue resistance and high compressive, tensile and shear strength.

No material has the perfect combination but some advances in tool material technology are more applicable than others. Coated carbides, ceramics, cubic boron nitride (CBN), & polycrystalline diamond (PCD) are good for nickel alloys, cast irons and steels but not so applicable to titanium. CBN and ceramics are found to be ineffective due to chemical reactivity with titanium, Hartung & Kramer [39] found

aluminium, nitrogen and oxygen had high solubility in titanium. CBN and ceramics also have high hardness and are therefore too brittle for the cyclic loading in titanium milling. Dearnley [13] found CBN and polycrystalline diamond to show good performance but they are very costly. Interstitial impurity elements; carbon, nitrogen and oxygen have detrimental effect on machinability.

The most common tool materials used for titanium milling are cemented carbides and high cobalt High Speed Steels.

i) *High Speed Steel (HSS)* tools can be recommended for intermittent cuts [53], or cuts where high deflection may be experienced as the mechanical shocking can chip carbides. HSS is found to be better than carbide at low speeds where max temperatures are below 600°C, above which temperature the HSS starts to soften, Edwards [54]. HSS tools are particularly popular in the USA where low surface speeds allow large MRR through process damping (chapter 5).

ii) *Tungsten carbides* have been found to have good hot compressive strength and to resist plastic deformation. The properties depend upon the cobalt content. Konig [3] found that high cobalt content performed better at low speeds and low cobalt content for high speeds. Cobalt increases toughness but reduces hardness. Most carbides perform better at high temperatures above 500°C in the 'tough zone'.

For the majority of applications coated cemented carbides showed greater wear rates than straight cemented carbides Hartung[39], Katayama, [55].

Zlatin & Field [2] found that the surface speed could be increased from 55ft/min to 150ft/min for a 30 minute tool life using carbides as compared with HSS.

Tool Geometry

i) *Rake Angle*

A highly positive rake angle results in lower strain than a negative rake angle and therefore lower feed force and temperature [15]. Very low strain can lead to a continuous chip formation thereby reducing temperature and stress and the heat affected zone (HAZ) moves away from the cutting edge reducing the risk of fracture. There is a danger that a highly positive rake and relief angle will weaken the edge increasing the risk of fracture and in some cases the flank face can be directly heated due to the thin edge. Positive rake angles up to 23° have been found to be good for milling, whilst low positive and negative rake angles can be better for turning as they

prevent heat transfer to the flank and strengthen the edge [3], [56]. The smaller edge section due to high rake angles is less of a problem in milling due to the lower peak temperatures. Turkovich & Durham [57] found that a change from -5° to +15° in rake angle accounted for a 10% reduction in temperature due to a reduction of shear strain in the primary zone.

ii) Relief Angle

A high relief angle reduces the frictional forces and will therefore reduce flank temperature due to friction. However, as mentioned above a high relief angle will also weaken the edge thereby transferring more of the shear temperature to the flank face. Kneisel & Illgner [58] found an optimum relief angle of 20° with a rake angle of 28°. Shallow relief angles lead to rubbing and below 4° severe adhesion can be observed.

iii) Helix Angle

Shaw [10] observes that the helix angle increases the effective radial rake and sends the chips in a different direction to the feed direction. The helix angle results in a longer contact period with lower maximum force and can reduce mechanical shocking and forced vibrations.

iv) Edge Radius

Increasing the edge radius of the tool increases the chip contact length and therefore produces longer contact times. "This effect almost doubles the respective contact zone temperature for an increase of the cutting edge radius rc =15 micron to rc = 50 micron."(Klocke et al. [59]).The edge radius and cutting forces and temperature also influence surface integrity [60], as the edge radius approaches the uncut chip thickness ploughing rather than shearing can occur.

Cutting Parameters

i) Feed Per Tooth

Vaughn & Quackenbush [44] raised some interesting issues regarding high speed machining of titanium. It is suggested that internal vibrations within the work piece may assist the chip segmentation process and consequently reduce energy consumption and tool tip temperature. It is stated that at high speeds the vibrations are induced whereby the segmentation occurs more freely. Small chip thickness can lead

to rubbing and high temperatures; at high speeds an increase in feed per tooth from 0.025 to 0.4 mm resulted in a two fold decrease in maximum tool tip temperature [21]. Vaughn & Quackenbush propose that these effects are due to increased chip segmentation. It is not clear whether these effects only occur at high speeds for light radial depths of cut (0.3mm), if the segmentation effect can help to minimize tool tip temperature at low speeds (3000 rpm) then there may be some advantage in increasing the fpt. The phenomenon is more pronounced in titanium than in steels due to the brittle nature of the material.

The effect of frictional "rubbing" for low feed per tooth has been widely discussed and there is a minimum chip load below which tool wear will increase. The rubbing phenomenon and the chip segmentation effect point towards an optimum chip load for all cuts where tool life may drastically diminish either side of a stable "chip bandwidth". In many shops this chip load is picked from experience or from conservative empirical data from tool suppliers.

Elbestawi [29]found that increases in feed per tooth resulted in the dominant failure mechanism changing from flank wear to chipping; flank wear dominated below 50 microns. Zlatin & Field [2] demonstrated that when the chip thickness is at its maximum the chip can weld to the tool causing failure. During conventional milling the chip is at its greatest on exit and can weld to the tool and break away the edge, for this reason climb milling is preferred to conventional milling.

ii) Surface Speed (Vs)

Rake and flank wear are known to increase with increasing feed and speed. It is widely understood that tool wear and tool temperature increase with increased cutting speed. Taylor's tool life equation has summarised the experience of many machining shops;

$$VsT_l^m = k \qquad (2.1)$$

Where Vs is the cutting speed, T_l is tool life, m is number of teeth and k is a constant. This concept must always be considered when attempting to increase cutting speeds to increase MRR, there will be a trade off against tool life. As the temperature increases with cutting speeds so does the tool wear, and no speeds have yet been found whereby the temperature begins to drop off as predicted by Salomon [38].

Palmai [37] proposed that cutting temperature increases with cutting speed to a certain limit, and in the case of intermittent cutting could reach a maximum and then reduce.

The empirical equation $T_l=C_tVs^{xt}$ was proposed by Palmai to link cutting temperature with cutting speed. C_t and x_t are empirical constants.

iii) Radial width of cut

Radial width of cut has a strong influence on tool wear as it controls the time in cut and the effective feed per tooth. Kneisel & Illgner [58] found an experimental increase in wear with radial immersion and Perez-Bilbatua [61] found a linear decrease in life with radial immersion at low speed. The influence of radial immersion on tool life has been noted and the hypothesis that radial immersion has a strong influence on tool wear due to thermal loading this is worthy of further exploration.

2.3 Chatter in the Milling Process

2.3.1 Background

For much of the last century work has been undertaken to understand the cause of chatter in milling. Chatter is a self – excited vibration that causes poor surface finish and can cause damage to cutting tools and spindles. Chatter has long been a limiting factor in the productivity of milling operations and has also limited the geometries that could be formed through milling.

Tlusty [6] identified in the 1960's that the stability of a milling process is dependant upon the structural dynamics of the machine tool system, the cutting tool geometry and the workpiece material properties. If the frequency response function of a machine tool- tool holder – cutting tool assembly is known then stable-cutting parameters may be selected. In order to control chatter and optimise the productivity of the milling process it is important to have a fundamental understanding of mechanical vibrations and machining dynamics, these subjects will now be covered in detail.

2.3.2 Self Excited Vibrations

When developing a milling process or optimising an existing one, it is important to understand the limitations on cutting performance and productivity. The limiting factor against increasing the material removal rate (MRR) in milling has in the past often been the machine capabilities. Cutter and machine tool specifications will still

place restrictions on the cuts that may be taken, especially in the case of titanium machining, but vibrations can restrict the process from running at an optimum. During the machining process vibrations can occur between tool and workpiece. These vibrations typically take one of three forms; free vibration, forced vibration or self excited vibration.

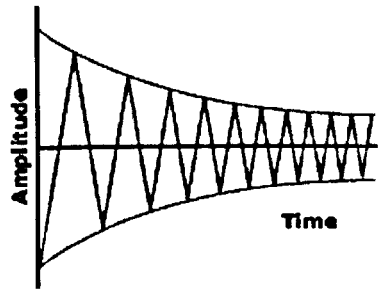

Fig2.2 Free Vibration

Free vibrations (Fig.2.2) are of the type seen when an initial impact is applied to a component and it is then allowed to vibrate freely as the vibrations decays with time, an example is the guitar string. A forced vibration may be cyclic force acting on a system, for example an unbalanced shaft and the vibration will occur at the frequency of the exciting force.

The amplitude of the vibration will be at its greatest when the exciting force equals that of the dominant natural frequency of the system and resonance occurs.
The cyclic impact of a cutting tooth on a workpiece, or the breaking of titanium chips could be a forced vibration. Koenigsberger and Sabberwal [62] investigated the magnitude of cutting force pulsations and the effect on the force of varying cutter geometry and cutting parameters.

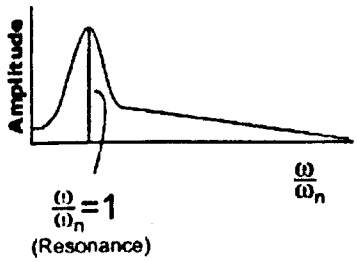

Fig2.3 Forced Vibration

Figure 2.3 shows the frequency response function (FRF) for a forced vibration. In milling terms there will be a high amplitude but stable vibration if the tooth passing frequency is equal to dominant natural frequency. This vibration may cause poor surface finish but will not cause catastrophic damage in the manner of chatter.

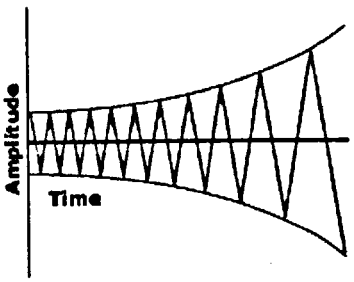

Fig 2.4 Self Excited Vibration

Self-excited vibrations (Fig 2.4) are self-generated from a steady energy source. Unlike a free vibration where the amplitude will decay with time, the amplitude of vibration increases through a feedback loop and becomes unstable. The amplitude of vibration will increase to a peak level that may be determined by constraints within the vibratory system. An example of a self-excited vibration is a whistle.

Chatter is a self-excited vibration and is one of the major causes for limiting the MRR during the machining process [63]. As a self-excited vibration the chatter amplitude will grow until a non-linearity in the machining process prevents further growth, for example the tool may jump out of the cut or the chatter amplitude is restricted due to process damping (Chapter 5). Chatter results in poor tool life, poor surface finish and noise pollution. Chatter must therefore be eliminated where possible from the machining process. If chatter can be understood and controlled then MRR and productivity can be optimised.

2.3.3 Regenerative Chatter

History of Chatter Research

For much of this century work has been undertaken to understand the cause of chatter in milling. Chatter is a self – excited vibration that causes poor surface finish and can cause damage to cutting tools and spindles. Chatter has long been a limiting factor in the productivity of milling operations and has also limited the geometries that could be formed through milling.

Early research on chatter started with Taylor [64], Arnold [65] and Hahn [66] in the 1940's and '50's. Chatter was thought by some to be negative damping in the machining process [67]whilst others have more recently claimed that in the case of titanium milling the oscillation in forces as the result of segmented chip formation can initiate chatter[34] . Tobias [63, 68, 69] was the first to develop the concept of the stability plot for turning. Tlusty [70] worked extensively on chatter theory and stability in cutting, looking first at continuous cutting processes and then at the intermittent milling process [71]. Merrit [72] led a research program from the Cincinnati Milling Machine Company, initially focussed on the dynamic stability

requirements for machine tools. Tlusty & Ismael [71] developed a time dependant simulation for chatter in milling that was further developed with Smith [73] that predicted cutting forces and deflection as well as stability of the cut. Altintas & Montgomery [74] proposed an alternative model that considered vibration of the tool and the work piece.

The first analytical stability lobe equations to predict the onset of chatter were developed in the 1960's [7],[6]. Tlusty [6] was the first to present a theory on machine tool stability explaining the significance of the variation in chip thickness as a result of subsequent wave forms being traced on the workpiece surface.

$$F_n = r_1 (Y_1 - Y_0) \qquad (2.2)$$

Where Y_0 is the amplitude of the surface that has been cut with a previous tool and Y is the surface being cut with the current pass. The limit of stability condition is defined as

$$Y_1/Y_0 = 1 \qquad (2.3)$$

The vibration is related to the cutting force and the transfer function:

$$Y_1 = F_n \Phi_{(w)} \qquad (2.4)$$

Where $\Phi_{(w)}$ is the transfer function of the system.

Despite there being a phase shift between the change of chip thickness and the change in force, the assumption is made that the real part of $\Phi_{(w)}$ can be taken for the calculation of stability for ease of calculation and based on observation that this should not cause substantial error. Tlusty relates the limiting depth of cut to the negative real values of the transfer function. Early works on chatter [65], explained chatter based upon the velocity principle. This principle assumes that a component of the cutting force is dependent upon and in phase with the velocity of the Y_1 vibration, this is represented by the real part of the transfer function and is discarded by Tlusty. Tobias [7] used the velocity and regenerative principles with the velocity principle being defined by a penetration rate. It is assumed that the phase shift between passes will adjust itself to that which corresponds with the maximum energy of self-excitation.

Tlusty presents a solution whereby the limiting depth of cut can be clearly related to the individual modes of the system, thus lending this technique to machine tool design and analysis [6].

Andrew was also amongst the first to identify chatter as being born of the machine tool dynamics and chip formation and not related to run-out and forced vibrations [63]

and went on to compare the theories of Tobias and Fishwick [75], and Tlusty and Polacek [6].

Tlusty and Polacek assumed that the cutting force is proportional to the steady state chip thickness, whilst Tobias and Fishwick believe that the cutting force varies with surface speed and feed velocity or penetration rate and also consider the number of teeth engaged in the cut. Andrew [63]describes an example where two cutters, one with one tooth engaged and the other with two teeth engaged, are both taking the same size of cut and feed. Although the force will be the same in each case, the variation in chip thickness will be greater for the cutter with two teeth engaged as the effective displacement is seen on each tooth, doubling the overall variation in chip thickness. Tlusty and Polacek consider the problem to be of forced vibrations, the wave produced in one cut exciting a further wave in the succeeding cut.

A combined model was produced by Tobias [7] incorporating the stability approach of Tobias and the modal analysis methods of Tlusty. Further significant developments came when Tlusty presented his stability lobes for milling [76] , simplifying the milling process to an orthogonal process such as turning. This algorithm did not however account for the time varying nature of the milling process and assumes an average cutting force direction.

The orthogonal cutting models developed by Tlusty and Tobias had a major impact on the machine tool industry with users combining intuition and simple adjustments to gain practical advantage from the models.

Tlusty simplified the milling model by orientating the cutting forces to the direction of the resultant force. Tlusty used the geometric mean of the immersion angles, whereas Opitz used an average value $A(\phi_t)$ [77] and used pitch angle to account for number of teeth engaged in the cut. These one dimensional models do not take account of the time variant nature of the milling process and each use an oriented transfer function.

Sridhar [78, 79] argued that milling has coupled dynamics and must be considered as a two dimensional problem, resolving the forces in the feed and tangential directions. Sridhar used numerical techniques to solve the forces. Minis & Yanushevsky [80] solved in the frequency domain using Floquet theory for delayed differential equations. Altintas & Budak further developed the coupled dynamics model and considered harmonics (ρ) of the periodic matrix. [81]

Davies created a chatter solution for low radial immersion where free vibration of the tool occurs when no teeth are engaged in the cut. Davies found that for instances of shallow radial immersion a second stability lobe appeared. This notion was further studied as Stepan [82] approximated regenerative time delay, Bayly [83] used time finite elements and Budak, Merdol and Altintas [84] developed a multi-frequency solution. These all predicted added lobes in the high speed range.

The Altintas solution [81] assumes that harmonics are low pass filtered where radial immersion is not too small. This simplifies the calculation and gives an efficient prediction for stability although it will exclude the second lobe effect.

The model is also expanded to a three dimensional chatter model. Considering the dynamic coupling between x and y direction modes leads to an eigenvalue problem as opposed to the scalar solution proposed by Tlusty.

The analytical models derived by Tlusty and Altintas will be covered in more detail and employed as a means of explaining the physics of chatter. The partial immersion models of Davies and Insperger are then discussed in more detail and an introduction to non-regenerative chatter, mode coupling is presented.

Chatter Mechanics and Analytical Stability Lobes

Analytical Stability Lobes – Tlusty

During a milling operation as the tooth cuts the workpiece material at a pre-determined mean chip thickness, the tooth will vibrate in the direction and frequency of a dominant mode of the machine tool system. If we assume a single degree of freedom perpendicular to the path of the tool then a waveform will be left on the cut surface. As the next tooth cuts this surface, removing the waveform, it too will leave a waveform on the surface of the material. These two waveforms will define the size of the chip to be removed. If the two waves are exactly in phase then the chip width, and hence the cutting force *(2.5)*, will remain constant.

Fig 2.5 Chip thickness variation

$$F_n = K_s\, b\, h \qquad (2.5)$$

Where K_s is the cutting stiffness, b is the chip length and h is the chip width.
If the second tooth is out of phase with the previous tooth, the chip width will vary and so too will the cutting force F_n. The variation in cutting force will further increase the vibration and there is a critical point at which this vibration loop becomes self - sustained. This is the cause of the self excited vibration known as regenerative chatter.
According to Tlusty [76], the phase difference is dependant upon the chatter frequency (close to modal frequency) and the tooth passing frequency as shown below;

$$\frac{60 \cdot f_c}{n \bullet m} = N + \frac{\varepsilon}{2\pi} \quad , \quad N = 0,1,..... \qquad (2.6)$$

Where N is an integer (lobe number)
fc = chatter frequency (Hz)
n= spindle speed (rpm)
m = number of teeth
ε = phase (radians)

The criteria for stability are related to the phasing of subsequent teeth, the cutting force F_n, and the transfer function of the excited mode.
Equation (2.5) states that the cutting force F_n is related to the cutting stiffness, chip width and chip length. As the tooth follows the waveform the chip width will vary such that at any point the chip is defined as the nominal feed chip width (h) less the current deflection of the cutter normal to the cut surface (Y_1) plus the previous deflection of the cutter (Y_0).

$$F_n = K_s * b * (h - Y_1 + Y_0) \qquad (2.7)$$

Whilst looking for the criteria for stability one can isolate the variable component of the cutting force;

$$F_v = K_s * b * (Y_0 - Y_1) \qquad (2.8)$$

The value of $Y_0 - Y_1$is related to the negative real part of the excited mode as represented in the Frequency Response Function in Figure 2.5.

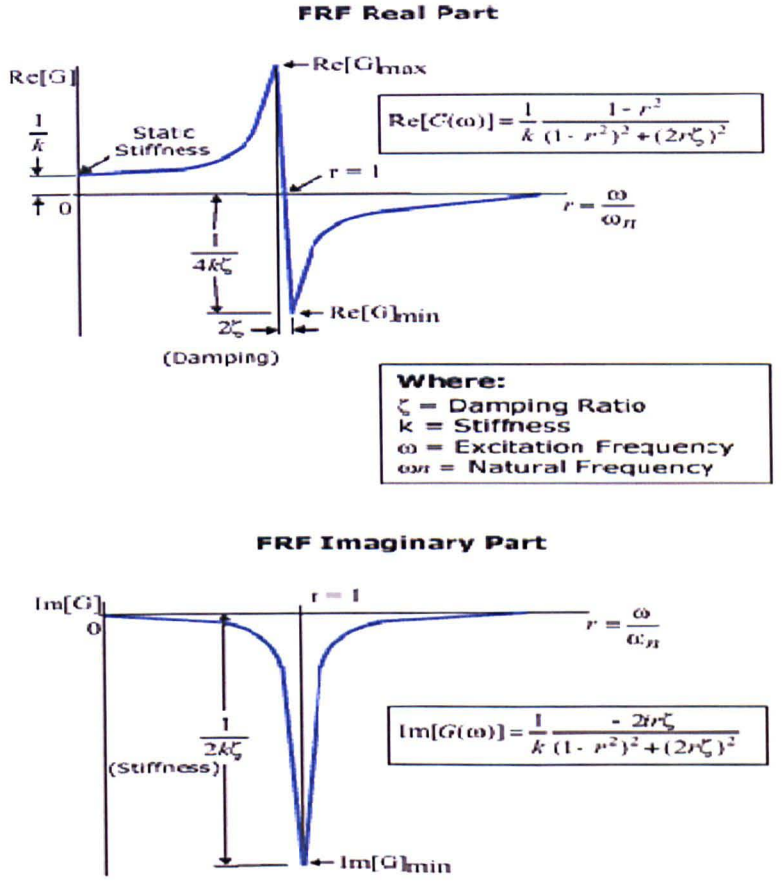

Fig. 2.6 Frequency Response Function (FRF) Real & Imag plots

It can be demonstrated with a phase plane plot that $Y_0 - Y_1$is is at its greatest for the minimum real value of the excited mode (Fig2.6). Tlusty [21]relates the stability limit to the real part of the FRF, the cutting stiffness, a directional coefficient and a value for the average number of teeth engaged in the cut as a mean approximation of the direction and magnitude of the force acting upon each tooth.

$$b_{\lim} = \frac{1}{2 \bullet Ks \bullet \mathrm{Re}[G] \bullet \mu \bullet m_{avg}} \qquad \textit{(2.9)}$$

Where b_{lim} is the limiting chip length, μ is the directional coefficient, Re[G] is the real value of modal transfer function and m_{avg} is the average number of teeth engaged in the cut (related to radial depth of cut).

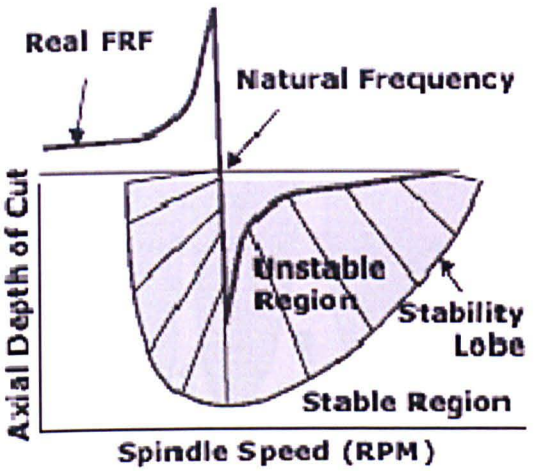

Fig. 2.7 Lobe Plotting from Real Part of FRF

There exists a critical chip length (axial depth of cut) below which all spindle speeds are stable and this is defined by Re[G]min;

$$b_{\lim crit} = \frac{1}{2 \bullet Ks \bullet \mathrm{Re}[G]_{\min} \bullet \mu \bullet m_{avg}} \qquad (2.10)$$

The boundary relationship between phase and the transfer function is derived from a phase plane plot (Fig 2.8);

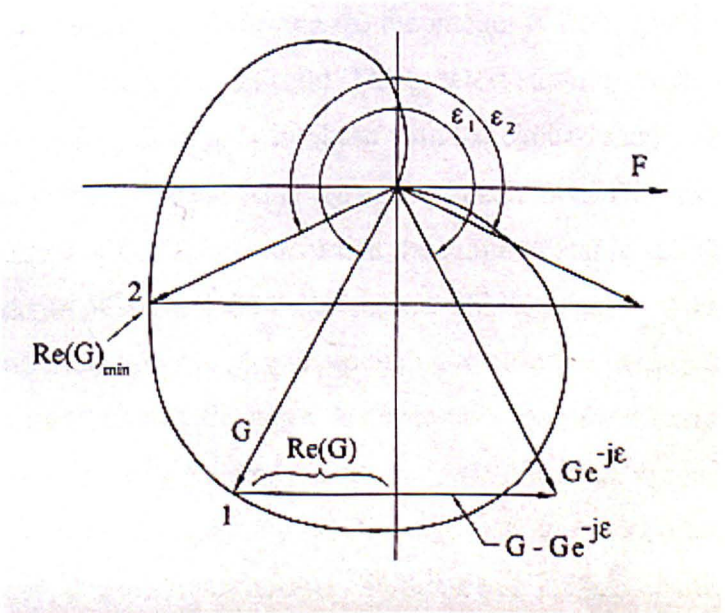

Fig. 2.8 FRF Phase Plane Plot [21]

It can be seen from the plot that the phase angle between subsequent teeth can be defined in terms of the real and imaginary values of the transfer function.

$$\varepsilon = 2\pi - 2\tan^{-1}\left(\frac{\mathrm{Re}[G]}{\mathrm{Im}[G]}\right) \qquad (2.10)$$

Thus if the transfer function of the system is known a criteria for stability can be plotted from equations (2.5), (2.9) and (2.10).

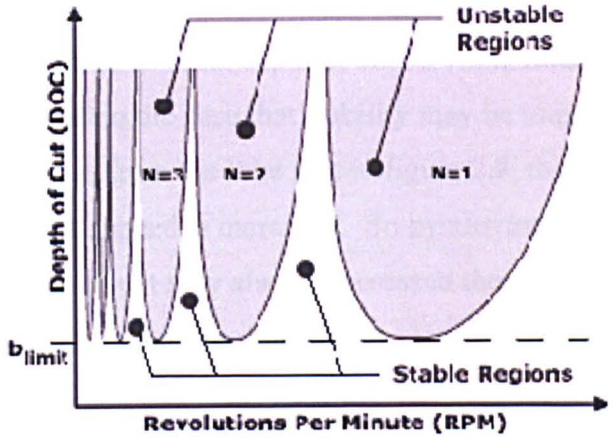

Fig.2.9 Stability Lobe Plots

In the *Fig2.9* the grey area above the boundary line represents unstable milling. At the boundary of stability line (b_{lim}) chatter will occur at a specific frequency plotted in the lower plot. The troughs of each of the lobes correspond to the $b_{limcrit}$ value and crossing the stability boundary at this point will result in chatter at the frequency of $\mathrm{Re}[G]_{min}$.

Each separate lobe relates to the integer N from equation (2.5) with the N=0 lobe being furthest to the right. The greatest stability exists when the tooth passing frequency is exactly in phase with the excited mode, i.e. when $f_c = N * n * m/60$. This condition is satisfied at the peak of each lobe. The vertical axis of the plot shows axial depth of cut. It is evident that the range of stable spindle speeds reduces as the axial depth of cut and the Fn increases. This is to say that although subsequent teeth may not be exactly in phase, producing a variation in chip thickness, the point at which this variation leads to chatter is dependant upon the mean cutting force. Beyond N=1 for tooth passing frequencies of $n * m > 2fc$ large ranges of stable milling exist.

Traditional machining practice has seen operators either reduce the axial depth of cut or reduce the spindle speed in order to eliminate chatter. As can be seen from the stability lobe plot both of these actions will eventually stabilize the cut either by reducing the cutting force below the threshold or finding a stable spindle speed. The

latter often occurs due to a phenomenon known as process damping which shall be covered in more detail at a later stage.

Reducing either spindle speed (which must see a proportional reduction in feed rate) or axial depth of cut will reduce the MRR for the process.

$$MRR = a_p * a_e * fr \qquad (2.11)$$

Where a_p is axial depth of cut, a_e is the radial depth of cut and fr is the feed rate.

It is often the case that stability may be improved by raising the spindle speed. As can be seen from the lobe plot in figure 2.8, the width of the lobes will increase as the spindle speed is increased. So by moving the cut to the right of the plot the axial depth of cut may also be increased thereby increasing the MRR further.

For any given machine tool – spindle –cutting tool configuration an optimum spindle speed can be identified if the transfer function is known. The measurement is taken using a hammer impulse on the tool tip that is recorded by an accelerometer located also on the tool tip. This direct measurement is recorded using a data acquisition card and a Fast Fourier Transform (FFT) is carried out to compute the transfer function of the system. The transfer function is then displayed in its real and imaginary form from which stability plots can be generated using the equations outlined in this chapter.

In this manner the dynamics of the machining system can be easily measured and interpreted on the shop floor and can assist manufacturing engineers or machine operators in selecting optimized stable spindle speeds. The assumption is made that the dynamics of the system as measured in the static condition will be representative of the system dynamics during the machining operation. This assumption shall be investigated in chapter 4.

Coupled Mode Solution

The Tlusty derivation of stability lobes became widely used during the 1980's [76]. As discussed at the start of the chapter it contains some simplifications, approximating the cutting force vector based upon the radial width of cut and the number of teeth engaged by calculating an oriented transfer function.

Altintas [81] proposed a coupled mode solution in an attempt to provide a more accurate interpretation of the stability lobes. The Altintas solution assumes that harmonics are low pass filtered where radial immersion is not too small. This

simplifies the calculation and gives an efficient prediction for stability although it will exclude the second lobe effect.

The model has also been expanded by Altintas and Campones to a three dimensional chatter model. Considering the dynamic coupling between x and y direction modes leads to an eigenvalue problem as opposed to the scalar solution proposed by Tlusty. The Altintas alagorithm will now be presented in detail as it forms the foundation for a model developed in chapter 4.

The tangential and radial cutting forces acting on tooth j can be expressed as:

$$F_{rj} = K_r F_{tj} \tag{2.12}$$

$$F_{tj} = K_t b h(\phi_j) \tag{2.13}$$

Where b is the axial depth of cut, h is the chip thickness, ϕj is the angular position of the tooth. K_t is the tangential cutting force coefficient, K_r is the radial cutting force coefficient, Ft is the tangential force, F_r is the radial force and j is the tooth number.

$$h(\phi_j) = g(\phi_j)\left[f_t \sin\phi_j + (v_{j-1} - v_j)\right] \tag{2.14}$$

Where;

f_t is the feed rate per tooth, v_j is the dynamic displacement of present tooth, v_{j-1} is the dynamic displacement of previous tooth and g(ϕj) is a step function to determine whether tooth is in cut.

$$g(\phi_j) = \begin{cases} 1 \leftarrow \phi_{st} < \phi_j < \phi_{ex} \\ 0 \leftarrow \phi_j < \phi_{st} or \phi_j > \phi_{ex} \end{cases} \tag{2.15}$$

Where;

ϕ_{st} is the start immersion angle of cut, ϕ_{ex} is the exit immersion angle of cut.

For cutter displacements (x) and (y) the radial displacement of teeth j and j-1 at time t become:

$$v_j(t) = -x(t)\sin\phi_j(t) - y(t)\cos\phi_j(t) \tag{2.16}$$

$$v_{j-1}(t - T_j) = -x(t - T_j)\sin\phi_j(t) - y(t - T_j)\cos\phi_j(t) \tag{2.17}$$

Where T_j is the time delay between teeth due to spindle rotation.

For a standard pitch cutter the time delay is equal to the rotational speed divided by the number of teeth.

The dynamic chip thickness equation can now be presented as:

$$h(\phi_j(t)) = g(\phi_j)\left[\Delta x_j(t)\sin\phi_j + \Delta y_j(t)\cos\phi_j(t)\right] \tag{2.18}$$

where

$$\Delta(x,y)_j(t) = (x,y)_j(t) - (x,y)_{j-1}(t - T_j) \qquad (2.19)$$

The dynamic chip load can be substituted into the tangential and radial cutting forces which are then resolved in the feed direction (x) and the normal direction (y), summing for the total number of teeth (m):

$$F_x(t) = \sum_{j=0}^{m-1}(-F_{tj}(t)\cos\phi_j(t) - F_{rj}(t)\sin\phi_j(t)) \qquad (2.20)$$

$$F_y(t) = \sum_{j=0}^{m-1}(F_{tj}(t)\sin\phi_j(t) - F_{rj}(t)\cos\phi_j(t)) \qquad (2.21)$$

The total dynamic milling forces can be represented in vector form:

$$\{F(t)\} = \frac{1}{2}bK_t\sum[A\ (t)]\{\Delta\ (t)\} \qquad (2.22)$$

Where ;

$$\{F(t)\} = \{F_x(t), F_y(t)\}^T \qquad (2.23)$$

$$\{\Delta\ (t)\} = \{\Delta x\ (t), \Delta y(t)\}^T \qquad (2.24)$$

[A(t)] is the matrix of time varying periodic directional coefficients; a_{xx}, a_{xy}, a_{yy}, a_{yx}. Where:

$$a_{xx} = \sum_{j=0}^{m-1} - g_j[\sin 2\phi_j + K_r(1 - \cos 2\phi_j)] \qquad (2.25)$$

$$a_{xy} = \sum_{j=0}^{m-1} - g_j[K_r \sin 2\phi_j + (1 + \cos 2\phi_j)] \qquad (2.26)$$

$$a_{yx} = \sum_{j=0}^{m-1} - g_j[(1 - \cos 2\phi_j) - K_r \sin 2\phi_j] \qquad (2.27)$$

$$a_{yy} = \sum_{j=0}^{m-1} - g_j[\sin 2\phi_j - K_r(1 + \cos 2\phi_j)] \qquad (2.28)$$

The matrix is periodic at spindle frequency and can be expressed as a Fourier series expansion.

$$[A\ (t)] = \sum_{\rho=-\infty}^{\infty}[A_{\rho j}]e^{i\rho wt} \qquad (2.29)$$

$$[A_\rho] = \frac{1}{T}\int_0^T[A\ (t)]e^{-i\rho wt}dt \qquad (2.30)$$

where (ρ) represents the harmonics. The harmonics have been demonstrated to have little influence on stability [85] and are therefore discounted and a solution is found for ρ =0. A_0 is only valid while the tooth is engaged in the cut:

$$[A_0]=\frac{1}{\phi_p}\int_{\phi_{st}}^{\phi_{ex}}[A_j(\phi)]d\phi=\frac{1}{2\pi}\begin{bmatrix}\alpha_{xx}\alpha_{xy}\\ \alpha_{yx}\alpha_{yy}\end{bmatrix} \qquad (2.31)$$

Where t:

$$\phi_p = 2\pi / m \qquad \text{(pitch angle)} \qquad (2.32)$$

And the integrated functions are:

$$\alpha_{xx}=\frac{1}{2}[\cos 2\phi - 2K_r\phi + K_r \sin 2\phi]_{\phi_{st}}^{\phi_{ex}} \qquad (2.33)$$

$$\alpha_{xy}=\frac{1}{2}[-\sin 2\phi - 2\phi + K_r \cos 2\phi]_{\phi_{st}}^{\phi_{ex}} \qquad (2.34)$$

$$\alpha_{yx}=\frac{1}{2}[-\sin 2\phi + 2\phi + K_r \cos 2\phi]_{\phi_{st}}^{\phi_{ex}} \qquad (2.35)$$

$$\alpha_{yy}=\frac{1}{2}[-\cos 2\phi - 2K_r\phi - K_r \sin 2\phi]_{\phi_{st}}^{\phi_{ex}} \qquad (2.36)$$

the resulting dynamic equation is:

$$\{F(t)\}=\frac{1}{2}bK_t[A_0]\{\Delta\ (t)\} \qquad (2.37)$$

where:

$$\{\Delta(t)\}=\begin{Bmatrix}x(t)\\ y(t)\end{Bmatrix}-\begin{Bmatrix}x(t-T)\\ y(t-T)\end{Bmatrix}=\{\eta(t)\}-\{\eta(t-T)\} \qquad (2.38)$$

η(t) represents the relative vibrations between tool and workpiece at time t whilst η(t-T) represents the vibration marks left by the previous tooth. The vibration at chatter frequency w_c is described as harmonic variables:

$$\left.\begin{aligned}\{\eta(iw_c)\}&=[\Phi(iw_c)]\{F\}e^{iw_c t}\\ \{\eta_0(iw_c)\}&=e^{-iw_c T_j}\{\eta(iw_c)\}\end{aligned}\right\} \qquad (2.39)$$

The relative transfer function matrix being:

$$[\Phi(iw)]=\begin{bmatrix}\Phi_{xx}(iw)\Phi_{xy}(iw)\\ \Phi_{yx}(iw)\Phi_{yy}(iw)\end{bmatrix} \qquad (2.40)$$

The regenerative displacements at a chatter frequency can be expressed as:

$$\{\Delta(iw_c t)\}=\{\eta(iw_c)\}-\{\eta_0(iw_c)\}=(1-e^{-iw_c T_j})[\Phi(iw_c)]\{F(t)\}e^{iw_c t} \qquad (2.41)$$

Substituting this into the dynamic milling equation we have:

$$\{F(t)\}e^{iw_c t} = \frac{1}{2} bK_t (1 - e^{-iw_c T_j})[A_0][\Phi(iw_c)]\{F(t)\}e^{iw_c t} \quad (2.42)$$

The above equation has a non-trivial solution when its determinant is zero:

$$\det[[I] - \frac{1}{2} K_t b\left(1 - e^{-iw_c T}\right)[A_0][\Phi\ (iw_c)]] = 0 \quad (2.43)$$

The oriented transfer function is the product of the directional factors and the transfer function.

$$[\Phi_0(iw_c)] = \begin{bmatrix} \Phi_{xx}\alpha_{xx} + \Phi_{yx}\alpha_{xy}, \Phi_{xy}\alpha_{xx} + \Phi_{yy}\alpha_{xy} \\ \Phi_{xx}\alpha_{yx} + \Phi_{yx}\alpha_{yy}, \Phi_{xy}\alpha_{yx} + \Phi_{yy}\alpha_{yy} \end{bmatrix} \quad (2.44)$$

The eigenvalue Λis represented as follows:

$$\Lambda = -\frac{m}{4\pi} K_t b\left(1 - e^{-iwt}\right) \quad (2.45)$$

Resulting in:

$$\det[[I] + \Lambda[\Phi_0(iw_c)]] = 0 \quad (2.46)$$

If Φxy =Φyx =0 the eigenvalue can be solved as a quadratic function:

$$a_0\Lambda^2 + a_1\Lambda + 1 = 0 \quad (2.47)$$

A complex solution can be found for the eigenvalue where the entry and exit angles and material stiffness values K_t and K_r are known.

The limiting depth of cut for stability can now be related to the eigenvalue:

$$\Lambda = \Lambda_R + i\Lambda_I = -\frac{1}{4\pi} K_t b_{\lim}\left(\cos w_c T - i \sin w_c T\right) \quad (2.48)$$

$$b_{\lim} = -\frac{2\pi}{mK_t}\left[\frac{\Lambda_R(1 - \cos w_c T) + (\Lambda_I \sin w_c T)}{(1 - \cos w_c T)} + i\frac{\Lambda_I(1 - \cos w_c T) - \Lambda_R \sin w_c T}{(1 - \cos w_c T)}\right] \quad (2.49)$$

As the axial depth of cut limit (b_{lim}) has a physical value the solution only exists when the imaginary part is zero and the real is negative.

Substituting

$$\kappa = \frac{\Lambda_I}{\Lambda_R} = \frac{\sin w_c T}{1 - \cos w_c T} \quad (2.50)$$

Into equation 2.44 the imaginary part vanishes giving the limiting chatter free depth of cut as:

$$b_{\lim} = -\frac{2\pi\Lambda_R}{mK_t}\left(1 + \kappa^2\right) \quad (2.51)$$

The stability lobes can now be solved by determining the phase shift of the eigenvalue for a chatter frequency w_c at tooth period T:

$$w_c T = -\cos^{-1} 2\psi \qquad (2.52)$$

The phase shift between the inner and outer modulations can be presented as:

$$\varepsilon + 2N\pi = \pi - 2\psi + 2N\pi \qquad (2.53)$$

Where N is the integer number of vibration waves during the cut period.

The spindle speed can then be solved as:

$$n = \frac{60 w_c}{N(\varepsilon + 2N\pi)} \qquad (2.54)$$

From equations 2.51, 2.53 & 2.54 the stability lobes can be computed for each lobe number N.

A Matlab algorithm for plotting lobes using this coupled mode solution has been written by the author producing sample lobes as presented in Fig.2.10. This model is developed further in chapter 4 as part of an investigation into the performance of variable pitch and helix tools.

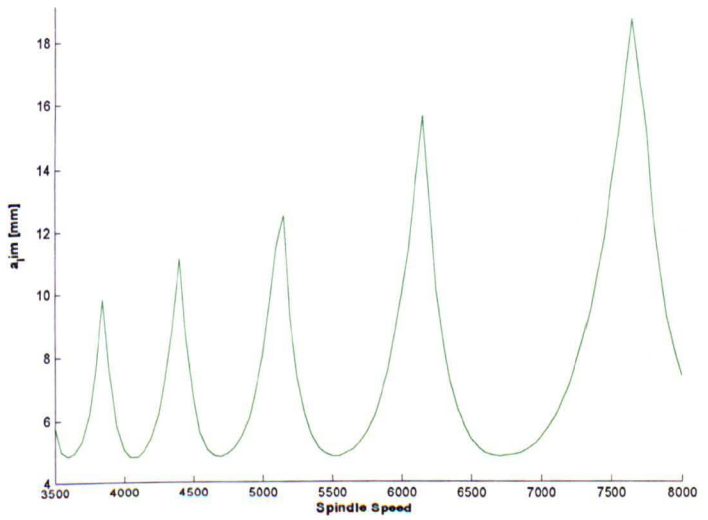

Fig.2.10 Sample stability lobes plotted using Altintas coupled mode solution

Delayed Differential Equations & Second Lobe

Davies [86]has verified an interesting stability characteristic for low radial immersion milling. The phenomenon is an extension of traditional stability lobe theory whereby stable cutting occurs when the vibrations and the tooth passing frequency are in phase. These stable conditions occur at multiples of the natural frequency of the system such

that the tool and workpiece contact always occurs at the same point in the vibration cycle and there is no change in chip width that can lead to regenerative chatter. If one looks at a sinusoidal vibration in one axis it can be seen that other than at the peaks and troughs, the vibration will pass through the same point twice per cycle. During low radial immersion <10% it can be assumed that modes in one direction only are dominant and that the vibration follows a sinusoidal waveform, rather than an elliptical vibration caused by deflection in two directions. It can also be assumed that for very small immersion where the contact is almost instantaneous, that the tooth stays in the same position of the vibration cycle throughout the contact time in the cut. With these assumptions it can be deduced mathematically (Davies [87]) that stable conditions can occur at twice the number of speeds suggested by traditional stability lobe theory. Consequently a stability lobe plot for these conditions exhibits an extra lobe for each value of N.

Insperger & Stepan [88]proposed a new mathematical method for determining stability in milling. Delayed differential equations with time-periodic coefficients are used. The delayed differential model incorporates the 'second lobe' effect.
Using this method a second region of instability is seen that can give the effect of islands of stability. This work has been furthered by Mann and Bayly[83, 89] at Washington University and Davies at NIST and UNCC and provides an alternative to the Altintas model presented here in depth. The Altintas model has been selected for further development in this thesis as it allows a detailed

2.3.4 Mode Coupling

A second chatter mechanism can exist if the relative vibration between tool and work piece can occur in two directions simultaneously in the plane of the orthogonal cut. If an end mill is considered to have vibrations in the x and y directions simultaneously, x being the direction of cut, the two vibrations having the same frequency and a phase shift between them, then an elliptical cutter path will occur. The force on the tool will be acting in the direction Fn shown in Fig2.10 and the tool will be moving at speed V in the direction of the feed.

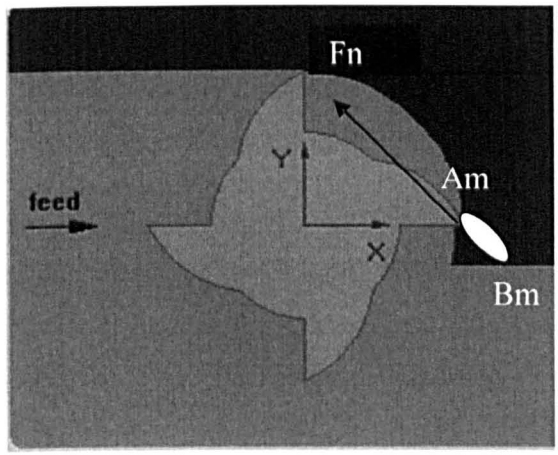

Fig. 2.11 Mode Coupling Effect

The ellipse represents the periodic path from Am to Bm followed by the cutter. The elliptical motion is caused by the two vibrations in the (x) and (y) directions that are of equal frequency but with a phase lag.

As the cutter moves along the elliptical path from Am to Bm the force Fn acts against this motion and takes energy away. As the cutter moves from Bm to Am the force drives the cutter and puts energy into the motion. As the motion Bm to Am is the latter part of the elliptical cycle it occurs as the tooth is engaged deeper into the cut, consequently the force is greater during the Bm to Am motion. If the energy gained or removed from the motion is proportional to the force Fn at that time, then the energy gained by the motion from Bm to Am is greater than the energy removed from the motion during Am to Bm. Consequently there is a periodic surplus of energy caused by this elliptical motion, which sustains the vibration against damping losses. This form of self-excitation can manifest itself as chatter, and can become more pronounced in long end mills. For this mechanism to occur the frequencies of vibration in both (x) and (y) must be equal.

A simple end mill would have equal flexibility and modal frequencies in each direction. Unequal flexibility in the two modes would lead to a variation in static deflection as the cutter rotates.

By altering the spring stiffness in one direction (x) the modal frequency in that direction is modified. As the frequencies are different, the effect of mode coupling is reduced. Ismael and Bastami [90] used a simulation and empirical data to demonstrate that once the ratio between the stiffness in the two directions is reduced below 0.4 the benefits are lost as the lower stiffness of the second mode becomes detrimental.

By grinding flats on opposite sides of a standard cutter the stiffness in one direction is altered. Changing the cross section of the tool at the design stage is another method of altering the stiffness ratio of the two modes.

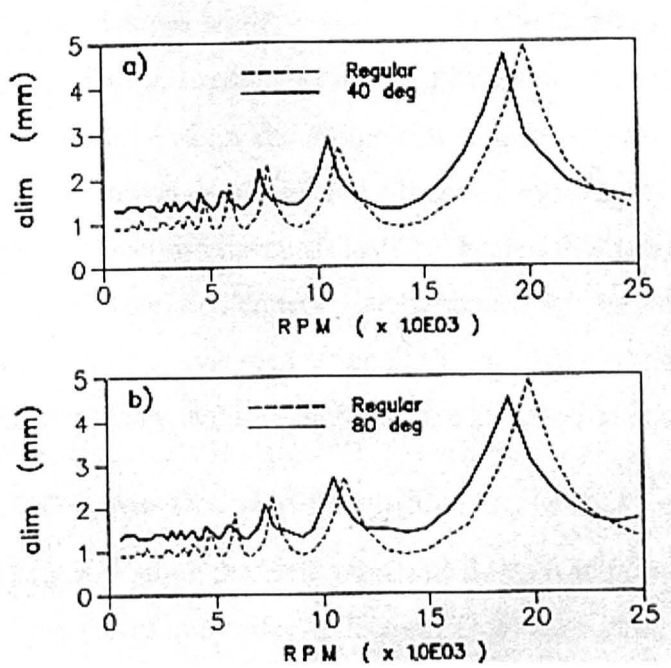

Fig2.12 Stability lobes for slotting (from Ismael , Vaderi 1990)

Ismael and Vadari [90]made investigations into the optimum angle of the flats with relation to the cutting tooth. For slotting operations the angle of the flat makes no difference, but performance of the modified tools are always better than standard. The stiffness ratio was found to give best results at 0.71. The optimum angle of orientation of the flats is 90°, with an orientation of 40° giving the worst results and maximum vibration.

The mode coupling effect becomes negligible at high speeds approaching n=f,f/2,f/3. At these speeds the regeneration of waviness is the primary cause of chatter.

2.3.5 Special Tool Geometries

An alternative to tuning the cutting parameters to stabilise the milling process is to break up the regenerative phasing using pitch variation. Variable pitch tools have been widely researched to this end. Variable pitch tools and waveform or variable helix tools are often used in industry although no analytical models exist for predicting the stability of the wavefrom and variable helix tools. Slavicek [91] first proposed variable pitch cutters using Tlusty's orthogonal chatter model. Slavicek's model proposed tools with two pitch angles, designed to give a 90 deg regenerative phase

shift during machining. Vanherck [92] also used an orthogonal model with more than two different pitch angles and a non-linear pitch angle variation. Varterasian [93] reported experimental results for randomly placed pitch angles and Stone [94] looked at serrated edges while Vanherick [92] also looked at variable helix cutters.
Tlusty (Tlusty, Ismael, Zlaton [95]) investigated the effects on stability of variable pitch, serrated edges and variable helix using chatter theory and numerical solutions. The serration also reduces the effective depth of cut, as the whole flute length will not be in contact with the cut. Tlusty [95]stated this as a reason for improved axial depth of cut with serrated cutters. Campomanes [96] presented a solution for serrated cutters using Altintas' average cutting force and average chip thickness model and showed that significant stability increases are achieved over standard cutters.

2.3.6 Time Domain Simulation

Tlusty and Smith pioneered the time domain solution for milling [97] [73] ,predicting cutting forces and cutter deflection. This was further developed by Altintas [74, 98] to incorporate the structural dynamic models of tool and workpiece.
The current tool-workpiece contact coordinates are subtracted from those created by the previous tool to evaluate the instantaneous chip thickness. The time domain solution will consider the non-linearities of the system and will therefore offer a more accurate prediction than analytical frequency domain solutions. Therefore any frequency domain chatter stability solution can be quickly assessed against a numerical, time domain solution.
Campamones & Altintas adapted the time domain solution to consider the mode shapes of the tool and the effect on ship size and machined surface [96]. Altintas points out that while finite element models are commonly used to model the plastic deformation trends at the chip interface, orthogonal to oblique cutting transformation and mechanistic models are most commonly used to predict cutting forces exciting machine tool vibrations [99]. Time domain models can be used to study the effect of tool geometries and parameters on cutting force, surface condition and stability. The available time domain models are all founded upon Tlusty and offer an accurate representation of the milling process.
Time domain is however computationally intensive and it is not a practical solution for determining optimum stability and parameters in a shop floor environment. For

this reason much research has focussed on analytical solutions to the chatter stability problem. [76] , [7], [100] , [101], [88], [81].

2.3.7 Process Damping

Equation (2.8) shows that the variation in cutting force is directly proportional to variation in chip thickness. This assumes that there is no phase angle between the two. In fact there is a damping action and a phase shift in the generation of the variable force. This damping action becomes significant at low cutting speeds. The stabilising effect can be used in practice to machine components that have low dynamic stiffness or where surface speed and tool wear limitations inhibit the use of high speed stability lobes. Roughing of titanium is often carried out at relatively low speeds and an understanding of process damping can improve MRR and reduce chatter.

It is believed that this phenomenon exists due to the variation on the actual clearance or relief angle of the tool whilst cutting a waved surface and its relation to the thrust on the cutter [21]. The variation in relief angle leads to variation in the thrust force component, being greater the smaller the relief angle. The variation in the thrust force is in opposite phase to the velocity and 90° out of phase with displacement. The out of phase force acts as damping. Figure 2.13 demonstrates that the actual clearance angle is at a maximum during the upward motion at position DD and the thrust force decreases, at position B the actual relief angle is very small leading to a greater thrust force. This means that while the velocity of the vibratory moment is acting downwards from A to C it encounters a greater reactive force than as it rises from C-DD. The variation in the thrust force is in opposite phase to the velocity and acts as damping.

The shorter waves have steeper slopes, causing the relief angle extremities and the consequent damping effect to be increased. The wavelengths (λ) are related to the cut velocity (V_s) and excitation frequency (w_c) as follows;

$$\lambda = V_s / w_c \qquad (2.55)$$

Consequently the damping effect is greater at low speeds.

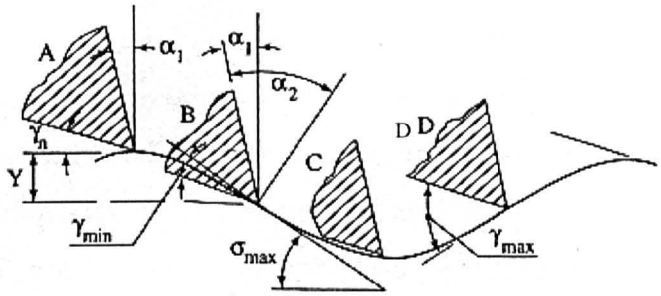

Fig. 2.13 Process Damping due to interference of clearance angle and cut surface. Taken from [21]

The damping effect should also be greater for tools with small relief angles.

Wu [102] showed that the interference between the cutting tool relief and the cut surface is the cause of the phase lag between the force and displacement.

Elbestawi et al [103] stated that the indentation of the tool into the machined surface is the source of process damping. The ploughing force caused by this indentation acts against the vibration velocity and consequently acts as a damping force.

Lee et al [104]used neural networks to model the process damping force generated during chatter vibration. The model was built upon the principle that the damping force is a result of the resistive force between the cutter and the undulated surface. During chatter the actual clearance angle may become negative as the cutting edge displaces work piece material. Lee stated that the resistive force is proportional to the volume of material displaced.

Altintas claims that 'modelling of process damping as a function of tool geometry, tool wear, cutting speed, work material and vibration frequency is yet to developed for effective prediction of chatter vibrations and stability in turning, boring, and low speed milling and drilling operations'[103].

Montgomery & Altintas [74] included Process Damping in their milling time domain model as did Tlusty and Smith [73], showing that it was dominant at low spindle speeds. Montgomery & Altintas attempted to model the interference between cutting tool and wavy surface using contact mechanics without satisfaction, producing high frequency bouncing of the tool.

Dynamic Cutting Force Coefficients (DCFC) and Process Damping

The cutting force coefficient Ks, a material and tool geometry related value, is used to predict the border of stability. Some research has suggested that the cutting force coefficient changes with Vs and that it is a complex number. Tobias first identified the cutting force coefficient to be a complex number [7], relating the rake angle of the tool, and the process damping between the slopes on the wavey surface and the relief face of the tool. CIRP formed a task force to identify the dynamic cutting force coefficients, led by Peters & Vanherck [105] and Tlusty [106].

They believed the dynamic cutting force coefficients to be responsible for the variation in stability at high and low speeds and ultimately contribute towards the process damping effect.

Tlusty [106] reviewed the CIRP research into dynamic cutting force coefficients (DCFC). The cutting force coefficient is taken as a real number in the limiting depth of cut equation, but Tlusty states that experience shows a cutting force coefficient value that varies with spindle speed and cutting parameters, with the limiting depth of cut ($b_{limcrit}$) tapering down from a high stability low speed region and gradually raising up again to settle out at low speeds.

Tlusty states that feed when increased in milling reduces blim yet in turning increases b_{lim} [67]. He takes this as evidence that damping is inherent in the cutting process that can influence chatter. The author proposes that the perceived reduction in blim from milling is due to a change in the contact stiffness between tool holder and spindle interface as a result of increased bending moment as identified by Smith [107]. Where no such reduction in contact stiffness occurs then an increase in feed may influence blim both in milling and turning- process damped region [107]. This proposition will be examined in chapter 5.

The CIRP DCFC tests were undertaken to establish the link between cutting data and chatter. It was believed that the DCFCs would also hold the key to modelling the low speed high stability process damping effect.

The chip formation and wave generation process is split into two distinct actions; the removing of a chip with an undulating surface is defined as wave removing and outer modulation, and the generation of a waved surface whilst removing the chip from a flat surface defined as wave cutting or inner modulation; Albrecht [75], Das [108].

Each cutting force coefficient (inner and outer) is considered to be complex. It is

concluded that stability is dependent upon the absolute value of the outer coefficients and the imaginary part of the inner coefficients which represents the damping in the process.

Outer modulation of cutting force is the effect of removing a chip from an undulated surface (wave removing).

Inner modulation of the cutting force is the effect of cutting with a tool vibrating in the direction Y normal to the cutting speed whilst considering a non-undulated cutting surface (wave cutting).

$$F_r = b(K_{di}\, Y + K_{do} Y_0) \qquad (2.56)$$

component of cutting force normal to surface (direction Y)

$$F_t = b\,(K_{ci}\, Y + K_{co} Y_0) \qquad (2.57)$$

component of cutting force tangential to surface (direction of av. Cutting speed)

Where each 'Kij' is a DCFC with a real and imaginary part;

$$K_{ij} = Re(K_{ij}) + j\, Im(K_{ij}) \qquad (2.58)$$

This approach founded in established stability theory led Tlusty [109] to identify positive and negative damping within the milling process. The negative damping (self –excited vibration) is caused by variation in the cutting force Fn and increases with an increase in rake angle of the tool. The negative damping is related to the imaginary part of the direct outer modulation DCFC.

The positive damping is believed to cause the process damping effect and is determined by the relief angle of the tool as described above. The positive damping relates to the imaginary part of the direct inner modulation DCFC. Tests were carried out on a lathe to determine the process damping coefficients and wavelengths for specific materials by cutting in an uncut groove to ensure that only the inner modulation effects were measured.

The concept of DCFC's led to an understanding of the causes of self- excitation and damping in the milling process but they are not directly applied to the currently used stability models presented earlier in this chapter. The real part of the outer modulation also determines stability.

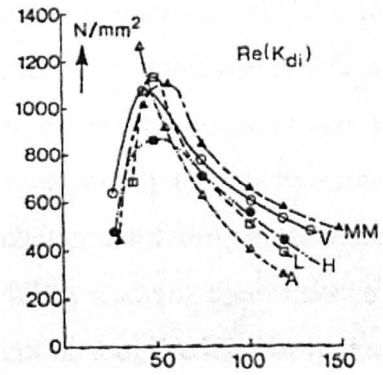

Fig. 2.14 DCFC vs Surface Speed. Taken from [70]

Efforts were made to measure these DCFC's using orthogonal cutting and an electrohydraulic excitation to give the regenerative effect. The tests were carried out on CK45N [110] and showed Im(Kdi) to be high at low speeds, representing process damping, reducing to a minimum at around 50m/min then increasing and levelling out at higher speeds. The various research laboratories struggled to obtain consistent data for these values. An alternative approach to understanding process damping will be discussed in Chapter 8.

2.4 Review of Current State of Research

2.4.1 Discussion

A detailed review of chatter theory and tool wear has been presented in this chapter. Much of the chatter theory relates to stability lobes and high speed machining and cannot be directly applied to titanium machining at lower surface speeds. When applied to high speed machining operations chatter theory yields significant gains, bringing difficult processes under control and increasing productivity. As outlined in chapter 1 a solution is sought for titanium milling operations, looking at alternatives to traditional stability lobes and shall be explored in the next section.

Tool wear, its mechanisms and causes have been widely studied for titanium machining. This is a vast subject and this chapter has presented a view of some of the important research to date. Radial immersion and surface speed are identified as having a dominant impact on max tool temperature and tool wear. Tool geometry is also a key factor, but in some cases the geometry requirement for extended life may counter those for stable milling. This is an example of the two fields coming together

and tool geometry shall be considered with relation to chatter stability in this thesis as much has already been researched and documented with relation to tool wear. The research into tool wear is often carried out in isolation from research into vibration, occasionally leading to erroneous observations such as chip segmentation causing chatter and failing to recognise the occurrence of chatter during tool life studies. When studying the influence of cutting parameters such as surface speed and depth of cut on tool life it is likely that chatter will be encountered at some point and should be recognised as an anomalous result. A thorough understanding of chatter along with tool wear mechanisms is essential for a comprehensive approach to titanium milling. In titanium machining it is proposed that neither dynamics nor tool wear can be studied in isolation as both can limit the process and have a strong influence over the other. The limiting surface speeds that are enforced by excessive tool wear mean that the stable regions for milling, available for higher speeds, cannot be used. The level of tool wear means that stable milling is limited to the slow process damped speeds or very low depths of cut. The stability lobe theory applied to high speed milling states that pockets of stable milling occur at tooth passing frequencies approaching the dominant modal frequencies of the tool [100]. These stable areas become smaller at lower spindle speeds and eventually become ineffective. If tool wear can be controlled enabling faster spindle speeds then greater advantage can be taken of stability lobes and structural modes can be avoided. Chatter and vibration in the milling process leads to excessive tool wear and chipping of carbide tools. In order to maintain acceptable tool life it is essential that stable milling conditions be maintained.
The studies of tool wear mechanisms and chatter in titanium machining have always been carried out in isolation. A lack of understanding of chatter theory can mislead the research findings. Some examples are listed below.

- Motonishi [34]claimed to have found force fluctuation from chip segmentation to correspond to the chatter frequencies, it is likely that he was picking up forced vibration rather than chatter. The chip segmentation frequency is a constant for a given set of parameters and cannot fall into the unstable phasing that leads to regenerative chatter.
- Observations where a change in alloying elements or material condition lead to chatter are likely to be due to a change in the cutting force coefficients

rather than directly related to the chip segmentation. Feed per tooth can also influence the cutting force coefficients.

- Tlusty claimed that feed reduces stability for milling but increases stability for turning [70], the influence of feed per tooth on stability in milling will be examined in chapter 5. An increase in feed per tooth will increase the bending moment on the bearings and at the spindle toolholder interface. Smith [107] showed that certain toolholder interfaces lose stiffness with increased bending moment and this can lead to a high feed per tooth reducing the system stability and inducing chatter.
- The influence of chatter on tool wear is often misunderstood, chipping being a common symptom of chatter. Kitaura [111] found that edge chipping was eliminated by increasing the feed per tooth from 0.05 mm to 0.08mm, it is likely that this increase in feed eliminated instability.
- Ber & Kalder [112] found that a honed edge reduced chipping and that chipping was more common on new tools. This could be as a result of micro burrs causing stress raisers but it is also likely that the honed edge reduces the sharpness and increases the process damping effect thereby eliminating chatter and chipping. This effect is common in new tools as they 'bed in' (chapter 5).
- Chatter stability should be ensured before embarking on any tool life tests or cutting force measurements. Observations within the literature review with regards to tool geometry also neglect certain aspects related to stability. The research relating relief angles to tool life focus only on the reduction in adhesion and friction and the issues of edge weakening. There is little direct evidence in the literature on the influence of rake and relief angle on tool stability and this will be explored in chapter 5.

2.5 *Research Areas*

2.5.1 Mapping of Research Areas

The mind map overleaf outlines some of the key factors limiting performance on any machining process. There have been great advancements in all these fields of knowledge and all are critical in controlling and optimising a machining process.

From the mind map, chatter and tool wear are taken as being the critical constraints in the titanium milling process, with tolerance and integrity to be taken as a qualifier for any change in parameters. Opportunities to advance the understanding in these areas to develop a generic titanium milling strategy are explored. Figure 2.15 demonstrates the possibilities to operate a stable milling process based upon the established milling stability theory outlined in this chapter.

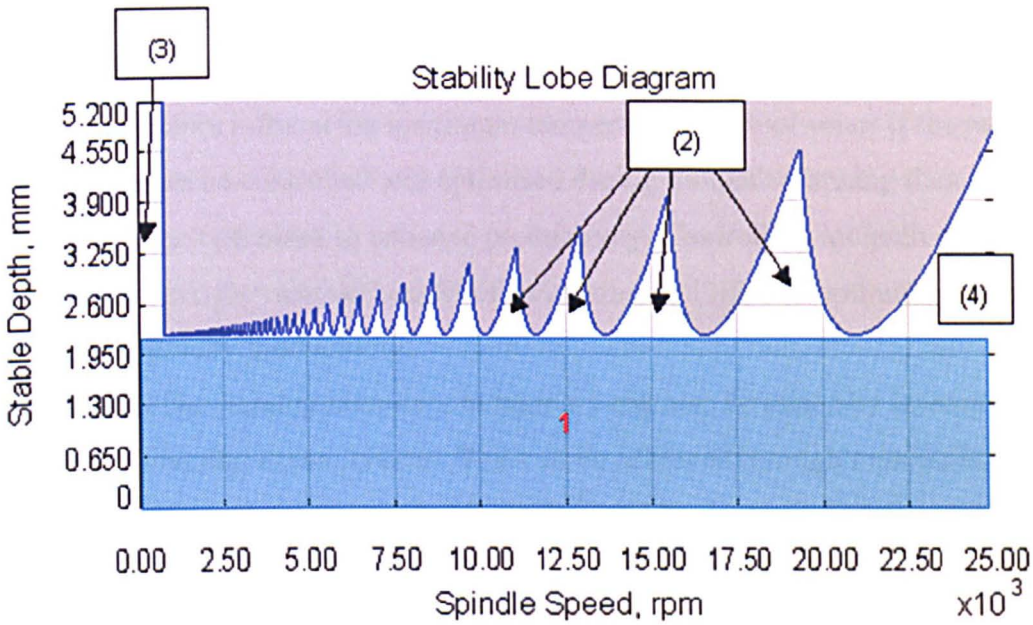

Fig.2.15 Regions of milling Stability

The regions in figure 2.15 represent the following:

Region 1 Below limit of stability for system – All speeds stable (proportional to dynamic stiffness of system)

Region 2 Stable lobe – tpf and f_n in phase – deep stable cuts

Region 3 Process damped region – Surface speed (Vs) low relative to f_n – deep stable cuts

Region 4 'Over the last lobe' – tpf high relative to f_n, stable machining

A stable milling process must lie in one of the 4 zones demarked in Fig2.15 and as tool wear in titanium milling becomes excessive at high surface speeds then regions 2 & 4 are often out of reach. To enhance titanium milling stability and productivity the objective must be to reach regions 2 & 4, raise the $b_{limcrit}$ thereby expanding region 1, or extend region 3 by increasing the process damping zone. The challenges and potential solutions for each of these regions are now explored.

Region 1

Problem- Region 1 is typically unproductive due to the high cutting force coefficients of titanium and the low depths of cut attainable without lobes. This region is often utilised by taking light radial depths of cut, thereby increasing Blim, but any increase in axial depth of cut will quickly induce chatter.

Proposal 1- It is possible that this could be optimised through ***toolpath strategies*** ensuring constant radial immersion, thereby limiting the maximum stable depth of cut. The research into tool wear mechanisms identifies surface speed and radial immersion as critical factors influencing maximum temperature and tool wear. If the radial immersion can be controlled and optimised during toolpath planning then surface speeds may be optimised to enhance productivity. Controlling toolpath strategies could then have the twofold benefit of increasing tool life and optimising axial depth of cut and thereby productivity.

Proposal 2-The stability boundary in region 1 can also be raised by interrupting the unstable phase that causes chatter. This can be achieved through manipulation of the spindle speed or the tool geometry. Anecdotal evidence suggests that ***special tool geometries*** can be used to raise the limiting depth of cut (Region 1) and manipulate the stability lobes (Region 2) but other than variable pitch end mills very little published data exists. It is possible that increased stability could be demonstrated through utilising tools with variable pitch and helix and that any advantage could be optimised through accurate modelling of the tool stability.

Region 2

Problem- Region 2 is the focus of most of the research carried out within the field and is only attainable when the tooth passing frequency approaches the dominant natural frequency of the system. Due to the tool wear issues detailed in this chapter such spindle speeds are not achievable unless the dominant frequency of the system is a low frequency structural or part mode.

Proposal- This means that research is required in the field of tool geometry and coatings to increase the practical surface speed range of milling cutters in titanium machining. Increasing surface speeds through tool development is a broad research topic with a great deal of attention from the research community and as yet no significant breakthroughs have been made beyond the introduction of tungsten carbide. This will not be a target of this thesis as it is felt that greater impact can be made elsewhere.

Region 3

Problem-Region 3 is the low speed process damped region and is where much titanium machining is carried out. Due to the low surface speeds required to employ process damping, and the lack of understanding of its boundaries and mechanisms, the process damping region is typically unproductive. Process damping is related to the surface speed and dominant natural frequency by a value known as the critical wavelength (λc). Little is known about this value or how it can be influenced.

Proposal- It is possible that if the value of λc can be increased and accurately predicted, the stable ***process damping*** region can be increased. If the ***system dynamics*** can also be manipulated to have only high frequency dominant modes then the stable spindle speed range may be increased to comprise the full range of operable surface speeds, making tool wear once again become the critical process constraint.

2.5.2 Toolpath Strategies

The research has outlined that radial width of cut, surface speed and chatter have a strong influence on tool life during titanium milling. During machining of pockets it is difficult to accurately control the parameters that influence tool life and stability and these are often neglected leading to poor productivity. Further research is required to establish the influence of controlled toolpath strategies where the focus is to maintain a constant radial immersion on the approach to pockets. Studies [113] at Boeing demonstrated the effects of increased radial immersion on tool wear and the potential benefits of carefully selected tool paths. Tests were carried out comparing tool life after cutting a circular pocket to cutting the equivalent perimeter of a square pocket containing corners. The tests showed that for the circular pockets the constant radial depths of cut exhibited low tool wear. For the square pockets a radial depth of cut was reached above which tool life began to improve rather than continue to decrease.
For each different radial immersion the same size of pocket was removed both for the square and the circular pockets. In the case of the square pockets, increased radial immersion meant fewer steps from the centre to the periphery of the pocket. Consequently the fewer steps that were taken, the fewer corners were machined and a certain radial immersion is reached whereby the reduction in corner milling outweighs the increased immersion throughout the rest of the cut. The research also demonstrates that the stability of a process is related to the area of the cut (bx a_e). That is to say that for a set number of cutting teeth, as the radial depth of cut increases the maximum

stable axial depth of cut will decrease. Developing pocketing strategies where the radial depth of cut is a constant should therefore maximise the stable axial depth of cut that can be achieved.

2.5.3 Special Tool Design

Altintas states that while stability of milling at high speeds is well understood and applied within industry, low speed milling and process damping require further research. It is suggested that solutions such as variable pitch cutters must be used in the low speed region at the expense of tool life Altintas[114],Budak [115],Vanherck [92]. If the regenerative effect can be broken up by disturbing the unstable phasing that supports chatter then depths of cut may be increased outside of the stability lobe range for a standard pitch tool. Waveform cutters and variable helix cutters are available on the market and anecdotal evidence suggests that they result in much greater stability and cutting performance than standard end mills. Waveform cutters and variable helix end mills have a pitch angle that varies from tooth to tooth and also up the length of the helix. No models exist for these tools and although good results are purported, the tool designs cannot be modelled or optimised.
Altintas acknowledges that solutions are not currently available for non-linearities due to change in machine tool FRF with position, variable cutting force coefficients due to process damping or variable chip thickness or cutting action. To achieve predictable enhanced stability when milling titanium a study into the performance and modelling of variable helix end mills would be beneficial.

2.5.4 Process Damping

While stability of milling at high speeds is well understood and applied within industry, low speed milling and process damping require further research [99]. Process damping of dominant tool modes allows for stable milling. In order to know the limiting surface speeds for which process damping of a mode will occur, the critical process damping wavelength for a specific tool/ work material combination must be empirically deduced. Once this is known the max spindle speed at which process damping will occur can be predicted for a given mode[1]. Therefore the higher

---

[1] *The process damping cut-off point is not a straight line and is actually a curve defined by the damping coefficient. To assume a straight line is a simplification and when operating at spindle speeds near to the process damping border the process damping effect may be seen to disappear with increase in depth of cut*

the frequency of the dominant modes, the higher the maximum stable surface speed for that mode.

As surface speed is proportional to the diameter of the end mill the MRR dictated by this limiting surface speed for a stated axial depth of cut (b), radial immersion ($I=a_e/D$) and feed per tooth (ft), will be the same for all tool diameters. In cases where part stability or structural stability inhibit high Metal Removal Rates (MRR), reducing the area of the cut will avoid chatter. When comparing a cutter diameter D to D/2, the smaller cutter can run at twice the spindle speed and feed rate for the same feed per tooth and surface speed. The smaller diameter cutter with an equivalent radial immersion (ae/D) can achieve a higher axial depth of cut and MRR without inducing chatter. This could therefore be an effective technique for optimising stability. Further benefits to optimising process damping and set-up for small tools can also be explored.

It is generally understood (Tlusty & Ismael [71]) that introducing a flexible mode to a system will influence other modes within the transfer function of that system. If the mode is flexible and high frequency relative to the other modes then the position of these modes on the y axis of the real plot will be raised. This is an important detail when considering the dynamic stability of a machining system as only modes with a negative real part can cause instability [69]. If the magnitude of the introduced mode is sufficiently high then all other modes, of lower frequency, may be pulled into the positive region of the real plot and will therefore become stable. Applying this theory to a tool holder/ spindle system, the addition of a flexible tool mode may stabilize all the mid range tool holder and spindle modes. This stabilizing effect comes at a price as the introduction of such a flexible mode would dramatically decrease the $b_{limcrit}$ level when considering the stability lobe plot. However if the frequency of this mode is high enough to be process damped, then all tool / tool holder/ spindle modes may be stabilized for the desired spindle speed.

This may be achieved by carefully selecting tool-holders, end mills, and end mill extensions. The smaller the diameter of the end mill the greater the stabilizing effect. Increasing the extension of a tool will decrease the dominant natural frequency but may raise the mid-range modes higher on the real plot. This creates possibilities for further research and useful strategies for milling titanium.

2.6 Research Hypothesis

Within this chapter an extensive review of titanium milling and machining dynamics has been carried out. It has been identified that these two areas of research, although typically addressed independently can have a significant influence on one another. Some of the key critical constraints on the titanium milling process have been identified from the current research to form the foundation of a holistic machining strategy for titanium. Three areas in particular have been identified as needing further research and these have been explored above. The three areas where research is lacking and a serious impact can be made are; toolpath strategies, process damping and special tool design. From the arguments developed within this chapter the following research hypotheses have been developed:

1 ***Tool life and chatter in titanium milling can be controlled through effective toolpath selection***

2 ***Variable helix end mills can provide enhanced stability and productivity and can be modelled using a frequency domain solution***

3 ***Process damping can be controlled and utilised to optimise milling stability through control of cutting parameters, tool geometry and tool set-up***

The following chapters will investigate these hypotheses with analytical and experimental techniques.

3 TOOLPATH STUDIES

3.1 Introduction

This chapter examines empirically the hypothesis presented in chapter 2 that significant gain in tool life and stability can be made to titanium milling operations through control of radial immersion and toolpath strategies. The background to the chapter revisits the issues pertaining to radial immersion in pocketing.

Before engaging in an empirical study, the proposition presented in chapter 2 that radial immersion has a strong influence on tool wear through raising peak temperatures is first explored using an established thermal friction-slider model from Stephenson, Shaw [ref]. The model is developed to consider the effects of helix on the thermal flux calculation and loading area. Results are presented from the model that support the proposition that radial depth of cut has a strong influence on peak temperature and is therefore likely to accelerate diffusion, attrition and thermo-mechanical wear mechanisms. Having explored analytically an observation from the lit review, an empirical pocketing study is now undertaken using the minimum and maximum radial depths of cut explored with the thermal model.

A square pocket is taken as the standard for the study, being representative of a typical aerospace weight reduction pocket. A standard pocket strategy is selected to represent current practice with the tool gradually stepping out in 3mm steps from the centre to the perimeter of the pocket. Four alternative toolpath strategies are presented graphically and explored experimentally, each aimed at controlling a constant radial immersion. A stability lobe analysis is undertaken for each of the tools and the results are displayed for a constant 3mm depth of cut and a maximum 11mm radial depth of cut, demonstrating that if the radial depth of cut can be controlled that axial depth of cut and productivity can be greatly enhanced. Each of the toolpaths are then evaluated, measuring flank wear under controlled conditions. The tool wear results are displayed and discussed demonstrating half the flank wear on the pockets with controlled radial immersion as compared with the standard whilst increasing cycle time by less than 10%.

The results are compared against predictions from a commercially available Finite Element based soft ware package (Third Wave Systems Production Module) that predicts cutter loads and calculates radial engagement throughout an NC toolpath. The results from the TWS simulation show spikes in radial engagement and force for the standard pockets and show a smooth cutter load for the best performing pockets.

This chapter contributes to the field of knowledge by experimentally demonstrating toolpath techniques that can control radial immersion and thereby greatly enhance both tool life and productivity for titanium milling. The strategies are particularly relevant to titanium milling as a reduction in radial engagement time and the thermal loading cycle controls the high peak temperatures seen in the titanium chip generation process, and maximises the axial depth of cut that can be taken without chatter despite high cutting force coefficients for titanium. These strategies have since formed part of a best practice titanium milling guide for Sandvik Coromant. The hypothesis that toolpath strategy can be controlled to reduce tool wear and optimise productivity is empirically supported.

3.2 Background – Corner Immersion

As outlined in chapter 2, radial immersion has been identified as having a strong influence on tool life when milling titanium and has been identified as one of the factors that can be readily controlled when programming titanium milling toolpaths. As titanium components become more common in aero-structural applications so do the occurrence of weight reduction pockets. Milling titanium pockets provides a challenge when programming toolpaths as it is difficult to maintain a constant radial immersion when approaching a corner (*Fig 3.1*). The increased radial immersion in corners is detrimental to tool life and can cause chatter. Smith [116] demonstrated that in aluminium pocketing routines, the maximum stable axial depth of cut could be increased through control of the radial immersion and the same applies to titanium milling.

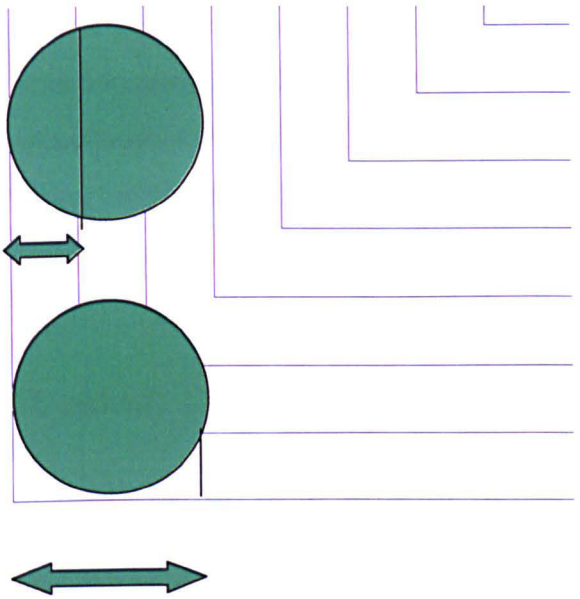

Fig. 3.1 Toolpath demonstrating corner immersion

Most CNC machines will experience a brief dwell in a 90° corner due to the change in direction and subsequent acceleration and deceleration required from the drives. This dwell will produce a chip thinning effect which can in turn lead to an increase in cutting force coefficients (chapter 4). As the chip reduces in size the chip mechanics change and the tangential frictional forces can become dominant. As the chip thickness becomes close to the nose radius of the cutting tool a ploughing action rather than a clean shearing action occurs causing frictional heat and accelerating tool wear. As well as accelerating wear the increased cutting force coefficient can induce chatter.

Summary of problems with corners:

- Increased radial immersion – reduces tool life.
- Increase in size of cut can cause chatter.
- Reduction in velocity leads to an increase in cycle time and can cause dwells in corners.
- Reduction in chip thickness due to dwell can increase wear and induce chatter.
- Increase in effective chip thickness due to tool centre feed control can overload the cutting edge and create high bending moments on spindle bearings and gauge line.

With the above considerations there are large gains to be achieved from controlling radial immersion during pocket milling, impacting on stability, tool life and cycle time. In this chapter a study is outlined to evaluate the effect of toolpath programming on controlling radial immersion and improving productivity through increased tool life and MRR.

3.3 Toolpath Strategy Investigation

3.3.1 Consideration of Thermal Effects

Constant radial immersion

A number of studies have indicated that tool life in titanium milling is strongly linked to radial immersion. Danly and Smith [117]investigated the effect of immersion on titanium milling and found that for passes of constant immersion, tool life dropped as the radial immersion was stepped up. It is believed that one of the factors leading to the decrease in tool life is an increase in maximum temperature at the cutting surface, [36],[37]. Initial studies suggest that the time in the cut relates to the peak temperature [35] and therefore would have a stronger influence than axial depth of cut. It has been demonstrated that for intermittent cutting the peak temperature rises to a maximum and then plateaus. This maximum temperature was shown to increase as the radial immersion is increased. Using a mathematical model based upon Shaw's friction slider [10] a study is undertaken here to predict the influence of radial immersion on cutting tool temperature. This model is designed to calculate the peak temperature for a set of constant input values and is used to examine the influence of milling parameters on peak temperature. In order to study the force loading on the cutting tool during the toolpaths explored within this chapter the Third Wave Systems Productivity module is used as this software has the capability to model an entire NC toolpath and predict instantaneous loads. The Third Wave Systems software generates plots that support and explain the experimental results but the derivations behind the software and the study of key parameters on tool life are not published therefore the Stephenson and Ali model [118] developed here offers a useful insight into the impact of key parameters such as radial immersion on peak tool temperature.

3.3.2 Thermal Model of the Milling Process

The model detailed here is developed from Stephenson's thermal model [118]. Stephenson took the friction slider model initially developed by Carslaw and Jaegger [119] and later developed by Shaw [10] to examine milling temperatures in interrupted cutting. It is assumed that the tool is a semi-infinite corner experiencing a square wave heat loading and cooling cycle. The model is based on a constant radial depth of cut and neglects any heat build up in the part itself. The manner in which the level of thermal flux (q_c) is determined is critical as will be demonstrated below. The model considers only thermal loading and there is no inclusion of mechanical or metallurgical aspects such as, chip curl, flank chip interface, chip segmentation and alpha-beta phase change. Initially the governing equations of Stephenson's model are presented in its original form, then with some modifications to allow an assessment of the impact of radial depth of cut and helix.

Stephenson & Ali Model [118]

Assumptions;

A The cutting cycle may be modelled as a semi-infinite rectangular corner experiencing a time varying heat- flux.

B The thermal properties of the tool are independent of temperature.

C Heat radiation may be neglected.

D Temperature at t=0 and t=∞ throughout the body treated as zero.

E All other boundaries are insulated.

F All energy consumed in the cut is converted to thermal energy

G Ratio of thermal conductivities between work piece and tool determines the heat seen by the tool.

Governing equations and boundary conditions;

$$\nabla^2 T_{emp} = \frac{1}{\alpha_s}\frac{\partial T_{emp}}{\partial t} \qquad (3.1)$$

$$-k_w \frac{\partial T_{emp}}{\partial z} = Q(x,y,t) \qquad z=0;\quad 0 \le x \le L_x, 0 \le y \le L_y \qquad (3.2)$$

where $L_x L_y$ are the dimensions of the heat source to be examined in this study and $Q(x,y,t)$ is the source of the heat flux. k_w is the thermal conductivity.

A spatially uniform source may be considered whereby the heat flux varies only with time in a linear relationship;

$Q(x, y, \tau) = q(\tau)$ *(3.3)*

Now considering an instantaneous heat source over the area $0 \le x \le L_x, 0 \le y \le L_y$, the average temperature over the heat source is given by;

$$T_{AVE}(t) = \frac{\alpha_s}{2 \cdot \sqrt{\pi \cdot k_w \cdot L_x \cdot L_y}} \int_0^t \frac{q(\tau)}{D} \cdot T_M(L_x, L_y, D) q(\tau) dy dx d\tau \qquad (3.4)$$

where

$$T_M(L,D) = 2L erf\left(\frac{2L}{D}\right) + \frac{D}{\sqrt{\pi}}\left[\exp\left(\frac{-4L^2}{D^2}\right) - 1\right] \qquad (3.5)$$

where L is length of uniform line heat source at time τ.

The heat input to the tool is modelled as a square wave function for interrupted cutting;

$$q(\tau) = \begin{cases} qc, s(\tau_1 + \tau_2) \le \tau \le s(\tau_1 + \tau_2) + \tau_1 \\ 0, s(\tau_1 + \tau_2) + \tau_1 \le \tau \le (s+1)(\tau_1 + \tau_2) \end{cases} \qquad s=0,1,2,\ldots \qquad (3.6)$$

where; q_c is the average heat flux entering the tool from the tool-chip contact during cutting. τ_1 is the time period that the tooth is in contact with the cut and τ_2 is the time period that the tooth is out of the cut. Therefore $(\tau_1 + \tau_2)$ is the time for one rotation of the cutter about its axis and is equal to;

$$(\tau_1 + \tau_2) = 60/n \qquad (3.7)$$

For a constant radial depth of cut (a_e) and cutter diameter (D) ;

$$\tau_1 = \left(\frac{\beta}{2\pi}\right) \cdot \frac{60}{n} \quad , \quad \tau_2 = 60/N - \tau_1 \qquad (3.8)$$

where χ the angle of immersion is given by;

$$\chi = \cos^{-1}\left(\left(\frac{D}{2} - a_e\right) \Big/ \frac{D}{2}\right) \qquad (3.9)$$

The heat flux (q_c) is calculated from the power consumed by the cut;

$$P = MRR \cdot K_s = (a_e \cdot b \cdot n \cdot m \cdot f_t) \cdot K_s / 60 \qquad \textit{(3.10)}$$

Due to the high specific heat and low thermal conductivity of titanium, relative to the carbide tool, most of the heat generated in the cut is transferred into the tool. However a proportion of this heat energy will be translated into the chip and the work piece. The ratio between the thermal conductivity of the work piece and the tool materials determines the percentage of the thermal energy that is transferred into the tool.

k_{wt} (thermal conductivity of titanium) = 7J/(sec m °C)

k_{wc} (thermal conductivity of carbide) = 75J/(sec m °C)

$$\text{Thermal energy ratio}_{(\text{carbide})} = \left(1 - \left(\frac{k_{wt}}{k_{wc}}\right)\right) \cdot 100 \ = 91\% \qquad \textit{(3.11)}$$

The average heat flux (q_c) can therefore be represented as the power per unit area seen by the tool surface;

$$q_c = \left(1 - \left(\frac{k_{wt}}{k_{wc}}\right)\right) \cdot \frac{(a_e \cdot b \cdot n \cdot m \cdot f_t) \cdot K_s}{60 \cdot L_x \cdot L_y} \qquad \text{MW/m}^2 \qquad \textit{(3.12)}$$

The dimension L_y is dependent upon the axial and radial immersions and the helix angle of the tool (a_e, b, ϕ). L_y is measured along the length of the cutting edge with Lx being the width of the contact area perpendicular to the cutting edge.

$$\text{For } b < \frac{a_e}{\tan\phi} \quad ; \quad L_y = \frac{b}{\cos\phi} \qquad \textit{(3.13)}$$

$$\text{For } b > \frac{a_e}{\tan\phi} \quad ; L_y = \left(\frac{a_e}{\tan\phi} \Big/ \cos\phi\right) \qquad \textit{(3.14)}$$

The dimension L_x is dependent upon the size of the tool chip contact area. This has been empirically observed as 1mm, *L_x is therefore taken as 0.001m.*

For given cutting parameters and tool parameters; (a_e, b, f, D, n, ϕ) we can determine the variables (q_c, $\tau_1\tau_2$, L_x, L_y) that allow us to determine the variation in T_{AVE} with time.

For the heat input (Equation 3.4) the expressions of temperature reduce to sums of time integrals over successive heating intervals. For a chosen time step (dt) the

integrals are calculated at each time step over all completed heating cycles using composite Gauss quadrature integration.

Modelling of Constant Radial Immersion

The standard tool path (Fig.3.10) used for experimentation in the next section has a radial immersion of 3mm along the straight, increasing to 11mm on the corners. The model developed by Stephenson uses $\tau 1$ and $\tau 2$ values to denote the time periods that the tool experiences thermal loading, and cooling respectively. $\tau 1 + \tau 2$ are equal to the time period of one revolution of the cutter about its axis (Equation 3.8). The model computes a number of cycles (N_c) of time $\tau 1+\tau 2$, each iteration using the tool temperature of the previous computation as T at time dt=0. The model is thus designed to determine tool tip temperature for a constant radial immersion and chip load. The heat flux is derived for this first iteration of the model as described above. In this format the Stephenson and Ali model can be used to illustrate the maximum tool tip temperature reached for different radial depths of cut.

This model has been developed to examine the influence of milling parameters on peak temperature for a range of toolpath studies aimed at optimising productivity and tool life for titanium milling. The five toolpath strategies that are being studied are detailed later in this chapter, the benchmark strategy starts from the inside of a square pocket and gradually opens out the pocket stepping out in 3mm radial passes. As each pass reaches a corner the effective radial engagement increases from 3mm to 11mm. The thermal model is used here to study the influence of the key process variables on peak temperature and compare the results for the 3mm radial immersion and the increased engagement of 11mm in the corners. The benchmark data for the simulation is therefore taken for a climb milling cut in titanium with 3mm a_e, 5mm b, 0.05mm fpt, 1750 rpm with the results shown in Fig. 3.2. The plots of temperature with time give a good indication of thermal shocking that is seen during the milling process and the peak temperatures seen. Although the results are not verified experimentally in this thesis, Stephenson's model in this form showed good correlation with empirical measurement and the results are taken here to give a qualitative assessment of the influence of key parameters on temperature.

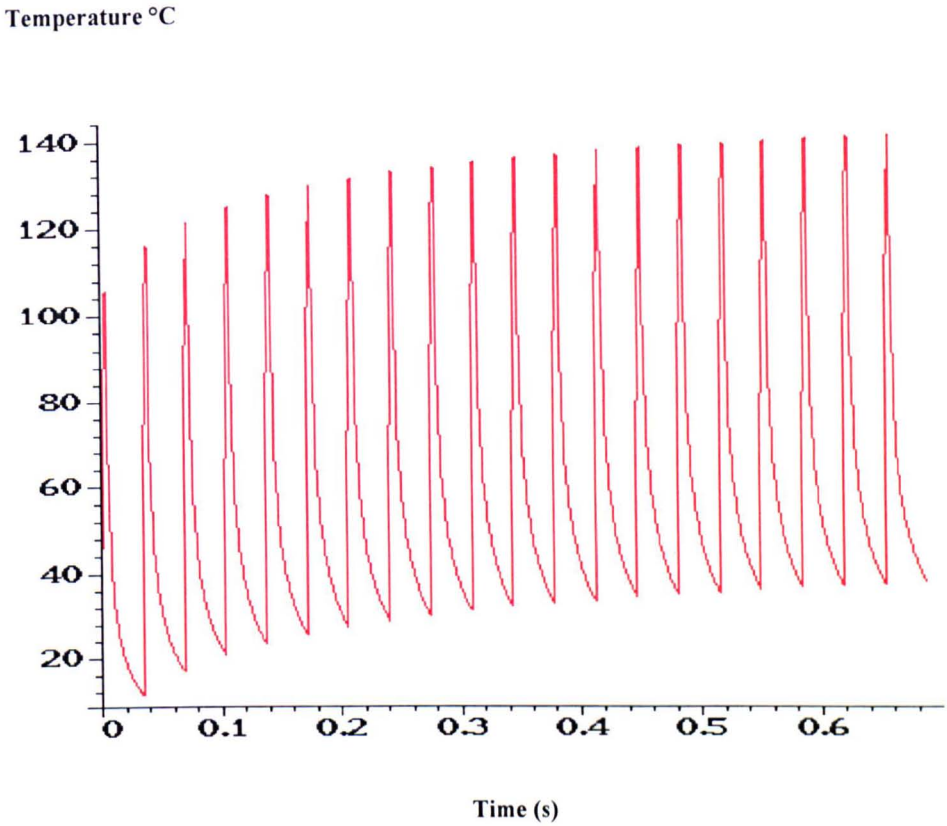

Fig. 3.2. Results from original model for ae=3, b=5, ft=0.05, n=1750, m=3

If the radial depth of cut is changed to 11 mm, the maximum immersion experienced during milling of the corners on the standard tool path then the results shown in Figure 3.3 are obtained. As expected the maximum temperatures are increased. Figures 3.2 and 3.3 indicate that the temperature of the tool increases with radial depth of cut and an increased rate of tool wear would therefore be expected.

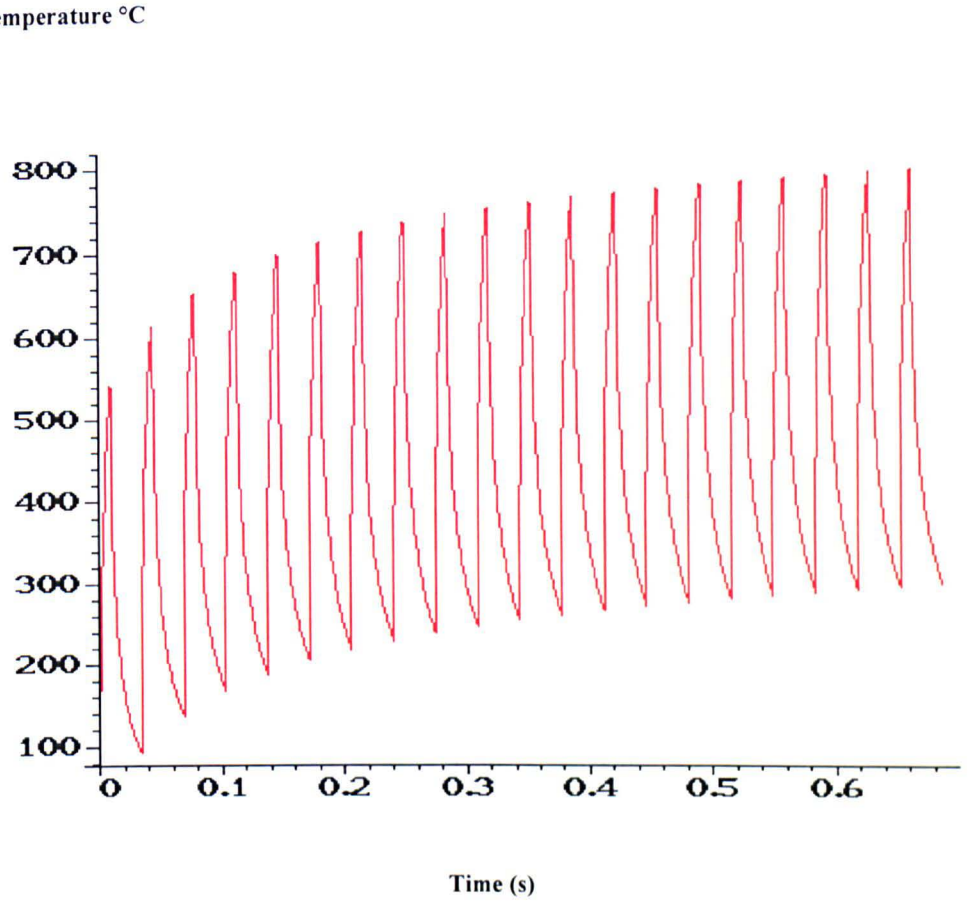

Fig. 3.3 ***Results from original model for ae=11, b=5, ft=0.05, n=1750, m=3***

Influence of cutting parameters (Limitations of initial model)

In order to model the maximum tool tip temperatures reached in the standard tool path it is necessary to vary the radial depth of cut seen by the tooth as it approaches and exits the corner. The values of τ 1 and τ 2 can be calculated for any given radial immersion and a relationship is required between radial immersion and time. Modification to the model is required such that $\tau 1$ and $\tau 2$ may vary with time. The model will also show the maximum temperatures reached when either radial depth of cut or feed per tooth are increased.

It is essential to consider the way in which q_c is calculated in this case. With the original format shown above, a 50% increase in either chip load or axial depth of cut will have the same effect on the maximum temperature. With the model in this form, increases in radial depth of cut will show the greatest increase in maximum temperature (relative to other input parameters) as this will proportionally increase qc

and also increase the heating period τ_2. An increase in radial immersion therefore has a twofold impact on peak temperature. The model has been used to study the influence of key parameters on peak temperatures in titanium milling. In each case a single parameter was increased by 50% from the standard in Fig3.2. and the peak temperature after 0.4 seconds recorded. The peak temperatures are compared against the standard set of parameters and represented in Fig 3.4.

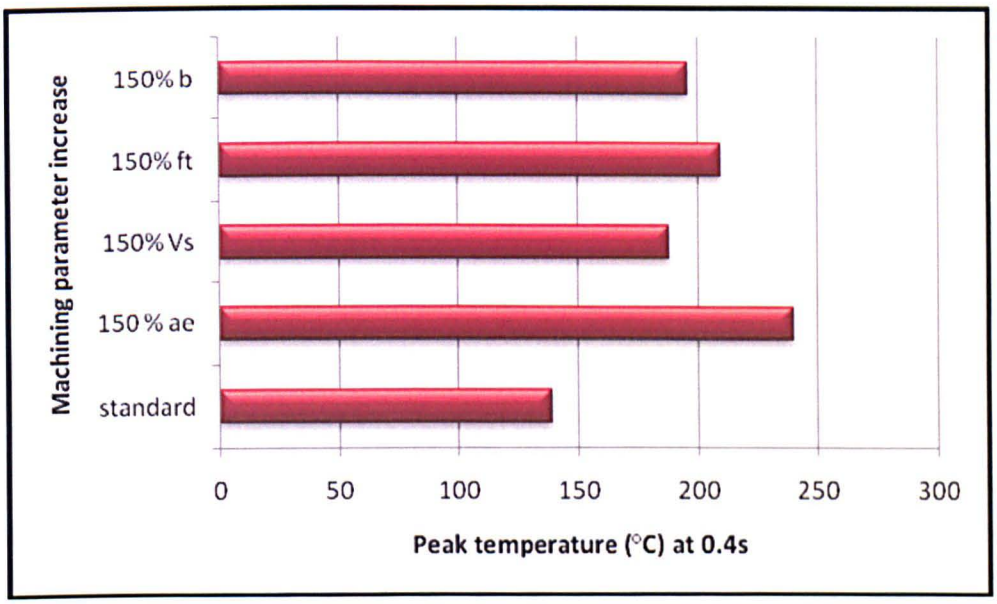

Fig.3.4 Peak temperatures as predicted after 0.4s varying key parameters by 50%

For a 50% increase in spindle speed we will again see a proportional increase in qc whilst the heating and cooling cycles τ_1, τ_2 will be shortened.

The model suggests that spindle speed (Vs) increases have a lesser effect on tool temperature than radial immersion (a_e) and chip load (f_t) increases. This is due to the decrease in heating and cooling cycle times as predicted by Palmai [37] . For a 50% increase in chip load there will be a 50% increase in qc. The plot indicates that chip load variations are more significant than spindle speed but less so than radial immersion.

For a 50% increase in axial depth of cut (b) there will be a 50% increase in power but the surface area of contact will also increase. The increase in b increases the area over which the flux is calculated, so the max temperature computed in the model is less than that for an equivalent increase in chip load. The increase in temperature with radial immersion as computed by the model is as expected. The increase in temperature with spindle speed is believed to be more than predicted. This may be due

to an over-simplification of the heat flux calculation, also the effects of friction and other phenomena should be considered.

Additional considerations

Chip thickness:

Increasing chip load increases the instantaneous cutting force on the tooth and can consequently lead to a greater likelihood of tool failure through other wear mechanisms such as chipping. Increasing chip load will also change the dimensions of the chip and affect the tool-chip interface, changing the size of Lx and maybe altering any thermal loading through friction.

Radial depth of cut v axial :

A Boeing study [113]stated the assumption that axial depth of cut does not have as much influence on tool wear as radial depth of cut. The thermal model and the results plotted in Fig. 3.4 support the assumption as the radial depth of cut relates to both the heat flux and the time in the cut.

For a helical end mill, an increase in radial depth of cut may see a greater increase in L_y than a proportional increase in axial depth of cut. Although an increase in b means that more of the flute length will experience the heating cycle throughout the cut, the instantaneous dimension L_y is more sensitive to changes in radial depth of cut. The fact that the leading portion of the edge L_y will enter and exit the cut before the trailing edge due to the helix angle is neglected in this model. It is assumed that the whole portion L_y experiences simultaneous heating and cooling.

The model is initially written with a straight edged insert in mind so the effects of helix are neglected. Also neglected is the fact that for $b > \frac{a_e}{\tan\phi}$, a portion of the flute length trailing L_y will experience the heating cycle. If we reject the idea of the instantaneous value of L_y and take L_{yt} to be the total length of the flute to be engaged in the cut throughout a cycle then we have $L_{yt} = \frac{b}{\cos\phi}$ for all values of a_e. Now this length L_{yt} is not entirely engaged in the cut at any given time but it is the length of flute that experiences the flux during the period of τ 2 and it is over this length of flute

that the power P consumed in the cut is generated. For large b/a_e, Ly_t is much greater than Ly and could make significant difference to the computation of qc and T_{AVE}.
To demonstrate the effect of interchanging L_y and L_{yt} the original computation has been made again but this time with an axial depth of cut (b) of 15mm (Figure 3.5).
For the new parameters we have;

b	15 mm
n	1750 rpm
a_e	3mm
L_{yt}:	17.3205 mm
L_y:	6 mm
τ_1:	0.0045s
τ_2:	0.0298s
qc_{Ly} =	71400 kW/m^2
qc_{Lyt} =	2.4734e+004 kW/m^2

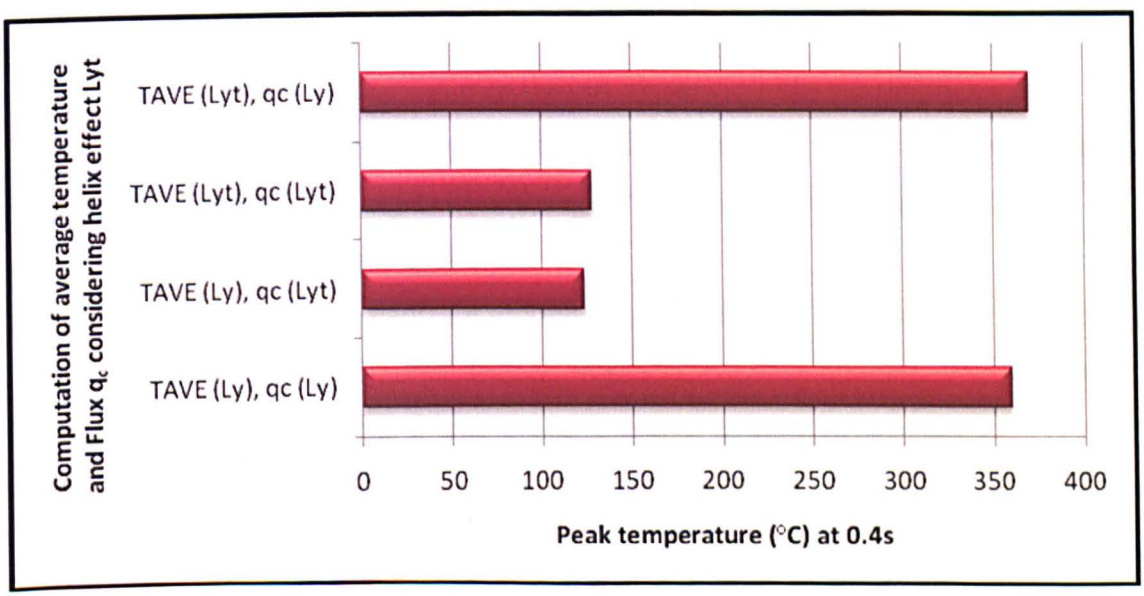

Fig.3.5. Study of impact on length of flute contact on flux and thermal loading calculation.

Using the initial parameters but substituting L_{yt} t for L_y in the computation of qc (Equation 3.13) a very low peak temperature is predicted.
As above but substituting L_{yt} for L_y in the computation of T_{AVE},(Equations ,3.2,3.5,3.6) a slightly higher peak temperature is predicted but still a huge reduction from the standard model from 360°C to 130°C. The length L_{yt} is the total length that experiences the heat cycle from the corner (as modelled) upwards.

If T_{AVE} is computed for L_{yt} and qc is computed for L_y then the results obtained show a slightly increased peak temperature to the standard.

It can be concluded that the model in the existing format is sensitive to changes in heat flux value but to a lesser extent the area to which the heat is applied.

A more accurate interpretation is to compute $qc_{(Ly)}$ for Power/ av no. of flutes in cut and use $qc_{(Lyt)}$ for the thermal loading function. The computation considers the area engaged in the cut at any given time and the total power generated in the cut. In relation to the power qc derivation shown earlier, the above derivation would lead to smaller values of qc for large radial immersion and high values of qc for slight radial immersion where there is not always a tooth in contact with the cut.

The effects of increased radial immersion shown with the original model will therefore be reduced. This is a more appropriate model as a_e will have a smaller impact on qc than b, the greatest influence on temperature of an increase in a_e is the increase in the loading and cooling periods τ 1 and τ2.

The time periods τ 1 and τ2 are calculated considering a single point on the perimeter of the cutter. Each point along Ly_t is in the cut for time τ 1 but the points are not instantaneously in the cut and experiencing the heat flux. The maximum length that may be loaded instantaneously is Ly although the location of the length Ly varies within the region Ly_t throughout the cut.

The model in this format is valid for modelling the spiral tool path and the rad-corn path presented in the experimental section where the radial immersion is kept constant throughout although some modifications are required to the flux derivation.

Modelling changing radial immersion

The time that the tooth spends engaged in the cut per cycle changes as the radial immersion of a cut changes. The level of heat flux experienced by the tool chip contact area also varies with radial immersion. The model must be altered to accommodate τ and qc values that vary with time.

Standard Toolpath

For corner milling, radial immersion can be assumed to increase linearly with time on approach to the corner and then decrease linearly on exit. The radial immersion at time t=0, t= ∞ will be the programmed immersion and the max radial immersion will be;

$$I = D/2\left(1-\cos\left(\frac{\pi-\chi}{2}\right)+2\sin\left(\frac{\chi}{2}\right)\right) \qquad (3.15)$$

where χ is a function of D and a_e as defined in (Equation 3.9)

The radial immersion will increase from a_e to I linearly over a time period equal to;

$(D/2+ a_e)$/feed *(3.16)*

(assuming that the previous pass was with the same tool radius)

Trochoidal

Stage 1

For a tool path following a trochoidal motion, the radial immersion varies from 0 to max programmed radial immersion (a_{emax}). This variation is assumed to be linear over a time period (t) of;

$0 < t < ¼ S$

where S is the cycle period for one revolution of a trochoidal pass.

Stage 2

The radial immersion then decreases from a to 0 over the time period;

$$¼ S < t < ½ S$$

Stage 3

The radial immersion remains at 0 for the time period;

$$½ S < t < S$$

at time t= S the time returns to t=0 and the cycle continues.

Summary of Thermal Model

There are some simplifications in the model as it does not consider the chip segmentation effect and is based wholly on continuous chip formation, however the trends are representative of those presented in the literature [43] and supports the proposition that radial immersion is a key variable influencing peak temperature. Stephenson showed good correlation with published temperature data for the original model [118] and the results are therefore taken to give a good representation of trends despite some simplifications. The model neglects the effect of helix on L_y but a brief study here suggested that although the thermal loading calculations change, the peak temperatures are not greatly influenced by helix angle.

The model also neglects the effect of chip thinning and increased frictional forces but provides an indicator and demonstrates that thermally activated tool wear is likely to be greater in cases where radial immersion is increased in corners of pockets.

Investigation into tool-wear through increased radial immersion

The Stephenson model that has been modified here shows some of the theoretical derivations of increases in temperature due to increases in radial immersion. The model suggests that radial immersion has the strongest influence on peak temperatures of all the cutting parameters studied, although simplifications seem to understate the influence of surface speed. The model has examined the proposition from the literature review that an increase in radial immersion influences tool wear through increase in peak temperatures. The next section of the chapter will examine five toolpath strategies to generate a square pocket to empirically evaluate the influence of radial immersion on tool wear. The standard toolpath serves as the benchmark whilst the other toolpaths are designed to reduce the impact of increased radial immersion in corners. A commercially available Finite Element based package, Third Wave Systems Production Module, is used to predict peak loads and immersion throughout each milling process. The Third Wave simulations calculate cutting loads and period of engagement of the cutting edge. The radial immersion predicted through Third Wave can be related to the temperature increases predicted for increased radial immersion with the thermal model presented in the early part of the chapter. The Third Wave model computes the load from an NC toolpath and therefore provides an appropriate means of estimating the influence of cutting conditions on load and temperature throughout the toolpath and can support the empirical findings. Dynamic stability can also be predicted for cases of constant radial immersion. The increased radial immersion on a corner means that the maximum stable axial depth of cut is reduced. Therefore by maintaining constant radial immersion the axial depth of cut may be optimised.

3.3.3 Experimental Design

Non Standard tool path programmes and trials

Tests carried out by Boeing [113]on equivalent square and circular pockets showed that tool wear was almost three times lower in the case of the circular pocket. It is believed that this is due to the increase in radial immersion when the tool enters a corner during the square pocketing routine. This is supported by the predictions with regard to thermal loading generated in the model presented in the previous section. The results of the Boeing experiments demonstrate that constant radial immersion is favourable to the increases in radial immersion experienced when milling a corner. As mentioned above, dynamic stability is predicted for cases of constant radial immersion. In the case where the tool path sees a change in radial immersion then it is the worst-case scenario for which stable cutting parameters are selected. This may mean that for much of the tool path the machine is running well below optimum parameters. For example a 3mm radial depth of cut may permit an 8mm axial depth of cut before chatter is induced, if the radial cut increases to 11mm in the corners then the maximum axial depth of cut that can be programmed for the entire pass will be less than 2mm. There are therefore multiple advantages in maintaining constant radial immersion in a tool path. The following toolpath study is proposed as a solution to the problem of increased radial immersion and cutter loading in pocket corners.
It is believed that the reduction in tool life for the square pocket is due to the increase in radial immersion when the tool enters a corner. In order to support this theory and find possible solutions to the problem, alternative toolpaths have been written for the machining of a 3.5" (88.9mm) square pocket. In all cases a 3mm radial and 5mm axial depth of cut is used with a 0.05mm feed per tooth (fpt). Screening tests showed a spindle speed of 1750 rpm and feed rate of 10.5 ipm (266.7 mm) to be dynamically stable and to give a reasonable level of tool wear, for purposes of both sufficient data points and titanium conservation.
For the cutting trials Robb Jack solid carbide end mills were selected with a TiN coating. The tools are described in Table 3.1

Material	Coating	Diameter	Helix angle	Rake angle	Relief angle	No of flutes
Carbide	TiN	19.05mm	35°	9°	11°	3

Table 3.1Description of cutting tools for pocketing trials

The tool geometries and coatings were selected to match the optimum used in the circular vs square pocketing trials undertaken by Stutzman et al [113]. It was found by Stutzman that although the TiN coating wore away quickly the overall performance with the above geometry was the most effective.

To monitor the tool wear after each pocket cycle, the tool was removed from the shrink fit holder and the flank wear was measured on a Voyager microscope and measurement system at UNCC. A fixture had been previously designed for the purpose of measuring flank wear. The fixture held the tool in place in a V-block and could be rotated to the helix angle of the tool to enable the flank edge to be parallel to the y-axis of the Voyager coordinate system. The tools were mounted in a Shrink Fit holder and the machine tool was a Cincinnati Maxim 4-axis horizontal machine tool at UNCC with a geared spindle and a maximum spindle speed of 6000 rpm. The tools were checked for runout using a clock mounted on the spindle housing and rotating the tool. For all trials the tools were maintained to a maximum run-out value of 12.7 microns.

Toolpaths for enhanced stability

Controlling the radial immersion throughout the toolpath will increase the maximum depth of cut that may be taken without inducing chatter. The frequency response functions of the tools were measured so that the tools could be analysed for stability (Fig. 3.6 -3.7).

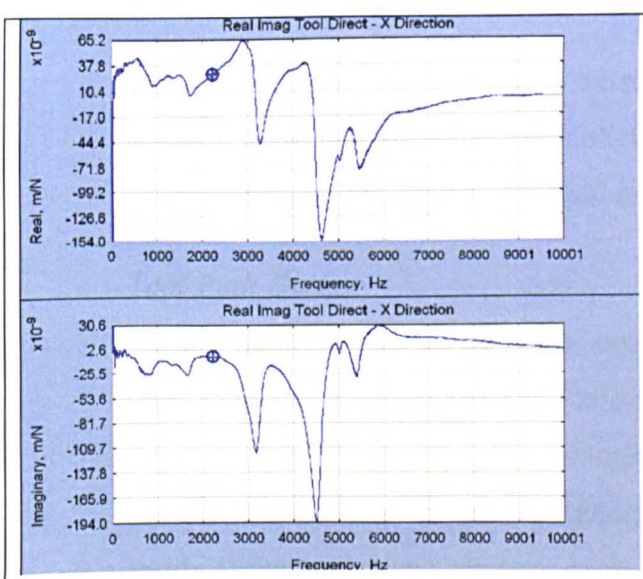

Fig. 3.6 X-directionFRF measurement of end mill described in table 3.1

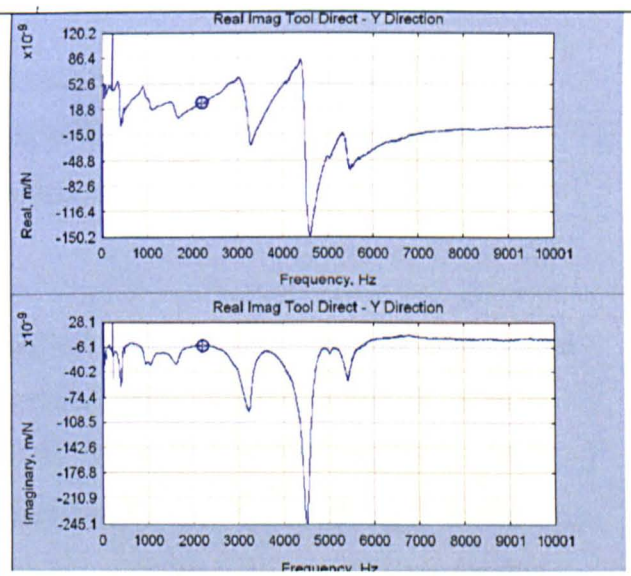

Fig 3.7 Y direction FRF measurement of end mill described in table 3.1

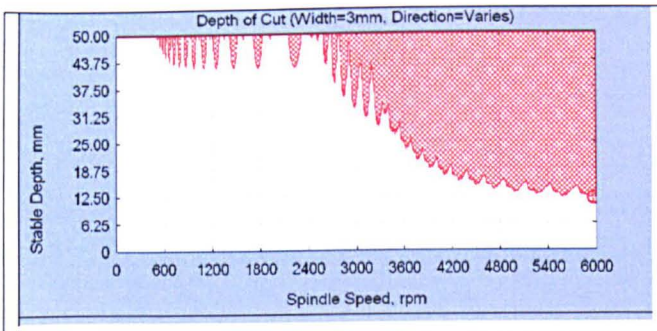

Fig. 3.8 3mm ae lobe plot (all directions) for end mill described in table 3.1

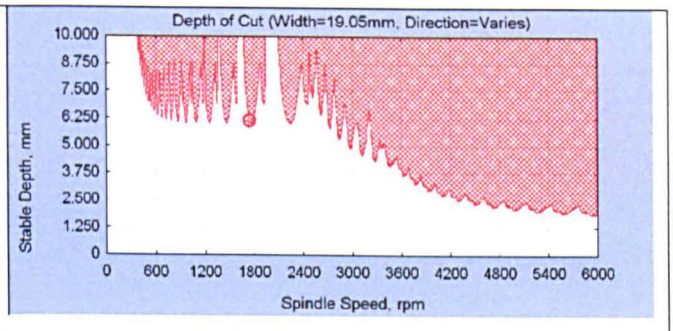

Fig. 3.9 Slot lobe plot (all directions) for end mill described in table 3.1

The drawbar force was measured and maintained as a constant at the start of each run using a drawbar dynamometer with a 50 taper interface. Variations in drawbar force have been proven to influence dynamic stability [120], and the introduction of chatter would cause rapid tool wear and render the tool life study invalid [121]. This is an essential precaution for any tool life study and is not always considered.

The stability lobes (Figs. 3.8- 3.9) are plotted for Ti6Al4V using a process damping wavelength of 0.6mm and are displayed as 12 directional plots overlaid, incrementing the feed direction by 30°. The plots show that the tool is just stable for a 5mm axial depth of cut at full slot which will be stable for all the toolpaths considered here. The first lobe plot is for a radial immersion of 3mm and it is evident that a much larger axial depth of cut can be taken up to 40mm if a radial immersion of 3mm can be maintained.

The lobe plots demonstrate that if the radial immersion can be maintained to a constant 3mm then the axial depth of cut and MRR will be 7 times greater than a pocket where sudden spikes in radial immersion occur.

Tool Path Design

Each of the following six toolpaths was designed with the objective of reducing radial immersion when approaching 90° or acute corners. The 'standard' toolpath taken as the control for the experiment was copied from the work by Stutzman [1997] and represents the default toolpath for many programming packages, starting from the inside of the pocket and working out towards the perimeter. The parameters for this toolpath are taken as the standard input for the temperature model in the first part of this chapter. Each of the toolpaths was programmed manually in Excel to ensure full

control over the tool trajectory. For each of the pockets the tool reaches full axial depth by ramping at an angle of 5°. As each toolpath was run at the same spindle speed and feed rate the different toolpaths resulted in different cycle times. The study offers a trade off between life and cycle time, the benefits of which can only truly be assessed with the relevant cost data for cutting tool and machine tool overheads. In the cases where radial depth of cut is maintained as a near constant there is the opportunity to increase the axial depth of cut and therefore increase productivity. The trials were maintained at a constant depth of cut to conserve material. The pocketing strategies are described below and are displayed in Figs. 3.10 -3.13. Each NC programme was developed manually for this study.

Standard Pocket (Figure 3.10)

This standard pocket strategy is taken as the control for the study. This is also a default strategy used by many CAM packages. The tool ramps to depth at the centre of the pocket and follows a square trajectory before stepping out by the programmed width of cut. This action is repeated until the full pocket is generated, encountering four corners and full radial immersion for each radial step.

Rad-corner (Figure 3.11)

This toolpath starts with a circle at the centre of the pocket and gradually morphs to the shape of the pocket. The radial immersion is controlled at the corners through an arced toolpath. This path leaves some final stock in the corners which is removed with 'rest milling', pecking away with 2 passes of constant radial immersion.

Pre-Slot (Figure 3.12)

The first operation for this toolpath is taken as a full slot at low speed. A full slot is the worst case scenario with relation to radial immersion so no reduction in tool life is seen as a result of increased radial immersion in corners. Two diagonal corner to corner slots (slotting at 650 rpm –101.6mm/min) are taken prior to the standard pocketing routine commencing at full speed, there by eliminating the corners during the standard routine. The trade off between radial immersion and surface speed was considered with the decision to reduce the spindle speed for the slotting operation.

The slower speed also increases the process damping performance and enables chatter free cutting for the larger axial and radial immersion.

Spiral (Figure 3.13)

This toolpath is another variation on the circular path. A true spiral tool path is employed up to the perimeter of the pocket, beyond which the remaining stock must be rest milled. The corners are cleaned up with arcs of increasing diameter around the centre of the pocket. The size of the spiral is restricted by the shortest dimension of the pocket, for a square pocket this is well suited, but for a rectangular pocket the spiral toolpath would leave a large proportion of the stock for rest milling.

Outside-in (Figure 3.14)

The outside- in tool path begins the pocket with a slot cut around the perimeter of the pocket at 650 rpm and 101.6mm/min feed. The tool path then follows the reverse of the standard tool path, working its way towards the centre of the pocket. The advantage of this tool path is that as the corners are on the inside of the tool path the tool does not see any increased radial immersion. The tool path also cuts the outer wall from thick stock and this would support the milling of thin walls as the walls are 'thick' and stable when cut.

This type of tool path however is ill suited for the milling of thin floors as the most flexible part of the floor is milled last when it has no inherent stability.

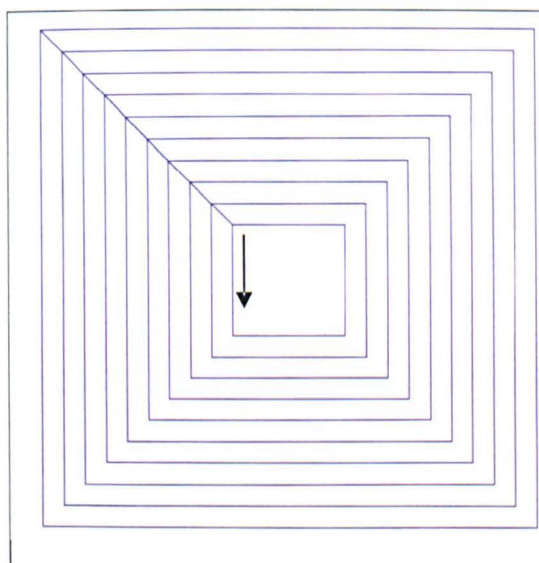

Fig. 3.10 Standard toolpath

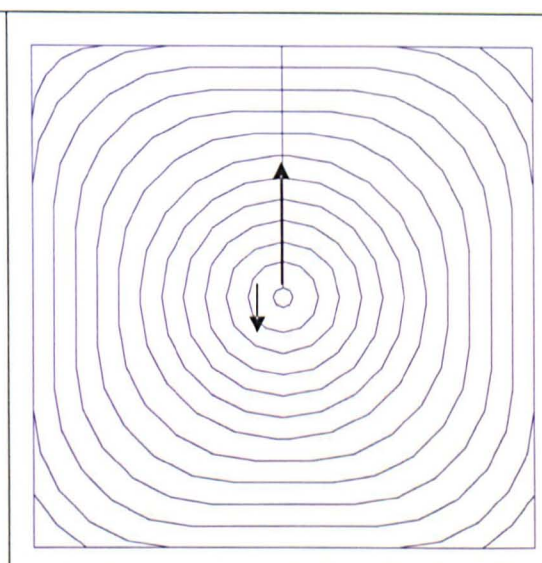

Fig. 3.11 Rad-corn toolpath

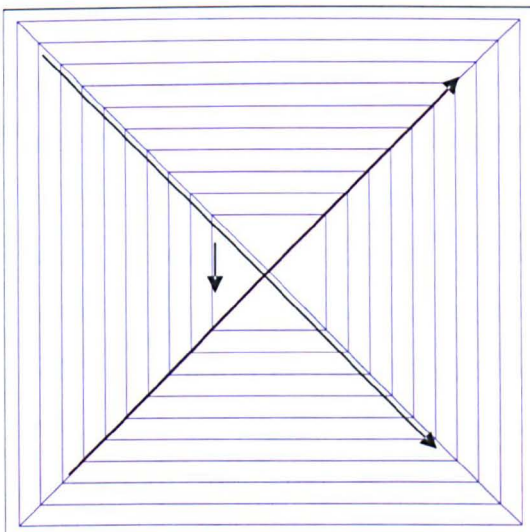

Fig. 3.12 Pre-Slot toolpath

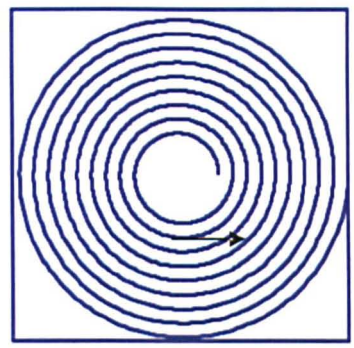

Fig. 3.13 Spiral toolpath

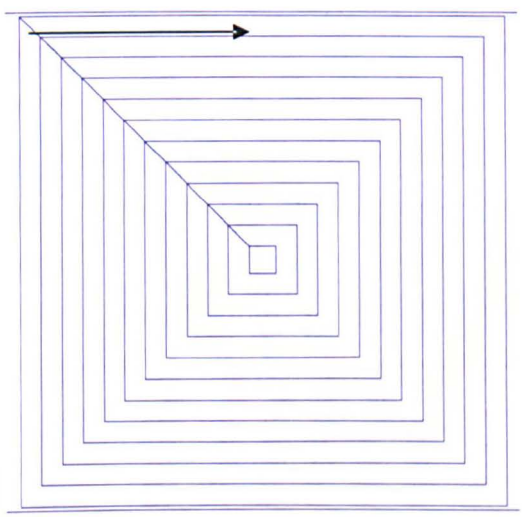

Fig. 3.14 Outside-In toolpath

3.3.4 Toolpath Simulation

Each of the toolpaths detailed in Figures 3.10-3.14 were simulated using Third Wave Systems Productivity Module. Third Wave Systems produce simulation software for machining processes, the core software AdvantEdge™ is a Finite Element package that models chip formation, forces and stresses experienced during the machining process. The Productivity Module references a database of cutting forces created with

AdvantEdge. The NC code workpiece and tool geometry are then processed to calculate cutting conditions, radial and axial engagements, at specified rotation increments of the tool. The cutting forces and radial engagement are then computed by referencing the database and can be presented in a time domain plot. This software package is useful for predicting peak loads seen during a milling process and can provide an estimate of varying radial engagement and cutting force throughout the NC cycle in a way that the analytical temperature model developed in the early part of this chapter cannot. The input toolpath parameters for each simulation are outlined in table 3.1 and the cutting parameters stated in the toolpath descriptions. Figures 3.15-3.19 present the time domain temperature and force plots for each of the five toolpaths.

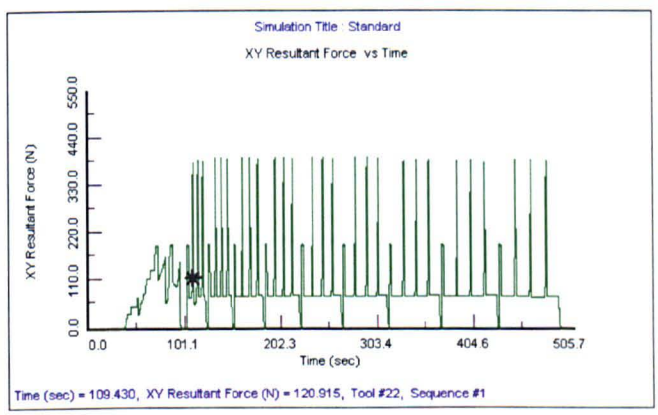

Standard toolpath– Simulated Force (N) vs time (s)

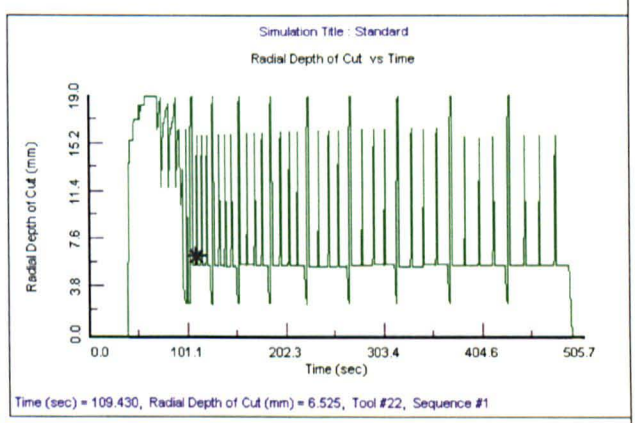

Standard toolpath –Simulated effective radial depth of cut (mm) vs time (s)

Figure 3.15 Standard toolpath 3rd Wave time domain plots

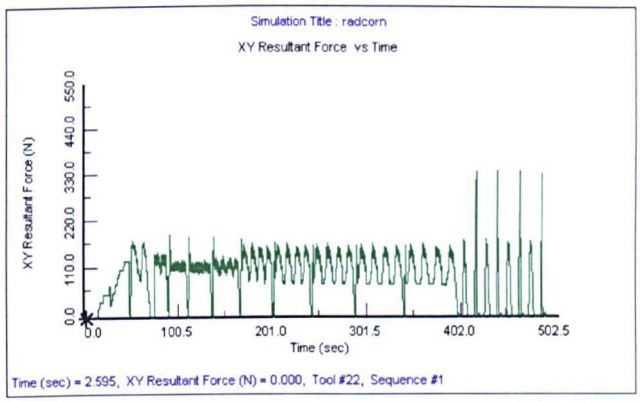

Radcorn toolpath– Simulated force (N) vs time (s)

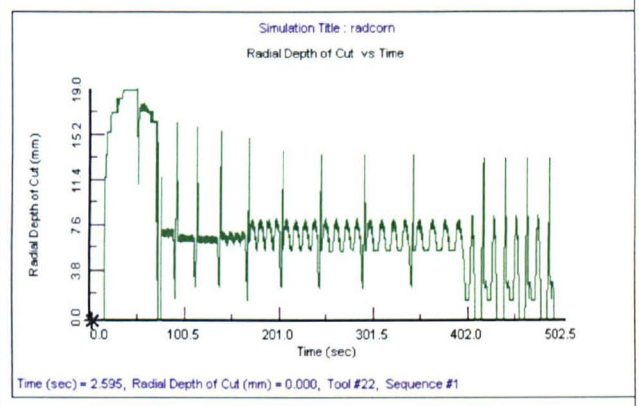

Radcorn toolpath- Simulated radial depth of cut (mm) vs time(s)

Figure 3.16- Rad-corner 3rd Wave time domain plots

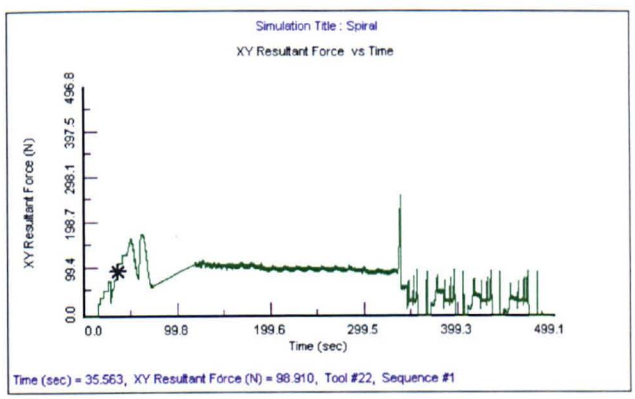

Spiral toolpath– Simulated force (N) vs time (s)

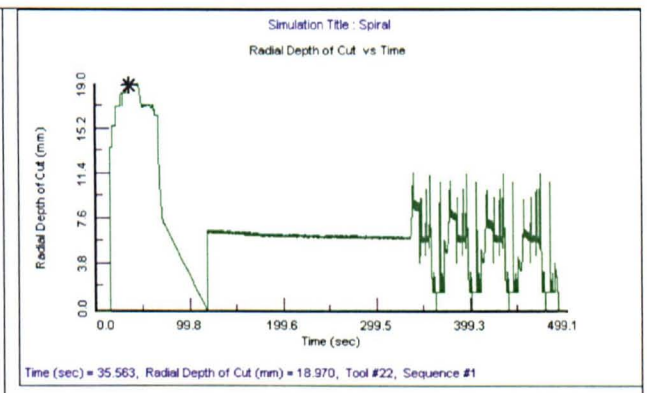

Spiral toolpath- Simulated radial depth of cut (mm) vs time(s)

Figure 3.17- Spiral 3rd Wave time domain plots..

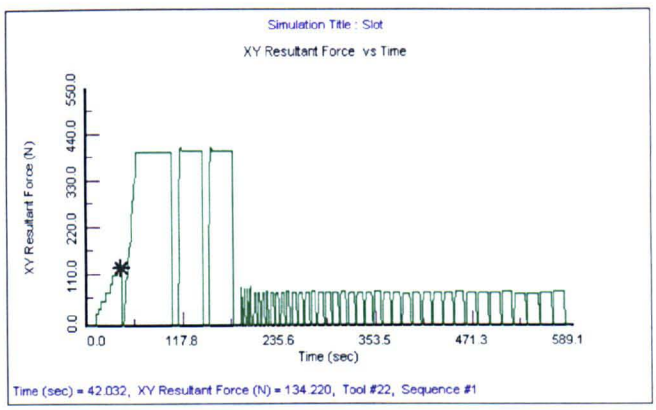

Slot toolpath– Simulated force (N) vs time (s)

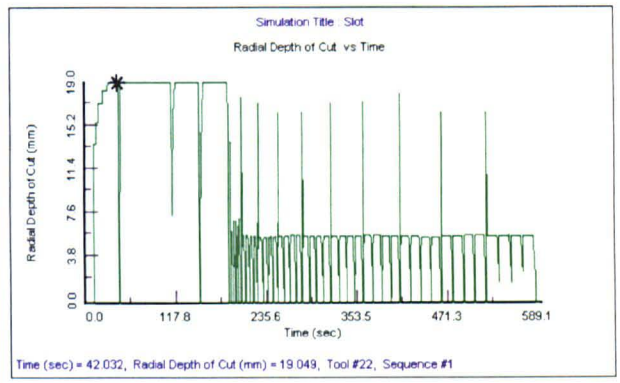

Slot toolpath– Simulated radial depth of cut (mm) vs time (s)

Figure 3.18- Slot 3rd Wave time domain plots

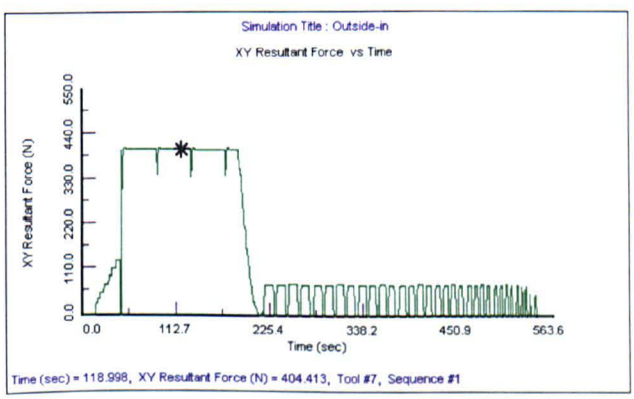

Out- In toolpath – Simulated force (N) vs time (s)

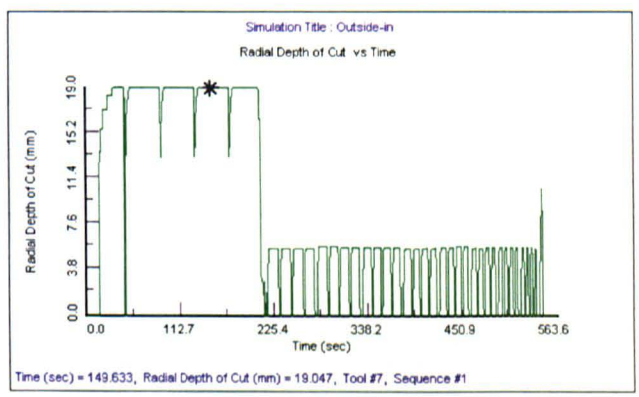

Out-in toolpath– Simulated radial depth of cut (mm) vs time (s)

Figure 3.19- Outside-In 3rd Wave time domain plots

3.3.5 Results of Toolpath Trials

Flank wear was measured after each pocket cycle, the Voyager measuring facility permitted a reference to be set from the unused cutting edge before scanning up the flute to the wear location. The measurement points were taken as the unused cutting edge and the outer limit of the wear band (Fig. 3.20).

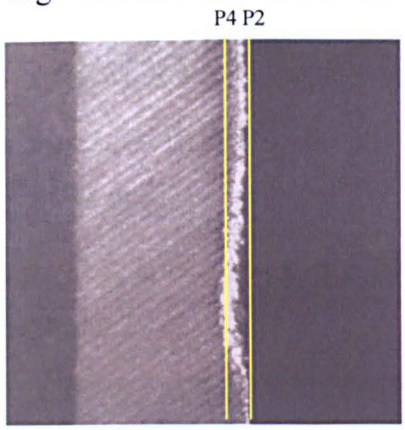

Figure 3.20 Wear Band (0.2mm)

Figures 3.21- 3.25 show the condition of each cutting tool at the conclusion of the trials. The flank wear was measured for each of the three flutes using the optical Voyager system and the average wear was recorded. The wear plots and cycle times are presented in Figs. 3.32 &3.33.

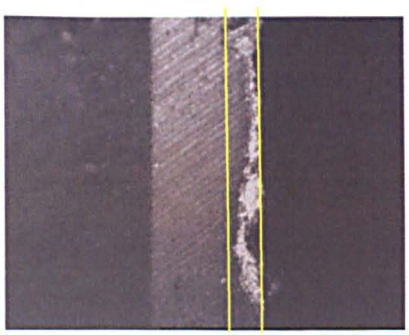

Figure 3.21 Flank wear for standard path

Flank wear after 6.7 standard cycles (cycle time 7 min 40 sec)

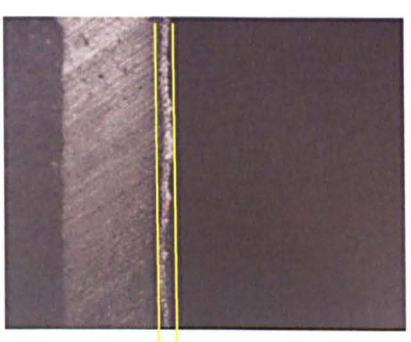

Figure 3.22 Flank wear for slot path

Flank wear after 7 slot cycles (cycle time 9min 51 sec)

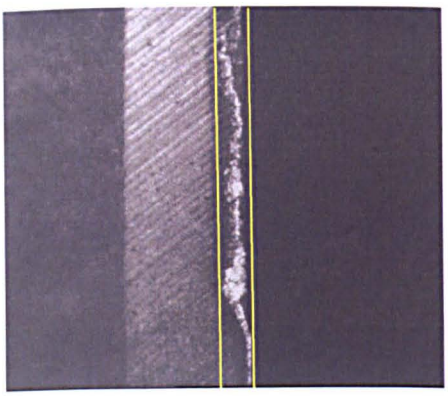

Figure 3.23 Flank wear for Rad-Corn path

Flank Wear after 7 rad-corner cycles (cycle time 8 min 20 sec)

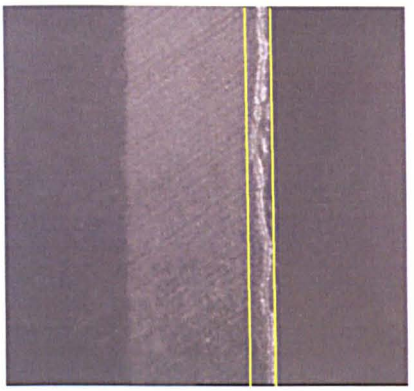

Figure 3.24 Flank wear for spiral path

Flank Wear after 7 Spiral cycles (cycle time 8 min 5 sec)

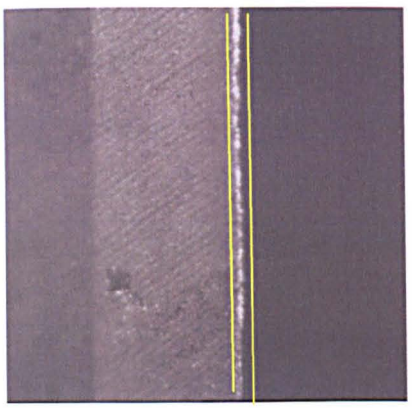

Figure 3.25 Flank wear for outside in path

Flank wear after 12 Outside In cycles

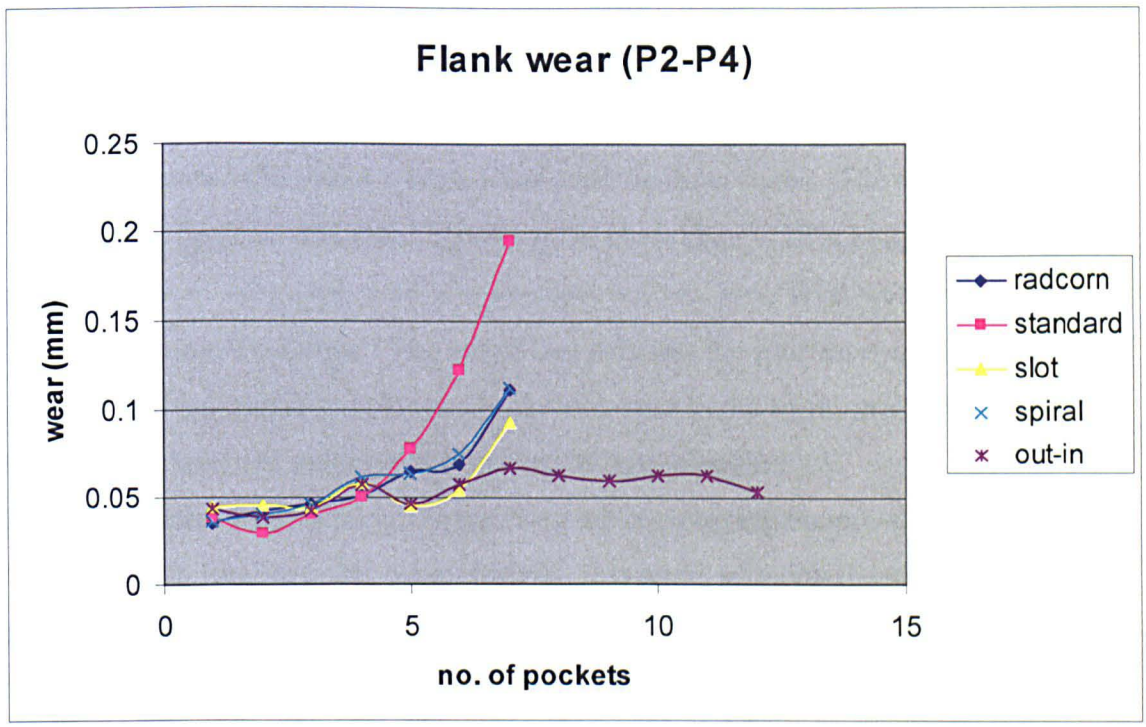

Fig. 3.26. Flank Wear plots for toolpath study

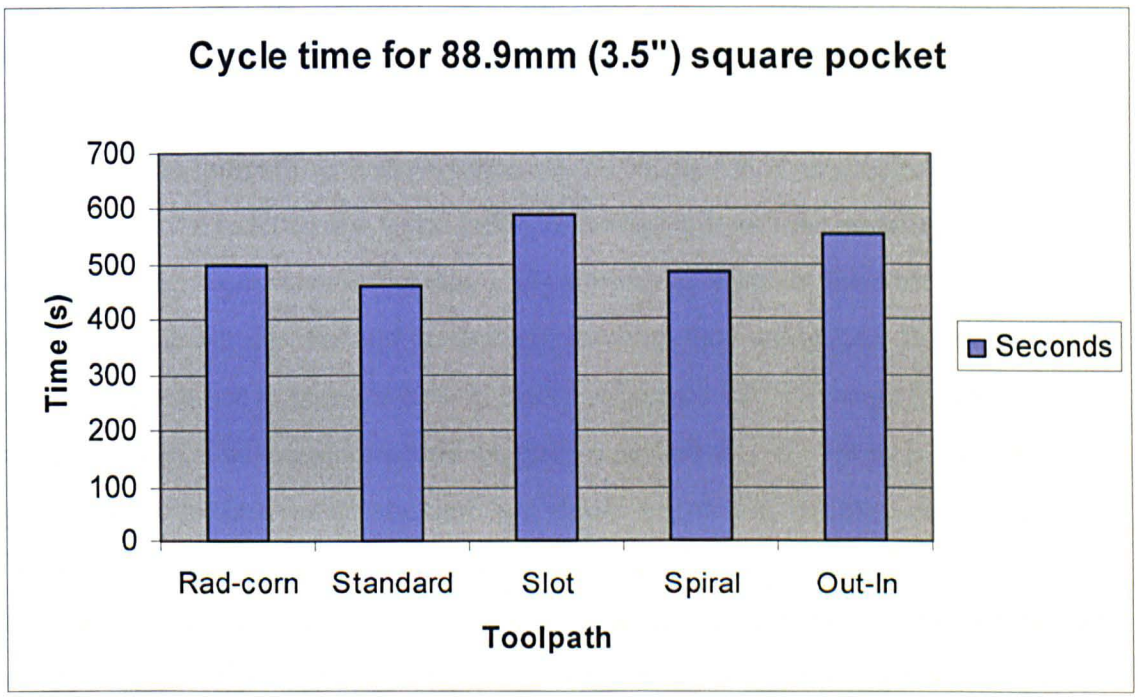

Fig.3.27 Cycle times for toolpath study

3.3.6 Analysis of Results

Experimental Results

Figure 3.26 shows the average flank wear over the three flutes. The outside-in tool path displays the least tool wear. However the cycle time is 28% longer than the standard. The spiral-morph cycle shows improved tool wear relative to the standard with a cycle time 9% longer. The spiral tool path has the shortest cycle time of the non-standard tool paths and shows similar tool wear to the spiral-morph tool path although as explained earlier it is restricted in its application.

The predominant form of wear for the two paths employing the pre-slot was flank wear, no notch wear or crater wear evident. This again supports the elimination of corners in the tool path. It is likely that a reduction in mechanical shocking reduces the amount of chipping and lower peak temperatures will restrict crater wear on the rake face which can also lead to edge chipping.

Simulation Results

The simulation results from Third Wave Systems Productivity Module show for the standard toolpath that the effective radial engagement varies between 5mm and 16mm throughout the toolpath with the resultant (x,y) cutting force varying between 60N and 400N. When the radcorn and spiral paths are compared with the standard the forces and engagement are much lower due to the smoothing effect at the corners, this in turn leads to lower thermal and mechanical loads on the cutting tool. Both the radcorn and spiral paths see maximum cutting forces of around 120N through the main body of the toolpath. These results would suggest improved tool life for both the radcorn and spiral toolpaths over the standard and would support the experimental findings. The slot and outside in toolpaths both see peak forces at around 400N whilst full slotting at a lower surface speed with the force then remaining below 60N whilst each toolpath maintains a constant radial width of cut at the full surface speed. For the main body of the toolpath the low cutting forces suggest even greater tool life when compared to the spiral and rad-corn toolpaths. The greatest wear is likely to be seen during the slotting operations where forces are predicted at around 400N. The successful performance of these toolpaths suggests that the reduction in surface speed for the slotting operation has a significant impact on temperature and wear.

The outside-in toolpath is somewhat smoother than the slot with no spikes in radial depth of cut once the first pass has been taken and a smoother force profile during the slotting portion. The outside in toolpath also has a slightly shorter cycle time than the slot path; all of these factors suggesting that 'outside in' should be the best performer.

3.4 Summary

In this chapter the hypothesis that tool life and chatter in titanium milling can be controlled through effective toolpath selection has been explored. experimentally As a tool approaches an external corner the radial width will temporarily increase to almost a full slot. The literature review suggested that radial immersion has a strong influence on tool life and that this may be thermally activated wear. A thermal model based upon Stephenson's thermal model for intermittent cutting is presented to explore the influence of radial immersion on cutting tool temperature with comparison to other variables. The model contains some simplifications and has been developed by the author so that comparisons can be drawn between the influence of axial and radial depth of cut on temperature. With support from the thermal modelling and from the literature it is proposed that radial immersion will have a stronger influence on peak temperature and tool wear than axial immersion, therefore toolpaths are sought that optimise axial immersion but maintain radial immersion at a controlled level.
The main contribution to the chapter is an experimental study into the influence of toolpaths that control radial immersion on tool wear and productivity. A number of toolpath strategies for an 89mm square pocket were developed, each controlling a constant radial immersion to varying extents and compared against a control toolpath with full immersion in the corners. Each of the pocketing strategies with corner immersion control had large gains in tool life over the standard toolpath, with less than half the wear for an equivalent number of pockets. It is clear that maintaining constant radial immersion throughout a tool path is advantageous in terms of tool wear. The two cycles where a pre-slot tool path has been employed have given the best results in each case. For toolpaths where constant parameters are sought, both the rad-corner and true spiral toolpaths are effective with a 10% increase in cycle time for half the equivalent tool wear.
Dynamic analysis of the milling tool showed that for the pockets where a_e is maintained at 3mm the maximum stable depth of cut is approximately4 times that of

the standard toolpath where radial engagement reaches 11mm. To support the findings a simulation has been run using Third Wave Systems Productivity Module software to evaluate cutter loading throughout each toolpath. The modelling supports the experimental findings, showing increased loading and immersion for the standard pocket.

The study proved that increased radial immersion in corners does have a negative effect on tool life and that the strategies presented here can greatly extend tool life through controlling the radial immersion. Of the five pockets the rad-corn and spiral were attractive as they required no heavy slotting to clear the corners and could be applicable to pockets with thin bases, resulting in very small increases in cycle time with comparison to the control pocket. The results support the theory that tool life may be increased if the high radial immersion on corners can be avoided. The optimised tool path may combine some of the traits of all these tool paths and may vary depending upon the work- piece geometry. This will be explored in the next section of the chapter.

Variations on the rad-corn tool path may be developed into curvilinear [122] tool paths that could be applied to any geometry. The spiral-morph toolpath is a combination of the rad-corn and true spiral and will avoid the increased cycle time and immersion as the tool steps out from each cycle. Bieterman [122] was interested in curvilinear toolpaths as a means of reducing the demand on the CNC and drives for acceleration and deceleration on approach to corners. By increasing the angle of curvature the change in acceleration is reduced as the tool can follow a near constant velocity.. This toolpath can now be generated with some CAM packages and was used as the foundation of a study by the author with Sandvik Coromant to establish best practice titanium pocketing strategies. Some of the strategies are presented in Appendix 1 and these are now presented in the Sandvik Titanium Coromant best practice titanium milling handbook.

In summary the hypothesis developed in chapter 2 that '***Tool life and chatter in titanium milling can be controlled through effective toolpath selection***' is supported experimentally within this chapter and contributes to the research field as the first experimental study into this problem with support from simulation. Since this work was completed it has been employed to influence industry best practice.

4 VARIABLE HELIX END MILLS

4.1 Introduction

This chapter examines the hypothesis that variable helix end mills can provide enhanced stability and productivity and can be modelled using a frequency domain solution. The chapter initially looks at methods of disrupting regenerative chatter and follows with an introduction to variable pitch and variable helix tools. A detailed discussion of research into variable pitch tools is followed by a study of the analytical model developed by Altintas, Engin and Budak [114] that will form the foundation of the variable helix model developed here. Stability lobes are presented which are developed from the Engin model with some modifications made by the author to enable clear identification of the boundary of stability. In addition to the analytical solution time domain modelling of variable pitch and variable helix tools is explored with a comment on chatter recognition criteria.

A new analytical model for variable helix end mills is then presented using an average pitch method to predict phase angle for each flute. Experimental validation of the new analytical solution and the Altintas & Merdol time domain solution is sought and the experimental procedure and tool selection are outlined. Many machine tools display non-linear dynamic responses between the static and loaded or at speed conditions, this may be due to variable preload, heating of the bearings or changes in contact stiffness. Before the experimental validation can begin a study is carried out to assess the linear dynamic response of the selected machine tool, a Makino A99. In order to plot the stability lobes the tool tip FRF and cutting force coefficients for the selected workpiece material are required. A detailed description is given on how to obtain the FRF and cfc data and a new methodology for the validation of stability lobes is detailed.

The variable helix tools have been selected with a range of pitch and helix variations, one tool with standard pitch at the tool tip and the others with varied pitch at the tip. For each variable helix tool studied, a standard helix equivalent is also used for comparison.

A discussion on the non-linearity of machine tool dynamics is presented. Any shift in dynamic response form the static empirically measured condition to the dynamically loaded condition can render stability lobes useless as lobe positions and stability limits shift. A number of solutions to this problem are discussed including FE analysis

of the changing bearing conditions and the Receptance Coupling method for combining measured and modelled FRFs suggesting areas for future work.
A study into the machine tool linearity is undertaken, plotting the stability lobes and chatter frequency within a selected spindle speed range as outlined in the stability lobe validation methodology. The linearity of the dynamics from the static condition is assessed with respect to any shift in lobe position and chatter frequency. The machine tool is found to have a predictable response up to 8000 rpm above which a contact stiffness associated with the spindle appears to drop and the dominant mode drops in frequency and dynamic stiffness. This new methodology for assessing the linear response of machine tool dynamics results in a suitable spindle speed range for the validation of the analytical variable helix stability lobes.
Once the operational spindle speed ranges have been established the same lobe proving methodology is applied to six end mills, three of which are variable helix and three standard helix equivalents, incorporating the same pitch variation as the variable helix tools. The results of the FRF and CFC measurements are presented along with the empirical, analytical and time domain lobe plots for each tool. A discussion of the results begins with an assessment of the time domain data and the criteria for chatter recognition within the time domain model.

4.2 Background

As outlined in chapter 2, one well-documented method for improving stability in the milling process is to interrupt the regenerative effect. This can be done through varying spindle speed [123] , varying vibration frequency [124] or varying the pitch of the teeth on the milling cutter [91]. If the unstable phasing of the subsequent teeth is broken up then Opitz [125] claims there will be a suppression of chatter, as there will be no superposition effect of the undulations from subsequent tooth passes feeding the chatter growth (fig 4.1).

Fig.4.1 Superposition of waves

The superposition and feedback loop takes a hold when an unstable phasing exists but the methods listed above will all vary the phasing between subsequent teeth through one of the three variables that define the phase shift:

$$N + \varepsilon = 120\pi . \frac{f_c}{m.n} \qquad (4.1)$$

$$\varepsilon = f_c l / Vs \quad [125] \qquad (4.2)$$

where l= tooth pitch and ε is the phase shift between subsequent teeth.

From equations 4.1 & 4.2 it can be seen that a change in frequency, pitch or rotation speed would change the phasing and a continuous variation in any of these three should serve to suppress the onset of chatter.

There have been alternative approaches to disturbing the unstable phasing between subsequent teeth that initiates regenerative chatter. This is achieved through varying the time period (τ_j) between the engagements of consecutive teeth and has been proven to be an effective method for chatter disturbance. Firstly this can be achieved through variation of the spindle speed on the machine tool [123]. Limitations to this method are the responsiveness of machine tools and the load on spindle motors are not designed to constantly change spindle speed or deliver sufficient bandwidth [123]. The success of this method is due to the disruption of the regenerative effect; the system cannot settle into an unstable phase.

The most practical solution is to use a milling cutter with variable pitch as this requires no advanced control on the machine tool or active control of the tool or workpiece. Tools with variable pitch offer a substantial benefit to titanium milling as more conventional methods of stabilising the process are unavailable at typical titanium milling surface speeds [126]. In addition to tools with different pitch angles between each flute with a constant helix, a number of tool designs exist which vary the pitch variation up the length of the flute. The aim is to further disrupt the regenerative chatter effect by introducing a broad range of phases up the length of the engaged flute relative to those of the previous flute. The target is to further reduce the chance of an unstable phasing taking a hold and forcing the process into a self-excited loop. Such tool designs in common use include serrated cutters, wave form or Krestcut ™ cutters and variable helix cutters.

Serrated edges on cutters result in a variation in cutter radius along the edge of the flute which in turn relates to a variation in pitch. The irregular distribution of teeth helps to break up the regenerative chatter effect and hence leads to greater stability in roughing operations. The variation in radius along the flute length leads to the waveform being imparted onto the part surface hence these tools are unsuitable for finishing operations.

It is established that the stability of serrated cutters is related to feed; when the feed is twice that of the serration amplitude the full form of the cutting edge will be engaged and the reduction in depth and variable pitch effect are both lost. The regenerative disturbance is only effective if subsequent teeth are not in contact with the workpiece as supported by simulation results. [127].

Wave form or Krestcut tools have a sinusoidal waveform down the flute length, such that the wave form is always set out of phase from the wave form on the previous tooth. This differs from the serrated edge cutters as the tool has a constant radius and the stabilising effect is purely down to the effective variation in pitch along the length of the cutter. Such tools are used successfully in HSS and carbide form although difficulty in regrinding the carbide form makes them relatively expensive. As the stabilising effect is a result of the change in pitch values up the length of the tool, best results are often obtained with large axial depths of cut. Limited successes are to be found when slotting at relatively shallow depths of cut.

Variable helix tools have a similar effect to the waveform cutters with the pitch variation changing along the length of the helix. These tools are typically used with a variable pitch at the end and then further changes in that pitch variation occur up the flute length. For any given slice of the tool the pitch variation will be different. The variable pitch at the tool tip means that the tools are not limited to large axial depth of cut applications, which often in turn mean shallow radial depths of cut , as with the waveform cutters. One limitation of variable helix is that with large pitch and helix variations the width between the flutes can be greatly reduced limiting chip clearance and leading to inconsistent tool wear. Over all there appear to be many benefits to using variable helix cutters as they provide a cheaper and more versatile solution than some of those described above. There has been relatively little documented work on variable helix cutters and a validated analytical stability model is sought in this chapter. All of the various special tool designs described above are founded on the

concept of variable pitch tools, the research history of which shall now be discussed in greater detail.

4.3 Variable pitch tools

Some of the first published work on variable pitch tools quickly followed the early modelling work on the stability of the milling process, indicating that they were already in common usage. In 1965 Slavicek [91] published one of the first pieces of work on variable pitch cutters claiming that altering the phase between subsequent teeth adjusted the feedback adjustment that initiated chatter and regeneration is annulled. This means that the two phases cannot adjust simultaneously to the optimum phasing for regeneration.

Slavicek expands equation (4.2) for a tool with two pitch angles $\varepsilon_1, \varepsilon_2$;

$$\varepsilon_1 = \omega l_1 / Vs, \varepsilon_2 = \omega l_2 / Vs, \qquad (4.3)$$

The mean value of the phase shift φ, its variation (Δ) and the irregularity of the tooth pitches are presented and equation (4.4) is now derived for the variable pitch cutter:

$$(\cos\Delta . e^{i\varphi} - 1) = \frac{1}{rF} e^{i(\varphi)} \qquad (4.4)$$

Slavicek predicts that the value of the coupling coefficient (r_c) (coupling the dynamic stifnness of the system and the depth of cut) at the limit of stability may be doubled for an irregular pitch cutter.

$$r = -\frac{1}{2G} \cdot \frac{1}{1 - \frac{\sin^2 \Delta}{2(1 - \cos\Delta\cos\varphi)}} \qquad (4.5)$$

the process has greatest stability at the frequency f1, where:

$$f1 == N.\frac{Vs}{4t} \qquad (4.6)$$

for a chatter frequency f1 and a surface speed Vs, the optimum tooth irregularity can be determined. Slavicek supported his theory experimentally demonstrating over double depth of cut achieved with the specially designed variable pitch cutters.

A drawback of this solution is that it works only for 2 pitch angles and is not fully integrated into the Tlusty or Altintas stability lobe algorithms that are now widely accepted. The paper does however show an understanding of the design and

performance of variable pitch cutters and demonstrates the improved performance over standard end mills.

Optiz [125] further expanded the research on variable pitch tools providing a solution that he integrated into stability lobes. He demonstrated that using a cutter with irregular pitch shifts the borderline of stability towards a higher width of cut for a considerable speed range. The pitch ratio determines at what spindle speed 'n' the stable area occurs. Outside of this area there is little benefit. Opitz [125] stated that a pitch ratio may be chosen for a practical spindle speed range.

Opitz claims that the single tooth milling models used at that time were found to be inaccurate when arc of contact is large and there are a number of dominant vibrations. He demonstrates the weakness of the single tooth average position method by taking as an example a slotting pass with the direction of feed normal to the one mode of vibration in the system. According to the simple model this process is infinitely stable but he demonstrates that in practice it will chatter as the teeth rotate and start to excite the dominant mode.

Opitz resolves the x-direction force as the sum of the components acting on each individual tooth engaged in the cut, the total force being related to time dependant direction coefficients. Opitz cannot propose an analytical solution for the time variant directional factors and so proposes an approximate solution where the time varying coefficient is substituted by its time average, taking the integral of the time varying factor from entry to exit multiplied by the number of teeth and divided by the immersion angle. He demonstrates good correlation with experimental data when using his average factor to generate stability lobes.

$$F_x = -Ks_1\left[(R_1 + R_2)x(t) - R_1.x(t - aT) - R_2.x(t - bT)\right] \qquad (4.7)$$

where;

aT , bT are the time delays for each pitch angle

R1,R2, are the directional factors for each set of pitch angles

Due to the nature of the time variant coefficients Opitz states that a computer simulation (time domain) is required for a true solution.

For the analytical solution an average coefficient is again proposed;

$$F_x = -Ks_1R_m\left[2x(t) - x(t - aT) - x(t - bT)\right] \qquad (4.8)$$

He concludes that the optimum pitch ratio can be defined as ;

$$\frac{l_b}{l_a} = \frac{240 f_c / m + n}{240 f_c / m - n} \qquad (4.9)$$

based upon the optimum phasing to prevent the superposition and regenerative effect of chatter.

Stability lobes are presented that show a broad band of stable spindle speeds for an irregular pitch cutter, but the cutter design is very much dependant upon one dominant chatter frequency. He notes good chatter stability within the 25 – 65 rpm range for an irregular pitch cutter whilst the standard cutter chattered and adhered to standard stability lobes (Fig.4.2).

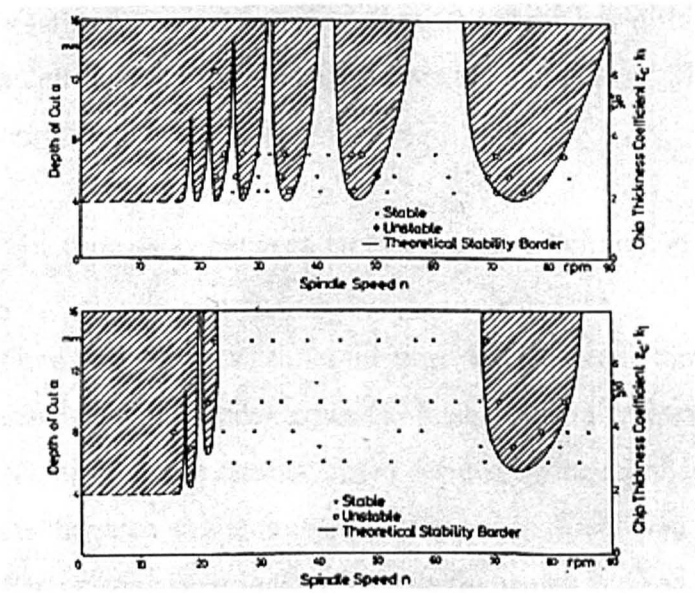

Fig. 4.2 Stability Charts for regular and irregular pitch cutters (ref Opitz 1966)

Altintas further advanced this work with his models for general end mills and with Budak [114] and Engin developed analytical models taking into account the directional nature of the cutting loads on each tooth for variable pitch end mills.

In 1995 Shirase and Altintas [128] developed a time domain model which showed that not only is chatter reduced by variable pitch but also that surface error is reduced. The non-uniform chip load due to the variable pitch results in a uniform chip thickness. The surface errors created by the teeth with large chip loads are removed by the subsequent teeth, which have smaller chip loads and reduced error. This is similar to the 'wiper' effect commonly used on finishing indexable face mills today. The non-uniform tooth loadings may result in reduced tool life.

4.4 Analytical model for variable pitch tools

As a first step to creating an analytical solution to variable helix end mill dynamics, an analytical model for a standard variable pitch tool is required.
None of the models discussed in the previous section sought a fully integrated theoretical solution other than that developed by Engin & Altintas [129] . Engin provides a solution adapted from the analytical stability lobes proposed by Altintas and Budak [81]. The solution demonstrates improved stability for variable pitch cutters and a method to determine optimum pitch angles for a known dominant frequency of the system. This solution will provide the foundation for an analytical solution for variable helix end mills and the key differences from the coupled mode solution expanded in chapter 2 are drawn out here. The solution starts with a representation of cutting forces:

Tj = time delay between teeth due to spindle rotation

For a variable pitch cutter the time delay for each tooth will be different to the standard pitch model expanded in chapter 2. For a standard pitch cutter the time delay is equal to the rotational speed divided by the number of teeth.
As the pitch angles are non-uniform each directional coefficient matrix is different. Each matrix is periodic at spindle frequency and can be expressed as a Fourier series expansion.

$$[A_j(t)] = \sum_{r=-x}^{x} [A_{rj}] e^{i\rho w t} \qquad (4.10)$$

$$[A_{\rho j}] = \frac{1}{T} \int_0^T [A_j(t)] e^{-i\rho w t} dt \qquad (4.11)$$

Where (ρ) represents the harmonics. The harmonics have been demonstrated to have little influence on stability [85] and are therefore discounted and a solution is found for ρ=0. A_0 is only valid while the tooth is engaged in the cut:

$$[A_0] = \frac{1}{2\pi} \int_{\phi_{st}}^{\phi_{ex}} [A_j(\phi)] d\phi = \frac{1}{2\pi} \begin{bmatrix} \alpha_{xx} & \alpha_{xy} \\ \alpha_{yx} & \alpha_{yy} \end{bmatrix} \qquad (4.12)$$

The resulting dynamic equation is:

$$\{F(t)\} = \frac{1}{2} bK_t [A_0] \sum_{j=0}^{m-1} \{\Delta_j(t)\} \qquad (4.13)$$

where:

$$\{\Delta_j(t)\} = \begin{Bmatrix} x(t) \\ y(t) \end{Bmatrix} - \begin{Bmatrix} x(t-T_j) \\ y(t-T_j) \end{Bmatrix} = \{\rho(t)\} - \{\rho(t-T_j)\} \qquad (4.14)$$

ι(t) represents the relative vibrations between tool and workpiece at time t whilst χ(t-Tj) represents the vibration marks left by the previous tooth. The vibration at chatter frequency w_c are described as harmonic variables:

$$\left.\begin{aligned} \{\iota(iw_c t)\} &= [\Phi(iw_c)]\{F\}e^{iw_c t} \\ \{\iota(iw_c(t-T_j))\} &= e^{-iw_c T_j}\{r(t)\} \end{aligned}\right\} \qquad (4.15)$$

The summation term for the teeth in the dynamic equation and the derivation of Δ_j are the key deviations from the standard coupled mode stability derivation.

The regenerative displacements at a chatter frequency for variable pitch can be expressed as:

$$\{\Delta_j(iw_c t)\} = \{\chi(iw_c t)\} - \{\chi(iw_c(t-T_j))\} = (1-e^{-iw_c T_j})[\Phi(iw_c)]\{F(t)\}e^{iw_c t} \qquad (4.16)$$

Substituting this into the dynamic milling equation for a variable pitch cutter we have:

$$\{F(t)\}e^{iw_c t} = \frac{1}{2} bK_t \sum_{j=0}^{m-1} (1-e^{-iw_c T_j})[A_0][\Phi(iw_c)]\{F(t)\}e^{iw_c t} \qquad (4.17)$$

The term Tj which represents the tooth period for each tooth pass constitutes the principle difference between the solutions for standard and variable pitch cutters. The inclusion of the term Tj means that an alternative solution for chatter is required. Equation (4.17) has a non-trivial solution when its determinant is zero:

$$\det[[I]\Lambda E[\Phi_0(iw_c)]] = 0 \qquad (4.18)$$

The eigenvalue Λ and regenerative delay E are represented as follows:

$$\Lambda = -\frac{1}{4\pi} K_t b \qquad (4.19)$$

$$E = m - \sum_{j=0}^{m-1} e^{-iw_c T_j} \qquad (4.20)$$

where

$$T_j = \Phi_{pj}/(2\pi n) \qquad (4.21)$$

ϕ_{pj}= pitch angle of tooth

Altintas proposed the following solution specifically for variable pitch cutters, expressing the chatter vibration wavelength (β) between each tooth pass (T)as:

$$\beta_j = w_c T_j = 2N_j\pi + \varepsilon_j = w_c \frac{\phi_{pj}}{2\pi n} \qquad (4.22)$$

The wavelength is assigned to an initial condition of β_0, giving the spindle speed for this case:

$$n = \frac{w_c \phi_{p0}}{2\pi\beta_0} \qquad (4.23)$$

The remaining wavelengths are then calculated using the known spindle speed which leads to the solution of regenerative delay term:

$$E = m - \sum_{j=0}^{m-1} e^{-i\beta_j} \qquad (4.24)$$

A value for E is therefore attained for the assigned chatter frequency (wc) and the calculated spindle speed for each tooth of the cutter.

The eigenvalue can now be solved, substituting E into Λ :

$$\Lambda = \Lambda_R + i\Lambda_I = -\frac{1}{4\pi} K_t b_{\lim} \qquad (4.25)$$

As the axial depth of cut limit (b_{lim}) has a physical value the solution only exists when the imaginary part is zero and the real is negative.

$$b_{\lim} = -\frac{4\pi\Lambda_R}{K_t} \qquad (4.26)$$

The stability lobes are constructed by scanning new wavelength B_0 and chatter frequency. Wavelengths can carry between 10° when spindle speeds are high relative to the vibration frequency to 3600° where 10 full wavelengths exist between each pass and the process damping begins to take hold. This method is much more computationally intensive than the analytical approach for standard stability lobes. The analytical model can be validated with experimental and time domain data.

A 19.05mm diameter end mill with 4 flutes is used to mill Al356 alloy at a range of speeds demonstrating stable and unstable parameters.

In the example the set-up is unstable at a desirable spindle speed and a variable pitch cutter is designed to stabilise the vibration at the desired speed. This is done by scanning the first pitch angle and the pitch increment.

$$n = \frac{w_c \phi_{p0}}{2\pi\beta_0} \qquad (4.27)$$

Engin [114] demonstrated that the analytical predictions match closely with both time domain and experimental data. The theory is successfully applied in the optimal design of the pitch variation and the process becomes stable at the desired cutting speed.

This model has been rewritten to provide the solution for variable pitch cutters and is used to predict the performance of the variable pitch tools in the experimental section. Fig 4.4 shows a stability lobe plot for a tool with the following parameters:

Pitch 1; 70, pitch2, 110, diameter 16mm

Machining parameters:

5mm ae, al7050,

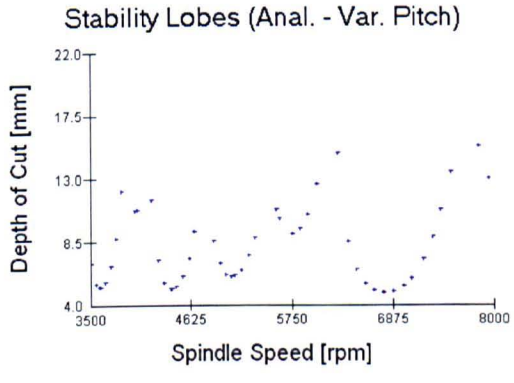

Fig. 4.3 Slot cut- Al 7050

Variable Pitch Stability Lobes, CutPro

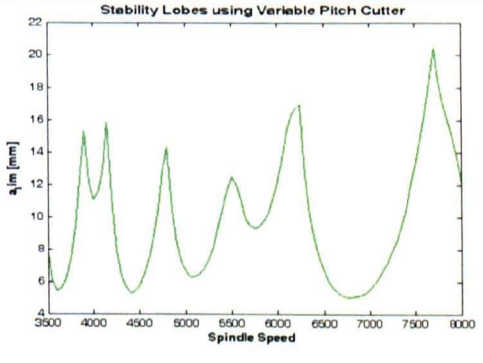

Fig. 4.4 Slot cut- Al 7050

Variable Pitch Stability Lobes, Turner

A modification has been made to the version developed by Engin and the commercially available solution available from MAL: As explained above the solution is sought through incrementing phase and frequency for each spindle speed value with a number of eigenvalue solutions available for each speed. The pre-existing solution presents the lobes as a series of points and there is no proposed method for determining the limiting depth of cut curve associated with most stability lobes. Schmitz presented a graphical manipulation method for plotting of lobes [130] but there are no methods for plotting continuous lobes from variable pitch lobes.

A solution is proposed here to determine the minimum depth of cut solution for the range of spindle speeds and present the lobe plot in a clearer fashion. The full algorithm is included in the variable helix Matlab model (Appendix II):
A new method for plotting stability lobe plots for variable pitch tools is used. The spindle speed range is divided into bins with width *dn (10rpm for the example in fig4.4)*. All corresponding depths of cut within the bin are scanned and the minimum depth of cut is selected and plotted against the average value of spindle speed (n) within the bin. The value *dn* defines the resolution of the lobe plot.

4.5 Time Domain Modelling of Variable pitch and variable helix end mills

The relevance of time domain vs frequency domain solutions has already been discussed. Time domain solutions provide the only fully accurate models for the time varying process that is milling. A time domain solution is required to predict the sum and direction of cutting forces acting on all teeth engaged in the cut at any moment in time. For variable pitch and variable helix cutters a time domain solution can consider the actual chip removal and surface generation at each point on the helix of the cutter and the workpiece surface. There is much publicised data on time domain solutions ([131], [97],[85], [80]) and the literature shows good correlation with experimental results.
Time domain solutions are computationally intensive and can take many hours or days (depending upon computing power) to compute a full stability lobe solution. A number of iterations are required to identify the onset of chatter for each spindle speed and depth of cut increment and this can greatly increase the computational time
The presence of chatter is determined in the time domain solution using the increase in the amplitude of cutting forces [73]. Sims developed a technique to determine the onset of chatter through identification of the damping loss factor in the periodic forces [132]. The time domain solution considers a number of nonlinearities in the cutting process such as the tool disengaging from the cut.
A time domain solution developed by MAL is used here to predict the stability of standard, variable pitch and variable helix end mills. Merdol & Altintas published a

paper on serrated cutters [127] where a time domain model is presented that accommodates the effective change in pitch along the flute of the tool. The bihelical model is based upon this model and the work by Altintas and Budak [114] with some modifications made by Merdol at UBC [133].

The stability criteria for the variable helix time domain solution is the same as that for the variable pitch cutters. The figures 4.5-4.8 compare a variable helix time domain output (on the right) with the time domain solution for the equivalent constant helix tool using the solution developed by Altintas & Merdol as part of the CutPro software suite.

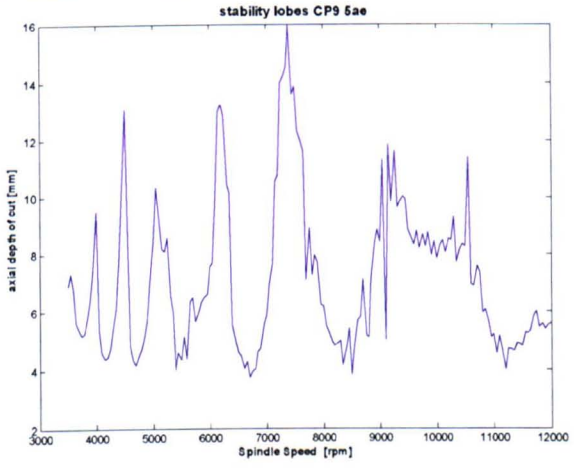

Fig. 4.5 ST 3 standard helix tool- time domain stability lobes for 5mm ae in aluminium

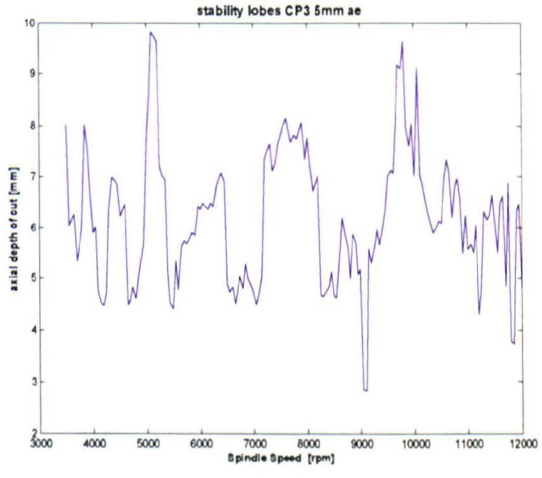

Fig 4.6 VH3 variable helix tool- timed domain stability lobes for 5mm ae in aluminium

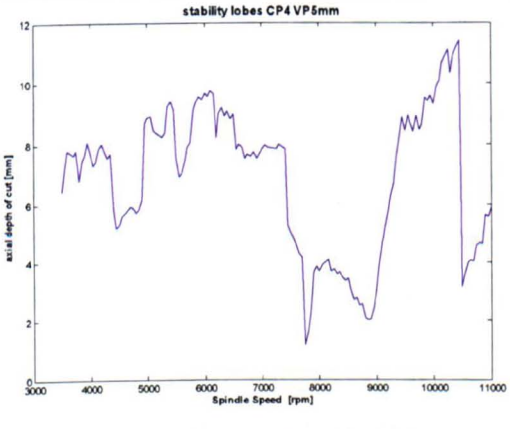

Fig 4.7 VP4 standard helix, variable pitch tool- time domain stability lobes for 5mm ae in aluminium

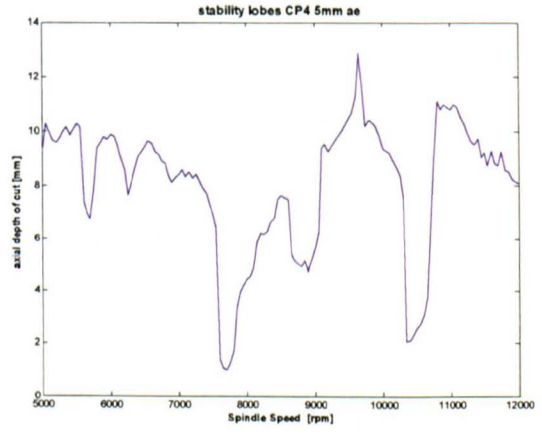

Fig 4.8 VH4 variable helix, variable pitch tool- timed domain stability lobes for 5mm ae in aluminium

As time domain solutions provide good correlation with experimental data it is proposed that this time domain model developed by Merdol be used to validate the analytical model developed here for a range of conditions.
As no published data exists to support the variable helix time domain model, experimental data is required to validate the time domain and analytical solutions for a selected number of process and tooling parameters. The frequency domain analytical solution for the stability of variable helix end mills will now be presented and then compared with the Merdol time domain solution.

4.6 A New Analytical Model for Variable Helix End Mills

An analytical model to represent the stability performance of variable helix end mills is presented in this section. Such a model is highly desirable as it will enable engineers to accurately predict the stability and productivity gains that may be obtained from such cutting tools and also to predict the optimum tool design for a selected machine tool and workpiece configuration.
The variable pitch analytical model as defined by Engin and Altintas has been outlined in some detail in the previous section as this is believed to be the most suitable foundation for the further development of a stability algorithm for variable helix tools.
A number of challenges have prevented the successful modelling of variable helix tools from being carried out to date. The stability predictions are non-linear as at any slice on the cutting tool the pitch differential will vary from a 'slice' at a different point. This means that the stability profile will vary with axial depth of cut. As axial depth of cut is an output of the calculation then some form of feedback loop will be required to predict stability for large axial depths of cut.

4.6.1 Average Pitch Method

The variable pitch analytical model developed by Budak and Altintas [114] is selected as a foundation for an analytical model for variable helix tools. Variable helix stability is dependant upon a feedback loop whereby the axial depth of cut dictates the range of pitch angles engaged in the cut, in turn determining the maximum stable axial depth

of cut. The target here is to develop a quick analytical model that offers good representation of the stability behaviour of variable helix.

The first assumption for the model is that the average pitch along the engaged flute can be calculated for each flute and the tool can then be modelled as a variable pitch cutter. The helix engagement is taken as the average depth of cut resulting from analytical stability lobes calculated for a standard helix tool with the same tool tip pitch variation.

The new method for plotting stability lobe plots for variable pitch tools is used as demonstrated in Fig4.9. For the plots displayed in this paper a resolution of dn=5 rpm was used. The Budak and Altintas [114] method is used to calculate stability for a uniform helix, variable pitch tool.

The dynamic milling expression has a non-trivial solution when the determinant is equal to zero.

$$\det[[I]\Lambda E[\Phi_0(iw_c)]] = 0 \qquad \textit{(4.28)}$$

This has two parts; real and imaginary, which can be solved by determining the eigenvalue (Λ) where E represents the regenerative delay, Φ_0 the oriented transfer function and w_c the chatter frequency.

$$E = N - \sum_{j=0}^{N-1} e^{-i\beta_j} \qquad \textit{(4.29)}$$

The solution for the regenerative delay term is found by scanning frequency, stability lobes (N) and teeth (j). β_j represents the wavelength between tooth j and its predecessor. The wavelength is assigned to an initial condition of β_0 to determine spindle speed (n) for a tooth pitch of ϕ_{pj}.

$$n = \frac{w_c \phi_{pj}}{2\pi\beta_0} \qquad \textit{(4.30)}$$

The chatter vibration wavelengths can now be calculated for the known spindle speed, where ε_j represents the phase delay in the waveform between subsequent tooth passes:

$$\beta_j = w_c T_j = 2k_j\pi + \varepsilon_j = w_c \frac{\phi_{pj}}{2\pi n} \qquad \textit{(4.31)}$$

The eigenvalue (Λ) can now be solved by substituting E into equation (4.45) :

$$\Lambda = \Lambda_R + i\Lambda_I = -\frac{1}{4\pi} K_t b_{\lim} \qquad (4.32)$$

The maximum stable depth of cut ($b_{\lim}$) can be calculated where K_t represents the tangential cutting force coefficient and Λ_R is the real part of the eigenvalue.

$$b_{\lim} = -\frac{4\pi\Lambda_R}{K_t} \qquad (4.33)$$

The stability results for the uniform helix tool are used to define the average axial engagement for the variable helix pitch calculation. The average pitch for each flute is calculated for the engaged flute length.

For: $n_{\min} \rightarrow n_{\max}$
$b_m = \bar{b}_{\lim}$

$$\phi_{pjm} = \frac{\left(\frac{\left(b_m/2\right)}{\tan\left(h_{j+1}\right)}\right) - \left(\frac{\left(b_m/2\right)}{\tan\left(h_j\right)}\right) + \left(\phi_{pj} \cdot D/2\right)}{D/2} \qquad (4.34)$$

Where D represents the tool diameter and h_j represents the helix angle for tooth j.

$$\beta_{jm} = w_c T_{jm} = 2N_j\pi + \varepsilon_j = w_c \frac{\phi_{pjm}}{2\pi n} \qquad (4.35)$$

For the new value of β_{jm}, the Altintas and Budak method is this time used to calculate the stability lobes for a variable helix tool using an 'average pitch method'.
The analytical results are displayed in Figures 4.22-4.37 alongside the time domain and experimental results.
The problem of depth of cut as an output and an input is likely to be of greater significance with extreme variations in helix angle. If the above concern is proven to be valid then the stability plots will be entirely non-linear with stability zones existing for a given spindle speed that vary with axial depth of cut. It may be possible to extend the depth of cut through an unstable region and then become stable again.
The Matlab program for the variable helix model is presented in Appendix II.

4.7 Experimental Methodology

Experimental validation is required for the time domain and analytical models. An explanation is given here of how the input data is collated and how the validation of stability lobes is carried out.

There are a number of advances in machine tool technology that introduce non-linearities into the dynamics of the machine tool system. That is to say that the modal characteristics of the machine tool as measured in the static condition are not always valid under the rotational speeds, bearing loads, cutting forces and temperatures when the machine is in cut. This will be discussed in more detail in the next section and experimental validation of time and frequency domain stability lobes for a number of machine tools will be presented and discussed.

The cutting forces are computed using the mechanistic model [134] which requires no knowledge of the shear angle but determines empirically the tangential and edge coefficients for the tool and workpiece combination.

As outlined in chapter 2, the following input data must be acquired for the computation of analytical and time domain stability lobes:

Tool and process parameters are also required as an input to the stability lobes (chapter 2). The tool geometries were checked against the drawings using a tool angle measuring system Helicheck ™.

Table (4.1) presents the measured tool parameters for all tools included in this study.

Tool	Diameter (mm)	Teeth	Helix 1 Degrees	Helix 2 degrees	Pitch 1 degrees	Pitch 2 degrees
ST3	16	4	30	30	90	90
VH4	16	4	35	40	107	73
VH3	16	4	40	42	90	90
VH7	16	2	35	40	150	210
VP4	16	4	35	35	107	73
VP7	16	2	35	35	150	210

Table 4.1 Measured Tool Parameters

4.7.1 Measurement of Transfer Function

As the cutting action, loads and deflections are directed at and around the tool tip, this is the point within the machine tool system where one must take a direct measurement of the transfer function. The transfer function of the cutting tool and machine tool system is measured using an impulse hammer to excite the tool tip. The hammer contains a calibrated load cell so that the input value is known and an accelerometer is mounted on the tool tip to measure the magnitude and phase response. A hammer impact will excite a broad range of frequencies and is a quick and practical measurement within a shop floor environment. One drawback of the hammer test is that the level of excitation across the desired frequency range can only be crudely controlled through hammer and tip selection. It is not always possible to get sufficient excitation at the high or low frequencies that may be of interest and sometimes a number of measurements with different hammer combinations are required to acquire the full range of desired data. An alternative to the hammer test is to use a shaker to excite the selected point at known frequency and levels of excitation. This method can give more controlled results but requires a greater level of set up for use on a machine tool and the measurement process is more time consuming. Hammer impulse tests are widely accepted as the standard methodology for measurement of the transfer function of cutting tools [135]. The apparatus are linked to a signal processor and then captured on a laptop via a data capture card.

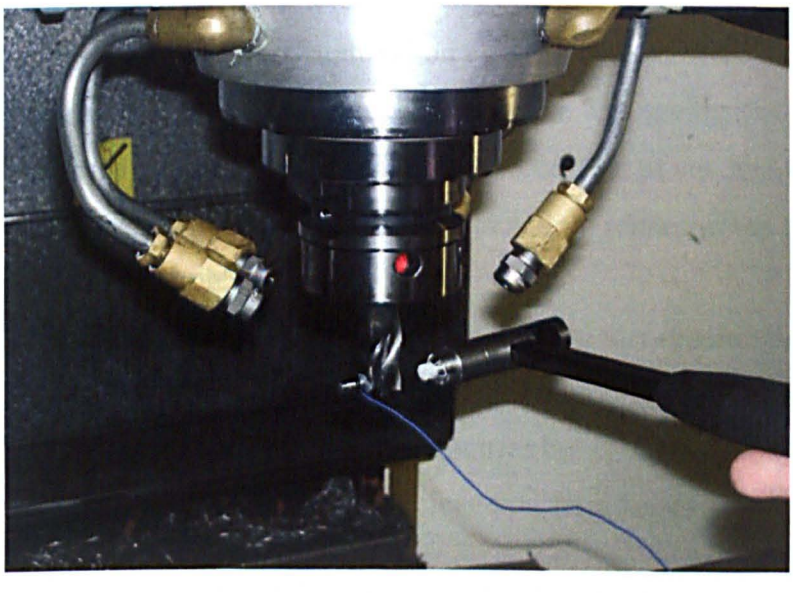

Fig. 4.9 Tap Test Measurement

An auto-range measurement is taken to scale the accelerometer and load cell responses and to ensure that the appropriate apparatus have been selected. The auto-scale simply scales the voltage response to optimise the measurement resolution. Five measurements are then taken in both the x and the y directions. Multiple measurements help to average out any measurement error and enable the coherence of the measurements to be assessed.

A Fast Fourier Transform (FFT) is computed to determine the response across the frequency range. The complex transfer function of the system can then be constructed, plotting the magnitude and phase response of the system to a known excitation.

The frequency response measurement is then used as an input into the stability lobe computation as outlined in chapter 2. For time domain simulation the modal parameters are extracted from the measurement, first using a curve fitting algorithm then identifying the modes for which the modal parameters are required.

4.7.2 Measurement of Cutting Force Coefficients

Both the time domain and frequency domain stability solutions are dependant upon accurate prediction of cutting force. For this knowledge of the cutting forces generated for a selected edge geometry and material property are required. This is done by following Altintas' mechanistic method.

Tests are carried out at three or more different feed rates at a set depth of cut and the forces for each cut are captured on a dynamometer. The x, y and z cutting forces are captured and plotted against chip thickness. The gradient of the curve represents the increase in cutting force proportional to the size of cut, and the point at which the curve crosses the y-axis (zero chip thickness) relates to the edge effect for the tool and workpiece combination [134].

This method provides a reliable cutting force that requires no knowledge of the shear angle or the chip formation process. A dynamometer is required and tests must be carried out for different edge geometries but it is an otherwise simple solution.

Example of cutting force coefficient data for a Sandvik end mill is presented below:

Test No:	Spindle Spd [rpm]	DOC a_p [mm]	Feed Rate ft [mm/th]	FR [mm/min]	Avg Fx [N]	Avg Fy [N]	Avg Fz [N]
1	100	2	0.03	12	5	-130	-20
2	100	2	0.05	20	-40	-180	-20
3	100	2	0.07	28	-60	-230	-20
4	100	2	0.1	40	-72	-290	-30

Table 4.2 Cutting Force measurements

The X,Y,Z average force data is plotted against feed per tooth. From the subsequent plot the X,Y,Ze and XYZc values can be determined.

$$\overline{F_x} = \overline{F_{xc}} \cdot G + \overline{F_{xe}}, \quad \overline{F_y} = \overline{F_{yc}} \cdot G + \overline{F_{ye}}, \quad \overline{F_z} = \overline{F_{zc}} \cdot G + \overline{F_{ze}} \qquad \textbf{(4.36)}$$

Where G is the gradient of the curve in Fig.4.12 and the edge effect $\overline{F_{ne}}$ is the force value when the feed per tooth is equal to zero, i.e. the point at which the curve crosses the Y-axis.

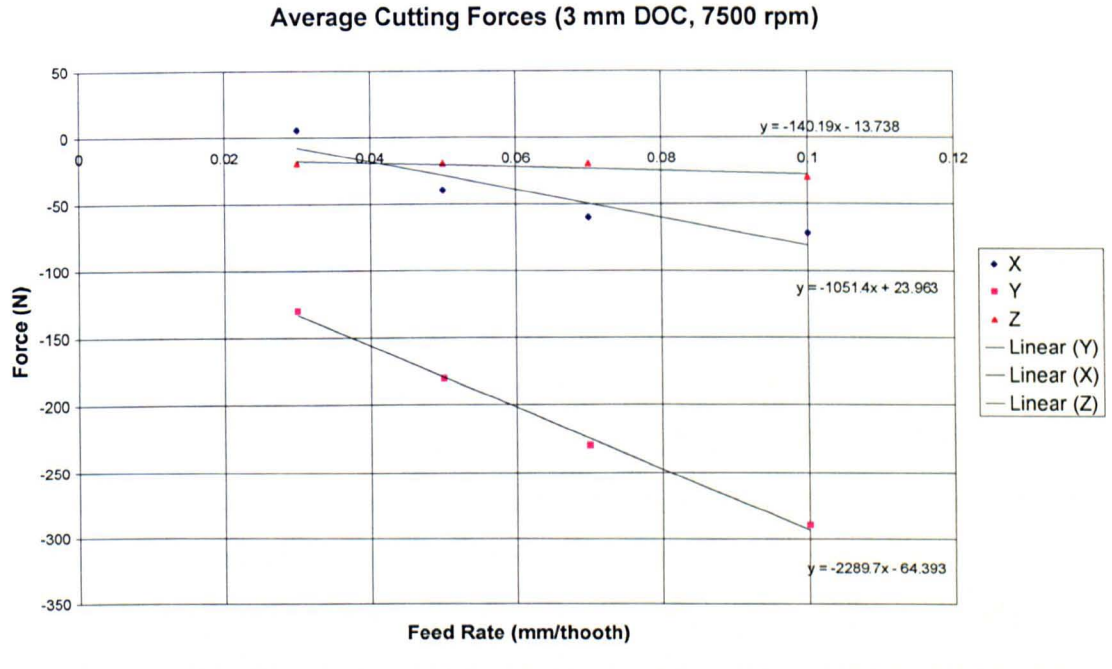

Fig. 4.10 Plot of Force vs Feed Rate to determine Ktc,Krc,Kac & Kte,Kre,Kae

The Kne and Knc values are then calculated as follows:

$$K_{rc} = \frac{4\overline{F_{xc}}}{m \cdot ap} \qquad \textbf{(4.37)} \qquad K_{re} = \frac{\pi \overline{F_{xe}}}{m \cdot ap} \qquad \textbf{(4.50)}$$

$$K_{tc} = \frac{4\overline{F_{yc}}}{m \cdot ap} \qquad (4.38) \qquad K_{te} = \frac{\pi \overline{F_{ye}}}{m \cdot ap} \qquad (4.51)$$

$$K_{ac} = \frac{4\overline{F_{zc}}}{m \cdot ap} \qquad (4.39) \qquad K_{ae} = \frac{\pi \overline{F_{ze}}}{m \cdot ap} \qquad (4.52)$$

For the above example the following values are obtained:

$K_{rc} = 200 \text{ N/mm}^2, K_{re} = 52 \text{ N/mm}^2$

$K_{tc} = -1000 \text{ N/mm}^2, K_{te} = 5.23 \text{ N/mm}^2$

$K_{ac} = -927 \text{ N/mm}^2, K_{ae} = -19 \text{ N/mm}^2$

4.7.3 Methodology for Validation of Stability Lobes

Equipment

To validate the stability lobes the boundary of stability for a range of spindle speeds must be found. This is done by first selecting a spindle speed range and setting an incremental spindle speed increase. For the tests presented in the next section the range was 3500 rpm-12000 rpm with an increment of 250 rpm.

The stability lobes should give good indication of what the depth of cut will be at each spindle speed so cuts are taken at the indicated depths around the limit of stability. Delio, Smith, and Tlusty [136], [137] suggested that audio detection offered one of the best methods for chatter detection and control. Other methods include dynamometers, accelerometers and strain gauges. Dynamometers have their own significant modal response, and this can affect part of the signal bandwidth. Dynamometers often do not have sufficient sensitivity above 1000Hz. As the cutting forces in end milling can be relatively low it is sometimes unclear when chatter begins. Accelerometers must be placed near antinodes in order to determine chatter. In some cases this does not occur or is not always possible as the nodal points may change with machining. If correctly placed, accelerometers will give a good indication of chatter, but the location is critical and some modelling is typically required in order to determine nodal points. Blum [138] and Liu and Liang [139] investigated the generation of acoustic emission during the machining process, and demonstrated that tool wear and cutting forces may be monitored. Teti [140] demonstrated that acoustic

emission (AE) may be related to cutting speed, feed rate, depth of cut and rake angle, and suggested that AE may be used for online control of the machining process. Microphones provide a good method of determining chatter as they can pick up signals across a large bandwidth and do not interfere with FRF of the system as proposed by Delio [136]. One problem is that microphones can be indiscriminate and will pick up background noise. This can be avoided by using reflection and direction techniques to ensure that the target sounds are picked up clearly.

Delio developed a chatter control system that offered a spindle speed correction based upon the chatter frequency recorded. The Harmonizer ™ software developed by Delio is now commercially available and is used in the following procedure to capture chatter frequencies.

In order to predict the tooth passing frequency and its harmonics, along with the stability plots for the system, certain parameters need to be input, including the spindle speed and number of flutes.

The software will accurately determine the actual spindle speed using a fine tune command. A chatter threshold is predicted which is set as a magnitude of the background sample and can be manually controlled.

When the cutter is engaged in the cut the sound of the cut is recorded. The ambient recordings will be filtered out of the sound spectrum, and any other frequencies that are not harmonics of the tooth passing frequency that are excited above the predicted chatter threshold will be identified as chatter frequencies.

Strategy

Once the stability lobe plots have been generated the tools described above can be used to validate the lobes by identifying stable and unstable cuts. With this in place the following steps are taken to validate the stability lobe plot:

1. ***Select spindle speed range***
2. ***Select spindle speed increment***
3. ***Carry out cut near to predicted limit of stability***
4. ***Record audio emission of cut using microphone***
5. ***Analyse FFT to find unstable frequencies***
6. ***If unstable***
    a. ***Record chatter frequency***

b. ***Reduce depth of cut incrementally (1mm) and repeat until stable cut is achieved***

7. ***If stable***

   a. ***Increase depth of cut incrementally until chatter is found and record frequency***

8. ***Move to next increment and repeat***

This strategy relies on the assumption that once a limit of stability is encountered at a specified depth of cut, chatter will always occur at any depth above that limit. Likewise stable cutting will always occur at any depth of cut below the limit. An example can be seen in Fig.4.11.

Below is an example of the time domain and FFT signals captured during the lobe validation process.

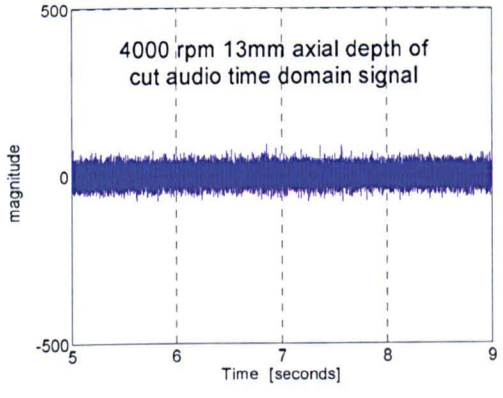

Time domain signal of stable cut

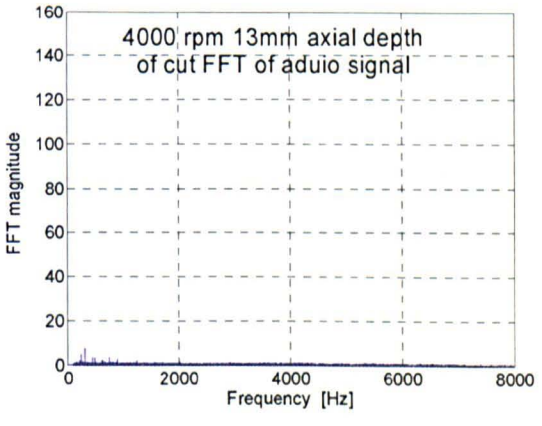

FFT of stable cut

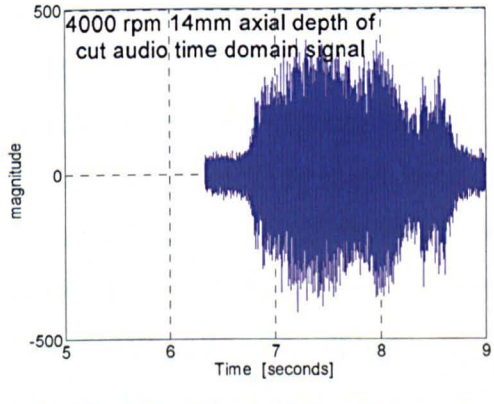

Time domain signal of unstable cut

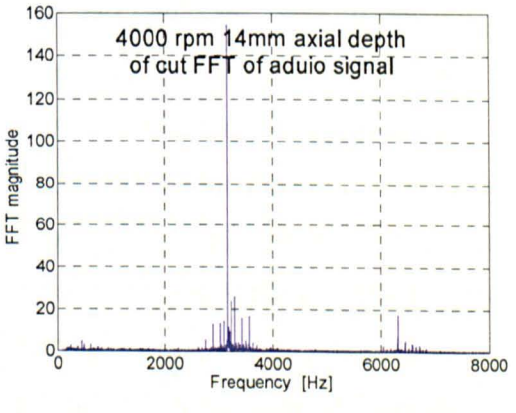

FFT of unstable cut

Fig. 4.11 Examples of stable and unstable cuts in time and frequency domain

4.8 Validation of machine tool linearity

4.8.1 Theory

Most of the accepted work on the stability of the milling process has acknowledged some simplifications in the analytical models. Non-linearities such as the teeth becoming disengaged from the cut and the process damping effect [103], have been well documented and are only included in time domain simulations. [141], [142], [143], [144].

One aspect of the system that much of this work appears to take for granted is the linearity of the machine tool system dynamics. As outlined earlier, a measurement is taken in the static condition with the spindle in a neutral gear and the axes stationary and with no load applied to the tool tip. During the cutting process the spindle is driven at speed which may result in varying pressures on the bearings, toolholder – tool interface and spindle- toolholder interface. The bending moment acting on the tool and spindle bearings may also change the system dynamics.

In addition to these fundamentals of the cutting process, variable preload on spindles is becoming more common and there are varying applications of spindle cooling or floating bearings to accommodate thermal effects on the spindle. There are also wide ranges of spindle interfaces available which behave differently under loaded conditions. It is the author's experience that the dynamics as measured in the static condition do not always match with the system dynamics during the cutting process.

Some recent research has stated that stability lobes are invalid for variable preload spindles [145] and variable preload spindles are now commonly seen as a suitable technology to protect spindle bearing life [146]. Spindle bearing life can also be protected by controlling chatter and current stability analysis techniques do not cater for variable preloads and therefore potentially reduce bearing life. Some advances in spindle dynamics research begin to offer solutions in this area. Simple Finite Element (FE) modelling of spindles has been developed and documented [147], [134] and these models can be built up from the spindle design, taking into account bearing stiffness and contact stiffness at the various interfaces. Using these techniques it is possible to accurately match a modelled and measured FRF. If the chatter frequency in the cutting process is measured as outlined above then a quick indication can be taken as to whether the system dynamics under cutting conditions tally with those

measured under static conditions. According to stability theory [76], [134] chatter will only occur at a frequency that has a negative real value, in the case of the coupled mode theory the eigenvalue must have a negative real value but his will still result in chatter at frequencies with low positive values and typically negative real values. If the chatter frequency is a long way from having a negative real value and does not correspond with any mode, positive or negative then it would appear that the system dynamics have altered under load. To gain an accurate assessment of the system dynamics then a full empirical stability lobe should be plotted as outlined in the previous section. The empirical lobe plot and chatter frequency plot can then be compared with the analytical prediction and any shift in dynamic behaviour becomes evident.

The FE spindle models can be modified to fit the system dynamics under load. To do this some idea of the spindle design and source of non-linearity is required. Three areas that have been documented are the bearings [145] and the spindle toolholder interface [148], and drawbar pressure [120]. If the FE model can be modified to represent the cutting conditions then an accurate prediction of the system dynamics under load is possible and stability lobes can be plotted. It may be that the system response changes with cutting force, bending moment, spindle speed or gear range and this means that a number of iterations of the FE model would also be required. This is an important area for further work. Smith [107, 149] has documented the influence of bending moment on stiffness of HSK and taper interfaces and demonstrates that a dramatic loss of stiffness can occur for high bending moments, particularly on HSK interfaces. The author has observed instances of this in industrial application where an increase in feed has apparently initiated chatter for large gauge line extensions on HSK interfaces. This is believed to be as a result of increased bending moment and reduction in contact stiffness and therefore limit of stability, as accepted chatter theory suggests that increased feed rate in milling should not have a detrimental influence on stability [21],[134].

A method is required to combine a static measurement with an accurate FE model of the spindle under the desired cutting conditions. One limitation of FE models is the inability to predict modal damping characteristics. In recent years there have been advances in the study of Receptance Coupling Substrate Analysis (RCSA), first presented by Schmitz and Davies [150] as a method for analytical prediction of the tool point dynamic response by combining frequency response measurements of

individual components through appropriate connections. The method uses vector manipulations to couple frequency responses.

The method is intended to reduce the machine downtime required for measurement of machine tools and cutting tool dynamic response. This can be achieved if the various components can be measured separately and then the various combinations can be modelled to give accurate predictions. The result would be a significant time saving as otherwise every single combination of machine tool, toolholder, cutting tool and cutting tool extension must be measured.

In RCSA direct and cross transfer functions are required to predict the response of the final assembly at any spatial coordinate. The FRF's are required only at the point of interest unlike FE or modal coupling techniques. In a simple example the system is represented as two bodies and a spring which are coupled through the equilibrium conditions for the various components and the direct and cross transfer function of the combined bodies are defined at a point on each, G11,G12,G21,G22 as a function of the measured transfer functions of the individual bodies.

$$G_{11}(w) = \frac{X_1}{F_1} = H_{11} - H_{11}\left(H_{11} + H_{22} + \frac{1}{k_c}\right)^{-1} H_{11} \qquad \textit{(4.53)}$$

$$G_{21}(w) = \frac{X_2}{F_1} = H_{22}\left(H_{11} + H_{22} + \frac{1}{k_c}\right)^{-1} H_{11} \qquad \textit{(4.54)}$$

$$G_{12}(w) = \frac{X_1}{F_2} = H_{11}\left(H_{11} + H_{22} + \frac{1}{k_c}\right)^{-1} H_{22} \qquad \textit{(4.55)}$$

$$G_{22}(w) = \frac{X_2}{F_2} = H_{22} - H_{22}\left(H_{11} + H_{22} + \frac{1}{k_c}\right)^{-1} H_{22} \qquad \textit{(4.56)}$$

The interface is modelled as linear and torsional springs and dampers representing the contact conditions between the tool and toolholder. Response functions are introduced relating displacement to moment and rotation to applied force and moment. Mobility FRF's are introduced relating force to velocity, accounting for the effects of viscous damping. The component FRF's are predicted analytically due to difficulties in measurement techniques for the free body states. The RCSA model has been tested for a number of tooling setups, showing good correlation with experimental results. It

is anticipated that once the contact conditions have been determined in this manner for a given toolholder-tool interface or spindle- toolholder interface that these can be taken as representative for that particular interface and can be reused for different geometries of tool or toolholder. This is not validated however, and the trial and error/ iterative method required determining the contact conditions represent the one serious weakness of this method.

Although little research has specifically addressed the issue of non-linearities in machine tool dynamics some of the relevant tools have been developed and this is a key area for future research. There are some publications [145] and many experienced engineers within the industry that claim that stability lobes are of no use as a result of these non-linearities, conversely there are many publications that neglect the existence or at least the popularity of machines with non-linear dynamics, believing that stability theory can be accurately applied to most or all machine tools [21].
Before any linear analytical models for milling stability can be validated it is important to first validate the linearity of the machine tool dynamics.
At the University of Sheffield AMRC with Boeing, the workshop contains a range of 3 and 5 axis machine tools representing those used in the aerospace industry. The Makino A99 will be tested for non-linearities in its dynamic performance and suitability for the validation of analytical milling stability models. The Makino is selected as it has a suitable spindle speed range up to 12,000 rpm and has a chilled spindle which limits any change in bearing load due to thermal expansion and subsequent changes in dynamic response at higher spindle speeds.

4.8.2 Empirical data

The reliability of the stability algorithm used here for a standard end mill has been well documented [81]with empirical data to support the models. As explained above the stability lobe predictions will only hold true if the system dynamics as measured in the static condition represent those that are seen during the cutting process at speed and under load. The validation of the linearity of the machine tool dynamics therefore requires measurement of the static tool tip FRF and the subsequent plotting and validation of stability lobes.

The Makino A99 has no preload or floating bearing mechanism designed to cope with increased pressure or loads at high speeds. Instead the machine has coolant delivery to the bearings. The spindle –toolholder interface is a Big-Plus ™ face and taper contact system. The face and taper system is designed to optimise contact stiffness under loaded conditions. Smith demonstrates that taper contact can be lost on standard taper interfaces whilst if face contact is lost on an HSK interface then stiffness is drastically reduced [107]. The Big-Plus system consists of a 50 taper with face contact and in theory represents the best of the taper or HSK approaches. The Big-Plus system is designed to offer maximum stiffness although sometimes this may come at the cost of damping. An increase in dynamic stiffness is directly proportional to an increase in limiting depth of cut and in some cases an increase in static stiffness may come at the cost of a decrease in damping, resulting in an overall reduction in dynamic stiffness and a subsequent reduction in stability [120].

The tool selected for measurement was tool CP9 as described in Table 4.5.

The tool was loaded into the Big-Plus toolholder with a 66mm extension from the face of the collet. The FRF was then measured as outlined in a previous section and the x and y direction measurements are presented in Figs 4.12 & 4.13.

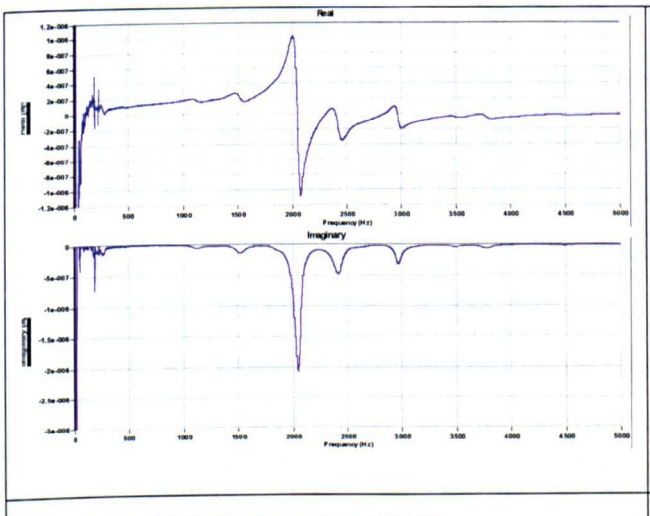

Fig 4.12 CP9 X-direction FRF
Makino A99 Big Plus 66mm extn

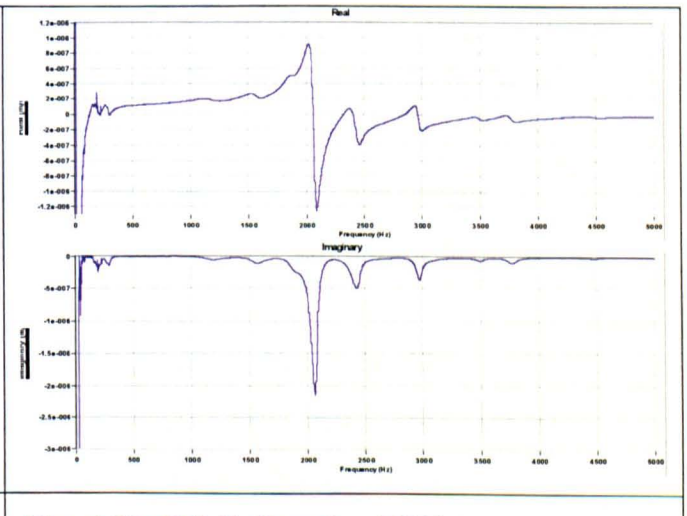

Fig. 4.13 CP9 Y-direction FRF
Makino A99 Big Plus 66mm extn

Stability lobe plots can now be created for this tool using the following input parameters:

D	16mm
a_e	5mm
M	4mm

Material	Al 7050
K_{tc}	400 N/mm^2
K_{rc}	160 N/mm^2

Table 4.3 Parameters for stability lobe plot

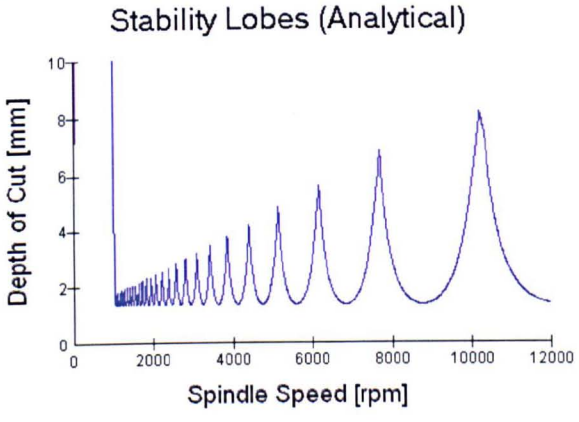

Fig. 4.14 CP9 X- direction lobes

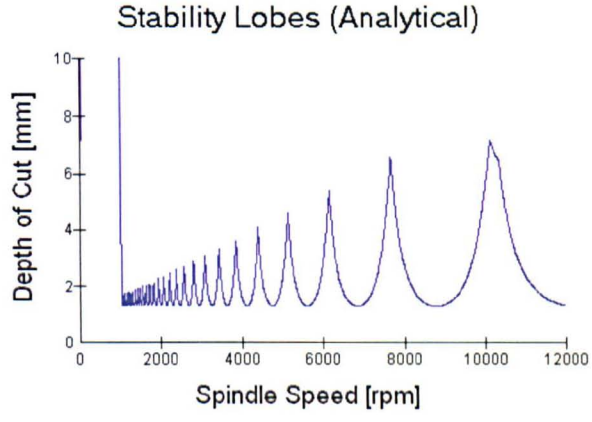

Fig. 4.15 CP9 Y direction lobes

The lobes were plotted for 5mm radial immersion for a number of reasons:

- Practical convenience, a slot can be opened up in steps of 5mm without leaving thin walls between cuts
- At less than full engagement there is clearance for chip evacuation for large depths and less process damping effect.
- The radial depth of cut is large enough that at least one tooth is always engaged in the cut, therefore the effects of decayed vibration outside of the cut can be neglected [86],[84].
- Taking a relatively low depth of cut will increase the limit of stability and will therefore better suit the observations on variable helix cutter for the next stage of the work, where full axial contact with the cut will broaden the range of tooth pitches engaged in the cut.

These lobe plots are validated as outlined in section 4.6.3.2. The spindle speed range is defined as 3500 rpm to 12000 rpm in increments of 250 rpm. The lower limit is taken at 3500 rpm as below this speed process damping effects may become stronger and these are not accommodated in the coupled mode algorithm. The depth of cut was monitored in increments of 1mm and the border for stability was taken as the depth of

cut 1mm above the highest measured stable depth of cut. Aluminium has been selected as it enables a wider range of surface speeds to be calculated for the lobe validation. The information can also be presented as an empirical lobe plot:

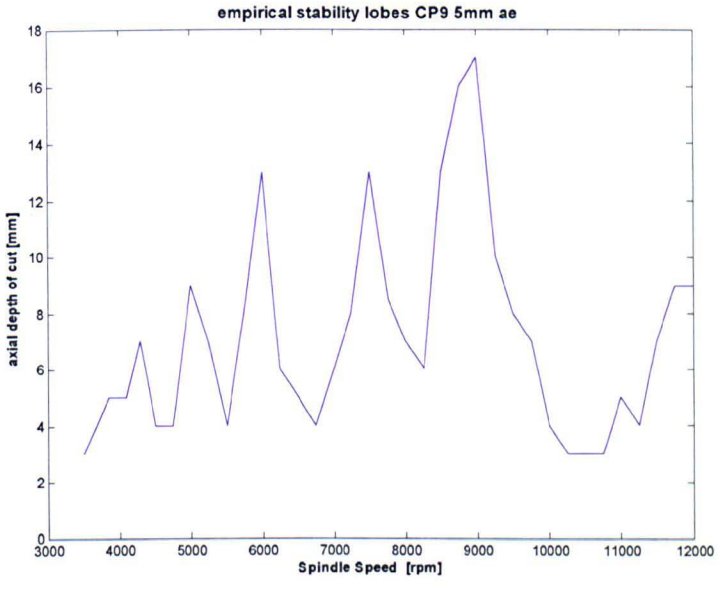

Fig. 4.16 Empirically measured lobe plots for A99, 16mm CP9 , 66mm extn,5mm ae

Fig. 4.16 shows good correlation with the predicted analytical lobes up to around 7500-8000 rpm. At around 9000 rpm an extra lobe appears that was not predicted through the initial stability analysis. At 10000 rpm there is no lobe and the limiting depth of cut has reduced from 4mm to 3mm.

This deviation from the predicted lobes must be a result of some inaccuracy in the stability lobe model or some inaccuracy in the input data. The model used here takes no account of the 'free vibration and decay of the tool' for shallow depths of cut. It has been well documented that for shallow depths of cut a second lobe may appear in between the standard lobes [84], [87], [82],[83]. The second lobe is followed by a subsequent drop in blim and then the standard lobe again takes form.

The parameters have been selected in this case such that the second lobe effect may be neglected due to a sufficiently large radial depth of cut and at least one tooth engaged in the cut at all time. The secondary lobes would not result in the shift or disappearance of the subsequent standard lobe where the tooth passing is in phase with a sub-harmonic of the vibration frequency.

A further understanding of these results can be obtained from analysis of the chatter frequencies at the border of stability. For each unstable lobe it is expected that the chatter frequency at the border of stability will change with spindle speed and phase.

The chatter frequency should gradually increase from the left to the right of the unstable region. The form of the lobe and the frequency of chatter correspond to the negative part of the real plot as outlined in chapter 2.

The range of chatter frequencies at the border of stability for each lobe should look the same with a gradual increase in frequency with spindle speed until the next unstable lobe begins and the frequency will drop sharply then continue the trend.

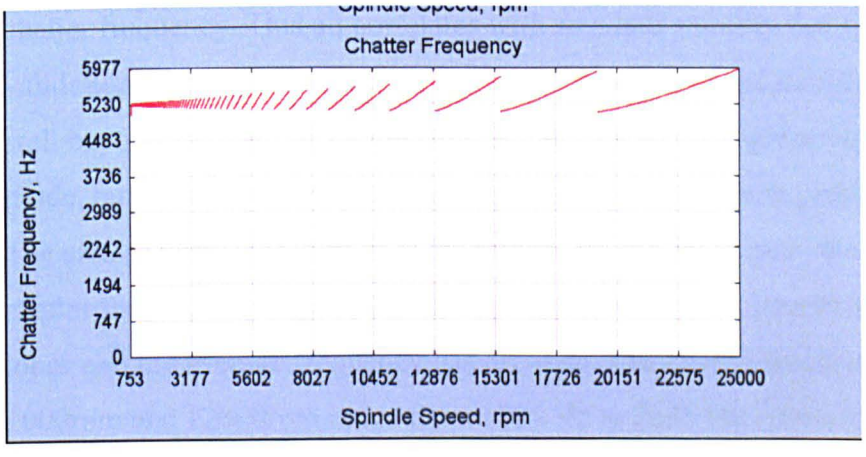

Fig. 4.17 Chatter frequencies for standard lobes

Figure 4.17 shows typical predicted chatter frequency trends with spindle speed at the border of stability. The chatter frequency vs spindle speed plot for CP9 is presented in Fig.4.18.

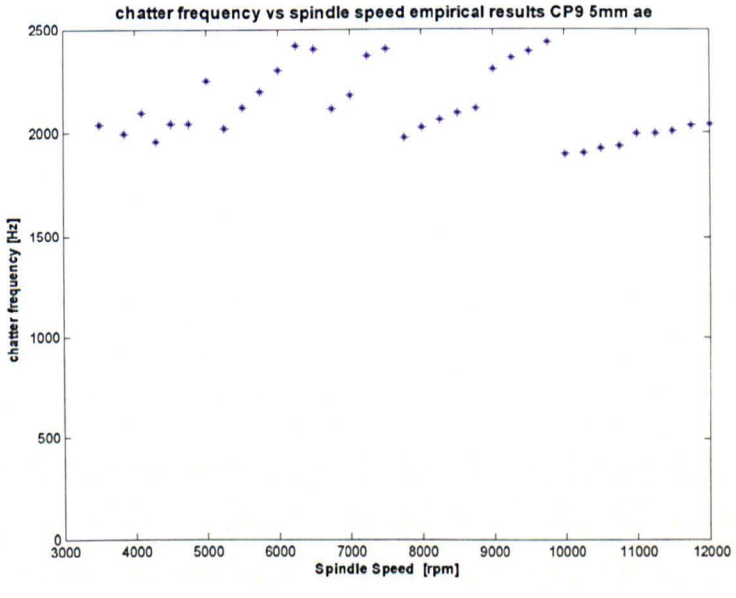

Figure 4.18 – Measured chatter frequency vs spindle speed

The plot for the measured chatter frequency against spindle speed shows two distinct chatter frequencies. The first frequency is around 2100 Hz and the second is around 2400 Hz. These both correspond with the measured FRF (Fig.4.13&4.14) , the 2100 Hz being the dominant mode and the 2400 Hz mode only causing chatter when the 2100 Hz mode is stable. This can be seen in the empirical lobe plot (Fig 4.17) as the 2100 Hz lobes are cut short at 6300 rpm, 7750 rpm and 9500 rpm by the 2400 Hz chatter frequency. This all correlates with standard stability theory and is a good validation of lobe theory and behaviour at the boundary of stability. In some instances well beyond the limit of stability the 2400Hz chatter has given way to the 2100 Hz mode, but at the boundary results matched very closely with prediction.
The area of particular interest is the region beyond 8000 rpm. We can see that the chatter frequencies from 7500-9000 rpm do not climb as steeply as with the previous lobes and the average frequency has dropped. The chatter frequencies between 1000rpm and 12000rpm range from 1895 Hz to 2036 Hz. The average frequency has dropped by around 150 Hz. The drop in frequency corresponds to a shift in the stability lobe positions. The stable speeds for the initial statically measured frequency of 2100 Hz and the recorded chatter frequency of 1930 Hz are calculated:

$$n = 60 * \frac{f_c}{m} * N$$

for fc= 2100 Hz and m=4 teeth and N= 3,4,5
n = 10500 rpm, 7875rpm, 6300 rpm, 5250 rpm

for fc = 1930 z=4, N=2,3,4
n= 14475rpm, 9650 rpm, 7237 rpm, 5790 rpm,

In the experimental lobe plot the region from 7500 rpm to 9000rpm represents the region where the system dynamics shift. The lobe plot (figure 4.17) clearly shows the start of lobe number 4 which then begins to fall away early due to the frequency drop. An unstable region forms that coincides with the frequency of 1930 Hz between lobes 2 and 3. Lobe 2 for the lower frequency can then be seen at 9000 Hz, the peak is removed by the 2400 Hz chatter frequency so that the peak spindle speed does not tie exactly with the maximum stable spindle speed of 9650 rpm. The plot then continues as expected for the 1900 Hz mode with the stability dropping off to a lower b_{lim} than

previously and beginning to climb again at 12000 rpm towards the N=1 lobe at 14475 rpm.

The lobe plot and frequency data clearly demonstrate a drop in frequency and stiffness in the dominant mode above 7500-8000 rpm. A reduction in modal stiffness would present itself as a drop in modal frequency and a reduction in the minimum stable depth of cut. Both of these are seen with a frequency reduction of approximately 150 Hz and a reduction in b_{lim} from 4mm to 3mm.

It would therefore appear that some contact stiffness is reduced above 8000 rpm. Below 8000 rpm the machine tool behaves as predicted and the recorded chatter frequencies match with those predicted from the FRF measurements with the spindle in the static condition.

One possible explanation for the change in stiffness could be heating of the spindle or bearings and thermal growth of the spindle. An investigation was carried out to ascertain whether the shift in frequencies did actually correspond to the suggested spindle speed range or whether it was a result of thermal growth from the spindle running for a period of time and independent of the operational spindle speed range.

A warm up cycle was run for 1hour with the spindle at 10000 rpm. After this the static measurements were repeated as were a number of cuts around the border of stability at both the high speed and low speed ranges.

The FRF data is presented in Figs 4.19 & 4.20:

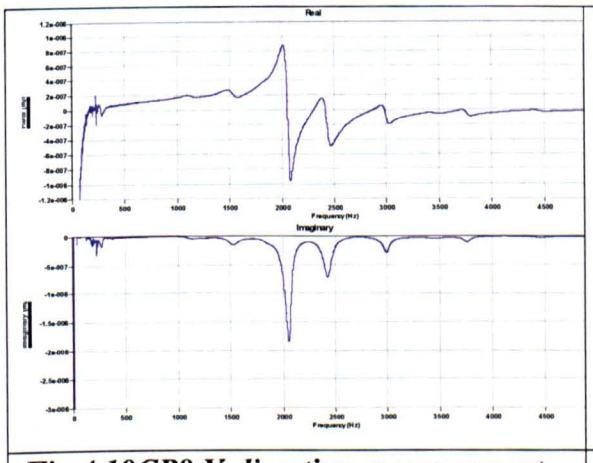

Fig.4.19CP9 X-direction measurement Makino A99 Big Plus 66mm extn after 1 hour warm up cycle

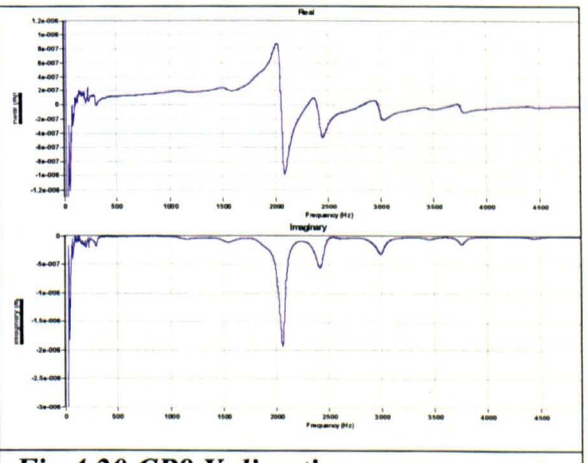

Fig.4.20 CP9 Y-direction measurement Makino A99 Big Plus 66mm extn after 1 hour warm up cycle.

The figures show there is little change in frequency or stiffness from the original measurement. If anything there is an apparent increase in dynamic stiffness of the

dominant mode which may be as a result of contact stiffness improving or could simply be within the limits of experimental error. There is nothing to indicate that the heating of the spindle alone has caused the shift in frequency and stiffness previously observed.

Stability tests were repeated at 4500 rpm and 1000rpm with exactly the same chatter frequency and stable depths of cut as previously observed. It can therefore be concluded that the reduction in modal stiffness above 8000 rpm is a function of the operational spindle speed range and below 7500 rpm the machine dynamics behave in a linear manner. Such deviations from linearity are not uncommon and it has been proven that analysis of the linearity of the machine tool dynamics is essential to determine a predictable operating range. It has now been comprehensively demonstrated that the Makino A99 has predictable dynamic behaviour below 7500rpm and therefore all speeds up to this limit are suitable for validating a linear stability lobe model.

4.9 Analysis of Results

4.9.1 Input Data

Measured FRF and CFC data

Measurement	Frequency (Hz)	Stiffness N/m	Damping
ST3,VH3 (x)	2062, 2400, 2956	1.337e7, 9.944e7, 2.031e8	0.0206, 0.0183, 0.0151
ST3,VH3 (y)	2063, 2388, 2957	1.259e7, 8.624e7, 1.575e8	0.0199, 0.0175, 0.0150
VH4,VP4 (x)	2061, 2609, 3032	1.932e7, 5.192e7, 4.433e8	0.0162, 0.0541, 0.0129
VH4,VP4 (y)	2058, 2444, 2992	1.886e7, 9.190e7, 1.902e8	0.0227, 0.0224, 0.0164
VH7,VP7 (x)	2160, 2478, 2985	2.208e7, 2.803e7 6.941e7	0.0157, 0.0191 0.0173
VH7,VP7 (y)	2145, 2468, 2983	1.875e7, 2.654e7,6.776e7	0.0206, 0.0178, 0.0190

Tool	Kte N/mm	Ktc N/mm^2	Kre N/mm	Krc N/mm^2
ST3	26	400	30	160

Table 4.4; Modal parameters and cutting force coefficients.

Tool Geometry Data

Tool	Diameter (mm)	Teeth	Helix 1 degrees	Helix 2 degrees	Pitch 1 degrees	Pitch 2 degrees
ST3	16	4	30	30	90	90
VH4	16	4	35	40	107	73
VH3	16	4	40	42	90	90
VH7	16	2	35	40	150	210
VP4	16	4	35	35	107	73
VP7	16	2	35	35	150	210

Table 4.5 Tool Geometries for Variable Helix Trials

The following plots show an overlay of the time domain, analytical and empirical results as laid out within this chapter.

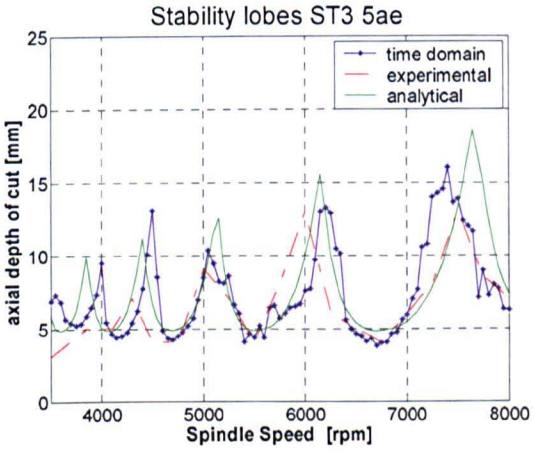

Fig.4.21 ST3 Lobes

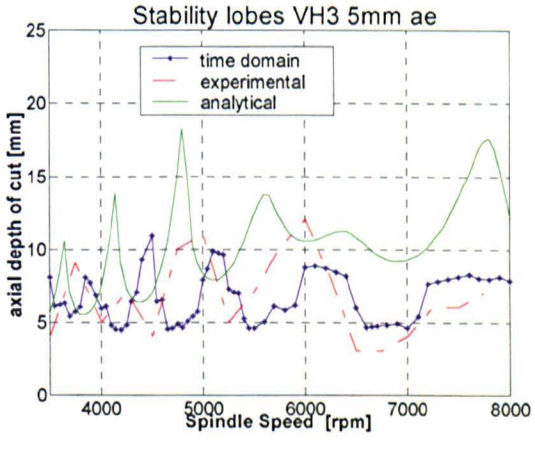

Fig.4.22 VH3 Lobes

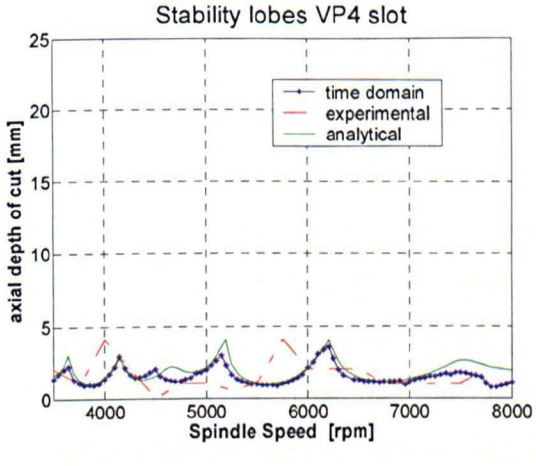

Fig.4.23 VP4 Lobes

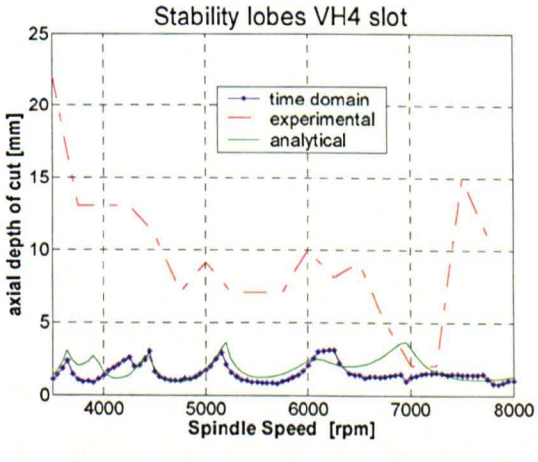

Fig.4.24 VH4 Lobes

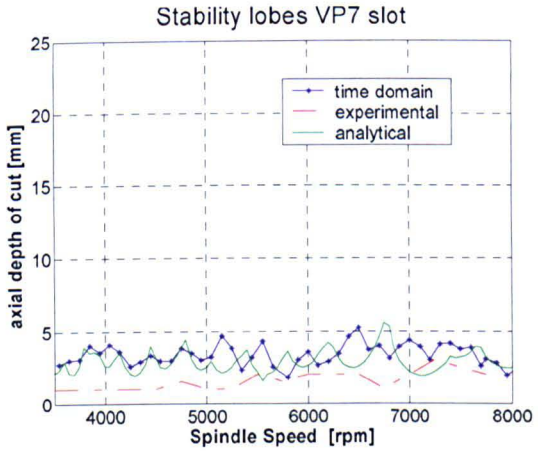

Fig.4.25 VP7 Lobes

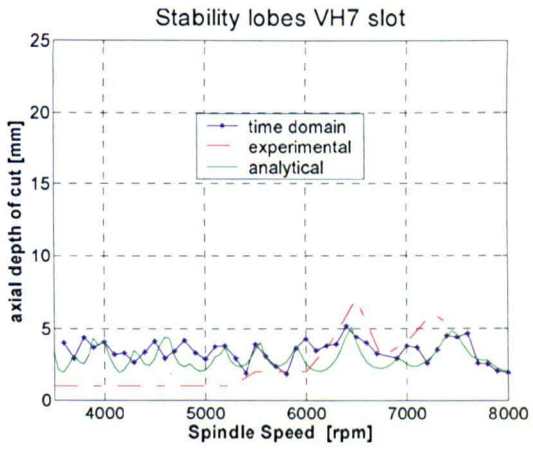

Fig.4.26 VH7 Lobes

4.9.2 Time Domain Chatter Recognition Criteria

It is expected that the time domain solution should give an accurate representation of the kinematics of the milling process. As the time domain results for the VH4 tool do not match with the empirical results it is possible that the chatter recognition method is not accurately detecting the stability limit. The chatter recognition method used for the time domain results in Figs 4.21-4.26 looks for the maximum static chip thickness along the length of the flute and uses this as criteria to determine chatter, judging a relative increase in chip thickness to be chatter. The variable helix tool will result in a large variation in chip thickness of adjacent flutes and variation in chip thickness down the length of the flute when the process is stable.

An alternative method for chatter recognition is sought that is not dependant upon chip thickness. Sims [132] proposed a chatter recognition criterion based upon the self-excited damping ratio of the system but the method requires filtering of the tooth passing frequency and cannot be applied to variable pitch tools.

Schmitz [151] proposed a variance method for chatter detection, demonstrating that the variance of tool tip position observed under once per revolution sampling grew with the onset of chatter. For comparison the Sims model [132]is used with the variance method to rerun the time domain stability lobe calculations.

The time domain stability lobes using the variance chatter recognition criterion for tool VH3 at 5mm radial immersion are displayed in Fig. 4.27. The results for the

variance method were close to those using the chip thickness chatter recognition criterion, neither method accurately predicting the increased stability for the VH4 tool. It was considered that the chip thickness chatter threshold of more than 20% of the static chip thickness may have been too low, for this reason a number of data points were computed with a chatter threshold of 50% of the static chip thickness with very little difference in the resulting stable depth of cut. In the case of the VH3 trials there appears to be a shift in the lobes between the analytical and time domain solutions, with the analytical solution being closer to the empirical results. The shift could be due to the calculation of the pitch angles and the influence of the average depth of cut assumption for flute engagement. The time domain has accurately predicted the axial depth of cut while the analytical solution has correctly predicted the stable speed regions.

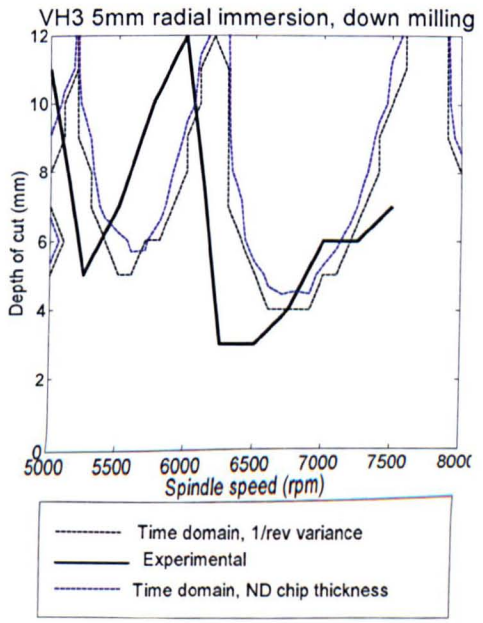

Figure 4.27. Lobe plots for VH3 using the once per revolution - variance chatter recognition criteria

4.9.3 Discussion of Results

As neither chatter recognition criteria correctly predicts the stability for VH4 it appears that the time domain model does not produce a stable outcome for the larger depths of cut, instead the time domain model predicts stability lobes that are close to the analytical average pitch results. The enhanced stability of the variable helix cutter VH4 is not represented in the time domain model and this may lend some insight into

the mechanics of variable helix end mills and the added stability. The experimental plot for VH4 bears resemblance to process-damped lobes; with a high depth of cut at low speed gradually reducing as the spindle speed increases. The fact that the lobe positions appear to match those predicted through the analytical and time domain solutions adds credence to this theory. All of the cutting tools bore the same edge geometry and it has been demonstrated that no process damping would occur within the selected spindle speed range under normal conditions. It may be possible that the inherent process damping in the 'layers' of the tool where the tooth period is stable inhibit chatter growth in the unstable 'layers'. Accurate modelling of process damping is not included in the time domain models and this would require further work.
It is also possible that the stabilising effect of the VH4 geometry is due to the disruption of the unstable tooth periods, preventing an unstable phase from taking hold in a similar manner to the spindle speed variation method [123]. The broad range of tooth periods along the length of the flute and varying between each flute may prevent any unstable phase from taking hold. This seems a likely explanation although it would be expected that the time domain simulation would accurately represent this phenomenon. The results for VH3 and VH7 suggest that for certain conditions the variable helix tools behave like variable pitch tools, the lobes are positioned by assuming the average pitch along the engaged flute length and no significant benefit in overall stability is observed over a variable pitch tool.

4.10 Summary

This chapter presented an analytical model for the prediction of stability for variable helix end mills, based upon the variable pitch model developed by Budak & Altintas. A new method for variable pitch lobe plotting is also described, showing the stability boundary as a continuous curve.
For validation a time domain solution is investigated and a technique for experimental validation of stability lobes is presented. An investigation into the linearity of machine tool dynamics is undertaken and it is demonstrated that under certain conditions the dynamics as measured in the static condition are not valid for the prediction of cutting dynamics at speed and under load. It is demonstrated that the chosen Makino A99 is linear between 3500rpm and 7500rpm and lobes are plotted analytically and experimentally for this range.

A comparison of the chatter stability of variable pitch and variable helix end mills has been presented, demonstrating that variable helix tools can show greatly enhanced stability and productivity. A new analytical model is presented for the stability of variable helix tools and shows good correlation with experimental and time domain results for cases where the helix variation is within a certain range.

Results from a time domain solution using the once per revolution variance method for chatter detection are presented and show good correlation with the chip thickness chatter recognition criterion. Neither model accurately predicted the stability for tool VH4 where the stability was much greater than the variable pitch, standard helix equivalent. It is possible that some form of process damping influences the stability, whereby the stable phases along the flute length inhibit the onset of regenerative chatter.

It is likely that the chatter suppression achieved with the variable helix tool in cases where a large axial engagement is permitted is a result of disturbance of the tooth passing time delay period along the length of the flute, preventing an unstable chatter period from taking hold. This suppression technique is akin to the spindle speed variation method rather than the stability lobe 'tuning' method. For this reason the analytical solution based upon an average pitch is only accurate for small axial engagement where the tool behaves as a variable pitch. It is also possible that process damping plays a part in the high performance of the variable helix cutter. The time domain model is believed to offer a comprehensive representation of the true kinematics of milling [99] but process damping is one of the known phenomena not included and could therefore offer an explanation for the observed empirical results. For larger axial engagements and to be able to model the full benefits of variable helix tools a new model is required that takes into account the pitch variation along the length of the flute. Such a model has to be iterative since one of the unknowns, depth of cut, forms a feed back loop as both an input and output of the solution.

The enhanced stability of variable helix end mills that has been demonstrated experimentally is of particular use in cases where machine tool linearity cannot be predicted as an overall increase in stability is observed, irrespective of spindle speed. Both the issues presented here of non-linearity of machine tool dynamics and of the inability of an established time domain model to predict stability of variable helix end mills make the study of the process damping phenomenon in Chapter 5 of particular interest.

5 PROCESS DAMPING AND TOOL OPTIMISATION

5.1 Introduction

The established theory on process damping has been explored in chapter 2. The desire to understand process damping was made clear through the CIRP initiative that led to a number of papers [106] that tried to explain and model process damping through speed dependant dynamic cutting force coefficients. Although the research provided an insight into the mechanism and manifestation of process damping no clear theoretical models were developed to predict process-damping effects. The majority of recent research on milling chatter has focussed on regenerative chatter and stability lobes [76],[81]. Good correlation between experiment and analytical results have been demonstrated using the various analytical and time domain stability lobe models [96], [129], [131],[97] but there has been less interest in process damping modelling, possibly due to the lack of success at accurate modelling.

The significance of process damping when machining 'difficult to cut' alloys, or materials where tool wear limits surface speed, has been discussed in chapter 2. Process damping provides the stability mechanism by which the majority of titanium machining can be achieved. A deeper knowledge of process damping is essential if accurate stability predictions and optimisation of parameters are to be achieved when milling titanium.

This chapter begins with a review of the process damping phenomena and the factors that can influence it. A procedure is then defined so that the process damping performance of a selected cutting tool and material can be characterised from which the influence of a number of parameters can then be explored. The influence of tool and cutting parameters on process damping performance are explored and FE analysis is used to support the findings and develop an understanding of the mechanics behind the process damping phenomena. Having established a means for evaluating process damping performance and understanding the parameters that strongly influence it, the second part of the chapter goes on to study the influence of process damping on desired cutting tool dynamics. A technique is developed whereby the FRF can be manipulated to result in stable milling parameters for solid carbide end mills for the full range of practical surface speeds so that chatter is no longer a critical path limitation on milling performance.

5.2 *Characterisation of Process Damping Performance*

5.2.1 Factors influencing process damping

To summarise the theory outlined in chapter 2; process damping is understood to be a result of rubbing of the relief face of a tool against the downward slope of a waveform traced by the tool on the surface of the workpiece due to vibration at a dominant frequency. It is widely understood that the gradient of the waveform is increased through reducing the surface speed and thereby reducing the wavelength of the vibration. The interaction is related to the relief angle of the cutting tool, the gradient of the waveform and the workpiece and tool material properties [103],[21].

Surface speed

Most practical understanding is focused on increasing the gradient of the waveform. This can be done by reducing the wavelength or increasing the amplitude of the vibration. As outlined in chapter 2 the wavelength is a function of surface speed of the tool and the frequency of vibration. Therefore either increasing the *frequency* of vibration or reducing the *surface speed* will increase the gradient of the waveform and increase the process damping effect (Fig 2.12). Later in this chapter the influence of chatter frequency will be studied in depth.

Feed per Tooth

Less research has been carried out on the influence of the amplitude of the waveform, the amplitude of vibration will be proportional to the cutting force and the stiffness of the machine tool system as seen at the tool tip [6]. Force can be increased through changes in axial depth of cut, number of teeth engaged in the cut, feed per tooth or tool geometry. An increase in axial depth of cut or radial width of cut can result in chatter [21] rather than stabilise it and the relationship between these parameters and process damping is therefore highly non-linear.

Feed per tooth or chip thickness does not directly influence regenerative chatter and the influence of feed upon process damping can readily be studied. The only other way that chip thickness is known to influence regenerative chatter is through changes to the cutting force coefficient. It is known that small chip thicknesses can lead to

work hardening of the chip material, increasing the cutting force coefficients and lowering the limit of stability at small feed rates [134]. When studying the influence of feed per tooth on chatter, tests will be carried out to distinguish between the influence on process damping due to the amplitude of vibration and the cutting force coefficient. As the stabilising mechanism in process damping is believed to be due to the 'rubbing' force between relief face and workpiece material, any increase in the friction force would be expected to increase the process damping influence [103]. It is therefore likely that increasing the cutting force through an increase in chip thickness will have a twofold effect of increasing the friction force and increasing the amplitude of the waveform.

Tool Geometry

The relief angle of the tool is believed to strongly influence process damping, for constant amplitude of vibration it is the relief angle of the tool that will dictate the level of interference. There may also be a rubbing effect at the tool nose, the phenomenon of 'bedding in' is commonly observed in milling and is considered in process monitoring techniques [152] [153]. During this initial wear period a new tool may chatter initially and then settle down to stability after a few minutes of operation. In such cases the tool loses its edge sharpness and the stability effect may well be down to the rounding of the nose radius and the effective reduction in the relief angle at a micro level. It is also common practice for experienced operators to run the edge of a new tool along a bench to dull the cutting edge slightly to avoid chatter. The influence of relief angle will be studied here and the effect of edge rounding will be discussed and proposed for a further study.

The other possible influence on tool geometry would be rake angle, as explained when discussing chip thickness, an increase in the cutting force would lead to a proportional increase in the frictional force and may therefore increase the process damping effect. Both the magnitude and direction of the shearing force or radial force could influence process damping.

In the next section an experimental design is outlined to study the effects of feed rate and tool geometry on process damping performance. One commercially available software package considers the influence of Process Damping when calculating stability lobes. Metal Max TXF ™ software uses a critical wavelength value to

determine the border of stability as defined by Tlusty [21] in terms of a spindle speed below which chatter will not occur. This provides a simple and effective method for characterising process damping and it is through the critical wavelength value that the process damping performance shall be assessed in the following tests. The software and research by Tlusty and Smith [76],[97] indicate that the border of process damping stability is in fact an exponential curve defined by a process-damping coefficient.

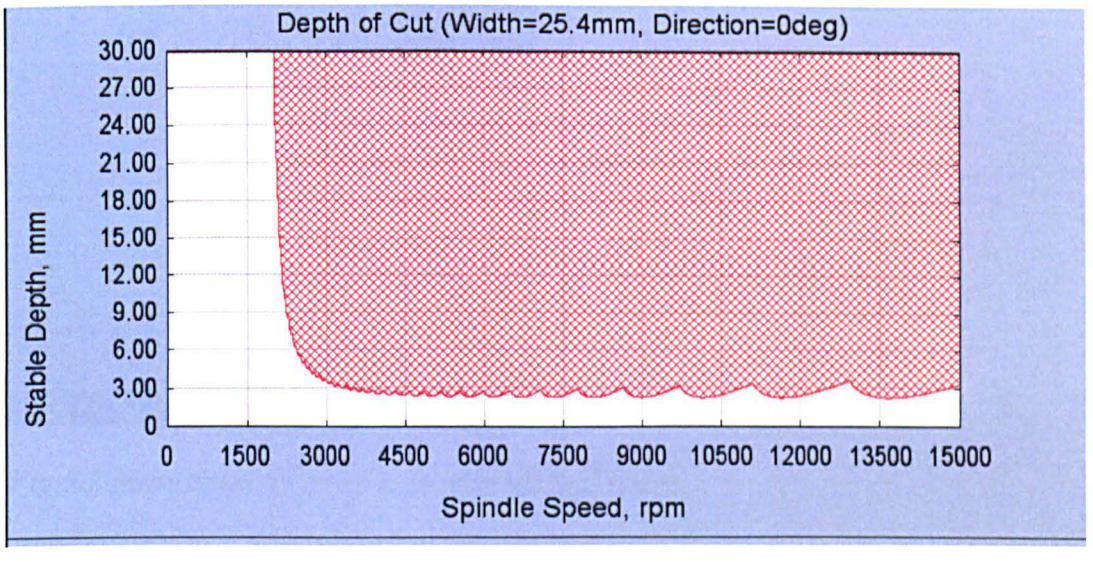

Fig.5.1 Example of process damped stability region

It is difficult to plot this curve experimentally or analytically and at large axial depths of cut, the curve becomes a vertical boundary on the stability lobe plot. It is for this reason that the 30mm axial depth of cut is selected in the experimental section and this simplifies the experimental procedure. In most practical cases for milling titanium b_{lim} is very low and for productive metal removal rates the axial depth of cut must be increased to the point where the process-damping limit is effectively a straight line boundary. Such examples shall be presented in the second half of this chapter.

5.2.2 Experimental Procedure

For the first phase of the trials a number of solid carbide tools have been designed so that the influence of chip thickness, relief angle and rake angle on process damping characteristics may be studied. For each of these tools tests were carried out to determine the critical process-damping wavelength for four different feed rates when

milling titanium. Each set of parameters was also repeated on a dynamometer so that the cutting force coefficients could be calculated. The tests were carried out on a Mori Seiki SV500 (Fig. 5.2).

Fig.5.2 Mori Seiki SV500 Vertical Milling Centre.

Cutting Tool Geometries used in Process Damping Tests

Name	Diameter	Rake	Relief	Helix
CP9	16	7	12	30
PD1	16	6.6	6	30
PD2	16	6.3	9.5	30
PD3	16	6.3	16	30

Table 5.1 Tool geometries for process damping trials

Parameter Matrix

Parameter	Test 1	Test 2	Test 3	Test 4
Hex (Max chip thickness mm)	0.03	0.05	0.07	0.1
a_p (mm)	30	30	30	30
a_e (mm)	1	1	1	1

Table 5.2 Parameter matrix for process damping trials

Determination of critical wavelength

The low radial and large axial depths of cut are selected to minimise the damage that may occur with the onset of chatter. The axial depth of cut must be sufficient to chatter the tool if process damping is not present, whilst the low radial depth of cut will minimise the damage. The feed per tooth is calculated from the maximum chip thickness value (hex) and is a function of the radial depth of cut and the cutter diameter:

$$hex = ft \cdot \sqrt{\frac{4ae}{D} - \left(\frac{2ae}{D}\right)} \qquad (5.1)$$

The spindle speed is incrementally increased during the test whilst maintaining a constant feed per tooth. The initial spindle speed is selected using a conservative estimation for the critical wavelength and consultation from the transfer function measurement. The spindle speed and feed rate are then increased together in increments so that a constant feed per tooth is maintained as the surface speed is increased. As the speed increases eventually chatter is encountered as the surface speed exceeds the critical limit. The chatter frequency is recorded and the critical process damping wavelength can be calculated.

In summary the procedure is as follows:

1. Measure FRF and plot stability lobes.
2. Select low radial and high axial depth of cut from stability lobes to ensure process damping curve is effectively a vertical boundary.
3. Select required hex value, e.g. 0.03mm, 0.05mm. Calculate the required feed per tooth from selected hex and radial depth of cut (a_e) using equation 5.1.
4. Select initial spindle speed by taking the frequency of the first dominant negative mode on the real part of the FRF and calculating from equation 5.2 using a conservative λc value.
5. Take a cut at set parameters and record audio signal.
6. Increment spindle speed and feed rate together to maintain a constant hex value until chatter occurs. Always increment speed and feed up and not down as a hysterysis effect can occur.

7. Record chatter frequency when audio signal exceeds threshold and note spindle speed.
8. Calculate λc.
9. Repeat for each hex value

Measurement of Transfer Function

The transfer functions of the tools are measured in both the X and Y orientations as outlined in chapter 4. The measurements for the reference tool, CP9, are presented in Fig.5.3 & 5.4.

It can be seen from the Y-direction FRF measurements and lobe plot that the 1st dominant mode is around 650 Hz. Although 650 Hz is not the frequency of the dominant mode, it is the first dominant frequency. At the borderline of process damping stability for the 650 Hz mode the mode at 2100 will be process damped and stable. The predictions for the spindle speed range are therefore based upon the 650

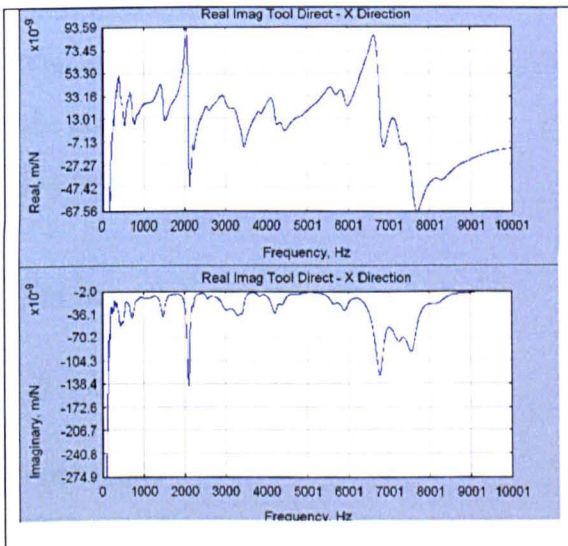

Fig.5.3 X direction FRF
60mm extension, Mori Seiki

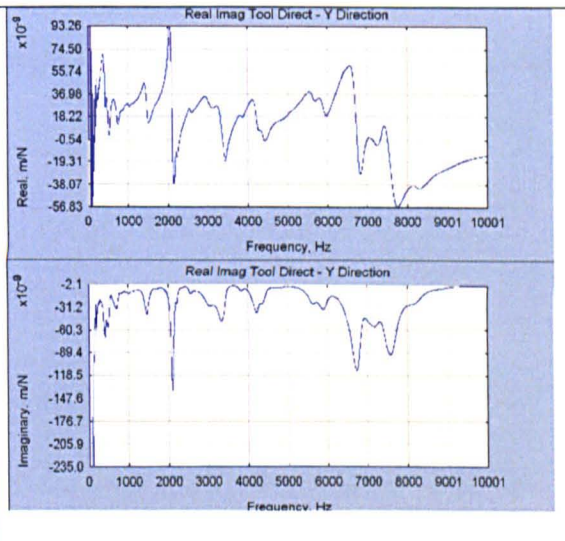

Fig. 5.4 Y direction FRF
60mm extension, Mori Seiki

Hz mode. If the 650 Hz mode could be stabilised then the 2100 Hz mode would become the first dominant mode and in accordance with equation 5.2 and a constant λc value, the maximum stable spindle speed would be increased by a factor of 3. This observation will be explored in more detail in the second part of this chapter.

$$\lambda_c = V_s / f_c \qquad \textit{(5.2)}$$

Chatter detection

As we are expecting chatter at 500-2100 Hz, this is well within the audio range, the audio monitoring system described in chapter 4 is appropriate [136],[154]. A sample is taken for the duration of the cut and as chatter encroaches, the magnitude of the audio response is viewed in the frequency domain after an FFT can be seen to grow. As the process damping phenomena 'damps' an unstable process there is no sharp boundary between stability and instability. The definition of stability in this case is defined as the magnitude of the chatter frequency passing a threshold limit when viewed in the frequency domain [136]. The chatter threshold is calculated as a magnitude greater than the RMS background signal before cutting commences. The surface finish of the component is also taken as an indicator as to when chatter is present. Unlike normal regenerative chatter, a peak can clearly be seen to grow at the unstable frequency as the speed is increased. Although some form of damped chatter is present, the chatter is at saturation point as a result of the process damping and will not grow any further in amplitude to the point at which it may be considered detrimental to tool life, spindle life or component quality.

The chatter limit is found by taking a long profile cut starting off at the lower limit for the critical wavelength, in this case 77 rpm. The feed rate is calculated from the feed per tooth and the spindle speed:

For hex =0.03mm, ae 1mm, D 16mm

$$ft = hex / \sqrt{\frac{4ae}{D} - \left(\frac{2ae}{D}\right)}$$

Fpt= 0.045

FR = m x ft x n

FR= 4 x 0.045 x 77 = 14 mm/min *(5.3)*

The speed and feed override dials are then increased simultaneously, maintaining a constant feed per tooth value until chatter is detected. Once chatter is detected the frequency of chatter and spindle speed at the onset of chatter are recorded and the critical wavelength is calculated.

The wavelength can then be used to calculate the limit of stability for that combination of edge geometry and workpiece material, irrespective of cutter

diameter, length or number of teeth. This method is particularly useful for inserted end mills where the repeatability of edge geometry is good. The process damping critical wavelength is then added to a database along with cutting force coefficients and used to calculate the stability of any relevant tooling set-up.

This newly defined methodology provides a robust and simple technique for measuring and predicting process damping performance in milling.

5.2.3 Results

The results for the process damping tests are presented below with the spindle speed and frequency at which chatter initiated listed, and the critical wavelength calculated.

All trials were run with a constant radial and axial depth of cut			**a_e (mm)**	**1**
			b (mm)	**30**
Tool	**F.p.t (mm)**	**RPM**	**Fc (Hz)**	**$\lambda_{c\,(mm)}$**
CP9	**0.03**	162	653	0.207
CP9	**0.05**	300	636	0.39
CP9	**0.075**	270	636	0.34
CP9	**0.1**	1170	681	1.439
PD1	**0.03**	117	663	0.147
PD1	**0.05**	180	646	0.233
PD1	**0.075**	473	644	0.615
PD1	**0.1**	568	677	0.702
PD2	**0.03**	105	645	0.137
PD2	**0.05**	162	641	0.212
PD2	**0.075**	378	647	0.49
PD2	**0.1**	454	677	0.562
PD3	**0.03**	162	661	0.205
PD3	**0.05**	272	641	0.355
PD3	**0.075**	270	688	0.32
PD3	**0.1**	936	686	1.14

Table 5.3 Experimental parameters and results for process damping wavelength trials

The results show a strong trend between chip thickness and process damping wavelength. An increase in chip thickness from 0.03mm to 0.1mm for tool CP9 resulted in approximately a seven fold increase in maximum process damped speed. This amounts to a 23 fold increase in productivity.
Surprisingly there is no clear relationship between relief angle and process damping wavelength evident. There does appear to be a slight trend for improved performance with an increase in relief angle. A trend is seen between rake angle and process damping wavelength. For these results it would appear that the impact of cutter angles warrants further investigation.

5.2.4 Repeat Tests – Investigation into effects of tool geometry

As the initial results go against the current theory that a shallow relief angle enhances process damping further trials were undertaken to examine the influence of tool geometry in more detail. The range of rake and relief angles has been broadened to enhance the effects. The tool geometries and cutting force coefficients are outlined in Table 5.4. Plots of the cutting force coefficient derivation in Fig.5.7 show that the cutting force coefficients are linear down to 0.03mm feed per tooth. No increase in force occurs due to work hardening or chip thinning.

Cutting Force Measurement

For the repeat trials the cutting force coefficients were measured for each tool so that a clear understanding of the influence of edge geometry on cutting force coefficients could be had. The cutting force coefficient investigation was also intended to explore whether the cutting force coefficients were linear for low feed rates and understand whether an increase in cutting force coefficients due to work hardening could account for the low λc for low feed per tooth encountered in the previous trials. The method for obtaining the cutting force coefficients is outlined in chapter 4. The cutting tests are carried out with a piece of Ti-6-Al-4V bolted down to a flat bed Kistler dynamometer (Kistler 9272). Cuts were taken at 16mm radial and 2mm axial depths of cut at speeds that were well below the process damped limit. The cutting force coefficients are then calculated for the number of teeth engaged in the cut and the effective chip thickness. Three feed values are required to compute the cutting force

coefficients and a total of four feed rates were used, simulating those used in the first process damping tests.

The cutting force coefficients are then calculated as in chapter 4. The radial and tangential cutting force coefficients Krc and Ktc can be combined to an overall Ks value which is the value used in Tlusty's analytical stability calculations.

$$K_s = K_{tc} \cdot \sqrt{1 + K_R^2} \qquad (5.4)$$

Where K_R is the ratio between the radial and tangential coefficients:

$$K_R = \frac{K_{rc}}{K_{tc}} \qquad (5.5)$$

Tool No.	Rake Angle (degrees)	Relief Angle (degrees)	Ks (mm2/N)
PD4	0	0	
PD5	0	6	1717,1813
PD6	0	12	2426,2770
PD7	6	0	
PD8	6	6	1713,1784
PD9	6	12	1516, 1507
PD10	12	0	
PD11	12	6	1519,1795,
PD12	12	12	1707,1622

Table 5.4 Tool geometries and Ti cutting stiffness

It can be seen from the plotting of the cutting force coefficients in Fig.5.6 that at low feed the cutting forces are low and the coefficients remain linear. The cutting force coefficient is unlikely to be the cause of chatter for low feed rates.

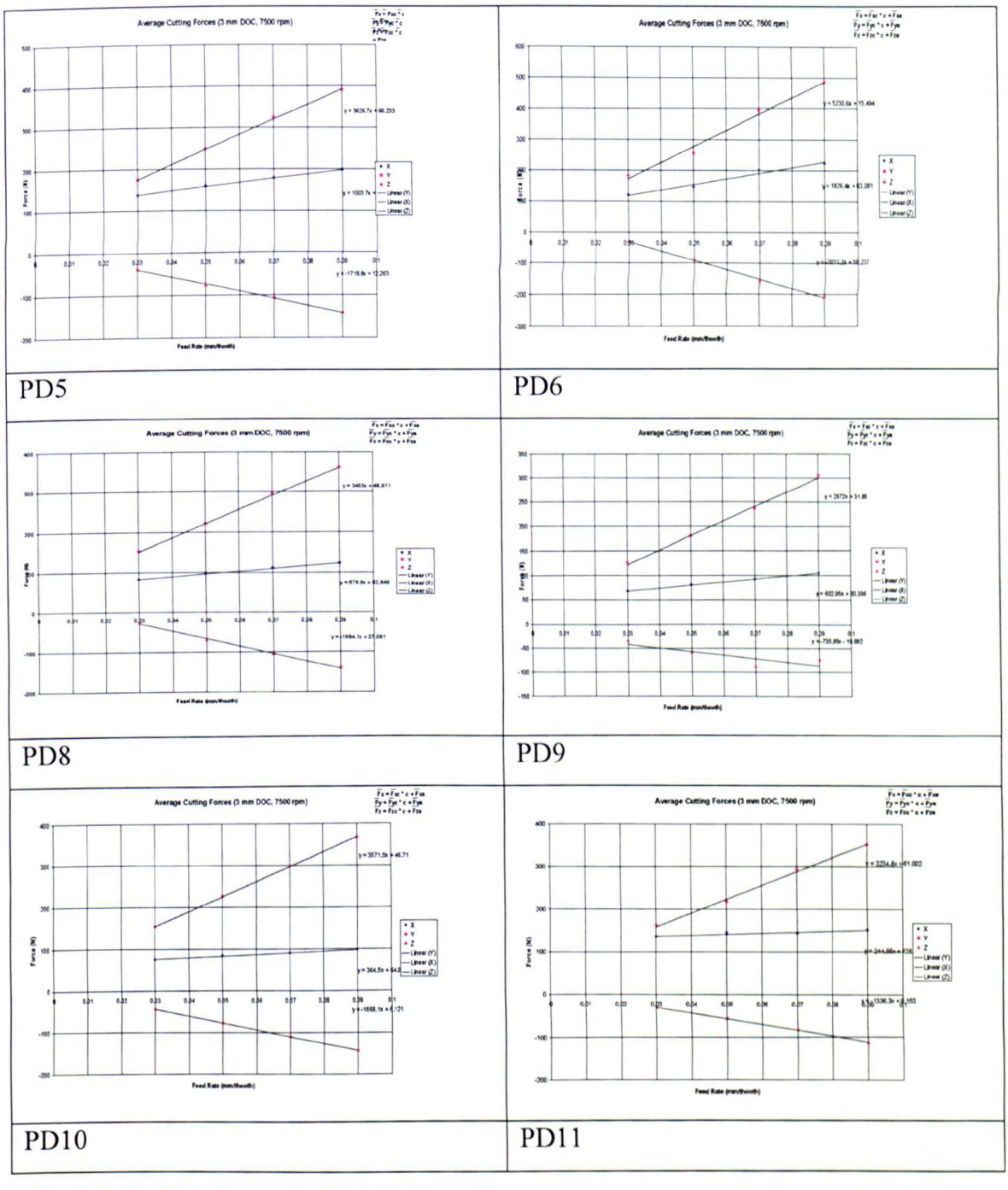

Fig.5.6. Cutting force coefficient linearity

Modelling of Geometry tests

The repeat tests are intended to further investigate the influence of tool geometry on process damping performance. The cutting tests are run at two feed values for the range of geometries. The aim of these trials is to evaluate the influence of rake and relief angles on process damping and in the case of the rake angle in particular to understand the influence and resultant direction of shear and friction forces. AdvantEdge ™ is a commercially available package provided by Third Wave

Systems. The software uses Finite Element techniques to model stress, strain and temperature in the cutting tool, chip and workpiece. Finite Element methods for modelling of cutting forces, temperatures and stresses form a broad field of research [155]. The Third Wave AdvantEdge FE model has been used previously to support cutting data for orthogonal chip machining operations and chip segmentation [156] [157].

The data is presented in graphic plots with a time domain signal of the cutting force for a single orthogonal cut. The fringe plots display plastic strain in the workpiece. High strain below the relief face of the tool could enhance the process damping interference effect. The Finite Element study shows the influence of rake and relief on chip shape and the area where high strain is induced. For the cutting force plots the X and Y relate to the tangential and radial directions respectively for milling applications. The results can be compared against the empirical results for the geometry tests and the cutting force coefficient data to investigate the influence of tool geometry on process damping conditions. The model does not take into account the cutting dynamics and the results represent the static condition. The results are displayed in Fig.5.7.

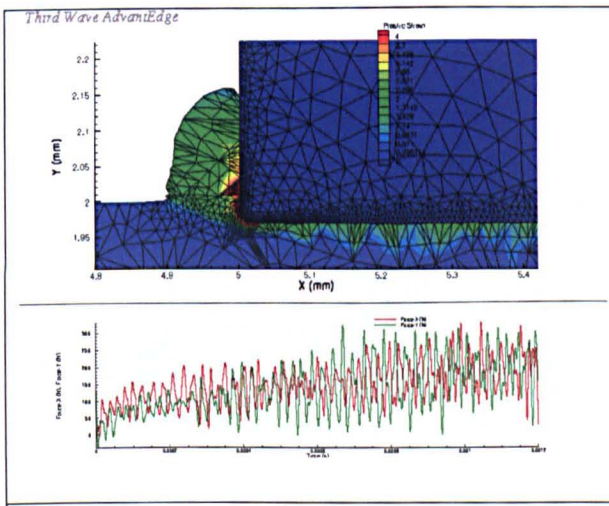

PD4 0.3, no coolant, 25m Vs

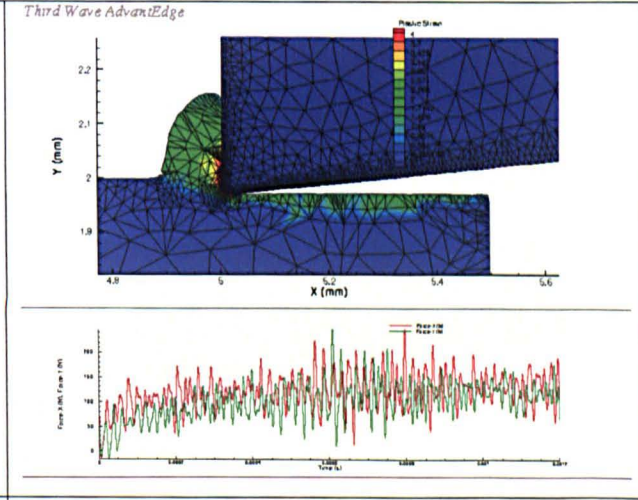

PD5 0.3, no coolant, 25m Vs

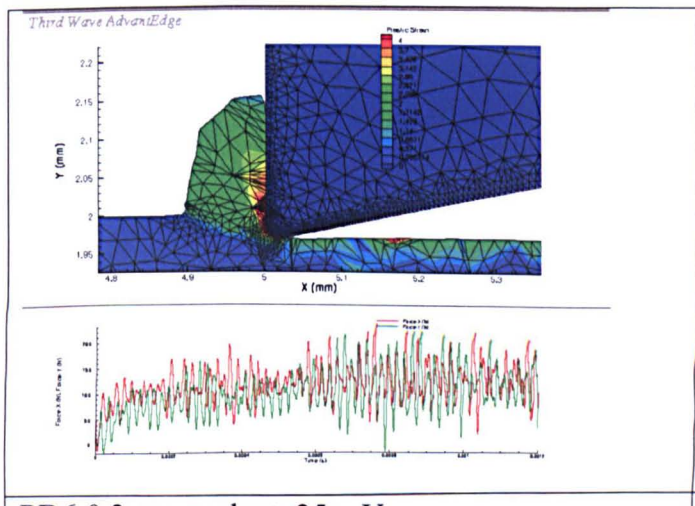

PD6 0.3, no coolant, 25m Vs

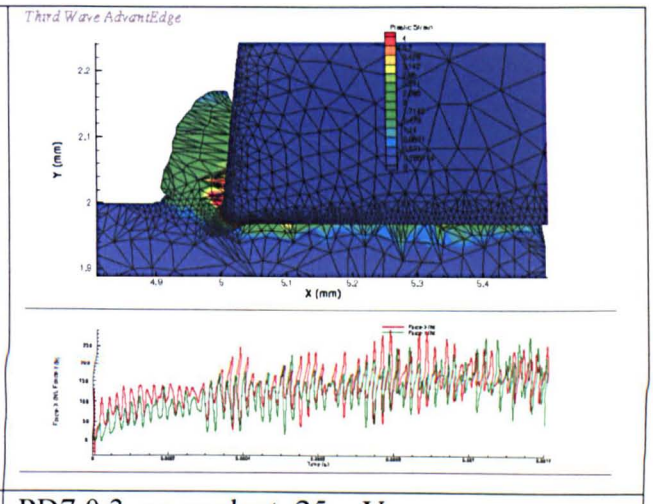

PD7 0.3, no coolant, 25m Vs

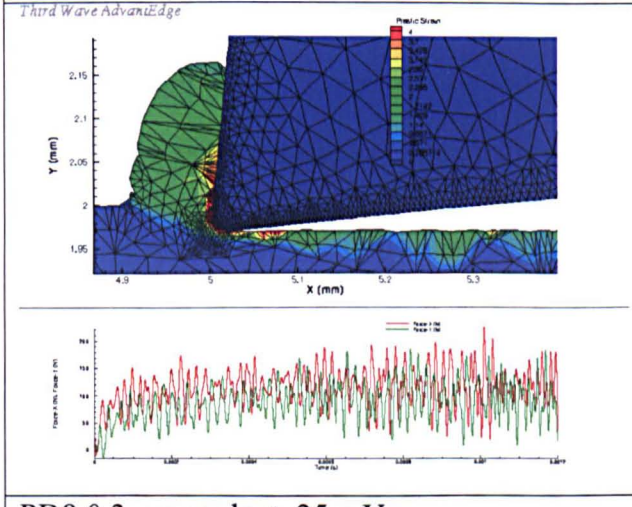

PD8 0.3, no coolant, 25m Vs

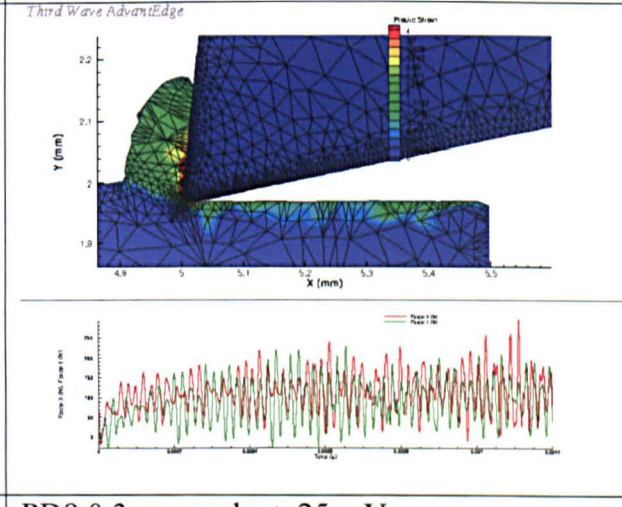

PD9 0.3, no coolant, 25m Vs

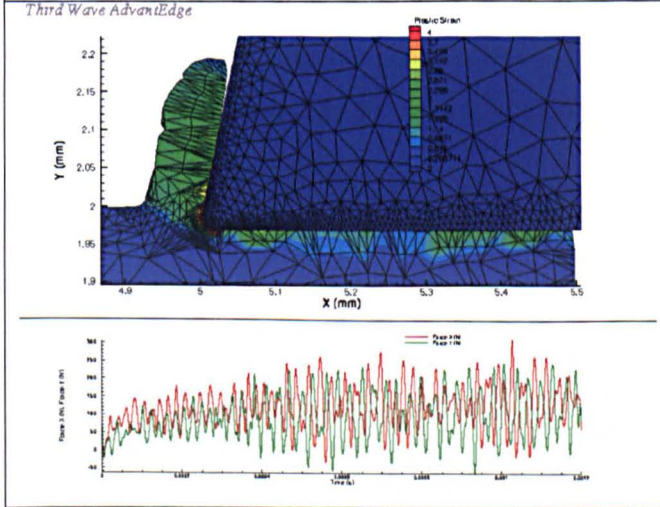

PD10 0.3, no coolant, 25m Vs

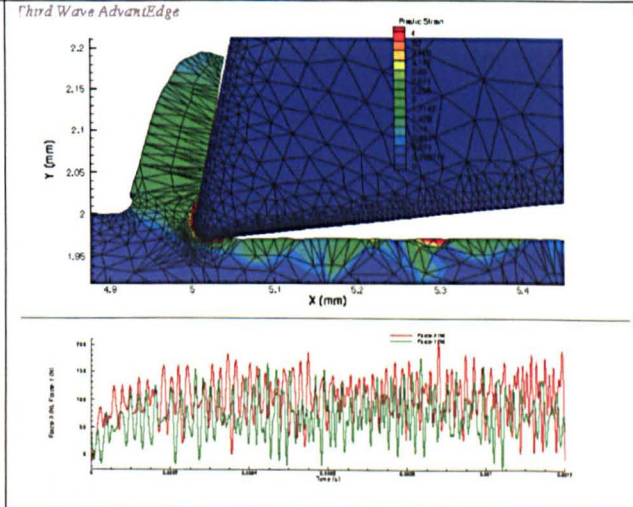

PD11 0.3, no coolant, 25m Vs

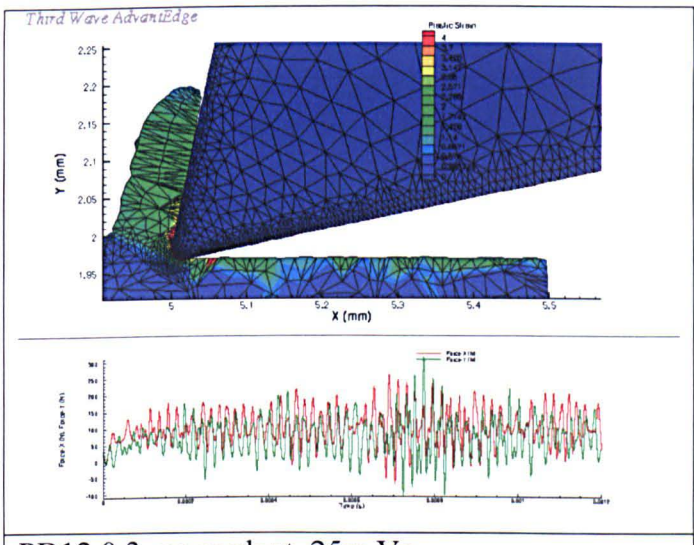

PD12 0.3, no coolant, 25m Vs

Fig.5.7 Third Wave™ plastic strain results for tool geometries.

The fringe plot represents plastic strain and the time domain plot represents radial and tangential cutting forces.

Discussion of Cutting Force Coefficient and FEM results

The zero relief tools (PD4,7&10) all see much higher cutting forces in the radial and tangential direction with high strain in the secondary zone behind the relief face of the tool. This will lead to high cutting force and temperature along the relief face and should be the best case for process damping performance. These tools would not be a practical production solution due to the high forces, temperatures, rubbing and adhesion on the relief face.

The highest strain on the cut surface appears to occur with the higher rake and relief angles, possibly due to the resultant force of the chip sliding up the rake face forcing the edge of the tool back into the cut.

Cutting force coefficients were not obtained for the zero relief tools as slot cuts were not advisable for zero relief due to the expected high force and temperature. Material quickly builds up on the relief face of the tool and the cutting action breaks down.

Of the remaining tools PD6 had the highest cutting force coefficients with PD5 being surprisingly low. The FE modelling indicates comparable cutting forces between the two tools but suggests higher strain on the cut surface with PD6. The cutting force coefficients were comparable for PD5 and PD8 both with 6° relief angles.

PD9 had the lowest cutting force with 6° rake and 12°relief angles, lower than PD 12 with the equivalent relief and higher rake angle. The FE model predicts low average cutting force for PD9. PD 12 has surprisingly high force relative to PD9 and the FE simulation predicts high strain around the edge radius and the previously cut surface. This could be a result of the edge radius and high relief face of the tool being pushed back into the cut zone by the resultant force acting upon the rake face.

Results of repeat tests

The experiments are repeated for the geometries outlined in Table 5.5, with the cutting force coefficients measured for four feed rates as presented in the table. The results from the second trials are presented in Table 5.7. For these trials the workpiece and cutting tools were set up so that the dominant cutting tool mode was the dominant mode for the system at around 1950 Hz. As this second phase of the study focuses on tool geometry every tool was run for only one hex value of 0.03mm, at a feed per tooth value of 0.045mm. The low hex value was chosen in order to conserve material as the first phase trials demonstrate that MRR increases greatly with an increase in hex. Example of MRR gain from first phase results for PD3:

- Hex = 0.03mm , ft =0.06mm , λc =0.205mm, rpm =159 ,Feed = 38mm/min,
- Hex = 0.1mm , ft =0.2mm , λc =1.14mm, rpm =884 ,Feed = 707mm/min,
- MRR increased 18 fold through optimisation of feed and λc

Screening trials were carried out for tool PD12 to determine optimum radial width of cut with 2mm radial immersion and 30mm axial depth of cut selected. This was to ensure that the programmed chip thickness was achieved and avoid rubbing and chip thinning due to push off. The results for PD12 are displayed in Table 5.6.

Tool	Ae (mm)	Ft (mm)	Hex (mm)	Ap (mm)	RPM	Fc (Hz)	$\lambda_{c\,(mm)}$
PD12	**1**	**0.05**	**0.025**	30	1000	1925	0.435
PD12	**2**	**0.045**	**0.03**	30	1200	1978	0.5

Table 5.5 Parameters and results for process damping screening trials

The trials above show a 16% increase in λ_c with an 11% increase in hex for the two sets of radial immersion. This compares to the gains seen in the first set of trials due to increase in hex. Fig.5.8 shows that for the larger radial immersion the chatter is much more clearly defined in the audio signal and the 2mm a_e value is therefore more

appropriate for the repeat process damping tests. The threshold setting (red horizontal line) is equivalent for each plot.

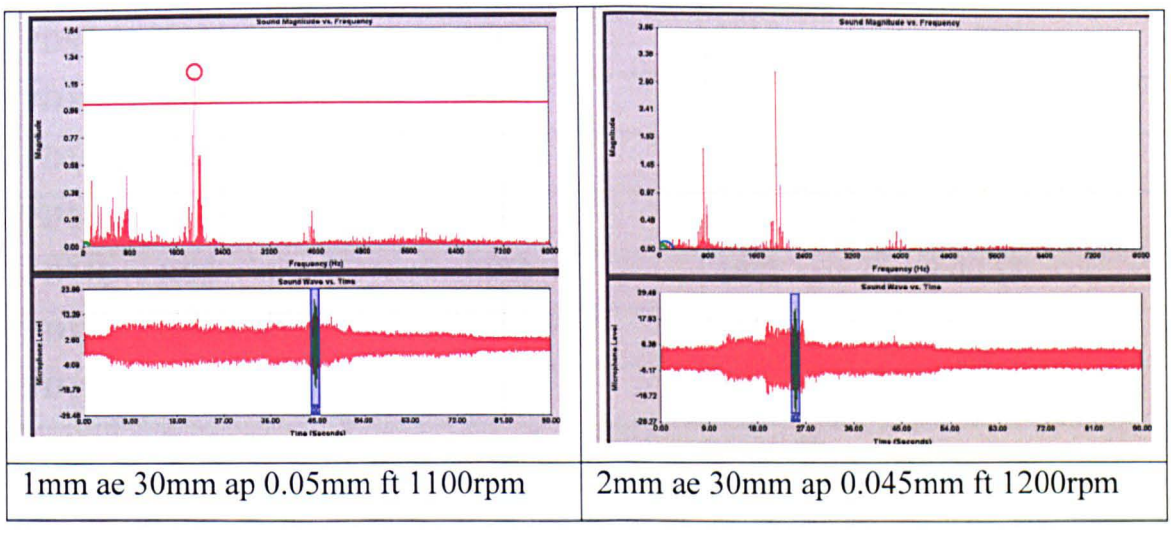

1mm ae 30mm ap 0.05mm ft 1100rpm	2mm ae 30mm ap 0.045mm ft 1200rpm

Fig.5.8. PD12 parameter screening with audio threshold as a constant

The full suite of tools was then run with the results outlined in the Table 5.6. The zero relief tools could not be made to chatter at any spindle speed. At speeds above 2500rpm, a surface speed of 125m/min, sparking occurred due to over heating and adhesion on the flank of the tool. The tests were only completed for PD7 as the X-axis of the machine was tripped out for PD4 and PD10 at speeds above 500 rpm but none of the three zero relief tools could be made to chatter.

All tests run at constant axial and radial depth of cut			**a_e (mm)**	**2**
			b (mm)	**30**
Tool	**Hex (mm)**	**RPM**	**fc (Hz)**	**$\lambda_{c\,(mm)}$**
PD4a	**0.03**	500	-	-
PD4b	**0.03**	-	-	-
PD5a	**0.03**	240	1780	0.113
PD5b	**0.03**	240	1955	0.1028
PD6a	**0.03**	210	1958	0.0899
PD6b	**0.03**	189	1956	0.08095
PD7a	**0.03**	2500	-	-
PD7b	**0.03**	2500	-	-

PD8a	**0.03**	180	1962	0.0769
PD8b	**0.03**	210	1962	0.0897
PD9a	**0.03**	210	1962	0.0897
PD9b	**0.03**	240	2012	0.0999
PD10a	**0.03**	-	-	-
PD10b	**0.03**	-	-	-
PD11a	**0.03**	300	1962	0.1281
PD11b	**0.03**	360	1921	0.157
PD12a	**0.03**	1200	1978	0.508
PD12b	**0.03**	600	1873	0.268

Table 5.6 Process damping wavelength experimental results

Discussion of Experimental Results

Other than the zero relief tools the best result was actually found with PD12 (12° rake, 12° relief). This does not follow the established theory that relief angle is the governing tool parameter. The FE modelling showed that for PD12, although the strain in the chip is much less than the tools with lower rake angles, the greatest plastic strain around the cut surface and the edge of the tool where the mesh is at its densest. PD12 had higher cutting force coefficients than all the other tools with the same rake or relief angles, excluding the zero rake and relief. As mentioned previously it is possible that the resultant force of the chip contact on the rake face pushes the edge back into the cut, increasing the rubbing on the relief around the cutting edge. High pressure around the cutting edge due to the sharper edge may also result in greater deformation of the material resulting in the high strain and a greater rubbing or process damping effect.

Of the other tools PD6 and PD8 were comparable, whilst PD9 had slightly better performance with the combination of 6° relief and 12° rake and also had the lowest cutting force coefficient. PD11 had around 50% higher performance than those mentioned above, again high rake angle leading to a higher λc and the FE model predicting high plastic strain on the cut surface and around the nose.

The results show a slight trend in increase of λ_c with an increase in rake angle. The influence of relief angle appears negligible until the relief angle is reduced to zero in which case chatter could not be found to occur and the rubbing due to zero relief becomes dominant.

In some cases different results were recorded for the same tool geometry between tool A and B. The variation for otherwise constant tool geometries is greater than the stated difference between the various geometries. When a tool has run for a period of time and has 'bedded in' then improved results are seen, as in the case of PD5 where a tool was used to prepare the workpiece material and a λ_c value of 2.5mm was achieved as opposed to the 0.1 achieved with a new tool. The results displayed in table 5.7 are for new tools only so edge condition for each tool was as supplied from the manufacturer. No facility was available to measure the edge condition and this is taken as a constant only through relying on the manufacturer's ability to produce repeatable tools to drawing. From the observation with the bedded in tool it is possible that the variation in performance from one otherwise identical tool to another is as a result of a change in edge condition. With facilities to measure and control the edge condition this would be an interesting topic for further research. In instances where a different result was achieved for the same tool geometry a new tool was trialled until two sets of comparable data were achieved.

Despite some fluctuations in performance for 'identical' tools, the following trends do stand:

- Increase in λ_c for increase in hex leading to up to 20 fold increase in MRR.
- Tendency towards higher λ_c for sharp tool geometry (high rake and relief).
- High λ_c for PD5 combination low rake and relief.
- No chatter achieved for zero relief tools.

5.2.5 Discussion

The results demonstrate that feed per tooth has the strongest influence on the critical process damping wavelength λ_c. The relief angle does not appear to have a strong influence on the stability other than with zero relief. For practical purposes this could be emulated with an eccentric cam relief. The greatest stability is seen with the high rake angle and high relief angle. There appear to be some interaction between the rake

and relief angles with good performance seen for tools with sharp geometries, high rake and relief, and strong edge geometries, zero rake and low relief. This is supported by the Advant Edge FE data as high strain is predicted around the cut zone and the cut surface for tools PD11 and PD12.

It is also evident that with zero relief, process damping severely inhibits chatter although this is not a practical tool geometry due to high friction forces and built up edge resulting in mounting cutting forces overloading the machine tool. It would appear that the typical geometries used for titanium machining (6 degree rake and 6 or 12 degree relief) give the worst performance. The PD11 & PD12 tools could result in reduced tool life for long lengths of cut as the sharp geometry results in a thin cutting edge which will see high localised thermal stresses and could result in premature fracture (Chapter 2). Equally PD5 with zero rake and 6 degree relief results in high cutting forces and temperatures, backed up by the AdvantEdge model, which would be linked to excessive tool wear.

The cutting force coefficient data shows that the cutting force coefficients are linear for the range of feed rates studied and that the influence of feed per tooth in the first set of trials is not linked to changes in the cutting force coefficients. The influence of feed is most likely due to increased amplitude of vibration, having the same effect as low surface speed on the slope of the wave form. This could also be combined with the resultant shearing force on the rake face pushing the relief and nose of the tool into the cut surface, particularly for tools with high rake angles.

It is likely that in the case of increased force from chatter, induced through raising the size of the cut, that process damping will eventually inhibit the growth of chatter. As outlined in chapter 2, chatter is a self excited vibration and will grow to infinity until a non-linearity in the process stops it from growing further. The tool jumping out of the cut and tool breakages are often quoted examples of such non-linearities [143],[101]. In reality it is likely that process damping prevents the chatter from growing to infinity. Although the cut is unstable, the frictional forces acting against the tool velocity created due to process damping prevent the chatter amplitude from growing further. This was observed during screening trials for the variable helix tools in chapter 4 when chatter was more severe for shallow radial cuts than for full slots, the tool being process damped in the slot due to the large contact forces with the workpiece during the chatter vibration cycle. The chatter was still evident but the

tools neither broke nor jumped out of the cut and instead were constrained by the contact forces with the workpiece.

In the case of the shallow radial immersion, the limit of stability was much higher, but when chatter did occur it was more severe, without the same level of contact pressure or process damping available to constrain the chatter growth. This is a fundamental change in the way that process damping is viewed and would suggest that efforts to determine the non-linear cutting force coefficients are misguided as process damping is a limit cycle and can act beyond the border of stability. Cutting force coefficients are used to determine behaviour up to the limit of stability only.

It is proposed that in the case of perceived 'stable process-damped' cuts the process damping prevents the chatter from growing rather preventing it from occurring. The increased amplitude of vibration due to chatter will increase the process damping effect and within a certain range this will prevent chatter from growing to an observable level. This effect can best be observed around the process damping border of stability. The boundary described in the experimental design of this chapter is not clearly defined and within a certain speed range the signs of chatter can be detected but it does not grow to a severe level. This makes the presence of chatter a subjective matter and for the purpose of the experiments outlined in this chapter the author has been consistent in his judgement, i.e. a threshold had to be exceeded before the cut was deemed to be unstable although the chatter frequency was clearly present. A hysterysis effect is also evident during the experiment to determine the wavelength; it was stated in the experimental design section that the spindle speed will start at a conservative value and then increase until the boundary is observed through chatter. If the initial spindle speed is to the right of the boundary and caused chatter and the spindle speed and feed are incrementally reduced the stability limit is observed at a lower spindle speed giving a more conservative value for the critical chatter wavelength. This occurs as the process damping forces are not strong enough to inhibit established high amplitude chatter, yet under the same speed and feed conditions can prevent the chatter from establishing itself when it begins at low amplitude. This demonstrates that the occurrence of chatter with relation to process damping is a subjective judgement based upon an amplitude threshold rather than the traditional Laplace domain stability criterion [158]. A time domain solution is required to model process damping to satisfaction as it is highly non linear.

It is for the above reason that process damping was suggested for the exceptional stability of some of the variable helix tools in the previous chapter. It was commonly observed that the chatter grew very slowly and the border of stability was much less clearly defined than in conventional lobe prove outs [132].
One major factor influencing process damping speeds and productivity is the frequency of vibration, this has been kept as a constant so far in this chapter. The next section of the chapter studies manipulation of the tool tip FRF to achieve broad spindle speed ranges within which the milling operation is process damped.

5.3 Optimisation of tooling set-up

5.3.1 Modal attenuation

Metal Removal Rates (MRR) for titanium milling are much lower than those of aluminium milling largely due to the excessive tool wear encountered when milling titanium at high speeds. As highlighted in earlier chapters, extensive research has been undertaken to understand the mechanisms of tool wear in titanium milling [13],[159], and advances in tool, coolant and material technology have made titanium milling more economical [56],[25],[160]. For roughing or semi-roughing operations, low speeds are generally employed and more acceptable tool wear levels are achieved. When tooth-passing frequencies are low relative to the dominant modal frequencies of the system, then little advantage can be made of the stability lobe effect. The limiting stable depth of cut is therefore defined by the stiffness of the dominant modes of the system. For this reason large diameter cutters are often employed.
The process damping phenomenon explored in the first part of this chapter allows large stable depths of cut to be taken at speeds that are low relative to the dominant modal frequencies. Machinists have taken advantage of the process-damping phenomenon since machining first began, often without understanding the effect, to facilitate stable cutting. It is still common to see machine operators slowing down the spindle speed to avoid the onset of chatter. Machining within the process-damping region can limit the machine tool to very low spindle speeds and MRR, well below the spindle speed and power capacity of the machine tool.

A new approach to optimising the stability of a machine tool system to achieve increased MRR is proposed and a practical application of the process damping theory explored in the first part of this chapter is developed. Although the theories outlined in this section will not replace heavy roughing of titanium, they will bring semi-finishing and finishing MRR close to those of roughing. The approach also aims to eliminate chatter incurred through spindle modes and is therefore ideally suited to machine tools that were not originally designed with titanium milling in mind.

As discussed in the early part of this chapter, process damping offers a practical means of controlling stability of the titanium milling process where surface speeds are too low to utilise the stability lobes to good effect. The first part of this chapter looked at the variables that influence the critical process damping wavelength and presented a method by which that value could be determined. Once the critical wavelength is known for a given tool, material and feed rate, stable cutting parameters may be obtained through manipulation of spindle speed or the dominant natural frequency. Tool tuning techniques have been studied for HSM where lobes can be placed at optimum spindle speeds and some modes can be attenuated [71]. Process damping is primarily focussed on the first mode to have a negative real part as this will limit the spindle speed range within which process damping can be utilised. Through optimisation of the process damping performance as outlined in the first part of this chapter and optimisation of the frequency response of the system significant gains can be made in metal removal rates for titanium milling. A novel method is proposed here for manipulating the tool tip FRF such that the tool, tool holder and spindle modes will not cause chatter within the practical spindle speed range.

The technique is most readily applied to titanium milling where tool wear limits the surface speed range. There may also be an application for this technique in micro-milling operations where small diameter tools < 5mm can be used at high spindle speeds. An advantage in the latter case is that direct measurement of the tool tip FRF is difficult and FE modelling may be sufficient to predict stability using this technique. FE modelling is often limited in machining applications due to difficulty in predicting the modal damping values and receptance coupling [150]. The advantage of the proposed method is that knowledge of the dominant modal frequency and stiffness of the tool may be sufficient to predict stability, providing that a suitable model or measurement exists for the spindle and toolholder. In this study the technique will be examined for titanium milling applications.

Desirable Dynamics

It will be demonstrated that if the cutting tool and tool holder are carefully selected then large ranges of stable machining can be made available for the full range of practical surface speeds. Past research has looked at designing inherent stiffness and damping into the system but this technique looks at manipulating the tool point FRF [161],[162].

Conventionally, when selecting a set up for titanium milling, stiffness is the primary concern. This often means employing rigid machine tools and spindles with large diameter end mills. The novel approach employed here strays from the traditional lines of thinking and employs tools of small diameter and low rigidity relative to the rest of the machine tool and spindle set up. As only the negative real part of a mode can cause chatter [21, 68], the introduction of a flexible tool mode may stabilise lower magnitude machine and spindle modes through attenuation [71]. Using Altintas' frequency domain model of coupled modes it is possible for a positive real value in the measured directions to cause chatter due to the consideration of coupled modes or with an oriented transfer function (OTF). This would happen when the negative peak of the modes have a low positive value and the OTF is accommodated in the MetalMax software used to plot the stability lobes presented in this study. Geng et al [163] demonstrated that the mode shapes can be corrected by considering modal residues. This technique can alter the position of the modes with relation to the y-axis on the FRF.

Modal Attenuation and Process Damping

The theory outlined here is valid wherever the influence of dominant modes can be attenuated and need not always result in infinite stability for the selected modes. The flexible tool mode is introduced through selection of a small diameter (low mass) tool with a balance between relatively high modal frequency due to low modal mass, and low stiffness. Cutting parameters are then employed that are within the process damping range for the dominant mode whilst all other modes are stabilised. It is desirable that the dominant tool mode is high frequency (low mass) and low stiffness relative to the tool holder and spindle modes.

The following plots in Fig. 5.9 are taken from an FE model to illustrate the effect of selecting small diameter tools. The FE model is one dimensional and created using the MetalMax SPA spindle modelling software, whereby lumped masses and springs are applied to nodes throughout the central axis of the spindle. The model is tuned to match empirical measurements by first matching the mode shapes and then fine tuning the stiffness and damping values of the springs so that the dominant modal parameters are close. The model can then be validated for a range of tool selections and a comparison for the Sajo model is presented in Fig.5.11.

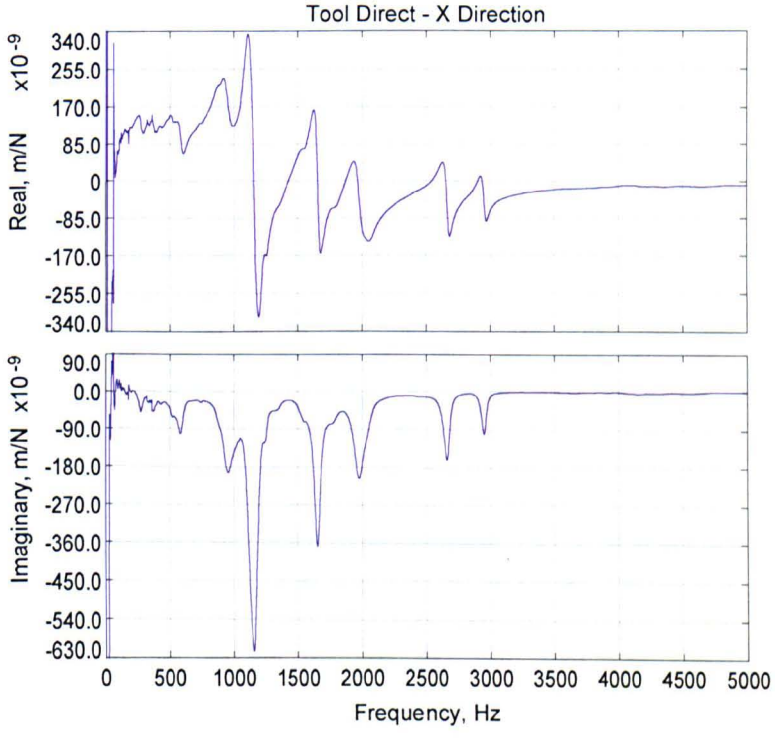

X-direction FRF for 19.05mm carbide rod (Measured)

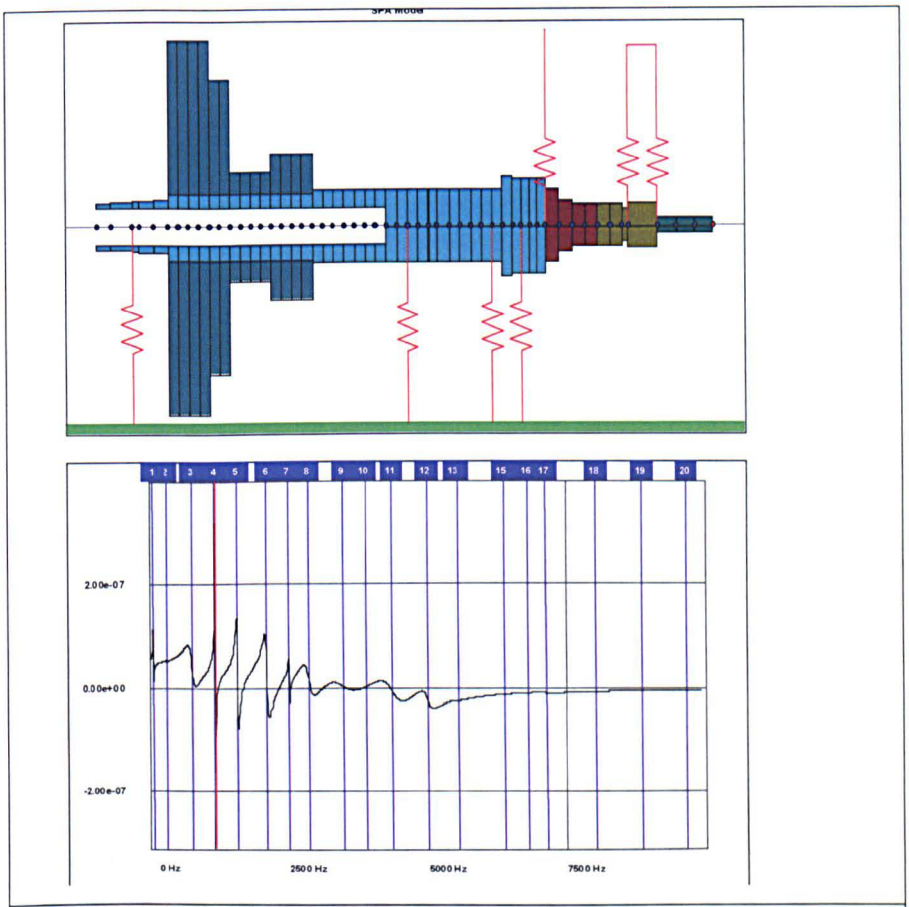

SPA FE model and tool tip FRF for 19.05mm carbide rod.

Fig. 5.9 Measured and simulated Frequency response plots for 19.05mm carbide

Figs. 5.10 & 5.11 show the real/imaginary FRF plot for a spindle and tool assembly generated from the model shown in Fig5.10. The same spindle model is used in each case, but with two tools of different diameter and equal length.

$1/k_c = 0.125e^{-8}$

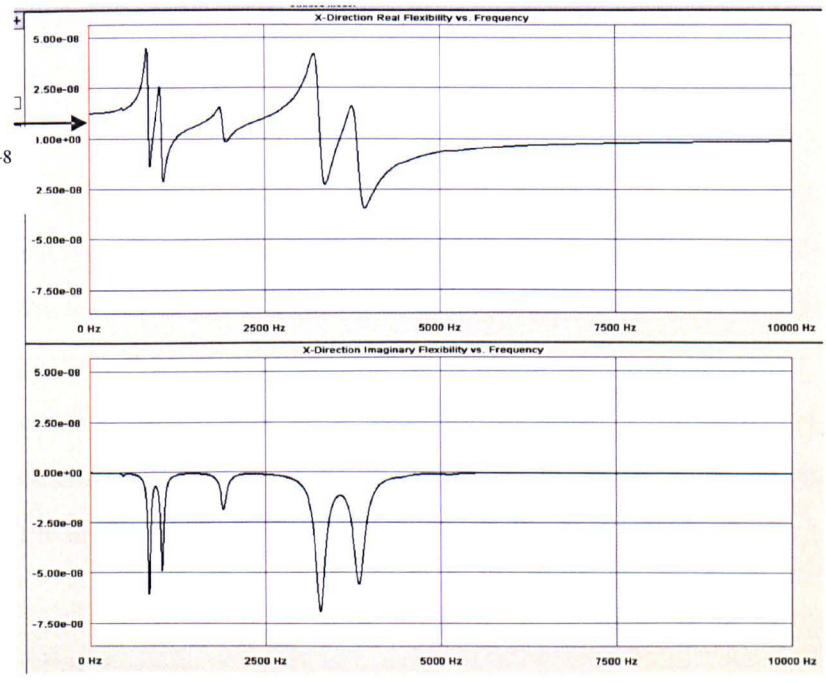

Fig. 5.10 Tool Tip FRF 32mm D end mill

$1/k_c = 0.2e^{-6}$

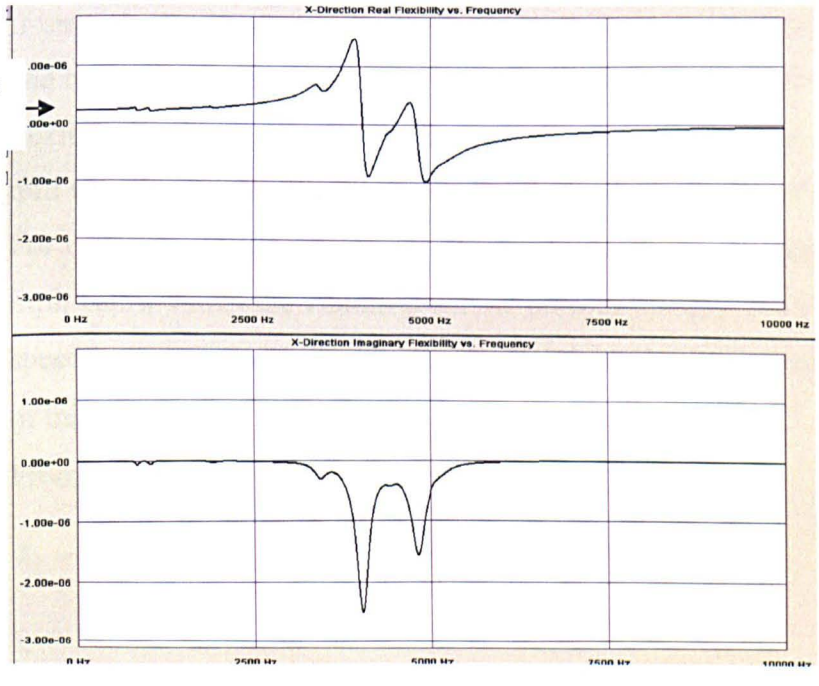

Fig.5.11 Tool Tip FRF 10mm D end mill

Fig. 5.10 shows the response of a 32mm diameter tool whilst Fig. 5.11 shows the response of a 10mm diameter tool. The introduction of the flexible modes with the small diameter tool has decreased the static stiffness of the system. The static stiffness is inversely proportional to the value of the real plot at 0 Hz. In Figs 5.10 & 5.11 the introduction of a flexible tool mode has reduced the static stiffness of the system by a

factor of 100. Decreasing the static stiffness of the overall system raises the lower frequency modes on the real plot, attenuating the effect of these modes on the machining system. If the stiffness of the introduced mode is sufficiently low, relative to the existing dominant modes, then the spindle and tool holder modes will be raised entirely into the positive region of the real plot. As the criteria for dynamic stability in the cutting process states that only modes with a negative real part can cause chatter [21] (eq 5.8), the spindle and tool holder modes have all been stabilised. Tlusty's stability lobe theory states that only the higher frequency dominant tool modes could cause chatter in the case of Fig. 5.11 as a positive real value results in a negative value for the limit of stability.

$$b\lim = \frac{-1}{2 \cdot Ks \cdot \mathrm{Re}(Min) \cdot \mu \cdot m_{avg}} \qquad (5.8)$$

If the two set-ups were to be considered for HSM applications then 32mm diameter end mill represented in Fig.5.12 would provide much greater stability. The high flexibility and low dynamic stiffness of the tool modes in the case of the 10mm end mill would result in a very low $b_{limcrit}$ value relative to that of the 32mm end mill.
For vibration at the frequency of the dominant tool mode there will be a surface speed limit below which the vibration will be process damped and chatter cannot occur. The speed is related to a critical wavelength and is calculated as outlined in the earlier part of this chapter.
From equation 5.1 the critical wavelength is defined as;

$$\lambda_c = \frac{Vs}{f_c} = \text{(Surface speed/ frequency of vibration)} \qquad (5.9)$$

It follows therefore that the higher the frequency of the vibration, the greater the surface speed range for which that mode will be process damped.
In the case presented in Fig. 5.10 for a critical wavelength of 0.6mm then stable milling can be achieved for full radial immersion and full axial immersion of the flute length for surface speeds up to 4000 rpm (Fig5.13). In reality the set up will be stable for all depths of cut within the full range of spindle speeds that would give acceptable tool wear. The red hatched area in Figs. 5.12 & 5.13 represents spindle speeds beyond the surface speed limit. The stiffer tool set up in Fig.5.11. has a much lower process

damping range and a comparison of Figs. 5.12 & 5.13 demonstrates the greater stability at low speeds with the small diameter tool.

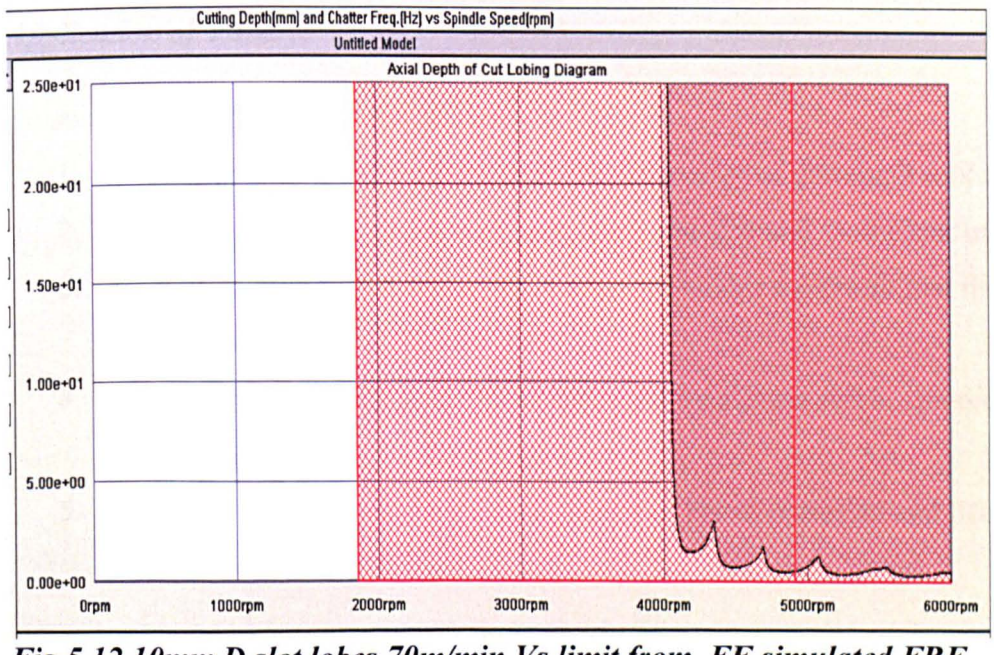

Fig.5.12 10mm D slot lobes 70m/min Vs limit from FE simulated FRF

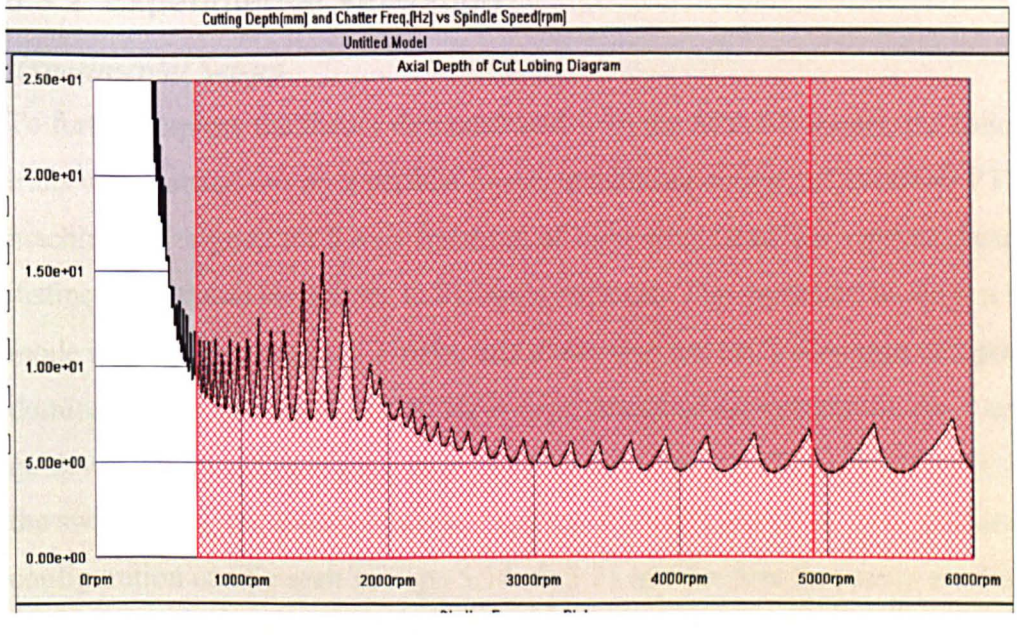

Fig.5.13 32mm D slot lobes 70m/min Vs limit from FE simulated FRF

As surface speed is proportional to the diameter of the end mill, the MRR dictated by the limiting surface speed for a stated axial depth of cut, radial immersion, number of teeth and feed per tooth, will be the same for all tool diameters. Therefore if switching

from a cutter diameter D to D/2 will increase the permissible ADOC then the overall MRR will increase.

Application of Theory:

To summarise the points outlined above:

1. Select small diameter tools to raise the frequency of dominant tool modes
2. Select toolholder to avoid high magnitude spindle and toolholder modes
3. Set tool length to attenuate spindle and tool holder modes so that they rise into the positive region of the real plot
4. Establish process damping wavelength and maximum stable spindle speed for tool mode
5. Use shallow radial and large axial depths of cut to optimise tool life and productivity

5.3.2 Experimental Validation

Experimental Set-up

To further explore the theory demonstrated with the SPA FE model, the following trials were carried out on a vertical 5-axis machining centre, a Cincinnati FTV5. The machine is designed for 5-axis finishing of light alloys and has a gimble head with distinct directional sensitivity in dynamic stiffness. The dominant mode is a spindle mode in the y-direction at 1270Hz, this mode also has an X direction component. A dominant y direction mode at 80 Hz is the C-mode of the column on the Y-axis guideways. In the X-direction there are lesser modes at 107 Hz and 370 Hz relating to the swinging of the column and the bending of the gimble head. The machine configuration can be seen in Figs. 5.14. & 5.15 and the low frequency modes in the x and y directions as measured on a 20mm solid carbide tool tip can be seen in Figs. 5.16 & 5.17.

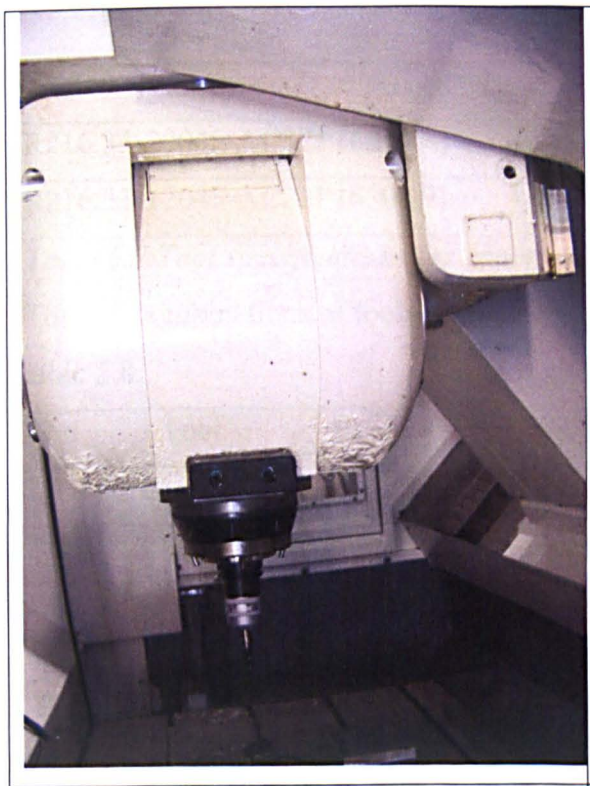

Figure 5.14
X-direction view of gimble head- FTV5

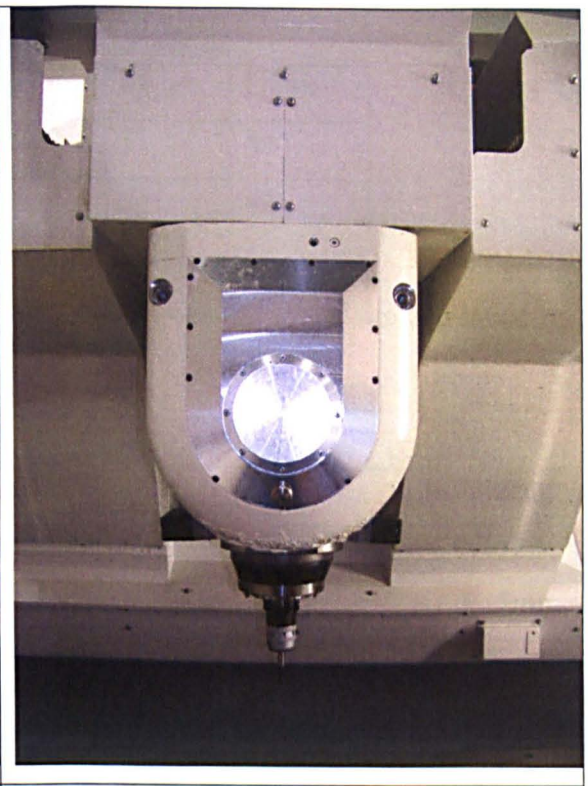

Fig 5.15
Y-direction view of gimble head- FTV5

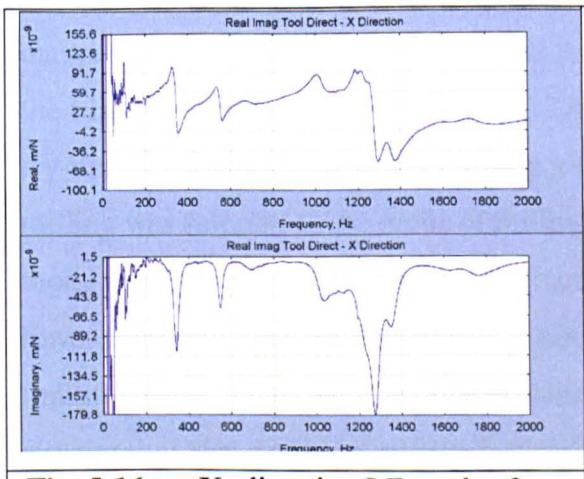

Fig. 5.16 X- direction LF modes for 20mm solid carbide FTV5

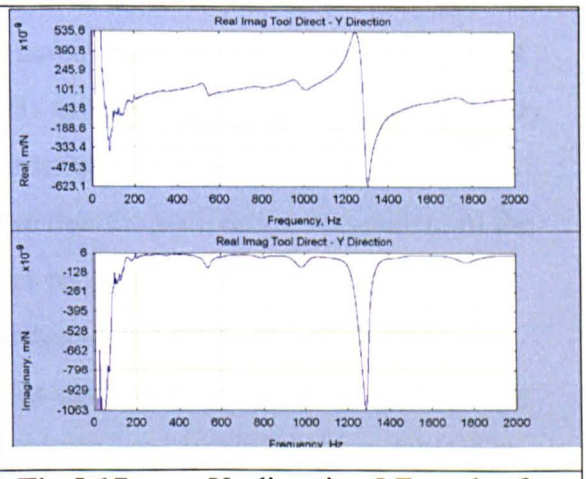

Fig 5.17 Y- direction LF modes for 20mm solid carbide FTV5

The FRF for solid carbide end mills of two diameters and different extensions have been measured and the stability lobes plotted in each case. A Nikken CM 20 chuck was used with a 20-12 collet for the smaller diameter end mill.

The tools used were Sandvik Coromant Plura each with the same edge geometry and process damping properties. The exact tool geometries and tool holder specifications are displayed in table 5.7.

Tool	D	m	Helix
R216.33-20045-AC32P1630 (A)	20	3	45
R216.33-12045-AC22P1630 (B)	12	3	45

Table 5.7 Tool specifications for experimental process damping trials

The full combinations of tools, tool extensions and tool holders tested are displayed in table 5.8.

Test	Tool	Extension	Tool holder	λc
1	(A)	47mm	Niken CM20	0.45mm
2	(A)	60mm	Niken CM20	0.45mm
3	(B)	47mm	Niken CM20 + 12mm collet	0.45mm
4	(B)	60mm	Niken CM20 + 12mm collet	0.45mm

Table 5.8 Tool extensions and tool holders for process damping trials

The critical process damping wavelength for the tools was determined as outlined in the first section of this chapter using a hex of 0.4mm.

For each setup the stability plots were predicted using the measured critical wavelength. Depths of cut were selected at up to 6mm so that the maximum process damped cuts were clearly above b_{lim} and the maximum lobe positions. The target of the trial was to attenuate the dominant 1270Hz spindle mode which is predominantly a y-direction mode but also has a strong x-direction component. X-direction slot milling was selected as the mode of milling so that the y-direction component of the mode would be minimised and the x-direction component could be attenuated. The lower frequency structural modes were not targeted and these may still provide a limiting depth of cut once the dominant modes have been stabilised. Low frequency structural modes would be approached with a traditional stability lobe optimisation rather than process damping. Across transfer measurement is required and it is not considered for this experiment.

The plots are displayed in Figs. 5.18 – 5.25 and from the predictions a spindle speed and depth of cut were selected near to the limiting operational surface speed, to compare the stability of the setups and to validate the plots.

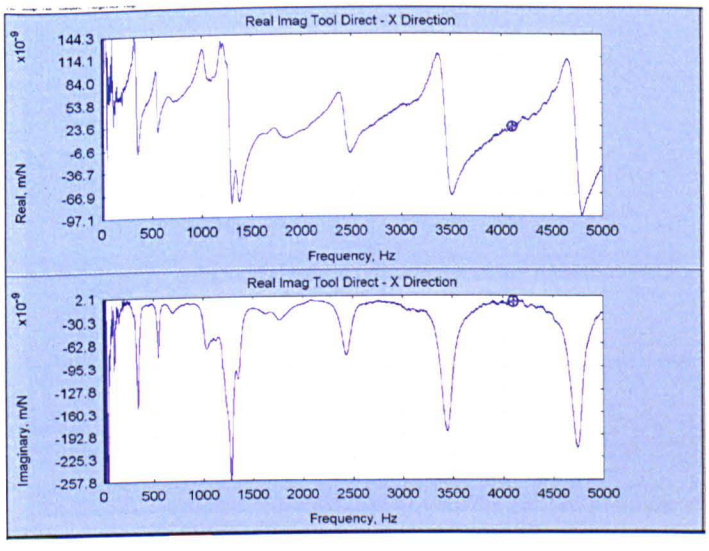

Fig.5.18 Test 1 – X direction FRF

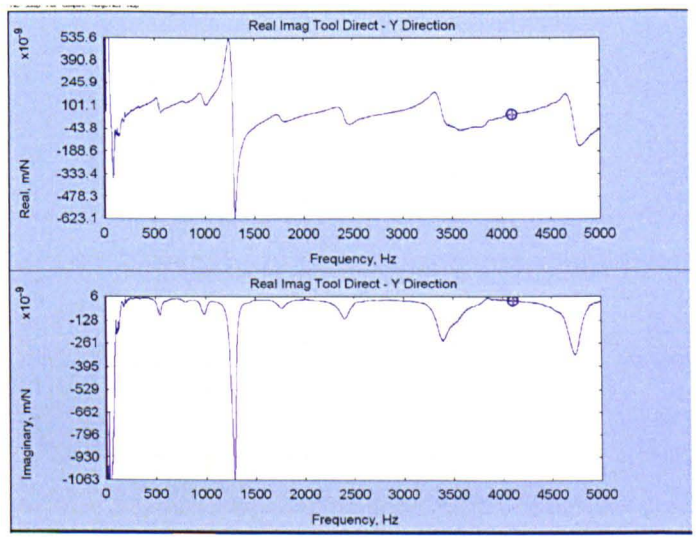

Fig. 5.19 Test 1 – Y direction FRF

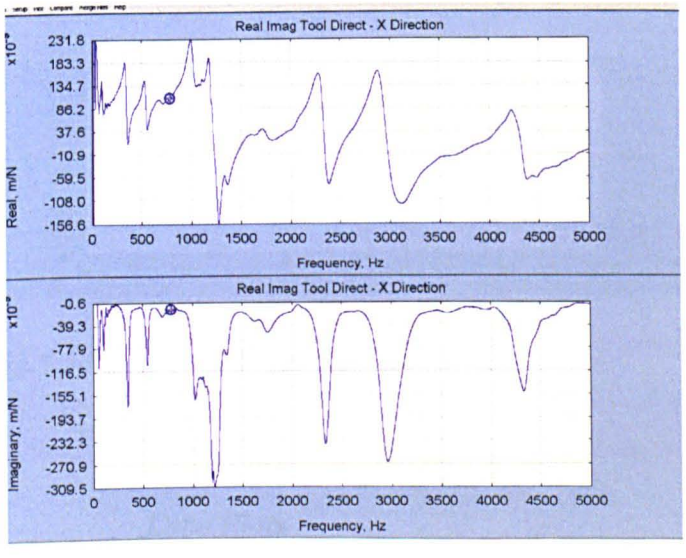

Fig.5.20 Test 2 – X direction FRF

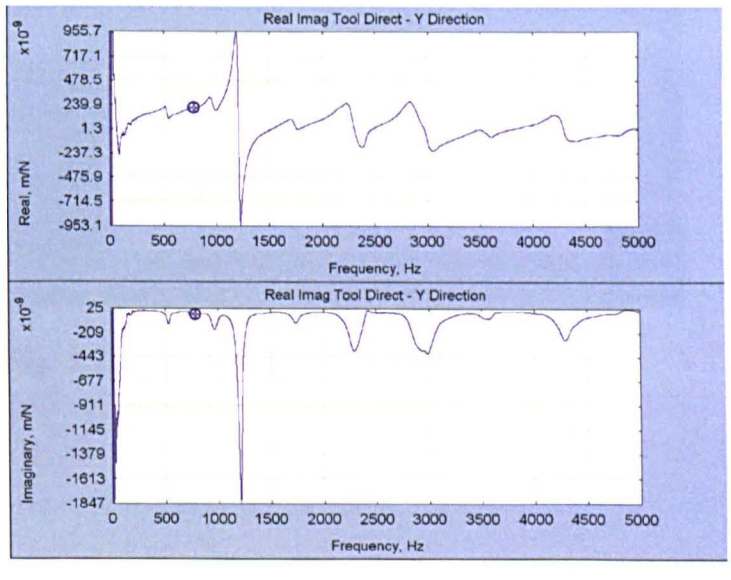

Fig 5.21 Test 2 – Y direction FRF

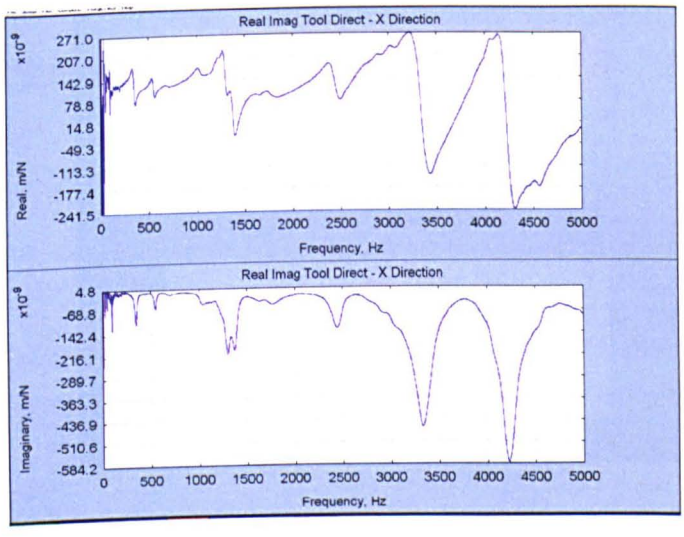

Fig.5.22 Test 3- x-direction FRF

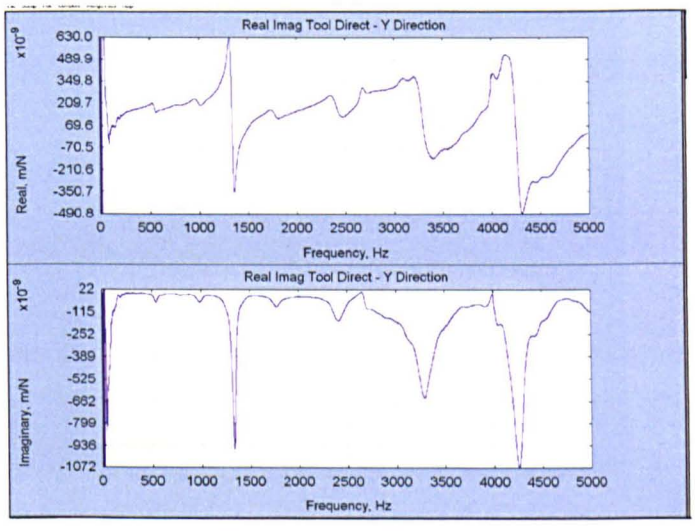

Fig 5.23 Test 3- y-direction FRF

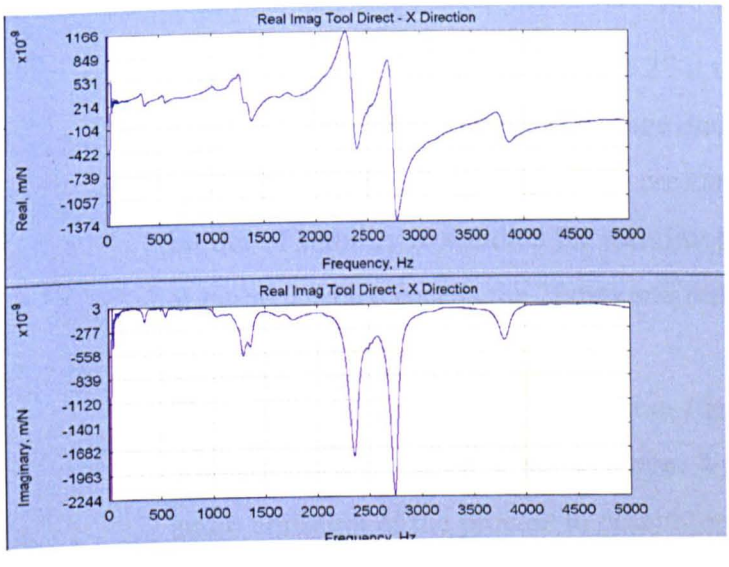

Fig.5.24 Test 4- x-direction FRF

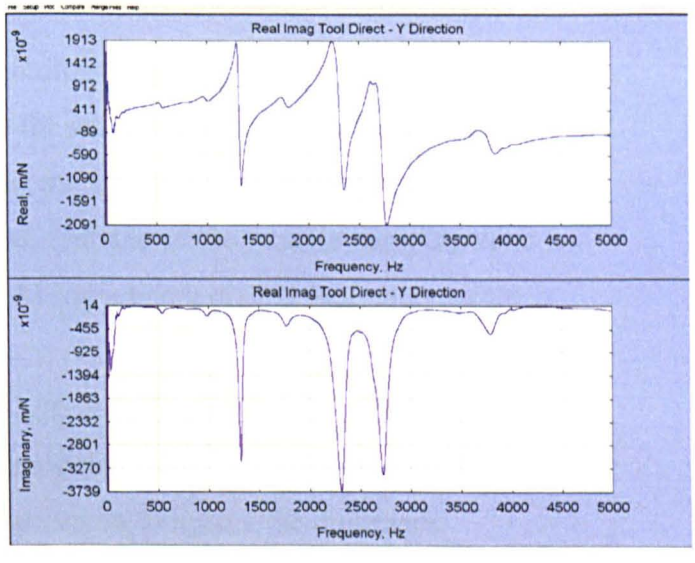

Fig. 5.25 Test 4- y-direction FRF

Lobe Plots

The lobe plots in figs.5.26 & 5.27 are taken for the 60mm extension tools. From the FRF figures 5.18-5.25 for the four set-ups it appears that the low frequency modes below 500Hz have a greater attenuation with the 60mm extension. The plots are generated with MetalMax™ TXF software as this permits predictions of the process damping zone using the critical wavelength approach.

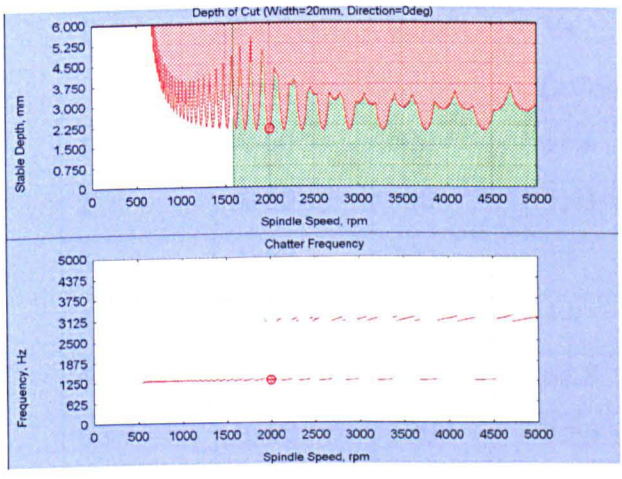

Fig.5.26 X-direction slot tool A-60mm

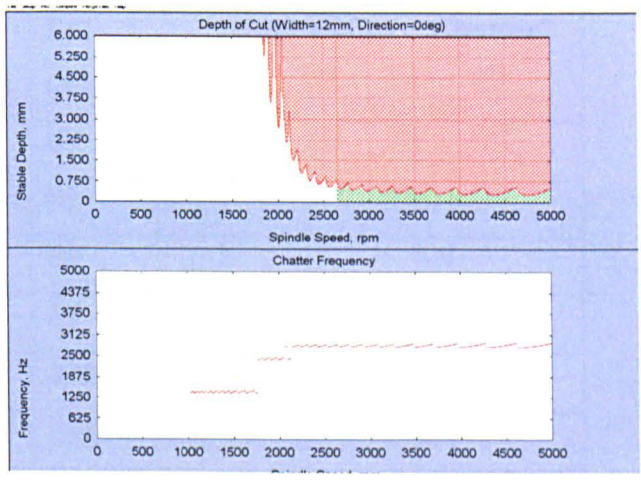

Fig.5.27 X-direction slot tool B-60mm

From the stability plots Fig5.26 & 5.27 it is predicted that setup B is more stable than setup A for the process damping range due to the attenuation of the 1270Hz spindle modes. A number of cutting trials were carried out for each setup around the predicted border of stability to validate the stability plots. Outside of the process damping zone at higher surface speeds the 20mm end mill (A) has a much greater b_{lim}, as expected for the stiffer tool.

The predicted chatter frequencies from Figs. 5.26 & 5.27 are between 1200Hz-4000Hz and are within the audio range. A microphone was selected to capture the audio emission of the process to determine stability and capture the dominant frequency. A visual inspection of the workpiece surface and judgement on the audible sound were all required to make a positive identification of chatter. If an audible vibration could be heard but no detection was made on the FFT then this was determined as borderline stability (B/L).The audio emission was captured using Harmonizer ™ software which was also used to compute an FFT of the time domain signal. The trials are detailed in Table 5.10 .All trials are slot cuts in the x-direction in a billet of Titanium 6-Al-4-V.

Trial	Tool-Length	RPM	Vs (m/min)	Fr (mm/min)	Depth of Cut (mm)	Chatter?
1	A-60	500	31.4	60	2	N
2	A-60	500	31.4	60	3	N
3	A-60	700	44	84	2	N
4	A-60	700	44	84	3	Y
5	A-60	1000	62.8	120	2	Y
6	A-60	1200	75.4	144	1	N
7	A-60	1200	75.4	144	2	B/L
8	A-60	1200	75.4	144	3	Y
9	A-60	1300	81.7	156	1	N
10	A-60	1300	81.7	156	2	Y
11	A-60	1300	81.7	156	3	Y
12	A-60	1500	94.2	180	3	Y
13	A-60	1990	125	239	2	B/L
14	A-60	1990	125	239	3	Y
15	B-60	1200	45.2	144	1	N
16	B-60	1200	45.2	144	3	N
17	B-60	1200	45.2	144	4	N
18	B-60	1990	75	239	3	N
19	B-60	1990	75	239	4	N
20	B-60	1990	75	239	6	B/L
21	B-60	2300	86.7	276	2	Y
22	B-60	2652	100	318	3	Y

Table 5.9 List of tool lengths, cutting parameters and chatter results

The experimental results detailed in Table5.9 are plotted against the predicted stability charts and displayed in Figs 5.28 & 5.29

Each trial is numbered, with green representing a stable cut, red an unstable cut and orange a border line cut.

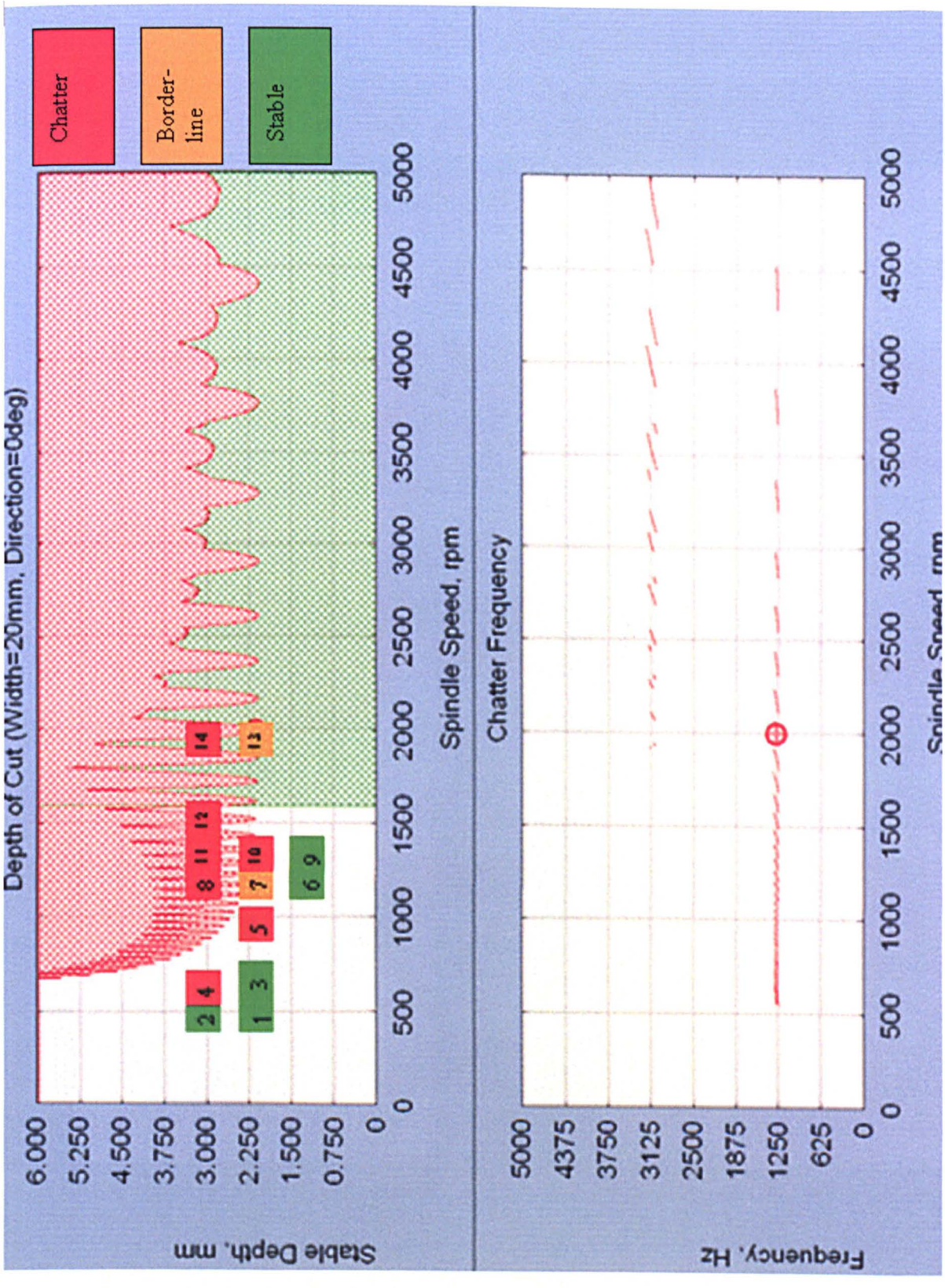

Fig 5.28 Experimental results against predicted stability A-60

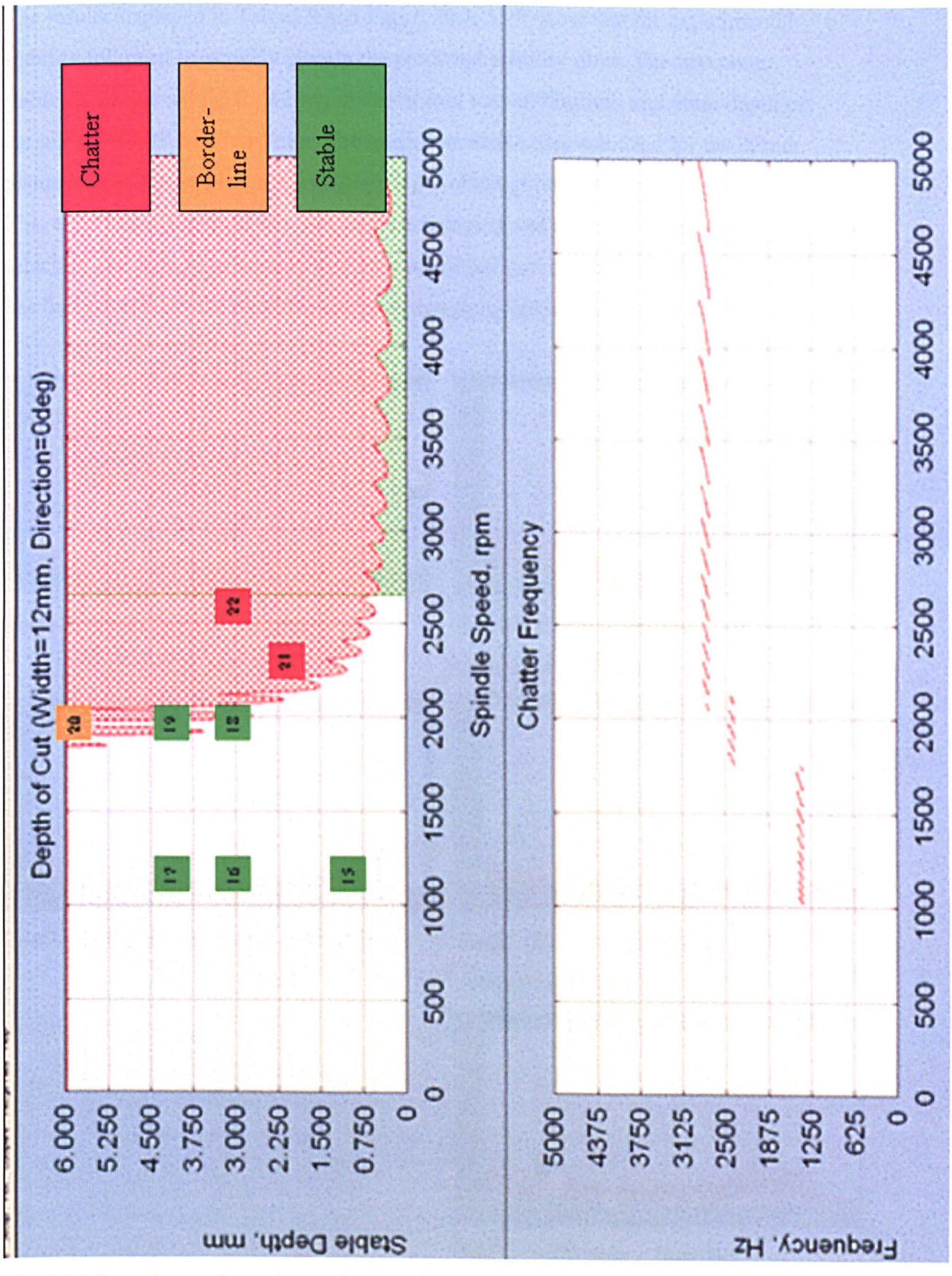

Fig 5.29 Experimental results against predicted stability B-60

The results displayed in Table5.9 and Figs 5.28 & 5.29 show that the experimental stability followed reasonably closely the predicted stability plots. The maximum stable data achieved for the 12mm diameter tool was at 75m/min and 6mm depth of cut giving a MRR of 17cm^3/min. The maximum stable data achieved for the 20mm diameter tool was at 44m/min and 2mm depth of cut giving a MRR of 3.4cm^3/min. This experiment demonstrates how process damping and optimisation of tool selection and set up can be used to obtain optimised tool data on a machine tool that has limited stability for roughing and semi-roughing operations.

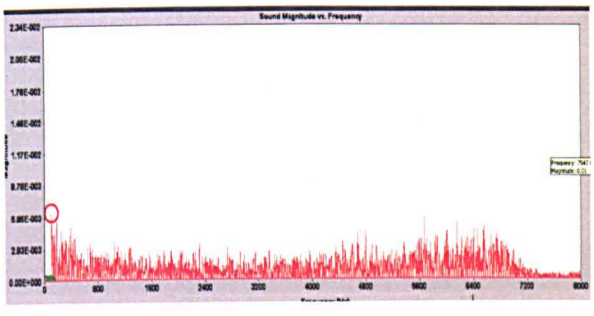

Test3-700 rpm 2mm slot (stable)

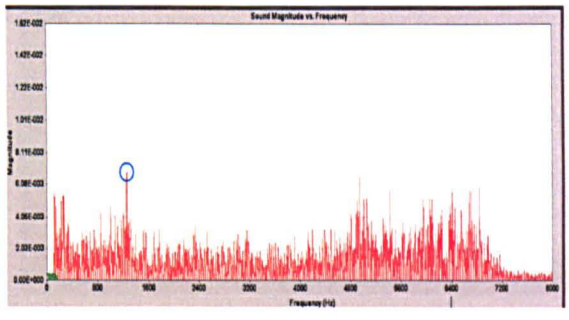

Test4-700 rpm 3mm slot
(chatter at 1270Hz)

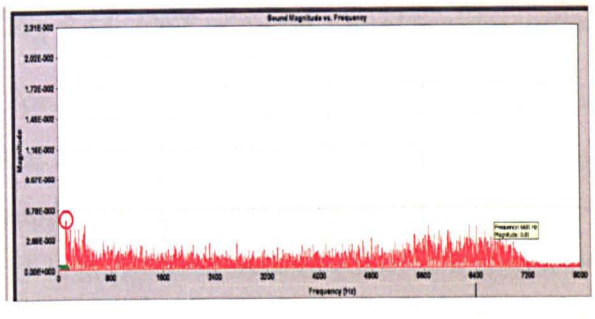

Test7- 1200 rpm – 2mm slot (borderline)

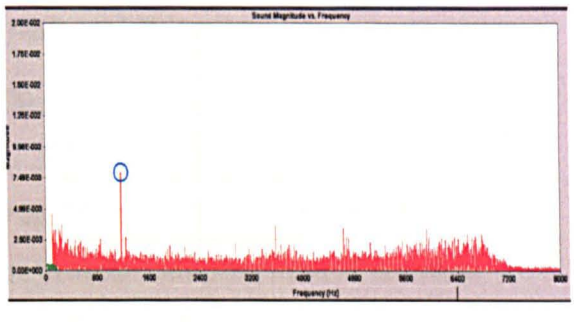

Test8- 1200 rpm -3mm slot
(chatter at 1270Hz)

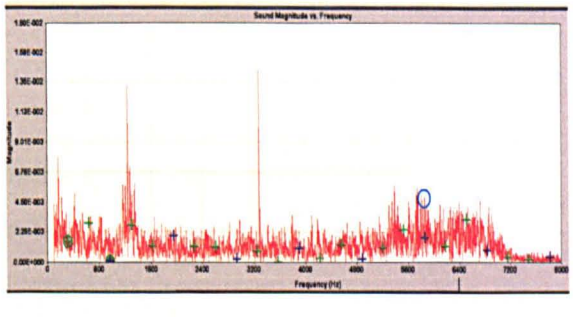

Test12- 1500 rpm – 3mm slot
(chatter at 1270Hz)

Fig 5.30 FFT of audio signal for slot milling with tool A in titanium

The FFT results for cuts 3,4,7,8,12,19 & 21 are presented in Figs5.30 & 5.31.
It can be seen that for tool A chatter is induced around the 1270 Hz spindle mode whilst for tool B chatter is induced at the 2830 Hz tool mode.
The audio signals near to the process damped limit are not as clear as the signals picked up during high speed milling of aluminium alloys but for each of the chattering passes there is a clear spike at around 1270 Hz whilst for the stable passes it is difficult to detect anything above the noise level. The chatter spikes do become more distinct as the spindle speed increases away from the process damped zone.

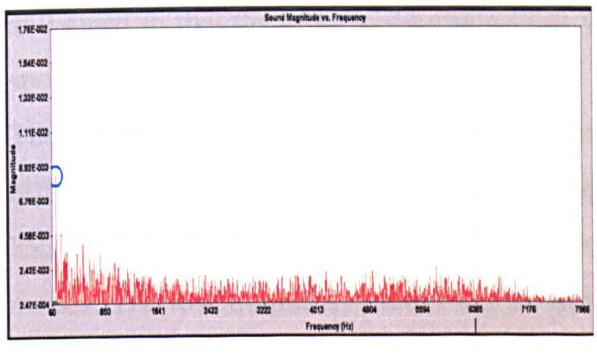

Test 19- 1990rpm 4mm slot (stable)

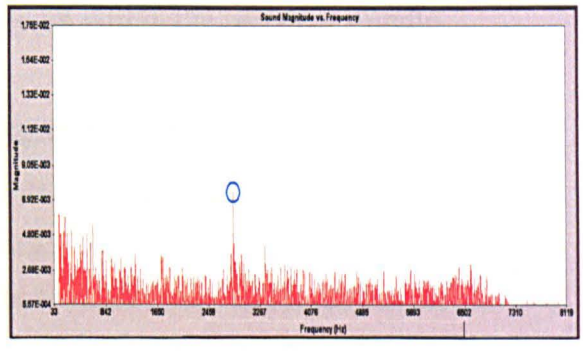

Test 21- 2300 rpm 3mm slot (chatter at 2800Hz)

Fig 5.31 FFT of audio signal for slot milling with tool B in titanium

For tool B a chatter plot is displayed for the 2300 rpm 3mm slot and a stable cut for the 1990 rpm 4mm slot. The chatter is at around 2800Hz, the predicted first dominant mode that is process damped for cut number 19 at 1990rpm. The chatter signal for cut 21 is fairly weak as with cut 4, as it is near to the process damping limit. Cuts were not taken far beyond the process damping limit in terms of spindle speed for tool B, as the process damping limit was already near the practical surface speed limit for tool wear.

Review of Experimental Results

The above results demonstrate that process damping theory may be used with manipulation of the frequency response function to achieve high productivity stable parameters to the extent that chatter is not a limitation on the system.
The FRF of setup B shows that the dominant modes of the machine tool structure have been attenuated by the introduction of a flexible tool mode. In case A this has occurred to a lesser extent and the maximum depth of cut that may be achieved before the structural mode induces chatter is 4 mm.

The FTV5 is a machine typically intended for 5-axis finishing and aluminium work and the stability of the machine would not permit titanium roughing under normal conditions. Through application of this technique efficient roughing parameters have been achieved and it is clearly demonstrated that modal attenuation combined with controlled process damping can deliver a solution where conventional approaches would fail. The feed per tooth could be further increased and the findings of the first part of this chapter would suggest that this would result in a significant increase in the process damping limit and in MRR. The feed per tooth for these trials was maintained at 0.4mm so that the process damping limit would lie within the practical spindle speed range for experimental convenience.

The structural modes below 500Hz have been largely neglected for this study as a different approach is employed to stabilise them. It is difficult to get accurate tool tip FRF data for the low frequency modes due to the high force required to excite these modes. The low frequency modes can be measured with a direct measurement on the spindle or machine tool structure.

A cross FRF measurement can be taken with an accelerometer mounted on the tool tip and excitation at various points on the machine tool structure. The limitation of the cross FRF measurement is that modal damping ratios cannot be accurately measured. A good assumption of the modal damping ratios can be made, and a low frequency stability lobe plot can be produced.

An added advantage of this technique is that it brings semi-finishing MRR close to that of roughing MRR. Conventionally aero structure parts are roughed, semi finished and finished resulting in 3 stages to achieve finished form from condition of supply. If semi finishing rates are close to those of roughing, then the part can be roughed close to form eliminating the need for an intermediary semi-finishing stage and enabling large productivity savings.

5.3.3 Summary of Process Damping and Modal Attenuation

The tap test measurements and cutting tests outlined above demonstrate that small diameter finishing tools can be used to achieve MRR equivalent to typical roughing processes for milling of titanium. The higher spindle speeds employed with the smaller diameter end mills may also mean that very low frequency structural modes will be avoided as the tooth passing frequencies will be higher than the modal

frequencies stabilising some structural modes with the 'over the last lobe' effect [4],[100].

Through introducing flexible tool modes, problematic spindle and tool holder modes can be attenuated and stabilised. This is particularly advantageous for machines that have complex modes and gears that would typically cause instability at the spindle speeds and cutting forces used for titanium milling. If correctly applied, this approach can lead to greater stable metal removal rates being available to a small end mill than a larger traditional roughing cutter. The limiting factor will then be tool wear and stability of the cutting process will be of no concern.

In theory this approach can be applied to any range of spindle speeds as long as the dominant tool modes are of sufficiently high frequency and flexibility. The approach has particular use in titanium machining because of the spindle speeds employed and the cutting forces incurred.

To use this method to accurately select a set up for optimum stability there must be confident predictions of the process damping properties as outlined in the first portion of this chapter. Dynamic repeatability of set up is also an issue [135, 149]. Further work on tool geometry and process damping properties is required along with an understanding of the repeatability of the process damping parameters from tool to tool. Repeatability of set up can often be poor for under damped tool modes as any slight variation in collet or drawbar force can lead to changes in damping of the dominant tool modes.

One limitation of the technique is static deflection of the tool if high cutting forces are induced. Low radial immersion may be required for finishing passes to limit static deflection.

5.4 Summary

Process damping has been studied by a number of groups over the last fifty years with no real success in modelling or manipulating the benefits of process damping. Process damping is particularly relevant to titanium milling as tool wear limits surface speed to ranges where stability lobes offer little benefit and process damping could be used advantageously if it can be predicted, controlled and optimised. Process damping is

believed to be caused by rubbing of the relief flank of the tool on the waveform traced on the cut surface.

A new method for evaluating process damping performance through measuring the critical process damping wavelength λc, has been presented at the start of this chapter. This method is then applied to study the influence of cutting parameters and tool parameters on the process damping phenomenon. In the first phase of trials feed per tooth is proven to have a strong influence on process damping performance with a six fold increase in the maximum speed at which process damping wavelength can occur with a 3.3 fold increase in feed per tooth, equating to over eighteen times the MRR through optimisation and control of process damping parameters.

From the first phase of trials little could be concluded with regards to the influence of rake and relief angles so a second set of trials were carried out with a broader range of rake and relief angles. These trials included some tool with zero relief which had the best process damping properties and could not be made to chatter although zero relief tools are not a practical application due to high temperatures and quick build up of material. This process damping effect may be emulated by employing cam relief tools, with an eccentric relief that offers some rubbing behind the cutting edge. Of the remaining tools, high rake angles appeared to have a positive influence on process damping particularly when combined with high relief angles. The experimental data was supported by measurement of the cutting force coefficients for each tool and Finite Element modelling using Third Wave AdvantEdge software. The FE results showed high strain on the cut surface for the tools with zero relief and also for high rake angles combined with high relief angles. It is proposed that this is a result of resultant force from the chip contact along the rake face pushing the cutting edge down into the cut material. The cases where high strain was predicted matched with good process damping performance and there appears to be a link between rake angle and process damping performance. If the rake angle is influencing the strain seen by the newly cut material and this is resulting in improved process damping properties then it is likely that the edge radius will also play a strong role. The edge radius has been specified as a constant for this study but there was no facility available to measure the edge radius and compare from one tool to another. It is possible that edge radius and edge preparation account for some of the disparity in results between tools of otherwise identical specification under identical parameters. In the case of tool PD5 one of the trials were run after the tool had been 'bedded in' preparing the workpiece

material. This bedding in process, removal of burrs and sharp edges from the cutting edge, resulted in improved process damping performance with a λc of almost 2.5mm. The study of the cutting force coefficients showed that they were linear for the small feed per tooth values tested and that work hardening and increase in cutting force coefficients could not be the cause of the poor process damping performance at low feed rates. It is concluded that the enhanced process damping performance at high feed is a combined result of increasing the amplitude of the vibration thereby increasing the slope of the waveform and the rubbing effect, and secondly increasing the resultant force seen on the rake face due to the travelling chip, thereby applying greater downward force on the cutting edge into the workpiece and increasing strain. The observations that the onset of chatter around the process damping limit and the vibration marks seen on stable cuts suggest that process damping does not provide a definitive border of stability. It is proposed that process damping acts as a limit cycle beyond the border of stability but when perceived to be a stable process, the process damping phenomenon prevents chatter from growing to notable amplitude. This would suggest that process damping is highly non-linear and should be modelled in the time domain and not through studying non-linear cutting force coefficients.
For practical manipulation and application of the process damping phenomenon a technique is developed in the second part of the chapter whereby modal attenuation is used to enhance stability for small diameter end mills to the extent that chatter is avoided within the practical surface speed range. Through introduction of high frequency, low stiffness tool modes the dominant spindle and toolholder modes from the machine tool system can be attenuated into the positive region of the real FRF plot. According to the defining equation for the limit of stability chatter cannot be induced by modes without a negative real part. Results of a single dimensional spindle FE model are presented to articulate the potential gains from employing this technique. A practical demonstration of the process is presented whereby introduction of a small diameter end mill stabilises the machine tool modes and enables greater MRR than with a more traditional approach with a large diameter end mill.
Utilising this technique eliminates concerns about chatter of spindles, tool holders and end mills. Once chatter is resolved then acceptable tool wear levels become the limiting factor in process optimisation. It has been demonstrated in this chapter that the set up is stable for surface speeds that are beyond the practical useful range for titanium machining due to tool life concerns. It is the objective of this approach to

eliminate chatter as a concern in the milling process. The hypothesis that process damping can be controlled and utilised to optimise milling stability through control of cutting parameters, tool geometry and tool set-up has been explored within this chapter. The first part of the chapter demonstrated that certain cutting and tool parameters can be controlled to optimise milling stability. The second part of the chapter demonstrated that control of tool set up and dynamic response can also result in optimised stability and performance.

6 CASE STUDY

6.1 Introduction

This chapter ties together the hypotheses investigated in chapters 3-5 and demonstrates how they are combined in practice to produce real gains when machining an aerospace component.

An aerospace landing gear part has been selected as a case study and the significance of the part and the primary features that are representative of titanium aerospace components are described. The aims set down by the landing gear manufacturer are outlined in context and a new approach to titanium milling strategies is required to hit the targets. A critical constraint analysis is then applied, targeting the factors that would restrict an increase in parameters and productivity. The theories developed in this thesis are each considered in detail to overcome the constraints. The different techniques are applied where appropriate and demonstrated on a number of production components. The success of these techniques on a real component is assessed and the overall success of the case study is assessed against the original objectives. In summary the chapter demonstrates the practical application of the theories developed in this thesis, putting them in an industrial context and demonstrating the huge rewards to be made through their application, thereby confirming the proposition in chapter 2 that there is a need for further development of titanium milling strategies. From this case study a list of rules of practice and risks for similar titanium aerospace parts are developed.

6.2 Case Study Background

The aerospace industry is continuously pushing for improved performance at reduced cost. Landing gear forms one of the most safety critical components on an aeroplane, being submitted to high impact and fatigue loading. The gear therefore requires very good strength and fatigue resistance whilst conforming to the aerospace trends of weight and size reduction.

One method of improving the performance / weight-size ratio is to move from steel to titanium components. Titanium 5Al-5V-5Mo-3Cr has been identified as a preferred material for its engineering properties and cost. Although titanium alloys have

become widely used in the aerospace industry for the reasons listed above, little machining data exists for Ti 5-5-5-3. Although the machinability of Ti 5-5-5-3 may vary to that of more common alloys such as Ti-6Al-4V, the same challenges exist; overcoming high tool wear, high cutting force coefficients and propensity to chatter. Ti5-5-5-3 has higher cutting force coefficients than Ti-6Al-4V and Arrazola [164]determined Ti-5-5-5-3 to have 56% of the machinability of Ti-6Al-4V.

At the outset of this project Messier Dowty were in the process of preparing a bid to supply the landing gear for the new Boeing 787. It was anticipated that much of the gear for the 787 would be produced in Ti 5-5-5-3 and a greater depth of knowledge of the machining and processing of this material was required to support the bid and potential long-term production.

A drag brace was selected as a sample component to demonstrate best practice titanium milling techniques and establish a cost model for the machining of titanium and compare it with the current Messier Dowty standard.

The drag brace contains a number of pockets and profiles that make it ideal for a demonstrator for the techniques outlined in this thesis.

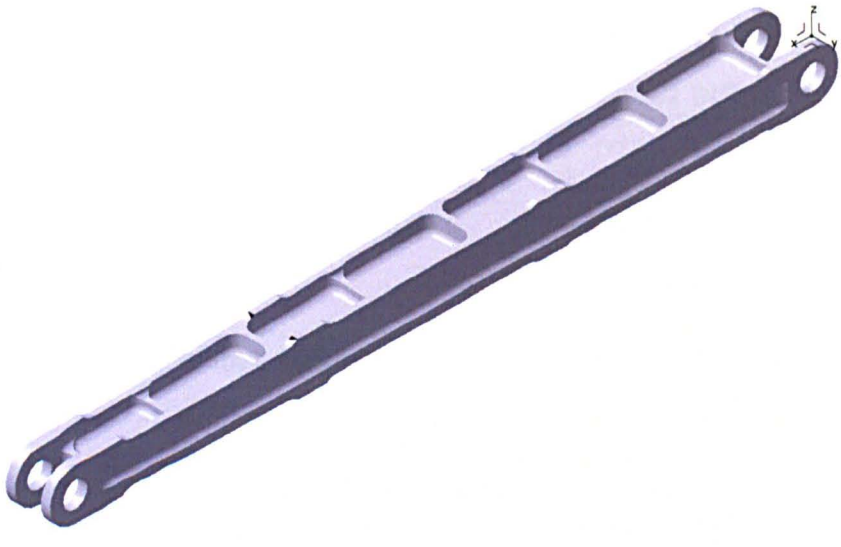

Fig. 6.1 Drag Brace

Initial screening tool life studies indicated that maximum surface speeds for Ti-5-5-5-3 were around 50% of those for comparable tool life in Ti6-4, therefore maintaining suitable tool life though strategy and parameter selection was paramount.

6.3 Aims

The case study had the overall aim of achieving comprehensive improvements in cycle times for the machining of Ti 5553 as compared with Messier Dowty and industry standards. To meet cost targets Messier Dowty set the target of machining titanium at the rates that they currently machined steel. As outlined in chapter 2, peak cutting temperatures and stresses are much higher when machining titanium than steel, the thermo-mechanical wear mechanisms combined with chemical effects mean that tool life when machining titanium alloys, and in particular Ti-5-5-5-3 will be significantly lees than steel. With higher cutting force coefficients than many steel grades the material is also more likely to induce chatter. In order to achieve the targets set out, a fundamental change in machining strategies is required. The current standard is to use large indexable cutters at depths of cut below the limit of stability to produce stable cutting parameters at acceptable tool life.

GOAL	BENEFIT
Machine 5-5-5-3 titanium at the same rates that Messier Dowty Limited currently machine steel	Support Messier Dowty bid to supply landing gear for Boeing 787.
Carry out all machining in the heat treated condition	Eliminate intermediary machining operations and set-up
Machine to finished surface	Eliminate the need for polishing, improve repeatability and quality.
Validate integrity of part after 'aggressive machining' conditions	Ensure optimum quality and productivity
Validate all machining parameters on a 'production' batch.	Obtain reliable cost data and address production issues

Table 6.1 Goals and benefits for Messier Dowty Ti5553 milling case study

6.4 Key features

The drag brace was 1.4m in length with a number of weight reduction pockets along each face and a through pocket or clevis at either end, each with a through bore (Figures 6.1,6.2). This part is typical of many titanium aerospace components, comprising of pockets with challenging corner and fillet radii, webs and thin floors, open profiles and undercuts and an enclosed U-shaped 'clevis' at either end requiring long L/D cutters to access and finish the corner radii.

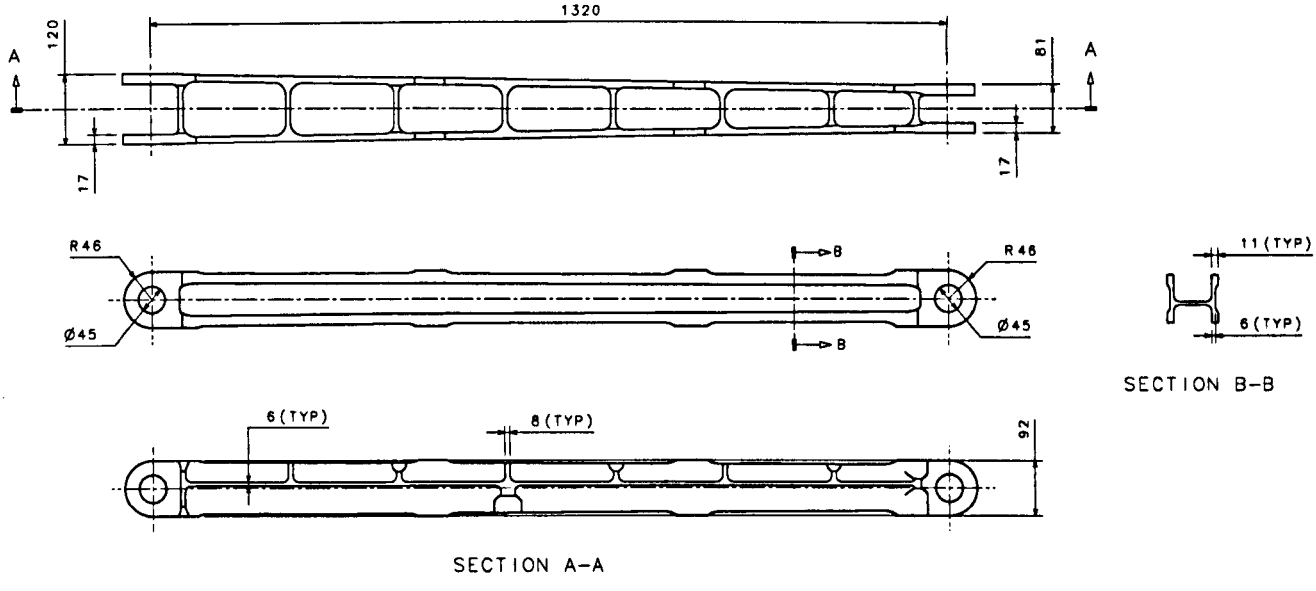

Fig.6.2 Drag Brace part dimensions

These are common features on structural aerospace components where shear and torsional strength is required combined with minimal weight. For these reasons parts requiring good strength and low weight are often produced from titanium, making the selected part highly representative of titanium components machined in the aerospace industry.

6.5 Critical Constraint Analysis

i. The first critical constraint on the machining of a drag brace of titanium Ti5-5-5-3 when compared with steel will be tool wear. In order to maintain acceptable tool life, milling strategies must be selected to optimise MRR and radial immersion. The pockets and outside profiles therefore provide the perfect opportunity to demonstrate the theory developed in chapter 3.

ii. The second critical constraint will be dynamic stability. The current practice is to employ large diameter indexable end mills and button mills to ensure rigidity of the cutter and enable high feed rates for relatively low depths of cut and surface speeds.

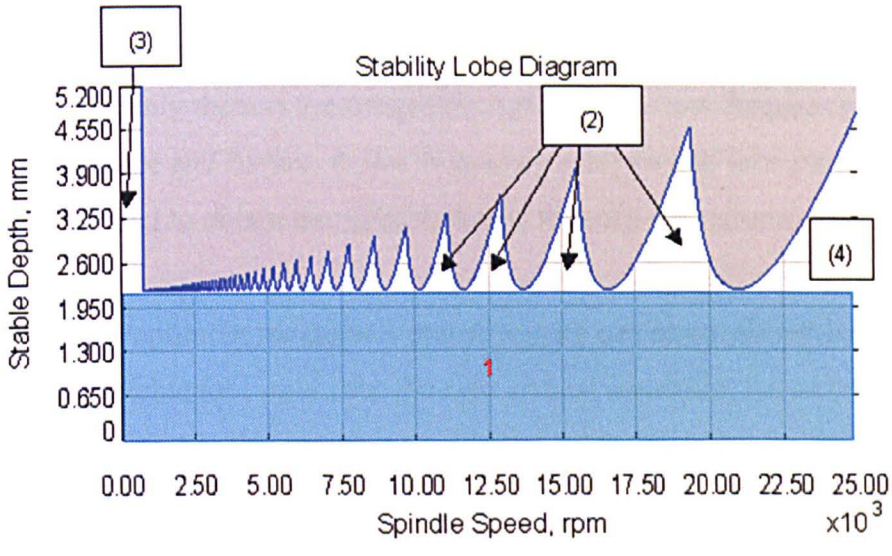

Fig.6.3 Regions of milling stability

The cutter selection often results in low dominant frequencies; as a result in figure 6.3 area 1 is the only region for stable cutting. To take larger stable depths of cut regions 2 or 3 must be accessed. As discussed in chapter 2, the stability lobes (region 2) cannot be reached due to surface speed restrictions, they can only become attainable by using tool geometries that will break up the unstable chatter phasing. Region 3 can be accessed for all tools, but as the maximum spindle speed is proportional to the frequency of the tool and the process damping wavelength then large diameter indexable cutters and button mills will result in low spindle speeds and feed rates. In some cases the stable speeds become so low that the speeds are impractical and the torque curves of the machine are exceeded,

meaning that region 1 again becomes the only practical option. When roughing enclosed geometries with large diameter tools, a semi-finishing operation is normally required to get close to finished form before a finishing pass can be taken. If comparable or better roughing rates can be achieved with smaller diameter cutters then the overall cycle time can be drastically reduced as semi-finishing is eliminated. There is therefore an opportunity to demonstrate the theories developed in chapters 4 and 5. The pockets will be used to demonstrate the process damping and toolpath strategies. The clevis ends require tools with high length/diameter ratios resulting in low natural frequencies and inefficient process damped speeds. The clevis therefore provides an opportunity to demonstrate the variable helix tool on a real feature.

iii. In cases where large diameter end mills can be process damped and used to rough efficiently there is the danger of chattering the low frequency modes of the machine and fixture. A low frequency analysis and lobe plotting is therefore required to obtain the stability limits for such operations.

iv. If the optimum parameters and strategies can be employed for stability and acceptable tool wear then the next critical constraint becomes the part integrity and size. For this reason a production batch of parts were produced and each were tested on a CMM for geometry and NDT tested for 'machining abuse'

6.6 *Application of Techniques*

6.6.1 Pocketing Strategies

Solid carbide roughing is very effective and can be more cost effective than using long edge indexable cutters where tooling costs are a major concern. In cases where machine tool stability is in question or part geometry limits accessibility for large diameter cutters, then solid carbide tooling is appropriate for roughing.
There are a number of advantages to using a small diameter end mill compared with a larger diameter roughing-cutter when roughing titanium:
Small diameter equates to higher rpm for equivalent surface speed (and higher feed).

Small diameter for an equivalent depth of cut means a smaller overall area of cut and thereby reducing the chance of exciting structural modes of the machine tool.
Small diameter equates to low mass and high frequency tool modes. The maximum stable process damped speed increases as the natural frequency increases and the diameter decreases. Therefore much higher stable speeds can be achieved with small diameter cutters.
The disadvantage is that tool life is linked to radial immersion (radial depth of cut/ diameter of cutter). It is therefore important to develop toolpaths where the radial depth of cut is maintained as a constant so that productive surface speeds and feed rates may be used without impacting on tool life.
From the toolpaths examined in chapter 3 it was demonstrated that the spiral-morph toolpath gave good results with regards to tool life and was also demonstrated to be practically applied to a range of pocket shapes during the Sandvik best practice study. A version of this toolpath has been selected to machine two of the seven pockets on one face of the drag brace and can be compared against more conventional techniques. An access hole is drilled in the centre of the pocket and then the 16mm end mill roughs the pocket base 1mm from the floor. The tool follows a trochoidal toolpath where the radial immersion of the tool is kept to a near constant and there are no sudden increases in size of the cut in the corners of the pocket. Maintaining a constant immersion in this manner increases tool life and avoids chatter.
The base is roughed up to the 12.5mm fillet radii and then the tool cuts around the perimeter of the pocket 12.5mm above the pocket base, leaving the stock in the fillet of the pocket. The overall cycle time for roughing with this technique was comparable to that of the large diameter long edge cutter, yet the load on the tool and machine at any given point was considerably less and tooling costs are drastically reduced. Once the tool is process damped this strategy is very effective as it is unlikely to chatter the part, machine or fixture and yields reasonable tool life compared to slotting with indexable carbide.

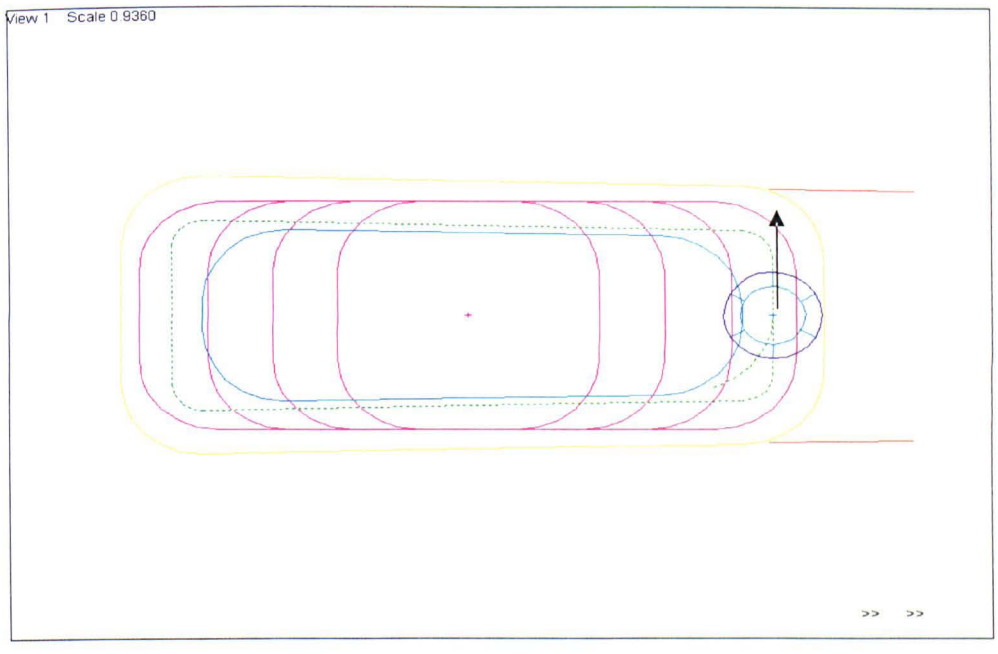

Fig.6.4 Pocket strategy A; adaptation of radius corner pocket strategy

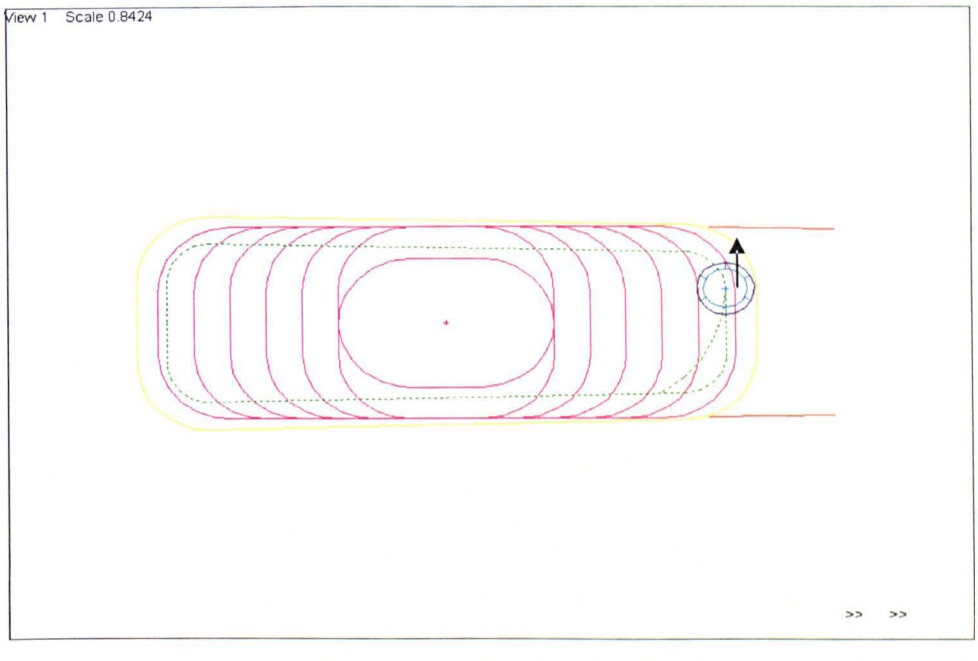

Fig.6.5 Pocket strategy B; Spiral strategy to control radial width of cut in pocket

Finishing of the pockets is best achieved using formed carbide tooling, due to the large fillet radius. In the case of the drag brace pockets the tool produced a good finish on the pocket walls whilst the speed and feed could be increased for the base to account for the reduced effective diameter of the cutter. A 38mm diameter cutter was used with 12.5mm corner radius to form the fillet. When milling the floor the

effective diameter was 13mm, meaning that the spindle speed could be increased three fold to maintain a constant surface speed. The large corner radius produces a chip thinning effect as shown in Fig6.6.

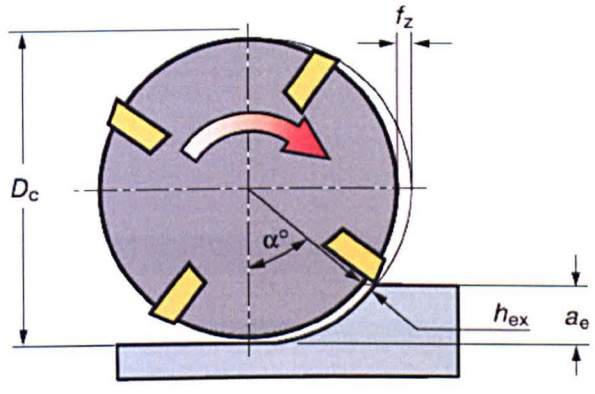

Fig.6.6 Chip thinning due to corner radius (ref Sandvik Coromant)

The feed per tooth can be increased to maintain a constant effective chip thickness or hex value.

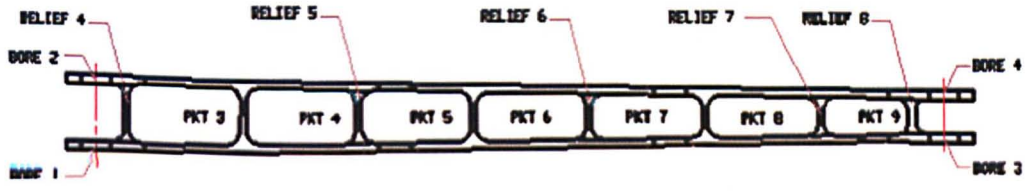

Fig.6.7 Machined Features

6.6.2 Modal attenuation/ process damping

As described, a number of the smaller pockets were roughed using process damped 16mm diameter solid carbide tools. The strategies are described in detail during the pocketing section but in each case the toolholders and tool length were set such that the dominant tool bending mode provided the only negative mode on the real part of the FRF. The best and worst cases for the analysed set ups are displayed in Figs. 6.8 and 6.9:

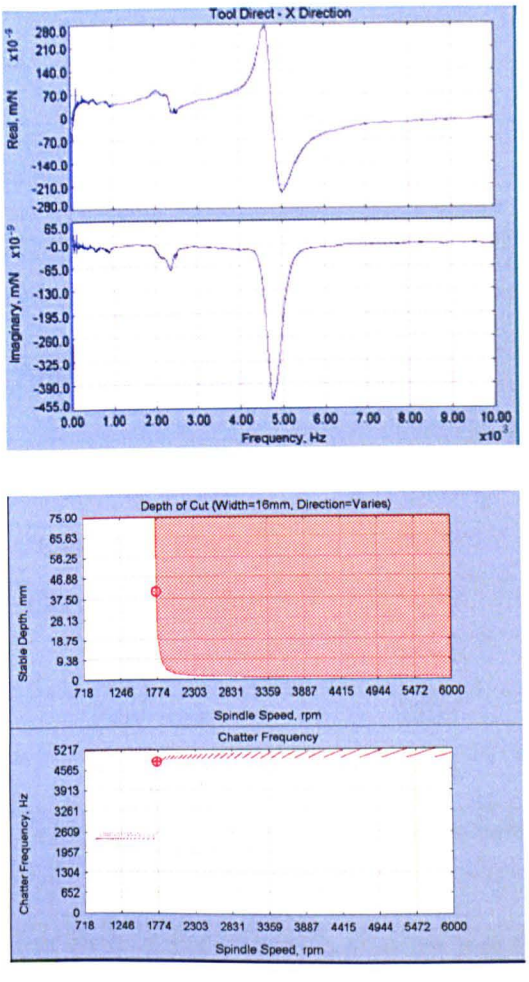

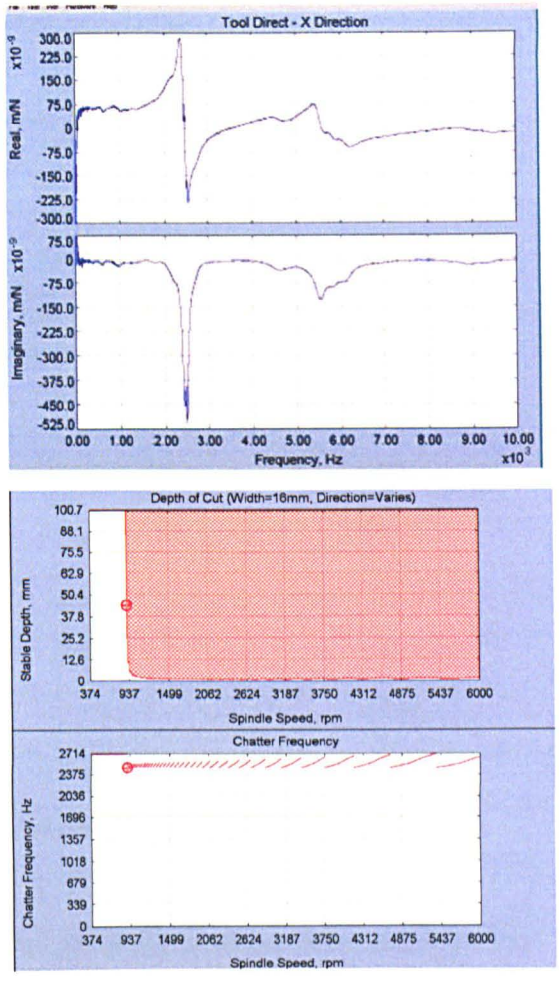

Fig.6.8 FRF & Lobes for Corogrip ***Fig.6.9 FRF & lobes for Rego – fix standard***

To generate the stability plots above it is important to know the critical process damping wavelength for the tools. These were measured using the technique outlined in chapter 5 and for the standard solid carbide end mills provided by Technicut and a feed per tooth of 0.1mm the process damping wavelength was found to be 0.8mm. Fig. 6.8 and 6.9 show the same tool measured in two different tool holders and therefore each has the same process damping properties. It is clear that the tool in the Sandvik Corrogrip holder has the highest frequency first negative mode and therefore the highest process damped cutting speed. The toolholders selected are in table 6.2 and the results of the toolholder analysis are displayed below in table 6.3.

Brand name	Type	Manufacturer
Corregrip special	Hydraulic	Sandvik
Corregrip standard	Hydraulic	Sandvik
Rego - fix	Hydraulic	Rego-fix
Posi-lock	Side lock	Gewefa
N / A	Shrink fit	Kennemetal

Table 6.2 Toolholder descriptions

Brand name	Frequency	Magnitude	Max PD Speed
Corrogrip special	4074	$-50\ e^{-9}$	1430
Corrogrip standard	5000	$-230\ e^{-9}$	1768
Rego - fix	2534	$-235\ e^{-9}$	900
Posi-lock	3205	$-5.73\ e^{-9}$	1280
Shrinkfit	2718	$-574\ e^{-9}$	950

Table 6.3 Tool holder modal parameters and maximum process damped speed

For each of the toolpaths shallow radial and full axial depth of cut were employed to maximise MRR and tool life and avoid chattering any part, fixture or machine modes. The process damping wavelength for the tool was determined as in chapter 4 and found to be 0.8mm at 0.1mm feed per tooth. The maximum process damped speed for each setup has then been calculated from the first negative mode on the FRF for λ_c = 0.8mm:

$$V_s = \lambda_c \times f_c \qquad (6.1)$$

Modal attenuation is used through optimisation of tool holder, spindle and tool modes. This resulted in the Corrogrip holder giving a maximum stable process damped speed of 1768rpm, almost twice the MRR of the incumbent Rego-fix tool holder.

The solid carbide process damped pockets were the most effective of all techniques when considering cycle time and tool life and cost. The metal removal rates were much higher than the existing benchmark using indexable tools and the small diameter solid carbides take the pocket close to form, effectively eliminating semi-roughing. The added advantage of the process damped carbide approach is that the machine tool was not required to pull high torque or require high stability. The next section looks at the structural stability requirements for the heavier cutting operations.

6.6.3 Machine Tool Tuning (Process Damping)

The most productive roughing technique found was to use large diameter brazed or indexable carbide with a tough grade and geometry. Where part geometry permitted, the heavy process damped depths of cut resulted in high metal removal rates. Tool life can be greatly improved by using through tool coolant at elevated pressures. The approach of using heavy, process-damped cuts is reliant on a stable machine tool and dynamic analysis may be required to optimise the tooling set up and parameters and select a stable lobe for the machine tool.

Dynamic analysis was conducted on a 50mm diameter, 6-flute, integral, brazed carbide and 38mm diameter, 4-flute, integral brazed carbide with a corner radius of 12.5mm. Testing was carried out in the X and Y directions on the 50mm diameter tool and in Z on the 38mm diameter. The focus of the analysis carried out in X and Y was to determine the optimum quill position for the Giddings & Lewis machining centre (Fig.6.10), to give the fastest process damped speed. The focus of the analysis in the Z direction, attained by tapping up the axis of the spindle, was to determine the optimum position to reduce the effect of a problematic spindle mode. This mode was around 200Hz, which became unstable when a cutter with a large corner radius was used for roughing operations as the resultant direction of cutting force changed from a radial direction to up the axis of the spindle.

The fastest process damped speed obtainable is predicted from the measured FRF. This prediction is related to the frequency of the first negative mode of the real part of the FRF.

Fig.6.10 Giddings & Lewis machining centre at Messier Dowty Gloucester

Within this particular investigation tuning of the first negative mode was accomplished by varying the spindle extension but it can also be done successfully using the tool length or modification of the tool holder set-up, as demonstrated with the solid carbide tools.

In the second stage of the analysis, where the mode in Z was investigated, the dominant frequency was too low for effective process damped parameters and an approach similar to more conventional lobe theory was taken. This means that the magnitude of the negative peak of the real FRF is now of primary concern, the FRF data is displayed for a 50mm end mill in Fig. 6.11.

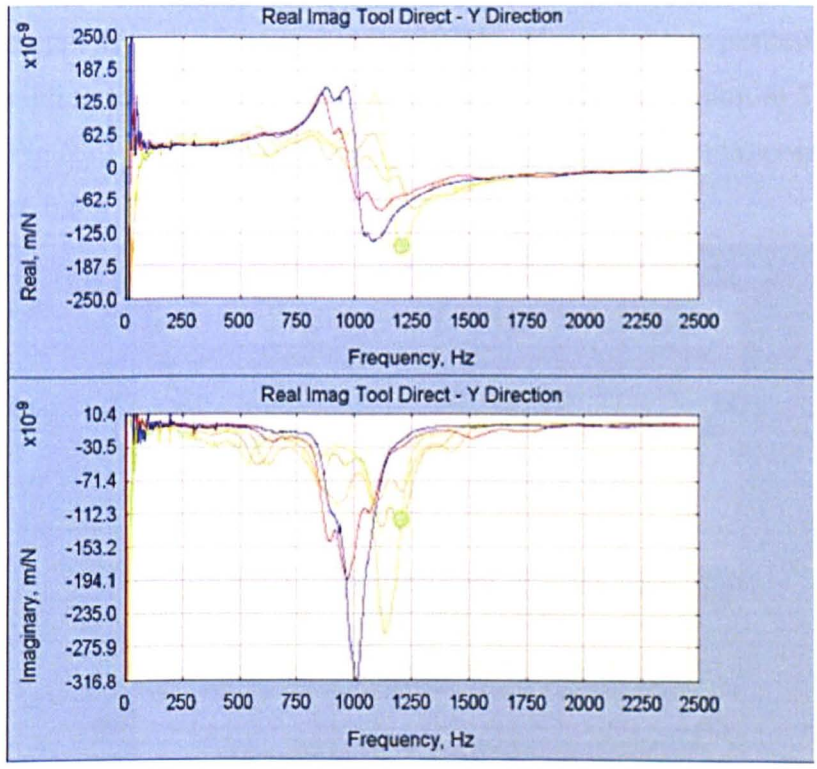

Fig.6.11 Y direction comparison of spindle quill positions

Blue – 0" Yellow – 8"(203.2mm)

The quill was tapped at 0, 2, 4.5, 6 and 8 inch extensions, in both X and Y directions. As the results from both X and Y were similar only Y is shown in Fig. 6.11. As stated earlier, the fastest process damped spindle speed is dictated by the negative peak of the real FRF, the higher the frequency, the faster the spindle speed. The results are summarised in the table 6.4.

Quill extension (mm)	1st Negative Real Peak Frequency (Hz)
0	1045
50.8	1008
114.3	982
304.8	1141
406.4	1207

Table 6.4 1st modal frequencies for different spindle quill positions

The quill extended at 8 inches (203.2mm) tunes the FRF of the set-up so that the first negative peak of the real is at 1207Hz. Hence for this particular set-up, when the cutting force was in the radial direction, a quill extension of 8 inches was used. Fig.6.12 shows the FRF data for the 38mm bull nose tool considering z direction stability.

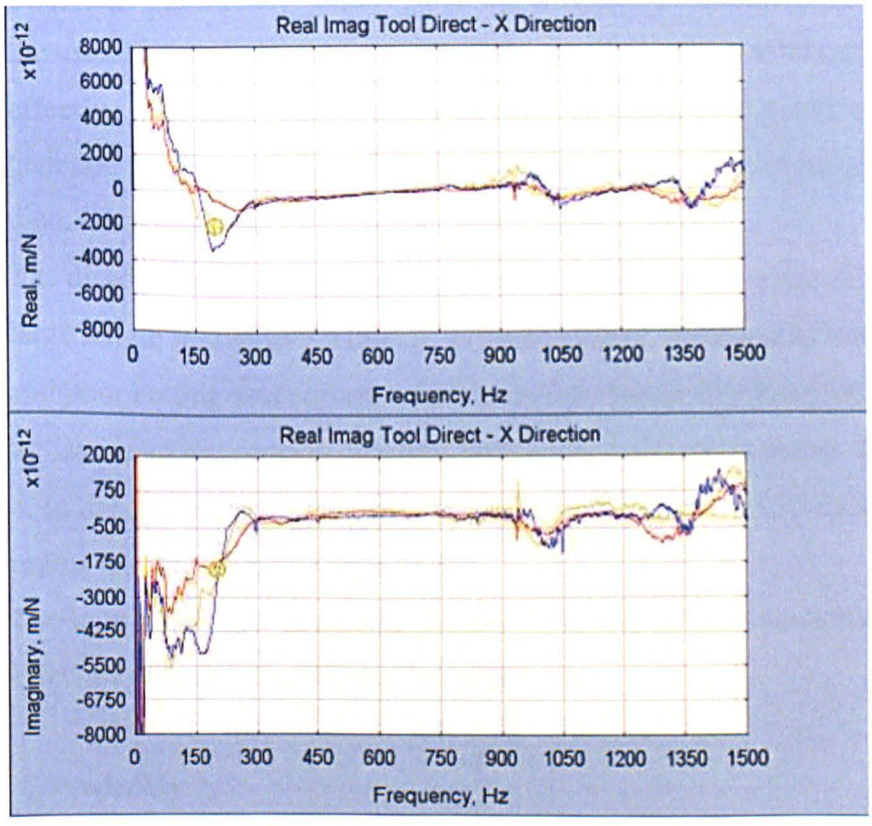

Fig.6.12 Z direction comparison of spindle quill positions

Blue – 0 Red- 50.8mm Orange- 127mm Yellow – 152.4mm

The quill was tested at 0, 50.8mm, 127mm and 152.4mm extension in the Z direction (Figure6.12). The four figures show that at positions 0 and 152.4mm, the magnitude of the negative real is larger than when the spindle is at 50.8mm or 127mm. This means the problematic mode has its greatest dynamic stiffness position at 50.8mm or 127mm. This is possibly due to wear of the quill at 0mm and 152.4mm as they could be more commonly used positions. It could be also explained by the possible modal interaction of the quill behind the taper face, which leads to a stiffening of the 200Hz mode at the 50.8mm to 127mm extension range. Using the results of this study, chatter was eliminated with both the 38mm and 50mm diameter tools through optimisation of the spindle quill position.

6.6.4 Variable Helix tools

The machining of the pockets demonstrated the success of small diameter tooling for roughing applications. Where small corner radii or other geometric features restrict the use of large diameter roughing tools, small diameter solid carbides are very effective. The advantages are that no semi-roughing is required as the tool can generate the finished form, and that feed rates can be increased relative to larger diameter cutters due to the higher stable spindle speeds.

The disadvantage of using small diameter tools to rough close to form is that often large length to diameter ratios (L/D) are required, resulting in low dynamic stiffness and poor cutting performance. Earlier in the chapter this has been addressed through utilisation of the process damping and modal attenuation theory developed in chapter 4. In the case of the clevis end, the depth of the feature with relation to the corner radius resulted in a L/D ratio of 5:1.

The long tool length increases the tool mass and reduces its stiffness, both having the effect of reducing the natural frequency.

$$f_n = \sqrt{(k_c/M)} \qquad (6.2)$$

The low dominant frequency means that the maximum process damping speed becomes too slow to be efficient. An alternative strategy is therefore sought, providing the opportunity to demonstrate the variable helix theory explored in chapter 4.

The bi-helical cutters were designed with 4 flutes and 24mm diameter so that the tool could be driven around the 12.5mm pocket radius without a dwell in the corner.
As demonstrated in chapter 5, variable helix tools of the correct geometry outperform variable pitch tools and were therefore selected. Despite the 24mm diameter the tool effectively full slots in the corner and this is the most challenging part of the feature.
The geometry relates to the successful variable tool tip pitch and helix from chapter 5. The parameters match the optimum parameters from the lobe plot. Although in chapter 5 it is demonstrated that the tool out performs the predicted stability limit the predicted speeds for maximum stability are accurate.
During initial trials of the variable helix tool a number of bands could be seen on the profile of the wall, appearing as though the tool was chattering at certain points along its length whilst being stable at others. This lends further insight into the mechanism of stability for variable helix tools.
The bands can be seen in Fig. 6.14. The 3mm radial cut was taken as two axial passes although chatter can clearly be seen in the centre portion of the pass.

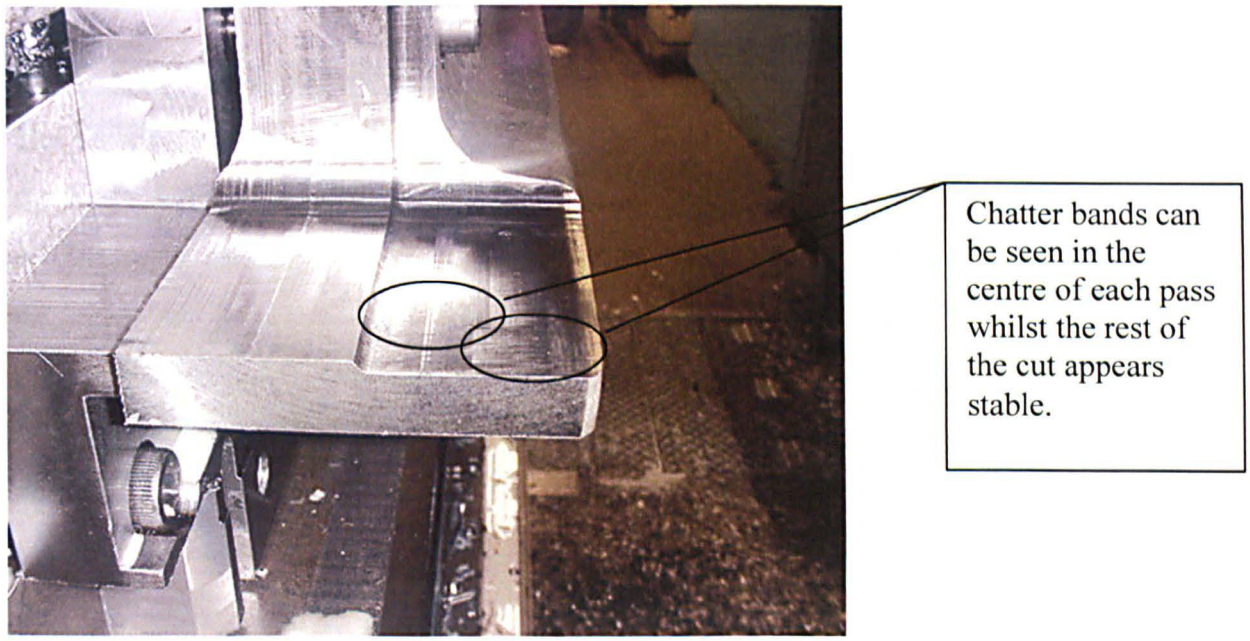

Fig. 6.13 Variable helix chatter bands on clevis.

The technique proved to be successful with the tool following a U-shape toolpath around the clevis perimeter, leaving 0.5mm on for finishing with two axial passes of 25mm depth from each side. The photograph of the 3mm radial roughing pass clearly shows multiple bands of chatter on two axial passes. This raises some possible insight into the high stability mechanism of the variable helix tool.

- If different 'slices' of the tool can be both stable and unstable at the same time this lends further credence to the theory that process damping combines with variable helix to result in enhanced stability.
- Stability models without damping would see chatter engage the entire tool once a portion of the tool begins to chatter as the localised high amplitude vibration increases the cutting forces along the length of the tool.
- Some non-linearity is preventing the chatter from taking hold of the entire tool, this could be due to the tool jumping out of the cut or process damping inhibiting the chatter growth in the stable portion of the tool.

6.6.5 Finishing Strategy

The variable helix tool was also used for a full depth finishing pass with 0.5mm radial depth of cut. In this case there was no chatter and a competitive cycle time was achieved. The alternative method was to use a two flute solid carbide end mill so that the tool would see no increased loading in the corners as only a maximum of one flute can be engaged at any time, therefore being 2.5 times more stable than a standard five flute tool. The two flute method is also successful but by using the variable helix tool productivity is increased by a factor of 2.5.

6.7 Results

The cycle times for the various features as recorded during a batch run of 5 components are presented in table 6.5

Operation	*Cycle Time*	*Strategy*
Profile 3 & 4 faces 1 - 4	**106min 38sec**	**50D brazed carbide**
Small Clevis	**15min 18sec**	**Bihelical**
Large Clevis	**30min 17sec**	**Bihelical**
Pocket 1	**70min 35sec**	**Indexable Carbide rough, brazed carbide finish**
Pocket 2	**89min 5sec**	**38mm brazed carbide rough & finish**
Reliefs 1,2,3	**34min 34sec**	**44mm indexable carbide- rough 38mm brazed carbide –finish**
Profile 1	**76min 9sec**	**50mm brazed carbide profile**
Profile 2	**86min 8sec**	**50mm brazed carbide rough Indexable 'Dream cutter' finish**
Pocket 3	**22min 50sec**	**Indexable carbide rough**
Pocket 4	**28min 58sec**	**Solid carbide, process damped trochoidal**
Pocket 5	**25min 43sec**	**Solid carbide, process damped trochoidal**
Pocket 6	**29min 30sec**	**24mm gator trochoidal roughing 38mm brazed carbide finish**
Pocket 9	**17min 16sec**	**24mm var helix spiral rough 25mm ball nose finish rads**
Pocket 7	**30min 20sec**	**Button mill ramp**
Pocket 8	**28min 42sec**	**38mm brazed carbide rough & finish**
Reliefs 4 - 7	**28min 52sec**	**44mm indexable carbide- rough 38mm brazed carbide –finish**
Relief 8	**6min 50sec**	**38mm brazed carbide rough &**

		finish
Bores 1 - 4	**11min 23sec**	**U-drill, boring bar**
Square Face Up	**13min**	**50D brazed carbide**
Total	**13hrs 16min 26sec**	

Table 6.5 List of part features with cycle time and brief description of strategy.

From Table 6.5 it can be seen that the average cycle times is **13 hours 16 minutes.**

Comparing the process damped solution of pocket 5 to the cutting tool provider solution of pocket 7 using a button end mill indicates that the solid carbide route gives a shorter cycle time and better tool life. With pockets with smaller radii this becomes even more effective.

The clevis ends, roughed and finished with bihelical cutters were 6 times faster than the standard approach provided by the tooling engineer. The high depth of cut and relatively high surface speed enabled by the bihelical cutter drastically increased productivity.

The highest MRR were achieved on the reliefs, where long edge cutters were tuned to the dominant spindle modes. The machine lobes also enabled high MRR on the 38mm end mills for semi-roughing of pockets. The positioning of the quill and the subsequent spindle speed selection eliminated chatter and proved that the tool was optimised for the part and material condition. The tool modes were process damped but in this case combined spindle and quill modes fell into the lobe region.

6.8 Summary

The theories developed in this thesis have been demonstrated and applied in an industrial context. The ultimate goal is to improve the productivity of titanium milling.

At the start of this case study the task was set to produce a titanium part at the same rate as a steel part despite the surface speed for 1hr tool life being 20m/min as opposed to 100m/min. The milling time was demonstrated at 13 hours 16minutes against an initial target of 30 hours for titanium. By Messier Dowty's estimating

method 30% is added to cutting time to account for non-cutting time and tool changes. By the same estimating method the following processes were also added at their standard titanium rates. With these considered the total process time for the component is shown in Table 6.6.

Operation	Time per part	Time per batch	Running Total (part)	Running Total (batch)
Forging Prep	1h	2h	2h	2h
Cutting Time	13h 16m	-	14h 16min	2h
Additional Machining Process time	4h 33 min	2h 30 min	18 h 49 min	4h 30min
Deburr	1h 30min	-	20h 19min	4h 30min
Machine Additional Details (greaser holes, spot faces etc) + 25%	5h	-	25h 19min	4h 30min
TOTAL			25h 19 min	4h 30 min

Table 6.6 Process times for part production

This total process time of 25hours 19minutes is comparable to the process time predicted for an equivalent steel part using the Messier Dowty estimating model (24 hrs) and less than half of the predicted time for a titanium component. This is despite only having influenced 50% of the process time through milling technology. On milling time alone the cycle time was 60% of that for a steel part (19 hrs) and 3 times faster than the cycle time predicted for the established titanium method.
The total cost of tooling on the first two forgings was £515.77, approximately £40/hour tooling consumption. This is taken as the AMRC standard rate for consumable tooling when machining Ti-6Al-4-V and demonstrates a reasonable and stable process. If the hourly rate of the machines is low then the surface speed can be slowed to reduce tool cost at an increase in machine running cost until an optimum cost is achieved.

6.8.1 Review of Case study goals

GOAL	RESULT
Machine 5-5-5-3 titanium at the same rates that Messier Dowty Limited currently machine steel	Ti-5-5-3 now machined at the estimated rate for steel .
Carry out all machining in the hardened condition	All machining carried out in the heat treated state at productive rates
Machine to finished surface	Polishing eliminated: Known surface quality.
Validate integrity of part after 'aggressive machining' conditions	NDT passed, repeatable integrity
Validate all machining parameters on a 'production' batch.	Actual cost per part, confidence in proposed strategies

Table 6.7 Review of goals and results of titanium milling case study

The results against the objectives demonstrate the successful application of the theories developed within this thesis.

7 CONCLUSION

7.1 Development of Research Hypotheses

The critical constraints on titanium milling are identified in chapters 1 and 2 as tool wear and chatter. None of the constraints should be considered in isolation as once one issue is resolved the critical constraint can move to another area and create further problems. It is proposed that chatter and tool wear in titanium milling in particular should not be considered in isolation and some examples are presented from the literature where considering either in isolation has led to erroneous or impractical conclusions. Following the literature review in chapter 2 a typical chatter stability plot was studied identifying the areas where enhanced stability can be achieved when milling titanium. It is concluded that through control of process damping or through raising of b_{lim} or repositioning of lobes it may be possible to improve titanium milling stability and performance. If the b_{lim} and lobes are to be utilised then it is essential that constant radial depths of cut are maintained as an increase in radial depth of cut will lower the maximum axial depth of cut before chatter occurs. Radial depth of cut is also identified from the review as a key process variable influencing titanium tool wear along with surface speed. Strategies are then sought that can address the issues of titanium milling stability through process damping and lobe form manipulation whilst controlling surface speed and radial depths of cut to levels where productive MRR and tool life may be achieved. Three areas are identified from this review. The first is the *study of toolpath strategies* to maintain constant radial immersion and thereby maximise tool life, stable axial depth of cut and MRR. The second is the *study of special tool geometries* to break up chatter and manipulate the blim and lobe positions such that they may benefit the titanium milling surface speed range. The third area of focus is characterisation and control of the *process damping* phenomenon so that the region may be extended to higher surface speeds enabling stable milling for the titanium surface speed range.

From the review of the current state of the literature and the identification of areas of research where further contribution could be made towards optimising titanium milling strategies the following research hypotheses were created.

1. ***Tool life and chatter in titanium milling can be controlled through effective toolpath selection***
2. ***Variable helix end mills can provide enhanced stability and productivity and can be modelled using a frequency domain solution***

3. ***Process damping can be controlled and utilised to optimise milling stability through control of cutting parameters, tool geometry and tool set-up***

7.2 Toolpath Strategies

In chapter 3 a study is undertaken to evaluate whether tool life and chatter can be controlled through toolpath optimisation as stated in the first hypothesis. A thermal model is developed and presented predicting that radial depth of cut will have a greater influence on tool temperature than axial depth of cut and that controlling radial depth of cut should reduce peak temperatures and enhance tool life. Five toolpath strategies are developed for an 89mm square pocket, each aimed at avoiding the increase in radial immersion that occurs when an internal corner is encountered. This is achieved by either slotting out the corners before the standard toolpath is initiated or by following curvilinear toolpaths to maintain near constant immersion. Stability lobe theory demonstrates that with the controlled immersion an increase in axial depth of cut can be achieved thereby improving both tool life and productivity. The experimental results are supported through simulation using Third Wave Systems Productivity module demonstrating that the new toolpaths see reduced loading throughout the pocket with minor increase in cycle time. The results supported the hypothesis leading to the following conclusions:

- Toolpaths can be generated that enhance that tool life through controlling a constant radial immersion.
- Through maintaining a constant radial immersion a larger axial depth of cut and metal removal rate can be achieved, optimising productivity.

The second part of chapter 3 investigates the application of the technique to a range of aerospace pockets. A range of pockets were selected by Sandvik Coromant to represent typical titanium pockets encountered within the aerospace industry. A number of strategies were defined by the author for each pocket, comparing the strategies developed within the first part of chapter 3 with more established pocket roughing techniques. A range of the successful strategies are presented in chapter 3 and most combine some roughing or semi-roughing with solid carbide end mills following curvi-linear toolpaths with heavy roughing using large diameter long edge indexable cutters. The long edge cutters produce the greatest MRR providing there is

sufficient stock to remove and sufficient machine tool stability. In the cases of unstable machine tools or set-ups the solid carbide roughing techniques are recommended. The toolpaths derived here are now used by Sandvik Coromant to train their aerospace application engineers globally and are currently accepted as Sandvik Coromant best practice for titanium pocket milling [8].

7.3 Special Tool Geometries

Chapter 4 investigates the application of stability lobe theory to titanium milling applications and explores the benefits of special form cutting tools to increase stability within a desired operational range. Non-linearities in modern machine tool dynamics are identified as a problem for the application of traditional stability lobe theory to titanium milling along with the limited surface speed range available. The performance of standard, variable pitch and variable helix end mills are explored experimentally after first defining a spindle speed range for which the machine tool in question showed a linear dynamic response, maintaining the frequency response as measured in the static condition.

The hypothesis developed in chapter 2 proposed that variable helix end mills would offer an improvement in performance over standard end mills through enhanced stability and that the performance may be modelled and controlled. An analytical model is developed within the thesis founded upon the stability theory of variable pitch end mills whereby the average pitch of each flute can be calculated and the stability of the process determined as a result of the phasing of each tooth pitch and the chatter frequency. The analytical model developed here is compared against a fully kinematic established time domain model developed by Altintas at UBC [74], refined by Merdol to incorporate variable helix end mills. The results of the two models are compared against the experimental results for a range of end mills and cutting conditions [163].

The experimental results show that the variable helix end mills behave in a similar manner to variable pitch for small changes in helix and pitch angle. In the case of VH4, the combination of large differentials in pitch and helix demonstrated greatly enhanced stability, the variable helix end mill outperforming the variable pitch end mill and standard end mill by a factor of 20. These results clearly support the first part of the hypothesis that variable helix end mills can result in significant productivity

gains through enhanced chatter stability. The conditions under which these benefits occur require large differentials in helix and pitch angles. The effect is greatest for profiling operations where a greater portion of the flute length may be engaged thereby introducing a greater range of phases into the cutting process.

The analytical results show good correlation with the time domain model and with the experimental results for the variable helix end mills with smaller differentials in helix angle, where the variable helix end mills behaved predictably like variable pitch end mills and the average pitch feedback loop gave good lobe positions. Both the analytical and time domain results failed to predict the enhanced stability demonstrated with tool VH4. With regards to the second part of the hypothesis, it has been demonstrated that variable helix end mills can be modelled under conditions of shallow axial depth of cut where they behave like variable pitch end mills, but no model has been created that accurately predicts the enhanced stability demonstrated by tool VH4 with exaggerated helix and pitch differentials.

The time domain model represents the full kinematics of the milling process yet fails to represent the mechanism by which the enhanced stability of variable helix end mills is realised. This leads to the theory that the stability mechanism is non-linear, the stability and depths of cut demonstrated by VH4 were greater than the maximum depth of cut in a lobe and could not therefore be modelled through manipulation of the chatter phases. It seems likely that the stability is increased as a greater range of stable phases are engaged in the cut. If the tool is represented in discrete slices each tooth on each slice will have a phase that tends towards stability or instability through traditional bifurcation theory. The tool that demonstrated the greatest stability had the most extreme range of these phases as a result of a broad range in helix angles, pitch angles and a large axial depth of cut, resulting in a greater number of discrete layers with a broader range of phases. Traditional stability lobe theory as applied within the analytical model developed here would state that unstable phases tend towards chatter and a stable phase would have a neutral effect. If this is indeed the case then the tool with the greatest range of phase angles should result in the poorest stability. However the tool with the greatest range of chatter phase angles results in the greatest stability. This puts an onus on the introduction of further stable phases. If this is the case the influence of a stable phase angle cannot be neutral and there must be some mechanism by which a stable phase angle inhibits the chatter initiated by an unstable phase at some other point in the cut. This would be highly non-linear and could be

explained by process damping, that is to say that the stable portions of the cut result in sufficient damping to suppress the unstable portions of the cut. This theory is supported by the results in the case study where Fig. 6.14 shows a profile cut with a variable helix end mill where at some portions of the flute length the cutter appears to be unstable whilst the majority of the cut is stable. This hypothesis will be covered in the further work section.

In conclusion the hypothesis that variable helix tools offer enhanced stability and performance and can be modelled has been supported in part, although no accurate model has been presented here for all scenarios. The following summary points are drawn from chapter 4:

- The Dynamic behaviour of machine tools is not always linear. This is demonstrated with an empirical lobe validation on a Makino A99 at the AMRC. At a certain spindle speed range the machine dynamics change and render the stability lobes based upon the static FRF invalid.
- The non-linearities make traditional stability lobes unreliable and mean that alternative techniques for enhancing cutter stability must be sought.
- Special tool design and process damping are two techniques that can be employed to enhance stability. Although knowledge of the system dynamics is required these techniques are not as sensitive to changes in the dynamics as traditional stability lobe theory.
- Variable helix end mills can vastly outperform variable pitch end mills when certain helix and pitch variation at tool tip are combined.
- A frequency domain model has been presented that shows in certain cases variable helix tools behave like variable pitch tools and their stability can be accurately predicted.
- In certain instances variable helix tools have high stability that is not represented within established time domain models and cannot be represented with a conventional frequency domain approach.
- The enhanced stability of variable helix end mills is likely to be caused through some non-linearity in the milling process such as process damping as this is neglected in the time domain model which otherwise represents the full kinematics of the milling process.

7.4 Process Damping

Chapter 5 investigates the phenomenon of process damping and seeks a method for measuring and controlling the process damping performance of a cutting tool and material combination. A procedure is presented for establishing the critical process damping wavelength and it is demonstrated that this value is dependant upon chip thickness. An experimental matrix is presented with a range of rake and relief angles with each tool tested at 3 feed rates. The variable with the strongest influence on the process damping wavelength is the feed per tooth with the rake and relief angles studied showing little influence. There was some increase in process damping performance with an increase in rake angle but this was negligible with relation to the influence of feed per tooth. The established theory states that relief angle has a strong influence on process damping performance. This was not evident from the first round of experiments so the tests were repeated with a broader range of rake and relief angles using the same experimental set-up. The tool parameters comprised of a two factor three level full factorial design of experiment with rake and relief angles of 0°, 6° and 12°. Two tools were run for each set of parameters and a Third Wave Systems FE model was run to study the predicted cutting forces and strain around the cutting zone. Cutting force coefficients were also measured for each tool taking 4 feed per tooth values to plot the curves. The cutting force coefficients determine the amount of force generated for a given cut and this is computed by plotting the feed and normal forces against a range of feed rates. The cutting force coefficients were shown to be linear for the range of feed per tooth studied, thereby discounting the possibility that process damping performance is improved at high feeds due to a decrease in cutting force coefficients. It is likely that the increase in process damping performance with increased feed is related to an increase in amplitude of the waveform traced by the tool, thereby increasing the gradient of the waveform and increasing the interference between relief face and workpiece. Reducing the surface speed has a similar and better understood effect upon process damping whereby for a given frequency of excitation as the surface speed is decreased the wavelength reduces and the gradient of the waveform becomes steeper increasing the process damping effect.

One other possible reason for the influence of feed per tooth on process damping comes from the resultant force on the rake face of the tool, as the chip increases in width the resultant force pushing the edge of the tool back into the workpiece

becomes greater. The second set of cutting trials and the Third Wave modelling both supported the argument that rake angle plays a significant role in process damping performance. The best results were seen with a high rake angle and for non zero values the rake had a stronger influence than the relief. In the case of the zero relief tools no chatter could be induced, but as surface speeds were increased build up soon occurred on the relief face resulting in high forces and temperatures as the tool rubbed rather than cut the workpiece. Zero relief tools are not a practical option although variants on zero relief may be effective such as eccentric cam reliefs. For all other positive values of relief angle there was little notable effect. There was a clear trend in improved performance with higher rake angle and the Third Wave simulation predicted high strain in the workpiece around and behind the cutting edge. This would support the theory that with highly positive rake angles the resultant force of the chip on the rake face pushes the edge of the tool back into the workpiece causing a greater rubbing effect. One factor that must be important is the edge condition and this was taken as a constant for all experiments. The edge condition was not measured and in some cases tools of identical geometry gave quite different results, it is possible that this was due to difference in edge condition. If such results occurred tests were repeated with new tools until two tools of the same geometry gave comparable results. In summary the hypothesis is validated and the following conclusions have been drawn:

- Process damping is highly non-linear and acts beyond the boundary of stability rather than influencing the cutting force coefficients that control the boundary.
- Feed per tooth is a key variable acting upon process damping performance.
- The influence of feed per tooth is not related to cutting force coefficients and is most likely related to the increase in amplitude of the vibration and equivalent increase in slope, and the resultant force of the chip sliding on the rake face pushing the tool back into the cut surface.
- An experimental procedure has been described for evaluating the process damping performance of a cutting tool for a range of feed rates.
- There is a possible interaction with edge radius. This would follow the theory that the rubbing occurs near to the tool edge and can be enhanced when the edge is pushed into contact with the cut surface due to a high resultant force on the rake face.

- There is a trend in improved process damping performance with an increase in rake angle. This may be due to the resultant force of the chip on the rake face pushing the tool edge into the cut material.

The second stage of chapter 5 used the findings from the initial experimental analysis and applied them to determine optimum cutting conditions for solid carbide tools. A theory is presented based upon established stability lobe theory and the process damping theory developed within this thesis. The tool tip FRF may be manipulated through selection of tool diameter, tool length from the face of the toolholder and toolholder selection. Through introduction of flexible tool modes the lower frequency spindle modes can be attenuated and moved into the positive part of the real FRF, thus according to the stability lobe theory described in chapter 2 rendering them stable and unable to initiate chatter. Further manipulation can be used to ensure that the first dominant tool mode is of high frequency and is the first negative mode in the tool tip FRF that can cause chatter. Through optimisation of the process damping wavelength this mode may be process damped whilst no other lower frequency modes can cause chatter as they have no negative real part. If the first tool mode is sufficiently high frequency and the process damping wavelength is optimised then the cutting tools can be chatter free for all practical surface speed and depth of cut ranges, effectively eliminating chatter as a problem and the critical constraint on the process once again becomes tool wear. The following conclusion can now be drawn:

- It has been demonstrated that through manipulation of the cutting tool and spindle dynamics for semi-finishing end mills, chatter can be eliminated from the operational spindle speed range.

7.5 Further Work

The hypotheses outlined in chapter 2 have been validated within this thesis although areas for further work have been identified. In the case of the toolpath strategies to demonstrate improved tool life and MRR, further work into the mechanisms by which increased radial immersion causes excessive tool wear may lead to further breakthroughs in enhancing tool life. Adoption of curvilinear toolpath techniques within leading CAM suppliers would broaden the application of the toolpaths proposed here.

The variable helix study clearly demonstrated that variable helix end mills under certain conditions behave like variable pitch end mills and can be modelled and controlled but to no great advantage over variable pitch. It was also demonstrated that for large variation in pitch and helix that a variable helix cutter can offer greatly enhanced stability over variable pitch and standard end mills. The analytical model developed here failed to predict this enhanced performance as did a well established fully kinematic time domain simulation. Further investigation is required into the mechanisms by which a variable helix cutter inhibits chatter. The fact that the time domain model could not predict the stability indicates that this is not a result of established stability theory. This leads to possibility that some non-linearity such as process damping plays a significant role as this is not included in the time domain model and would explain why portions of the tool length can be in stable and unstable phasing at the same instant whilst chatter is not able to grow to high amplitude. It is proposed that the stable phasing and regions along the flute length experience a degree of process damping that inhibits chatter growth along the unstable portions. The photograph from the case study at Messier Dowty supports this theory as stable and unstable bands can be seen along the side of the workpiece where a single pass has been taken, clearly near to the limit of stability for the tool but some non-linearity is preventing the chatter in the unstable phasing from fully taking a hold of the process.

This hypothesis has been developed within the thesis but not validated and further work is required to understand and model the stability of variable helix end mills. If the stability can be controlled then great gains can be made in productivity of titanium milling.

The experimental study into the key variables influencing process damping in chapter 5 highlighted the strong influence of feed per tooth on process damping performance. The methodology for determining the process damping wavelength can be readily applied to a milling setup but requires chatter to be recorded in order to determine λc. Further modelling of the process damping phenomenon is essential and will lead to greater understanding and manipulation of the key variables. The study into tool geometries surprisingly showed a strong influence for rake angles and this is a subject that could further be studied through simulation, leading to optimum tool design. One aspect of tool geometries that was not studied but identified as a possible key variable is tool edge radius. It is recommended that further work be undertaken on this subject

to understand and control the effects of edge condition on process damping. If all these variables can be simulated then optimum tool geometries can be defined and λc can be predicted and applied to the technique demonstrated in the second part of chapter 5 to optimise milling performance.

7.6 Summary

This thesis identifies that there is a perceived lack of understanding about the strategies for milling of titanium and optimisation of titanium milling processes. Whilst there is much published work on tool wear, tool geometries and grades there is little research combining these fields with research into chatter during titanium milling and milling strategies to optimise productivity.

After a review of the literature three novel areas are identified as opportunities for further development from which three strands of the research question are formed. The findings for each of the three core chapters are demonstrated in practice on a titanium aerospace component in a production environment. Through successful application of pocketing strategies, variable helix tools and process damping a titanium 5-5-5-3 landing gear part was machined at 50% of target cost.

In conclusion this thesis contributes to the field of research through;

- demonstrating the importance of radial immersion in titanium milling operations and a means of controlling it,
- developing a model demonstrating that under certain conditions variable helix end mills behave as variable pitch end mills whilst demonstrating experimentally that under certain conditions variable helix tools greatly outperform standard helix tools,
- demonstrating that process damping performance can be controlled and manipulated to enhance cutting performance and productivity.

Bibliography

1. Fersing, L. and D.N. Smith, *Machinability research with J&L tool dynamometer on Titanium 150A.* ASME paper No. 53-A-207, 1953.

2. Zlatin, N. and M. Field, *Procedures and precautions in machining titanium alloys.* Titanium science and technology- Volume 1, Ed. Jaffee R.I. and Burke H.M., Massachusetts Institute of Technology, 1973: p. 489-503.

3. Konig, W., *Applied research on the machinability of titanium and its alloys.* Proceedings of the 47th Meeting on AGARD Structural and Materials Panel, CP256, 1978: p. 1.1-1.10.

4. Smith, S. and J. Tlusty, *Current trends in high-speed machining.* Transactions of the ASME, 1997. **119**: p. 664-666.

5. Smith, S. and D. Dvorak, *Tool path strategies for high speed milling aluminum workpieces with thin webs.* Mechatronics, 1998. **8**(4): p. 291-300.

6. Tlusty, J., *A method of analysis of machine tool stability.* Proceedings of the 6th MTDR Conference, 1965: p. 5-14.

7. Tobias, S.A., *Machine Tool Vibration.* First ed. 1965: Blackie and Son, Glasgow.

8. Coromant, S., *Application Guide, Titanium Machining,.* 2004, Sandviken: Sandvik Coromant. 119.

9. Wright, P.K. and A. Bagchi, *Wear mechanisms that dominate tool life in machining.* Journal of Applied Metal Working, 1981. **1**(4): p. 15-23.

10. Shaw, M.C., *Metal cutting principles.* 1996: Clarendon Press Oxford.

11. Venuvinod, P.K., W.S. Lau, and C. Rubenstein, *The role of discrete contact at the flank wear land in determining cutting tool temperature in orthogonal cutting.* International Journal of Machine Tool Manufacture, 1983. **29**(4): p. 245-261.

12. Bhattacharyya, S.K., A. Jawaid, and J. Wallbank, *Wear of syalon tooling in the high speed machining of aerospace materials.* Trans. ASME Production Engineering Division, 1984. **12**: p. 245-262.

13. Dearnley, P.A. and N.A. Grearson, *Evaluation of principal wear mechanisms of cemented carbides and ceramics used for machining titanium alloys IMI 318.* Materials Science and Technology, 1986. **2**: p. 47-58.

14. Hoshi, T. and K. Okushima, *Optimum diameter and positions of a fly cutter for milling steel at light cuts.* Trans. ASME Journal of Engineering for Industry, 1965. **87**: p. 442.

15. Wright, P.K. and A. Bagchi, Proceedings of the 8th North American Manufacturing Research Conference, 1980. **8**: p. 277-284.

16. Zorev, N.N., *Interrelationship between shear processes occurring along tool face and on shear plane in metal cutting.* Trans. ASME International Research in Production Engineering, New York, 1963. **42**.

17. Chanrasekaran, h., *Thermal fatigue studies on tool carbides and its relevance of milling cutters,.* CIRP Ann., 1985. **34**(1): p. 125-128.

18. Wright, P.K. and E.M. Trent, *Metallographic methods of determining temperature gradients in cutting tools.* Journal of Iron and Steel Institute, 1973. **211**: p. 364-386.

19. Kramer, B.M., *On the materials for high-speed machining.* Trans. ASME Production Engineering Division, 1983. **12**: p. 127-140.

20. Kramer, B.M., *On the tools for high-speed machining.* Trans. ASME Journal of Engineering for Industry, 1987. **109**: p. 87-91.

21. Tlusty, G., *Manufacturing Processes And Equipment.* 1 ed. 2000: Prentice Hall, Inc.

22. Tonshoff, H.K. and S. Bartsch, *Wear mechanisms of ceramic cutting tools.* Ceramic Bulletin, 1988. **67**(6): p. 1020-1025.

23. Suh, N.P., *New theories of wear and their implications for tool materials.* Wear, 1980. **62**: p. 1-20.

24. Merchant, M.E., *Mechanics of the metal cutting process II: Plasticity conditions in orthogonal cutting.* Journal of Applied Physics, 1945. **16**: p. 318-324.

25. Alberti, N., et al., *Effects of the fracture, chipping and wear of cemented carbide tools on the determination of the optimum metal cutting conditions.* CIRP Ann., 1980. **30**: p. 67-69.

26. Trent, M.E. and P.K. Wright, *Metal Cutting, 4th Edition.* 2000.

27. Siekmann, H.J., *How to machine titanium.* Tool Engineer, 1955: p. 78-82.

28. Eckstein, M., G. Lebkuchner, and D. Blum, *End milling of titanium alloys using high cutting speeds, Part 2: Finish machining.* VDI-Z (Translation), 1992. **134**(6).

29. Barnet-Ritcey, D., R. Hachmoller, and M.A. Elbestawi. *Milling of titanium alloy using directed through spindle coolant.* in *NAMRI/SME.* 2001.

30. Trigger, K.J., *Progress Report No.2 on ATool chip interface temperatures.* Transactions of .ASME, 1949. **71**: p. 163-174.

31. Loewen, E.G. and M.C. Shaw, *On the Analysis of Cutting Tool Temperatures.* Transactions of the ASME, 1953: p. 217-231.

32. Komanduri, R., *Some clarifications of the machanics of chip formation when machining titanium alloys.* Wear, 1982a. **76**: p. 15-43.

33. Komanduri, R., *Further work on chip formation characteristicswhen machining titanium alloys, Annual Technical Report on 'Advanced Machining Research Program (AMRP).* by the General Electric Company, Corporate Research and Development, Schenectady, NY, to the Defense Advanced Research Project Agency, 1982c: p. 11-3 to 11-47.

34. Ashiura, Y. and H. Motonishi, *Titanium Processing Technology I. Machining.* Titanium Zirconium 1987. **35**(3): p. 131-141.

35. Tlusty, J., *High-speed machining.* Ann. CIRP, 1993. **42**: p. 733-738.

36. Maekawa, K., I. Oshima, and I. Nakano, *High-speed end milling of Ti-6Al-6V-2Sn titanium alloy, in Advancement of Intelligent Produciton.* Ed. Usui, E., Elsevier Science B.V. / The Japan Society for Precision Engineering, Amsterdam, 1994: p. 431-436.

37. Palmai, Z., *Cutting temperatures in intermittent cutting.* International Journal of Machine Tools and Manufacture, 1987. **27**: p. 261-274.

38. Salomon, C., *Process for machining metals of similar acting materials when being worked by cutting tools*, G.P. Office, Editor. 1931: Germany.

39. Hartung, P.D. and B.M. Kramer, *Tool wear in titanium machining.* CIRP Ann., 1982. **31**(1): p. 5-80.

40. Smart and Trent, *Temperature distribution in tools used for cutting iron, titanium and nickel.* International Journal of Production Research, 1975. **13**(3): p. 265-290.

41. Jensen, J.T., *High speed milling of titanium.* 1983: MIT.

42. Chao, B.T. and K.J. Trigger, *Cutting temperatures and metal cutting phenomena.* ASME Paper No.50-A-43, 1950.

43. Stephenson, D.A., *Assessment of Steady State Metal Cutting Temperature Models Based upon Simultaneous Infrared and Thermocouple Data.* Journal of Engineering for Industry, 1991. **113**: p. 121-128.

44. Vaughan, R.L. and L.J. Quackenbush, *The high speed milling of titanium alloys.* ASME Technical Paper 1966: p. 66-151.

45. Tyler, P., *High Speed Milling of Titanium*, in *Dept of Mechanical Engineering.* 2000, The University of Sheffield: Sheffield.

46. Cook, N.H., *Visual Study of the Machining of Titanium.* 1953, MIT Metal Cutting Lab.

47. Brown, C.J. and B.K. Hinds, *Force and temperature effects when machining titanium.* Manufacturing Engineers Transactions, 1985: p. 238-244.

48. Loladze, *Wear of cutting tools.* 1958, Mashqiz, Moscow.

49. Ernst, H., *Physics of Metal Cutting.* Machining of Metals 1938: American Society for Materials.

50. Merchant, M.E., *Mechanics of the Metal Cutting Process. I. Orthogonal Cutting and a Type 2 Chip.* Jounal of Applied Physics, 1945. **6**(15): p. 267-275.

51. Von Turkovitch, B.F., *Shear stress in metal cutting.* ASME Jnl of Engineering for Industry, 1970. **92**(1): p. 151-157.

52. Turley, D.M., *Slow Speed Machining of Titanium.* 1981, Materials Research Labs Ascot Vale (Australia): Melbourne. p. 35.

53. Machado, I.R. and J. Wallbank, *Machining of titanium and it's alloys- a review.* Proc. Institute of Mechanical Engineers, 1990. **204**: p. 53-59.

54. Edwards, R., *Cutting Tools.* First ed. 1993: Institute of Materials.

55. Katayama, S. and T. Imai, *Effects of Tool Materials on Tool Damage When Machining Titanium Alloys.* Trans. Iron Steel Inst. Japan, 1986. **26**(10): p. 329.

56. Komanduri, R. and W.R. Reed, *Evaluation of carbide grades and a new cutting geometry for machining titanium alloys.* Wear, 1983. **92**: p. 113-123.

57. Von Turkovitch, B.F. and D.R. Durham, *Machining of titanium and its alloys.* Proceedings of a symposium on Advanced Processing Methods for Titanium, 1981: p. 257-274.

58. Kneisel, T. and H.J. Illgner, *High speed machiing of difficult-to-cut materials, in High speed machining.* Verlag Munchen-Wien, 1996: p. 59-70.

59. Klocke, F. and S. Hoppe, *Mechanisms of chip formation in high speed cutting.* Scientific Fundamentals of High Speed Cutting, ed. H. Schulz. 2001, Munich: Drukhaus.

60. Hughes, J.I., A.R.C. Sharman, and K. RIdgway, *The effect of tool edge preparation on tool life and workpiece surface integrity.* Proc. Institute of Mechanical Engineers Journal of Engineering Manufacture, 2004. **218**(9): p. 1113-1123.

61. Perez-Bilbatua, J., et al., *Conventional and high speed machining of titanium alloys.* Informacion Technologica, 1997. **8**(2): p. 43-49.

62. Koenigsberger, F.S., A.J.P., *An Investigation into the cutting force pulsations during milling operations.* International Journal of Machine Tools Design and Research, 1961. **1**: p. 15-33.

63. Andrew, C. and S.A. Tobias, *A critical comparison of two current theories of machine tool chatter.* Internationjal Journal of Machine Tool Design & Research, 1961. **1**: p. 325-335.

64. Taylor, F.W., *On the art of cutting metals.* Trans. ASME, 1907. **28**: p. 31-350.

65. Arnold, R.N., *The mechanism of tool vibration in cutting of steel.* Proc. Inst. Mech. Eng., 1946. **154**: p. 261-284.

66. Hahn, R.S., *Metal-cutting chatter and its elimination.* Trans. ASME, 1953. **75**: p. 1073-1080.

67. Tlusty, G., *Analysis of the state of research in cutting dynamics.* Ann CIRP, 1978. **27**: p. 583-589.

68. Tobias, S.A. and W. Fishwick, *Theory of Regenerative Machine Tool Chatter.* The Engineer, 1958: p. 199-203.

69. Tobias, S.A. and W. Fishwick, *Theory of Regenerative Machine Tool Chatter (II).* The Engineer, 1958: p. 238-239.

70. Tlusty, J., *Analysis of state of research in cutting dynamics.* Ann. CIRP, 1978. **27**: p. 583-589.

71. Tlusty, J. and F. Ismael, *Special aspects of chatter in milling.* ASME, Journal of Mechanical Design, 1981: p. 1-9.

72. Merritt, H.E., *Theory of self-excited machine-tool chatter.* Trans. ASME J. Eng. Ind., 1965. **87**: p. 447-454.

73. Smith, S. and J. Tlusty, *Efficient simulation programs for chatter in milling.* CIRP Annals, 1993. **32**: p. 463-466.

74. Montgomery, D. and Y. Altintas, *Mechanism of Cutting Force and Surface Generation in Dynamic Milling.* trans. ASME J. Eng for Ind, 1991. **113**: p. 160-168.

75. Albrecht, P., *Dynamics of the metal cutting process.* Trans ASME, J. Eng. For Ind., 1965: p. 429.

76. Tlusty, J., *Dynamics of high-speed milling.* J. Eng. Ind., 1986. **108**: p. 59-67.

77. Opitz, H., *Investigation and calculation of the chatter behaviour of: Lathes and milling machines.* CIRP Ann. , 1969. **18**: p. 335-342.

78. Sridhar, R., R.E. Hohn, and G.W. Long, *A stability algorithm for the general milling process.* Journal of Engineering for Industry, Trans. ASME, 1968: p. 330-334.

79. Sridhar, R., R.E. Hohn, and G.W. Long, *A general formulation of the milling process equation.* Journal of Engineering for Industry, Trans. ASME, 1968: p. 317-324.

80. Minis, I. and R. Yanushevsky, *A new theoretical approach for the prediction of chatter in milling.* J. Eng. Ind., 1993. **115**: p. 1-8.

81. Altintas, Y. and E. Budak, *Analytical prediction of stability lobes in milling.* CIRP Annals, 1995. **44**(1): p. 357-362.

82. Insperger, T., et al., *Stability of up milling and down milling, Part I: Alternative analytical methods.* Intl. J. Machine Tools and Manufacture, 2003. **43**: p. 25-34.

83. Bayly, P.V., et al., *Stability of interrupted cutting by temporal finite element analysis.* ASME Journal of Manufacturing Science and Engineering, 2003. **125**: p. 220-225.

84. Merdol, D. and Y. Altintas, *Multi Frequency Solution of Chatter Stability for Low Immersion Milling.* ASME Journal . Manufacture, Science and Engineering, 2004. **126**(3): p. 459-467.

85. Altintas, Y. and P. Lee, *A general mechanics and dynamics model for helical end mills.* CIRP Annals, 1996. **45**(1): p. 59-64.

86. Davies, M., et al., *The stability of low radial immersion milling.* CIRP Annals- Manufacturing Technology, 2000. **49**(1): p. 37-40.

87. Davies, M., et al., *Stability prediction for low radial immersion milling.* Journal of Manufacturing Science and Industry, 2002. **124**: p. 1-9.

88. Insperger, T. and G. Stepan, *Stability of the Milling Process.* Periodica Polytechnica-Mechanical Engineering, 2000. **50**(2): p. 47-57.

89. Bayly, P.V., M.T. Lamar, and S.G. Calvert, *Low-frequency regenerative vibration and the formation of lobed holes in drilling.*

ASME Journal of Manufacturing Science and Engineering, 2002. **124**: p. 275-285.

90. Ismail, F. and V.R. Vadari, *Machining chatter of end mills with unequal modes.* Journal of Engineering for Industry, 1990. **112**: p. 229-235.

91. Slavicek, J., *The effect of irregular tooth pitch on stability of milling.* Proceedings of the 6th MTDR Conference, 1965: p. 15-22.

92. Vanherck, P. *Increasing milling machine productivity by the use of cutters with non-constant cutting-edge pitch.* in *Proceedings of the 8th MTDR Conference.* 1967. Manchester: Pergamon Press.

93. Varterasian, J.H., *White Noise; a deterrent to milling cutter chatter.* Manufacturing Engineering and Management, 1971.

94. Stone, B.J., *The effect on chatter behaviour on machine tools of cutters with different helix angles on adjacent teeth.* Proceedings of the 11th International MTDR Conference, 1970: p. 169-180.

95. Tlusty, G., F. Ismael, and W. Zaton, ***Use of Special Milling Cutters Against Chatter.*** **NAMRC 11 University of Wisconsin - Madison, SME,** 1983: p. 408-415.

96. Campomanes, M.L. and Y. Altintas, *An Improved Time Domain Solution for Dynamic Milling at Small Radial Immersions.* trans ASME, Manufacturing and Engineering and Science, 2003. **125**: p. 416-422.

97. Smith, S. and J. Tlusty, *An overview of modeling and simulation of the milling process.* Journal of Engineering for Industry, 1991. **113**: p. pp.169-175.

98. Altintas, Y., D. Montgomery, and E. Budak, *Dynamic peripheral milling of flexible structures.* Journal of Engineering for Industry, 1992. **114**: p. 137-145.

99. Altintas, Y. and M. Weck, *Chatter Stability of Metal Cutting and Grinding.* CIRP Ann. Manuf. Tech., 2004. **53**: p. 619-642.

100. Smith, S. and J. Tlusty, *Update on high-speed milling dynamics (1990).* Trans. ASME J. Eng. Ind., 1990. **112**: p. 142-149.

101. Davies, M., et al., *On the dynamics of high speed milling with long slender endmills.* CIRP Annals, 1998. **47**(1): p. 55-60.

102. Wu, *A New Approach of Formulating the Transfer Function for Dynamic Cutting Processes.* Journal of Engineering for Industry, 1989. **111**: p. 37-47.

103. Elbestawi, M.A., et al., *Modelling machining dynamics including damping in the tool-workpiece interface.* Journal of Engineering for Industry, Transactions of the ASME, 1994. **116**(4): p. 435-439.

104. Lee, B.Y., Y.S. Tarng, and S. Ma, *Modeling of the process damping force in chatter vibration.* International Journal of Machine Tools and Manufacture, 1995. **35**(7): p. 951-962.

105. Peters, J., P. Vanherck, and H. Van Brussel, *The measurement of the dynamic cutting coefficient.* CIRP Ann., 1971. **21**(2): p. 129-136.

106. Tlusty, G. and M. Weck, *Report to STC 'Ma' of CIRP: Present state of the cooperative project dynamic cutting coefficients.* Report WZL Aachen, 1978.

107. Smith, S. *Toolholder Interfaces.* in *NCMS 4th Annual Fall Workshop Series.* 2000.

108. Das, M.K. and S.A. Tobias, *The relation between the static and the dynamic cutting of metals.* Int J. MTDR. 7: p. 63-89.

109. Tlusty, G. and S.B. Rao, *Verification and Analysis of some dynamic cutting force coefficient data.* Proc 6th NAMR Conf., U. of Florida, SME., 1978: p. 420-426.

110. Tlusty, G., T. Moriwaki, and B.S. Goel, *The Dynamic Cutting Force Coefficient for Some Carbon Steels.* McMaster University MWRG Report no 76., 1976.

111. Kitaura, S., et al., *Cutting characteristics of carbide end mills.* Kobelco Technology Review 1994. **17**: p. 16-19.

112. Ber, A. and S. Kaldor, *The first seconds of cutting wear behaviour.* CIRP Ann., 1982. **31**(1): p. 13-17.

113. Stutzman, H.J., Talley T., *Frasia Cutter Analysis and Titanium Machining Strategy.* 1997, The Boeing Company: St Louis.

114. Altintas, Y., S. Engin, and E. Budak, *Analytical prediction of chatter stability and design for variable pitch cutters.* Journal of

Manufacturing Science and Engineering, Trans. ASME, 1999. **121**: p. 173-178.

115. Budak, E., *An Analytical Design Method for Milling Cutters with Non-Constant Pitch to Increase Stability, Part I: Theory, Part II; Application.* Trans ASME Journal of Manufacturing Science and Engineering, 2003. **125**: p. 29-38.

116. Smith, S., E. Cheng, and C. Zamudio, *Computer-aided generation of optimum chatter-free pockets.* Journal of Materials Processing Technology,, 1991. **28**(1-2): p. 275-283.

117. Danly, G., *Milling study of titanium helicoptor yoke*, in *Centre for Precision Metrology*. 2000, UNCC: Charlotte.

118. Stephenson, D.A. and A. Ali, *Tool Temperatures in Interrupted Metal Cutting.* Jounal of Engineering for Industry, 1992. **114**: p. 127-136.

119. Carslaw, H.S. and J.C. Jaeger, *Conduction of Heat in Solids*. 1959: Clarendon Press.

120. Smith, S., T.P. Jacobs, and J. Halley, *The effect of drawbar force on metal removal rate in milling.* CIRP Annals - Manufacturing Technology, 1999. **48**(1): p. 293-296.

121. Tlusty, J. and Z. Masood, *Chipping and breakage of carbide tools.* Journal of Engineering for Industry, Trans. ASME, 1978. **100**(4): p. 403-412.

122. Bieterman, M., *Curvilinear Tool Paths for Pocket Machining.* Society of Manufacturing Engineers High Speed Machining Tech Conference, 2002.

123. Altintas, Y. and P.K. Chan, *In-process detection and suppression of chatter in milling.* Int. J. Mach. Tool Manufact., 1992. **32**(3): p. 329-347.

124. Sims, N.D. and Y. Zhang. *Piezoelectric active control for workpiece chatter reduction during milling.* in *Proceedings of SPIE, Smart Structures and Materials 2004: Smart Structures and Integrated Systems.* 2004.

125. Opitz, H., E.U. Dregger, and H. Roese. *Improvement of dynamic stability of the milling process by irregular tooth pitch.* in

Proceedings of the 7th International MTDR Conference. 1966. Manchester: Pergamon Press.

126. Budak, E., *Improving productivity and part quality in milling of titanium based impellers by chatter suppression and force control.* CIRP Annals- Manufacturing Technology, 2000. **49**(1): p. 31-36.

127. Merdol, D. and Y. Altintas, *Mechanics and Dynamics of Serrated and Tapered End Mills.* ASME Jounal of Manufacturing Scinece & Engineering, 2004. **126**(2): p. 317-327.

128. Shirase, K. and Y. Altintas, *Cutting Force and Dimensional Surface Error Generation in Peripheral Milling with Varial Pitch Helical End Mills.* International Journal of Machine Tools and Manufacture, 1996. **36**(5): p. 567-584.

129. Altintas, Y. and S. Engin, *Generalized Modelling of Mechanics and Dynamics of Milling Cutters.* CIRP Ann. Manuf. Tech., 2001. **50**: p. 25-30.

130. Schmitz, T., *Automatic Trimming of Stability lobes.* International Journal of Machine Tools and Manufacture, 2002. **42**(13): p. 1479-1486.

131. Tlusty, J. *Forced vibration, chatter, accuracy, in high speed milling.* in *13th NAMRC, North American Manufacturing Research Conference Proceedings*. 1985. Berkeley, CA.

132. Sims, N.D., *The Self-Excitation Damping Ratio: A Chatter Criterion for Time Domain Milling Simulations.* Journal of Manufacturing Science and Engineering, 2005. **127**(3): p. 433-445.

133. Merdol, D., *Incorporation of variable helix into CutPro time domain engine*, S. Turner, Editor. 2006: Vancouver.

134. Altintas, Y., *Manufacturing Automation.* First ed. 2000: Cambridge University Press.

135. Medicus, K. and T. Schmitz, *Evaluating the Tool Point Dynamic Repeatability for High-Speed Machining Applications.* Proceedings of the 16th Annual ASPE Meeting, Arlington, VA, 2001: p. 357-360.

136. Delio, T., J. Tlusty, and S. Smith, *Use of audio signals for chatter detection and control.* Journal of Engineering for Industry, 1992. **114**(2): p. 146-157.

137. Smith, S. and T. Delio, *Sensor-based chatter detection and avoidance by spindle speed selection.* Journal of Dynamic Systems, Measurement and Control, Trans. ASME, 1992. **114**: p. 486-492.

138. Blum, T. and I. Inasaki, *A study on acoustic emmision from the orthogonal cutting process.* Journal of Engineering for Industry, 1990. **112**: p. 203-211.

139. Liu, M. and S.Y. Liang, *Analytical modeling of acoustic emission for monitoring of peripherical milling process.* International Journal of Machine Tools Manufacture, 1990. **31**(4): p. 589-606.

140. Teti, R. and D.A. Dornfeld, *Modeling and Experimental Analysis of Acoustic Emission from Metal Cutting.* Jounal of Engineering for Industry, 1989. **111**(3): p. 229-237.

141. Wiercigroch, M. and E. Budak, *Sources of nonlinearities, chatter generation and suppression in metal cutting.* Philosophical Transactions of the Royal Society of London, Part A, 2001. **359**: p. 663-693.

142. Moon, F.C. and T. Kalmar-Nagy, *Nonlinear models for complex dynamics in cutting materials.* Philosophical Transactions of the Royal Society of London, Part A, 2001. **359**: p. 695-711.

143. Balachandran, B., *Nonlinear dynamics of milling processes.* Philosophical Transactions of the Royal Society of London, Part A, 2001. **359**: p. 793-819.

144. Tlusty, J. and F. Ismail, *Basic non-linearity in machining chatter.* CIRP Ann. Manuf. Tech., 1981. **30**: p. 299-304.

145. Fiedler, U. and A. Sahn, *An den Grenzen der Hochgeschwindigkeitsbearbeitung- Ein Blick uber den Tellerrand.* 4th International Conference on Metal Cutting and High Speed Machining, 2003.

146. Kamman, *Preload Varies in Spindle Bearings.* American Machinist, 1984: p. 86-88.

147. Tlusty, J., S. Smith, and W.R. Winfough, *Techniques for the use of long slender end mills in high-speed- milling.* CIRP Annals, 1996. **45**(1): p. 393.

148. Agapiou, J., E.I. Rivin, and C. Xie, *Toolholder Spindle Interfaces for CNC Machine Tools.* CIRP Annals, 1995. **44**(1): p. 383-387.

149. Smith, S., et al., *The Effect of Dynamic Consistency in Spindles on Cutting Performance.*

150. Schmitz, T., M. Davies, and M. Kennedy, *Tool point frequency response prediction for high-speed machining by RCSA.* Journal of Manufacturing Science and Engineering, 2002. **123**: p. 1-8.

151. Schmitz, T.L., K. Medicus, and B. Dutterer, *Exploring once-per-revolution audio signal variance as a chatter indicator.* Machining Science and Technology, 2002. **6**(2): p. 215-233.

152. Kerr, D., J. Pengilley, and R. Garwood, *Assessment and visualisation of machine tool wear using computer vision.* International Journal of Advanced Manufacturing Technology, 2006. **28**(7): p. 781-791.

153. Wilcox, S.J., R.L. Reuben, and P. Souquet, *The use of cutting force and acoustic emission signals for the monitoring of tool insert geometry during rough face milling.* International Journal of Machine Tools and Manufacture, 1997. **37**(4): p. 481-494.

154. Smith, S. and W.R. Winfough, *The effect of runout filtering on the identification of chatter in the audio spectrum of milling.* Transactions of NAMRI/SME, 1994. **22**: p. 173-178.

155. Mackerle, J., *Finite- Element analysis and simulation of machining: a bibliography.* Journal of Materials Processing Technology, 1999. **86**: p. 17-44.

156. Marusich, T.D. and M. Ortiz, *Modelling and Simulation of High Speed Machining.* Int. J. Numerical Methods in Engineering, 1995. **38**: p. 3675-3694.

157. Kumbera, T.G., et al., *Numerical simulations of ductile machining of silicon nitride with a cutting tool of defined geometry.* Machining Science and Technology, 2001. **5**(3): p. 341-352.

158. Tlusty, J. and M. Polacek. *The stability of the machine tool against self excited vibration in machining.* in *ASME Proceedings of the Engineering Research Conference.* 1963. Pittsburgh, PA.

159. Wang, M. and Y. Zhang, *Diffusion wear in milling titanium alloys.* Material Science and Technology, 1988. **4**: p. 548-553.

160. Machado, I.R., et al., *Tool performance and chip control when machining Ti-6AL-4V and Inconel 901 using high pressure coolant supply.* Machining Science and Technology, 1998. **2**(1): p. 1-12.

161. Ema, S. and E. Marui, *Suppression of chatter vibration of boring tools using impact dampers.* International Journal of Machine Tools & Manufacture, 2000. **40**: p. 1141-1156.

162. Rivin, E.I., *Interrelation of Stiffness and Damping in Machine Tool Dynamics.* Trans. NAMRI of SME, 2001: p. 137-143.

163. Geng, Z., K. RIdgway, and S. Turner, *Linear Improvement of the Machining Stability Lobes and Application in Milling Process Prediction.* I Mech E Proc. IMechE Journal of Engineering Manufacture, 2007. **221**: p. 369-378.

164. Arrazola, P.J., Garay,A., Iriarte,L.M,Armendia,M.,Marya,S.,Le Maitre,F., *Macinability of titanium alloys (Ti6Al4V and Ti555.3).* Journal of Materials Processing Technology, 2008: p. in print.

165. Degarmo, E.P., J.T. Black, and A.R. Kohser, *Materials and Processes in Manufacturing.* Eighth ed. 1997: Prentice Hall, Inc.

APPENDIX I

Pocket strategies

Strategy 2-1

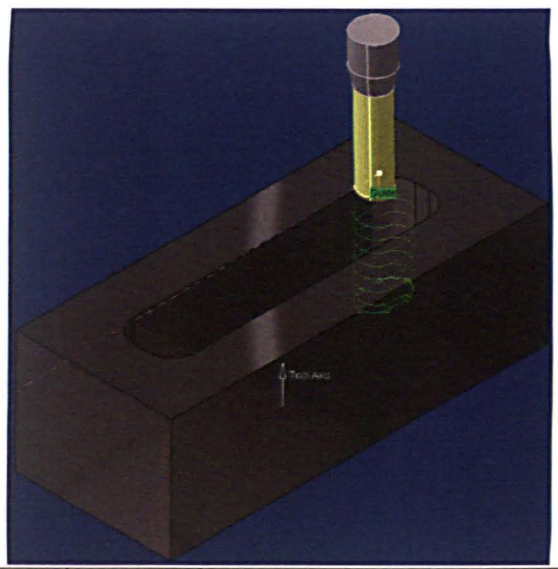

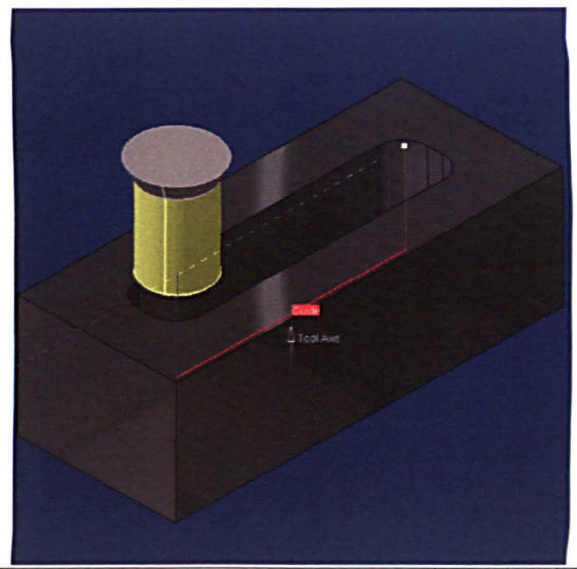

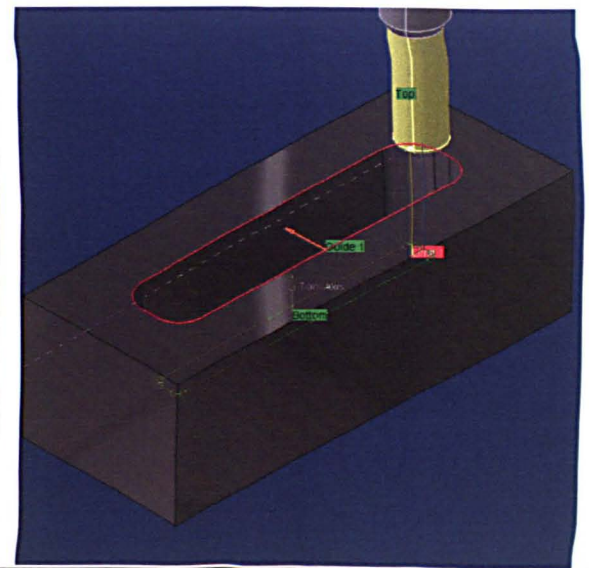

Strategy	Sequence	Tool	Action	D	Z	RPM	Vs (m/min)	Feed	FPT	Ae	Ap	Time
2-1	S10	T13 R216.35-16045-AK50N	Helical interpolation of oval (16mm x 26mm) ramping to depth	16	5	1320	66.35	198	0.03	16	6	225
	S20	T8 R390-032C6-45M	Plunge down pre-drilled hole, slot length of pocket	32	3	596 497.36	59.92 50	214.5 149.21	0.12 0.1	32	40	62 90
	S30	T6 R216.35-20045-AK55N	Run around perimeter of pocket at full depth	20	4	2500	157.08	750	0.075	0.25	40	96
Total Time				383								

Strategy 2-2

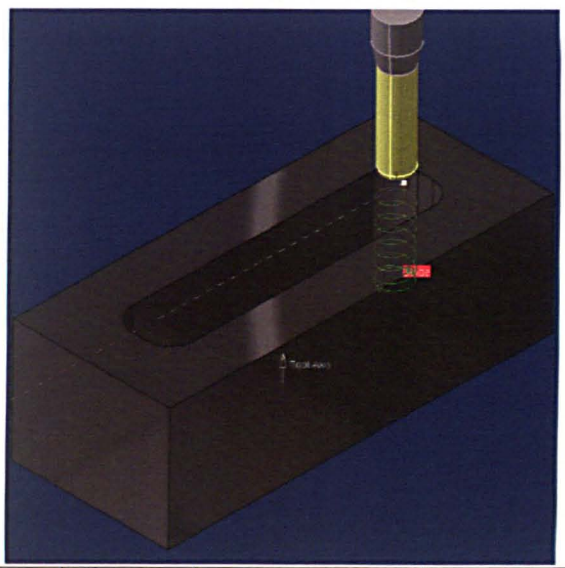

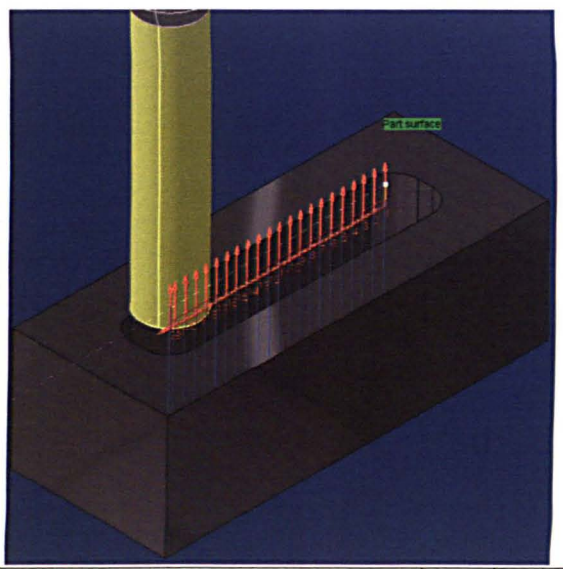

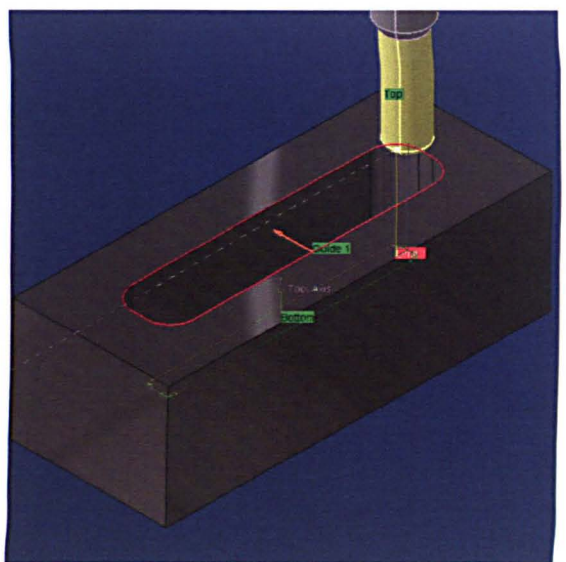

Strategy	Sequence	Tool	Action	D	Z	RPM	Vs (m/min)	Feed	FPT	Ae	Ap	Time
2-2	S10	T13 R216.35-16045-AK50N	Helical ramp to depth (16mm Radius)	16	5	1320	66.35	198	0.03	16	6	126
	S20	T10 R390-030A25L-11L	Plunge mill starting from hole	30	2	796 530.5	75.02 50	170 53	0.1 0.05	5.5	40	454 1456
	S30	T6 R216.35-20045-AK55N	Run around perimeter of pocket at full depth	20	4	2500	157.08	750	0.075	0.25	40	96
Total Time				676, 1678								

Strategy 2-3

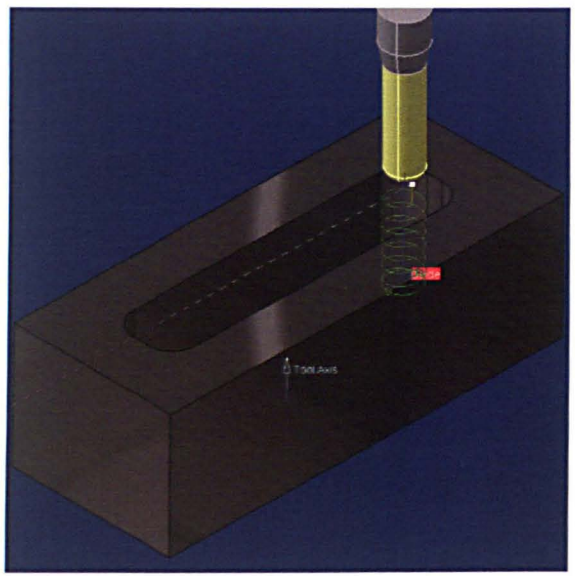

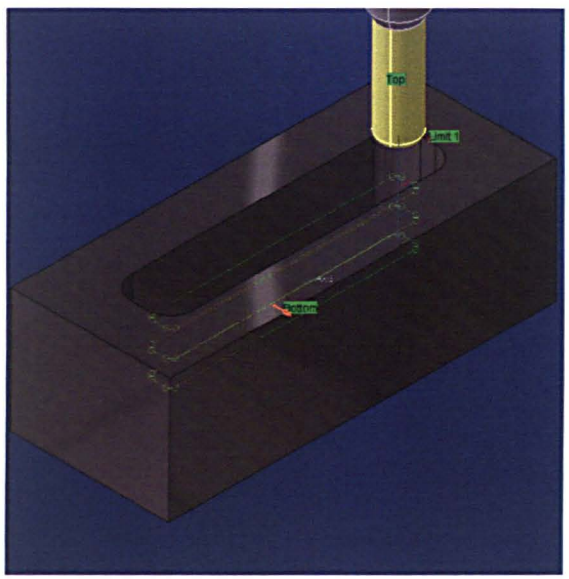

Strategy	Sequence	Tool	Action	D	Z	RPM	Vs (m/min)	Feed	FPT	Ae	Ap	Time
2-3	S10	T13 R216.35-16045-AK50N	Helical ramp to depth (16mm Radius)	16	5	1320	66.35	198	0.03	16	6	126
	S20	T6 R216.35-20045-AK55N	Slot around perimeter of pocket at full depth – slot to finish	20	4	905	56.86	181	0.05	20	13.5	310
Total Time				436								

Strategy 2-4

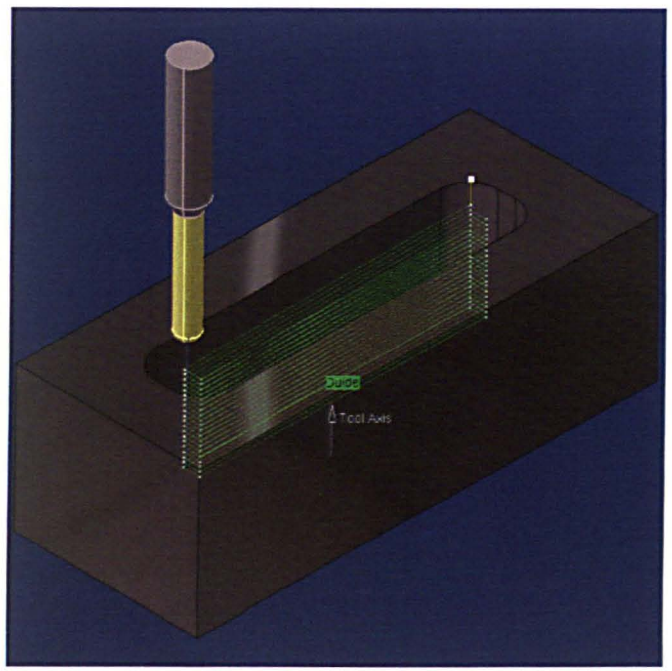

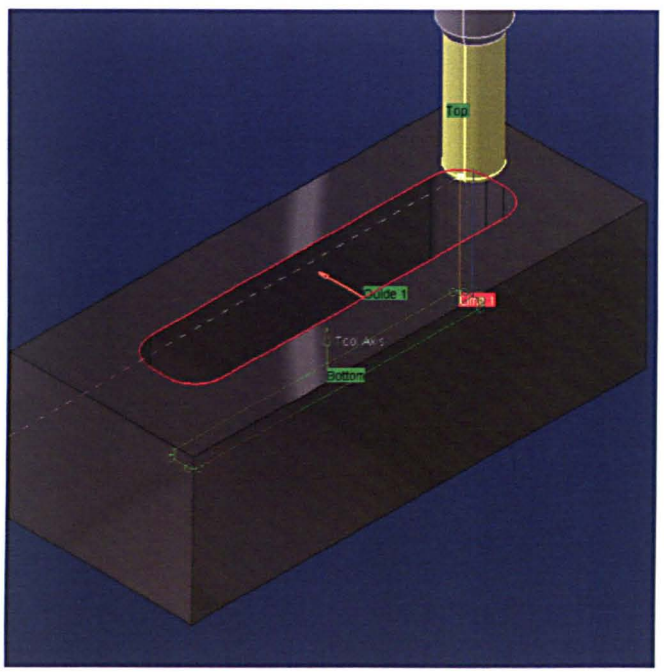

Strategy	Sequence	Tool	Action	D	Z	RPM	Vs (m/min)	Feed	FPT	Ae	Ap	Time
2-4	S10	T12 R300-025A32L-12L	Ramp at 2mm down to depth, continuous ramping on straight sections	25	2	763	59.93	458	0.3	25	2	716
	S20	T6 R216.35-20045-AK55N	Run around perimeter of pocket at full depth	20	4	2500	157.08	750	0.075	0.25	40	96
Total Time				812								

Strategy 2-5

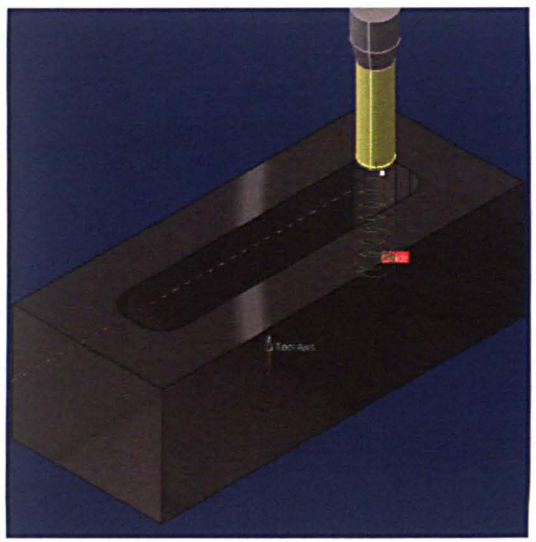

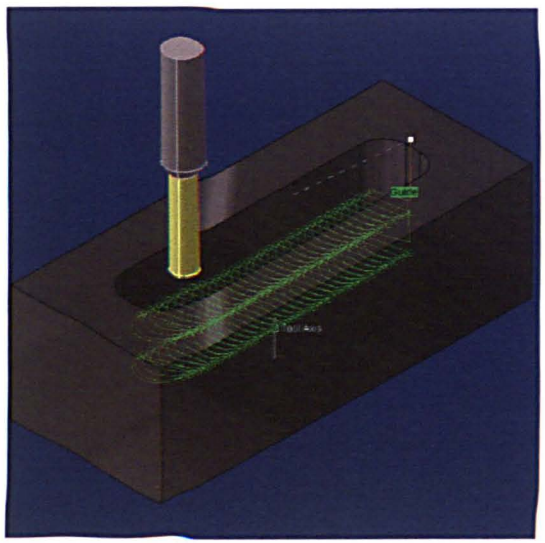

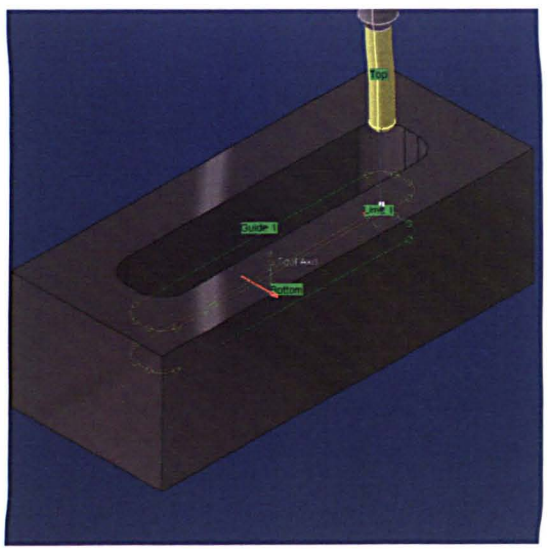

Strategy	Sequence	Tool	Action	D	Z	RPM	Vs (m/min)	Feed	FPT	Ae	Ap	Time
2-5	S10	T13 R216.35-16045-AK50N	Helical ramp to depth (16mm Radius)	16	5	1320	66.35	198	0.03	16	6	126
	S20a	T2 R216.34-10050-AK22P	Trochoidal tool-path to end of pocket	10	4	3180	99.9	512	0.04	4	20	278
	S20b	T2 R216.34-10050-AK22P	Finish perimeter	10	4	3180	99.9	764	0.06	0.5	20	
Total Time				404								

Strategy 3-1

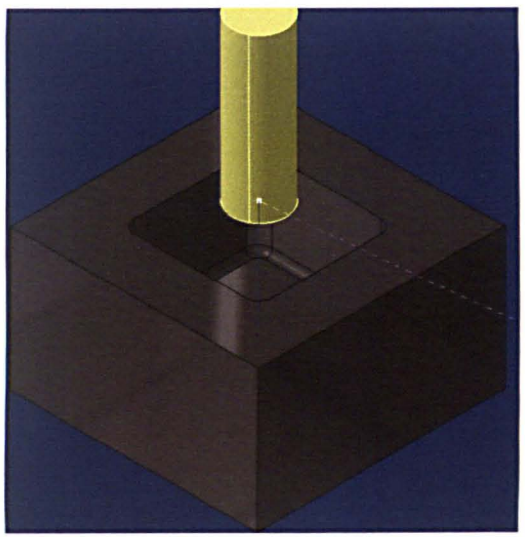

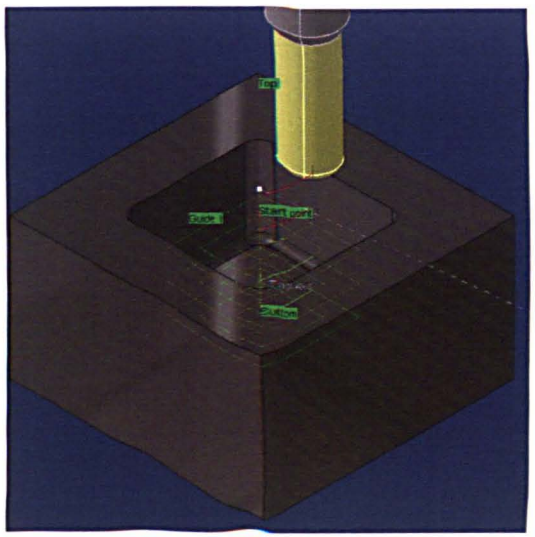

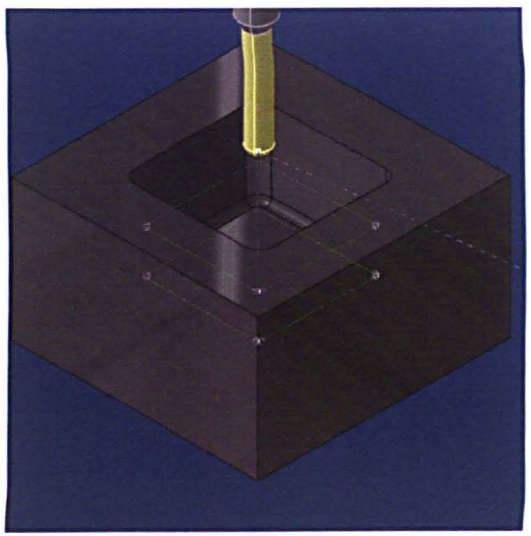

Strategy	Sequence	Tool	Action	D	Z	RPM	Vs (m/min)	Feed	FPT	Ae	Ap	Time
3-1	S10	T11 R416.2-0250L25-31	Drill centre of pocket	25	2	1528	120.01	275	0.09	25	40	15
	S20	T6 R216.35-20045-AK55N	Plunge down pre-drilled hole, slot perimeter of pocket and step-out	20	4	905	56.86	181	0.05	20/8	13.5	375
	S30	T2 R216.34-10050-AK22P	Finish perimeter	10	4	3180	99.9	512	0.04	0.5	20	63
Total Time				453								

Strategy 3-2

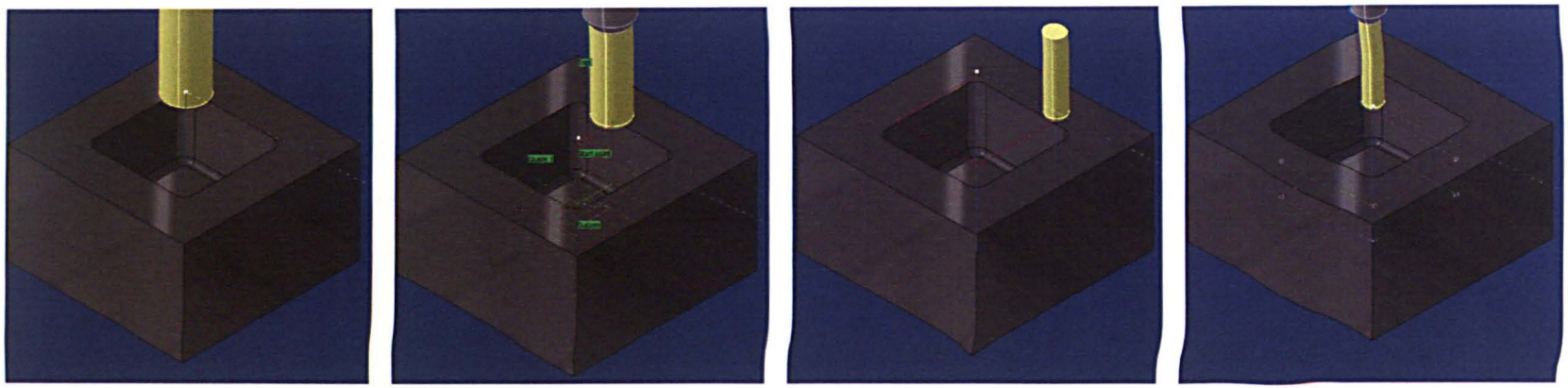

Strategy	Sequence	Tool	Action	D	Z	RPM	Vs (m/min)	Feed	FPT	Ae	Ap	Time
3-2	S10	T11 R416.2-0250L25-31	Drill access hole towards corner of pocket	25	2	1528	120.01	275	0.09	25	40	15
	S20	T6 R216.35-20045-AK55N	Plunge down pre-drilled hole, slot perimeter of pocket and step-in	20	4	905	56.86	181	0.05	20/8	13.5	383
	S30	T26 R230.2412000-AP048H1	Plunge corners	12	2	1590	59.94	500	0.079	3.6	40	31
	S40	T2 R216.34-10050-AK22P	Finish perimeter	10	4	3180	99.9	512	0.04	0.5	20	63
Total Time				492								

Strategy 3-3

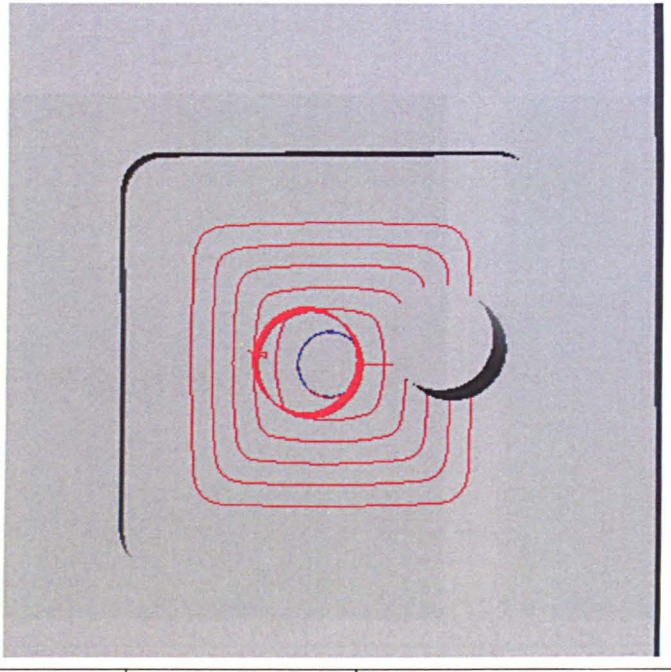

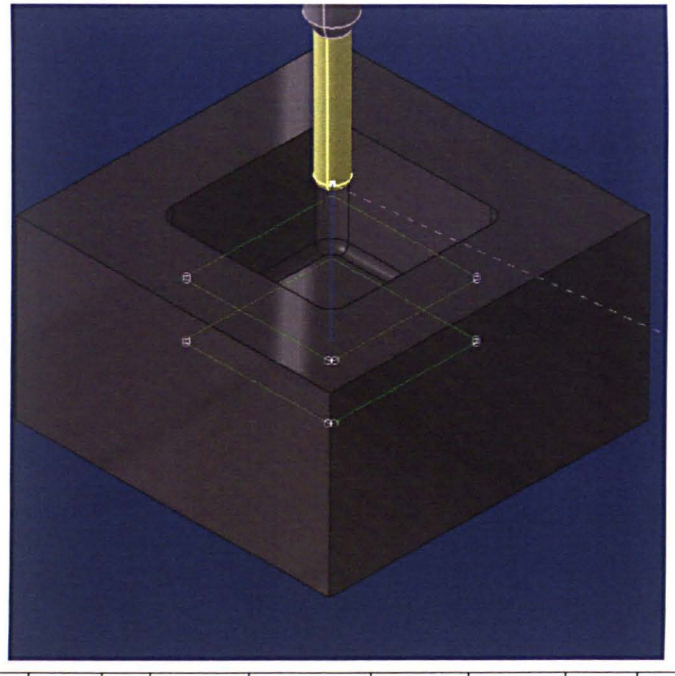

Strategy	Sequence	Tool	Action	D	Z	RPM	Vs (m/min)	Feed	FPT	Ae	Ap	Time
3-3	S10	T13 R216.35-16045-AK50N	Helical Ramp to depth and spiral from circle to pocket perimeter	16	5	1320	66.35	198	0.03	6/40	40	305
	S20	T2 R216.34-10050-AK22P	Finish perimeter	10	4	3180	99.9	764	0.06	0.5	20	54
Total Time				359								

Strategy 3-4

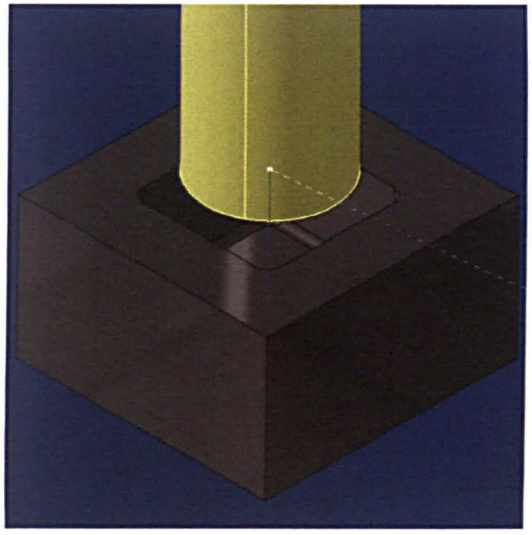

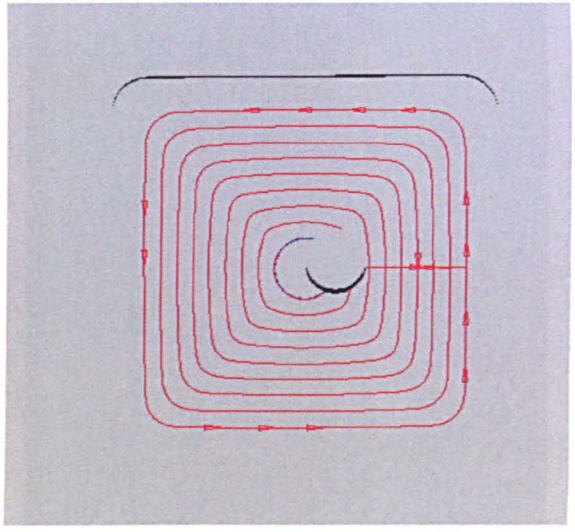

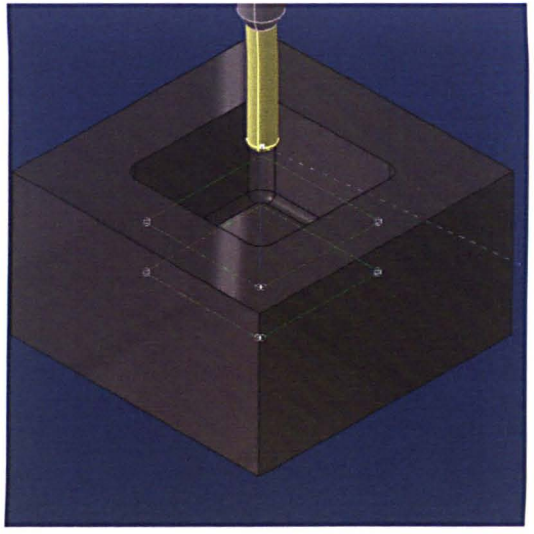

Strategy	Sequence	Tool	Action	D	Z	RPM	Vs (m/min)	Feed	FPT	Ae	Ap	Time
3-4	S10	T14 R416.2-0580L40-21	Drill centre of pocket	58	2	412 439	75.07 80	62 131.7	0.075 0.15	58	40	58 28
	S20	T13 R216.35-16045-AK50N	Spiral-morph from hole to pocket perimeter	10	4	3180	100	512	0.04	4	40	180
	S30	T2 R216.34-10050-AK22P	Finish perimeter	10	4	3180	99.9	764	0.06	0.5	20	54
Total Time				292								

Strategy 3-5

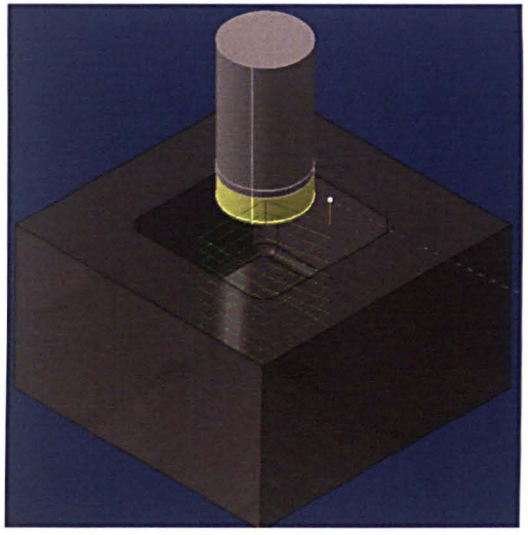

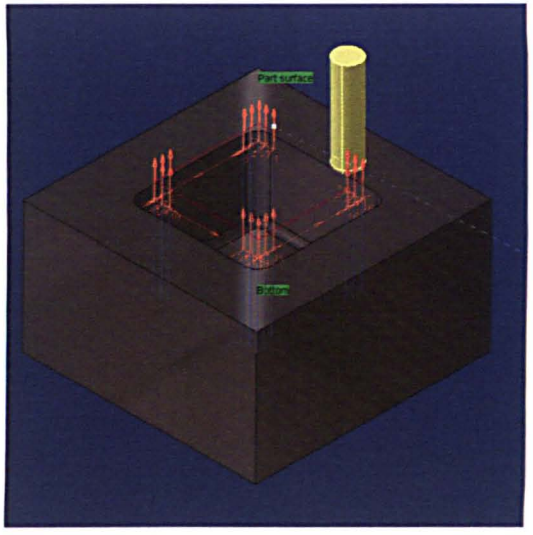

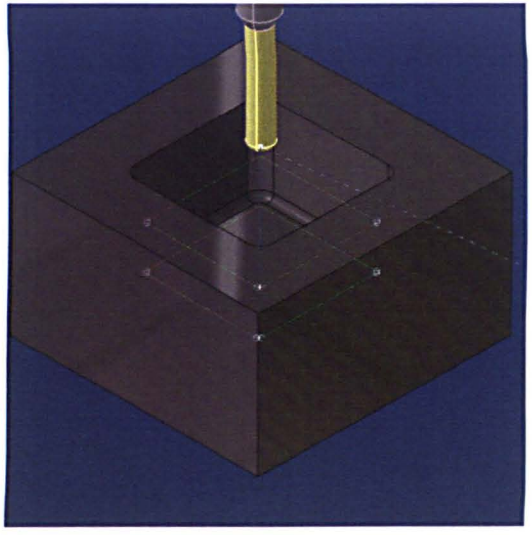

Strategy	Sequence	Tool	Action	D	Z	RPM	Vs (m/min)	Feed	FPT	Ae	Ap	Time
3-5	S10	T15 R790-032C552-11M	Ramp at 5mm Depth working in to depth	32	4	270	27.14	97.2	0.09	32	5	575
	S20	T26 R230.2412000-AP048H1	Plunge corners	12	2	1590	59.94	500	0.079	3.6	40	125
	S30	T2 R216.34-10050-AK22P	Finish perimeter	10	4	3180	99.9	512	0.04	0.5	20	90
Total Time				790								

Strategy 3-6

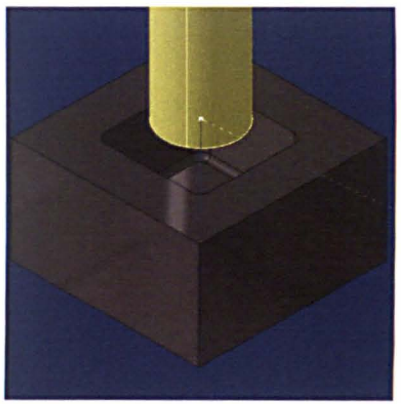
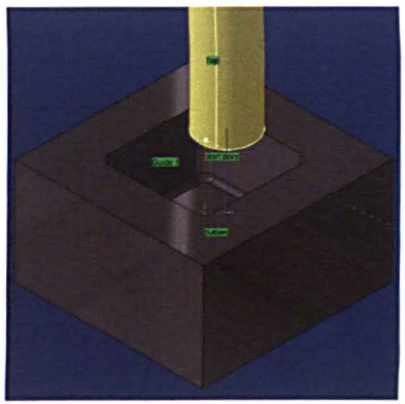
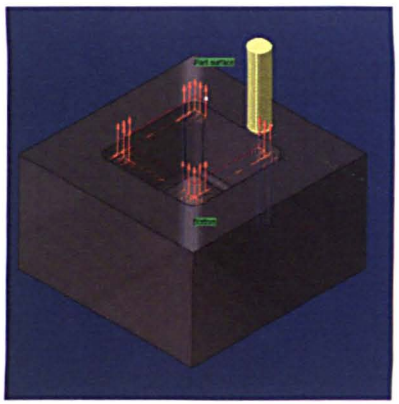
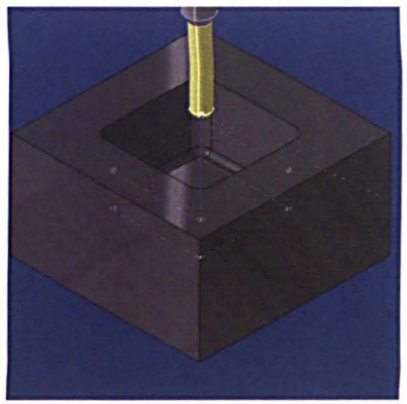

Strategy	Sequence	Tool	Action	D	Z	RPM	Vs (m/min)	Feed	FPT	Ae	Ap	Time
3-6	S10	T3 R416.34-10050-AK22P	Drill hole in centre	44	2	542.5	74.99	81.4	0.075	44	40	47
	S20	T8 R390-032C6-45M	Step-Out to perimeter	32	2	596	59.92	214.5	0.12	32	40	67
	S30	T26 R230.2412000-AP048H1	Plunge Corners	12	2	1590	59.94	500	0.079	3.6	40	125
	S40	T2 R216.34-10050-AK22P	Finish perimeter	10	4	3180	99.9	512	0.04	0.5	20	90
Total Time				329								

APPENDIX II

Variable Helix Matlab Solution

```
%
**********************************************************************
**
%           Chatter analysis program  for the milling cutter with
%                        nonuniform helix angles
%        This program is written by Sam Turner 2004 - 2006  (AMRC)
%
**********************************************************************
**
clear all;
%close all;
pi = 3.1415926;      %


i5 = 0;               % counter
wcs = 1000*2*pi;              % starting frequency
wci = 1*2*pi;              % increment
wce = 4000*2*pi;              % ending frequency
kmin = 0.1;           % min. number of lobes
kmax = 10;               % max. number of lobes
es = kmin*360;
ee = kmax*360;
ei = 5;               % increament
itec = 5e5;           % iteration constant
salim = 30;      % set alim
D=16;                 % Diameter of cuter
ae=16;                 % radial depth of cut
H1=35;                % Helix angle 1 (degrees)
H2=35;                % Helix angle 2 (degrees)

fip10=90;              % 1st pitch angle
L=30;                 % flute length (mm)
d=1;                 % number of elements taken up length of cutter

nmin=3500;
nmax=12000;
dn=50;
N=4;
Kt= 400e6;
Kr= 160e6/Kt;
minpitch=25;         % minimum pitch angle (degrees)
milldirection=1;           %0=conventional, 1=climb, 2=slot

Modal_inputCP3;

%%%%%%%%%%%%%%%%%%%%%%%%%%%%%%%%%%%%%%%%%%%%%%%%%%%%%%%%%%%%%%%%
%%Helix allocation
%%%%%%%%%%%%%%%%%%%%%%%%%%%%%%%%%%%%%%%%%%%%%%%%%%%%%%%%%%%%%%%%
dc=1;
h(1)=H1*pi/180;
h(2)=H2*pi/180;
for j=(3:N)
    h(j)=h(j-2);
end
h(N+1)=h(1);
r=D/2;
```

```
%%%%%%%%%%%%%%%%%%%%%%%%%%%%%%%%%%%%%%%%%%%%%%%%%%%%%%%%%%%%%%%%%%%%%%%%%%%%%%%%
%%%%%%%%
%%  DISCRETE PITCH METHOD
%%%%%%%%%%%%%%%%%%%%%%%%%%%%%%%%%%%%%%%%%%%%%%%%%%%%%%%%%%%%%%%%%%%%%%%%%%%%%%%%
%%%%%%%%%%%%%
L1=0
for L1=(0:1)
%%%Define average pitch angles for flute j , Helix H1, H2 and depth
of cut L
if L1==1
dl=L/d;

for j=(1:N)
    dz(1)=0;
    if j==1
        fipj(j,1)=fip10*pi/180;
    else
        fipj(j,1)=((2*(2*pi)/N))-fipj(j-1,1);
    end

    for dc=(2:d+1)
        fipj(j,dc)=(((dl*(dc-1))/(tan(h(j+1))))-((dl*(dc-
1))/(tan(h(j))))+(fipj(j,1)*r))/r;
        dz(dc)=(dc-1)*dl;
    end
    %p(j)=(sum(fipj(j,:)))/(d+1);
end

fipd=fipj*180/pi;
mf=min(fipd);
if min(mf)<minpitch
    error('pitch becomes too small, must reduce L or modify H1,H2 and
fip10 to increase pitch angles')
else
    fipd
end

figure;
plot(fipd(1,:),dz)
xlabel('Pitch Angle  [165]','FontWeight','bold')
ylabel('z position [mm]','FontWeight','bold')
title('pitch angle','FontWeight','bold','FontSize',12)
for j=(2:N)
    hold on;
    plot(fipd(N,:),dz,'r')
end
else
    dc=1;
    for j=(1:N)
    dz(1)=0;
    if j==1
        fipj(j,1)=fip10*pi/180;
    else
        fipj(j,1)=((2*(2*pi)/N))-fipj(j-1,1);
    end
    end
end
%%%%%%%%%%%%%%%%%%%%%%%%%%%%%%%%%%%%%%%%%%%%%%%%%%%%%%%%%%%%%%%%%%%%%%%%%%%%%%%%
%%%%%%%%%%%%%%%%%
%%%%%%%%%% Entry & exit angles, directional coefficients
```

```
%%%%%%%%%%%%%%%%%%%%%%%%%%%%%%%%%%%%%%%%%%%%%%%%%%%%%%%%%%%%%%%%%%%%%%
%%%%%%%%%%%%%%%%%%
if ae==D
    milldirection==2
end

if milldirection==0
    fist=0;
    fiex=acos(((r)-ae)/(r));
end
if milldirection==1
    fist=pi-(acos(((r)-ae)/(r)));
    fiex=pi;
end
if milldirection==2
    fist=0;
    fiex=pi;
end



axx=0.5*(((cos(2*fiex))-(2*Kr*fiex)+(Kr*sin(2*fiex)))-((cos(2*fist))-
(2*Kr*fist)+(Kr*sin(2*fist))));
axy=0.5*(((-sin(2*fiex))-(2*fiex)+(Kr*cos(2*fiex)))-((-sin(2*fist))-
(2*fist)+(Kr*cos(2*fist))));
ayx=0.5*(((-sin(2*fiex))+(2*fiex)+(Kr*cos(2*fiex)))-((-
sin(2*fist))+(2*fist)+(Kr*cos(2*fist))));
ayy=0.5*(((-cos(2*fiex))-(2*Kr*fiex)-(Kr*sin(2*fiex)))-((-
cos(2*fist))-(2*Kr*fist)-(Kr*sin(2*fist))));

A0=[axx axy ; ayx ayy ];

%%%%%%%%%%%%%%%%%%%%%%%%%%%%%%%%%%%%%START SCAN
%%%Start Scan
dd=1;
 for dd=(1:dc)
            p=fipj(:,dd)

    ct=1;
    for n=nmin:dn:nmax;
        slb1 = 0;
        slb2 = 0;
        slb3 = 0;
        i5=0;
    for wc = wcs:wci:wce;




%%%%%%%%%%%%%%%%%%%%%%%%%%%%MODAL%%%%%%%%%%%%%%%%%%%%%%%%%%%%%%%%%%%%%
%%%%%%

%%%%%%%%%%%%%%%%%%%%%%%%%%%%MATRIX%%%%%%%%%%%%%%%%%%%%%%%%%%%%%%%%%%%%
%%%%%%

%%%%%%%%%%%%%%%%%%%%%%%%%%%%%%%%%%%%%%%%%%%%%%%%%%%%%%%%%%%%%%%%%%%%%%
%%%%%%
```

```
%      % Reconsructed TFs from modal analysis
       GXY = 0; GYX = 0; GXZ = 0; GZX = 0; GYZ = 0; GZY = 0;
%
       GXX = 0.;    % Initialize first
       for mode = 1 : No_modex;  % Scan all the modes
           %  sum the modes contributing to the transfer function
           GXX = GXX + (wnx(mode)^2 / kx(mode)) / ((i*wc)^2 + 2 *
cetax(mode) * wnx(mode) * i * wc + wnx(mode)^2) ;
       end;

       GYY = 0.;
       for mode = 1 : No_modey;
           GYY = GYY + (wny(mode)^2 / ky(mode)) / ((i * wc)^2 + 2 *
cetay(mode) * wny(mode) * i * wc + wny(mode)^2 );
       end;

       TF_Matrix = [GXX GXY  ; GYX GYY  ];


%%%%%%%%%%%%%%%%%%%%%%%%%%%%%%%%%%%%%%%%%%%%%%%%%%%%%%%%%%%%%%%%%%%%%%%%%%%%
%%
       %%%%%%%%%%%%%%%%%%%%Scan flutes



           for j=(1:N)
               B(j)=60*(wc*(p(j)))/(2*pi*n);
               ep(j)=exp(-B(j)*i);
           end
           %%
           %%Define time loss factor for wc
           E=N-(sum(ep));



           A01 = A0.*E;



           %TF_Matrix = [GXX 0  ; 0 GYY ];

           sol = eig(eye(2),(A01 * TF_Matrix));
           if real(sol(1)) > 0     % choose the positiv-e first
eigenvalue
               if imag(sol(1)) * slb1 < 0, % choose, if the
imaginary part1=0
                   if abs(imag(sol(1)) - slb1) < itec,

                       i5 = i5 + 1;
                       w=wc;
                       %n0s(i5) = n;
   %                     for i1 = 1:N;
   %                         em(i5,i1) = beta(i1) * 180 / pi;
   %                     end;
                       sl(i5) = imag(sol(1));
                       al(i5) = 1000 * real(sol(1)) * 4*pi / Kt;
                       if sl(i5)<0
```

```
                        al(i5)=NaN;
                    end;
                end;
            end;
            slb1 = imag(sol(1));
            rs1 = real(sol(1));
        end;

        if real(sol(2)) > 0     % choose the positive second
eigenvalue
            if imag(sol(2)) * slb2 < 0, % choose, if the
imaginary part2=0
                if abs(imag(sol(2)) - slb2) < itec,
                    i5 = i5 + 1;
                    w(i5)=wc;
                    %n0s(i5) = n;
    %                 for i1 = 1:N;
    %                     em(i5,i1) = beta(i1) * 180 / pi;
    %                 end;
                    sl(i5) = imag(sol(2));
                    al(i5) = 1000 * real(sol(2)) *4*pi/ Kt;
                    if sl(i5)<0
                        al(i5)=NaN;
                    end;
                end;
            end;
            slb2 = imag(sol(2));
            rs2 = real(sol(2));
        end;

    end;
    alim(ct,dc)=min(al);
n0(ct)=n;
ct=ct+1;
end;

end
M=mean(alim);
L=M;
L1=L1+1;
end

col=[ 'r' 'g' 'b' 'c' 'm' 'y' 'k' '.' '*' '<' '>' 'p' 'h' '.-']



%
% plot(n0, alim(:,1),'b');          figure;
for dc=(1:d+1)
    hold on;
    plot(n0,alim(:,dc),col(dc))
%     if dc/2>floor(dc/2)
%         plot(n0, alim(:,dc),'r');
%     else
%         plot(n0, alim(:,dc),'b');
%     end

end
```

```
hold on;

xlabel('Spindle Speed ','FontWeight','bold')
ylabel('a_lim [mm]','FontWeight','bold')
title('Stability Lobes using Variable Helix
Cutter','FontWeight','bold','FontSize',12)
% legend('tool
tip','d1','d2','d3','d4','d5','d6','d7','d8','d9','d10','d11','d12')
axis([min(n0), max(n0), 0 ,25]);        grid;
save VH7alimslot.dat alim -ascii
save VH7

%n.dat n0 -ascii        hold on;
% plot(n0, alim(:,2),'r');
% xlabel('Spindle Speed ','FontWeight','bold')
% ylabel('a_lim [mm]','FontWeight','bold')
% title('Stability Lobes using Variable Helix
Cutter','FontWeight','bold','FontSize',12)
% %axis([min(npa(:,1)) max(npa(:,1)) 0 max(npa(:,2))]);     grid;
```